Optimization strategies for blind multiuser detection in strong interference scenarios

Stanley Smith

le cnam

École Doctorale Informatique, Télécommunications et Électronique

Centre d'Études et de Recherche en Informatique et Communications

THÈSE DE DOCTORAT

présentée par : **Stanley SMITH**

soutenue le : **19 décembre 2019**

pour obtenir le grade de : **Docteur du Conservatoire National des Arts et Métiers**

Discipline : **Génie informatique, automatique et traitement du signal**
Spécialité : **Informatique**

Optimization strategies for blind multiuser detection in strong interference scenarios

THÈSE dirigée par

M. Terré Michel	*Professeur, CNAM*

et co-dirigée par

Mme Pischella Mylène	*Maître de Conférences, CNAM*

RAPPORTEURS

M. Palicot Jacques	*Professeur, Centrale Supelec*
M. Ros Laurent	*Maître de Conférences, INP Grenoble*

PRÉSIDENTE DU JURY

Mme Liénard Martine	*Professeur, Université Lille 1*

EXAMINATRICES

Mme Fijalkow Inbar	*Professeur, Ensea*
Mme Niang Keita Ndeye	*Maître de Conférences, CNAM*

Remerciements

Je remercie le CNAM et l'EDITE de Paris pour m'avoir donné le privilège d'effectuer cette thèse et financé ces trois années de recherche.

Mes remerciements vont ensuite à l'ensemble des membres du jury, envers lesquels je suis extrêmement reconnaissant pour l'attention et de la bienveillance qu'ils ont portée à mon travail, et qui ont fait tout leur possible pour assister à ma soutenance malgré des difficultés de transport exceptionnelles. Je remercie Jacques Palicot et Laurent Ros pour leur lecture scrupuleuse de mon manuscrit et leur précieuses remarques, ainsi que Inbar Fijalkow, Martine Liénard et Ndeye Niang Keita pour leur intérêt et les discussions très constructives qu'elles ont apportées lors de la soutenance.

J'adresse ma profonde gratitude envers mes deux encadrants, Michel Terré et Mylène Pischella, qui m'ont accompagné et suivi tout au long de ces trois années, m'ont fait bénéficier de leur expérience et de leur expertise, et auprès de qui j'ai énormément appris. Je suis particulièrement reconnaissant de la confiance qu'ils ont exprimée à mon égard et de l'implication dont ils ont fait preuve lors de ces derniers mois de thèse, que ce soit par leurs relectures assidues du manuscrit en devenir ou les nombreuses répétitions à l'aube de la soutenance.

Je remercie chaleureusement l'ensemble des membres du laboratoire CEDRIC et de l'équipe LAETITIA qui m'ont accueilli et aidé à bien des égards. Mention spéciale à Christophe Alexandre, que j'ai dérangé mille et une fois pour des dépannages informatiques, mais aussi à Anne-Cécile Madec, Kim Ahn Nguyen, Pascal Chevalier, Didier Le Ruyet, Abdel Ghamraoui, Louison Monrose, Hmaied Shaiek, Iness Ahriz, Ali Dziri, Samuel Garcia, Daniel Roviras, Salim Faci, Luc Féty, Anne-Laure Billabert, Viviane Gal, Catherine Algani, Annie Thieulon, Rafik Zayani pour leur gentillesse et leur disponibilité. J'adresse une pensée particulière à mes collègues Wafa et Luan, dont j'ai partagé le bureau et le plus clair de ces trois années, et à qui je souhaite tout le meilleur pour la suite de leur parcours. Mes sincères remerciements à l'administration du CNAM et en particulier aux membres du bureau des études doctorales pour leur patience et les nombreuses sollicitations dont ils ont fait l'objet pour m'orienter dans les méandres des procédures administratives.

Ce manuscrit n'aurait finalement pu voir le jour sans le soutien inestimable de mes ami·e·s et de mes proches. Je pense à Elsa, Marion et Chloé, dont la présence et l'aide m'auront été salutaires dans les instants les plus tumultueux ; à Nico et Chacha, avec qui j'aurai passé tant d'inoubliables moments, et dont les encouragements et la venue à ma soutenance m'auront beaucoup touchés ; à Arnaud, Jibé et Hélène, qui auront bravé vents et marées pour être présents également, et auprès de qui j'aurai souvent trouvé refuge pendant ces trois années ; à Fabien, Charlie, Martin, Daga, Séb, Pierre, Louis, Fanny, Antoine, Quentin, Charly, et toutes celles et ceux qui auront, de près ou de loin, par leur soutien, leur

affection, ou simplement leur présence, œuvré à rendre ce moment possible ; à ma famille, mon frère, ma sœur et enfin mes parents, pour qui je ne saurais exprimer l'étendue de ma gratitude et de ma fierté.

À toutes et tous, merci d'être à mes côtés.

Contents

List of acronyms

ASK	Amplitude Shift Keying
AWGN	Additive White Gaussian Noise
BCA	Bounded Component Analysis
BER	Bit Error Rate
BIRCH	Balanced Iterative Reducing and Clustering using Hierarchies
BLUE	Best Linear Unbiased Estimators
BPSK	Binary Phase Shift Keying
BS	Base Station
BSS	Blind Source Separation
cdf	cumulative distribution function
CDMA	Code Division Multiple Access
cf	characteristic function
CLINK	Complete-Link
CMA	Constant Modulus Algorithms
CP	Cyclic Prefix
CPM	Continuous Phase Modulation
CRLB	Cramer-Rao Lower Bound
CSI	Channel State Information
DBSCAN	Density-Based Spatial Clustering of Applications with Noise
DFT	Discrete Fourier Transform
DMT	Discrete Multi-Tone
DSL	Digital Subscribe Line
EM	Expectation-Maximization
FDMA	Frequency Division Multiple Access
FFT	Fast Fourier Transform
FLAME	Fuzzy Clustering by Local Approximation of Membership
FSK	Frequency Shift Keying
GA	Genetic Algorithms
GLS	Generalized Least Squares
GMM	Generalized Moment Method
GMSK	Gaussian Minimum Shift Keying
IBI	Inter-Block Interference
ICA	Independent Component Analysis
ICI	Inter-Carrier Interference
IDFT	Inverse Discrete Fourier Transform
IGID	Information Geometric Identification
ILSE	Iterative Least Squares with Enumeration
ILSP	Iterative Least Squares with Projection
IoT	Internet of Things

ISI	Inter-Symbol Interference
IUI	Inter-User Interference
LLS	Linear Least Squares
LSE	Least Squares Estimators
MAC	Multiuser Access Channel
MIMO	Multiple-Input Multiple-Output
MISO	Multiple-Input Single-Output
ML	Maximum Likelihood
MLE	Maximum Likelihood Estimators
MM	Majorize-Maximization
MMSE	Minimum Mean Square Error
MSE	Mean Square Error
MUI	Multiuser Interference
MVUE	Minimum Variance Unbiased Estimators
NLLS	Non Linear Least Squares
NOMA	Non Orthogonal Multiple Access
NRMSE	Normalized Root Mean Square Error
OFDM	Orthogonal Frequency Division Multiplexing
OFDMA	Orthogonal Frequency Division with Multiple Access
OLS	Ordinary Least Squares
OMA	Orthogonal Multiple Access
OPTICS	Ordering Points to Identify the Clustering Structure
OQAM	Offset Quadrature Amplitude Modulation
PAM	Pulse Amplitude Modulation
pdf	probability density function
PSK	Phase Shift Keying
QAM	Quadrature Amplitude Modulation
QPSK	Quadratic Phase Shift Keying
SCA	Sparse Component Analysis
SER	Symbol Error Rate
SIC	Successive Interference Cancellation
SINK	Single-Link
SINR	Signal to Interference plus Noise Ratio
SIR	Signal to Interference Ratio
SISO	Single-Input Single-Output
SML	Stochastic Maximum Likelihood
SNR	Signal to Noise Ratio
SVD	Singular Value Decomposition
TDMA	Time Division Multiple Access
UDM	Underdetermined Mixtures
UE	User Equipments
WLS	Weighted Least Squares
ZP	Zero-Padding

Mathematical notations

a scalar number
$\mathbf{a}$ vector
$\mathbf{A}$ matrix
$\mathbf{A}^T$ matrix transpose
$\mathbf{A}^\dagger$ matrix hermitian transpose
$\mathbf{A}^{-1}$ matrix inverse
$\mathrm{Tr}\left[A\right]$ trace operator
$\mathbf{vec}\left(A\right)$ vectorization operator
$\mathrm{rk}\left(A\right)$ matrix rank
$\parallel A \parallel_F$ Frobenius norm
$\mathbf{A} \otimes \mathbf{B}$ Kronecker product
$\langle \mathbf{a} | \mathbf{b} \rangle$ Hermitian scalar product
$\mathbf{a} \circledast \mathbf{b}$ cyclic convolution

$\mathcal{A}$ continuous set
$\mathscr{A}$ finite set
$|\mathscr{A}|$ cardinal of a set
$\mathcal{A}^c$ complement of a set
$\mathcal{A} \cap \mathcal{B}$ intersection of sets
$\mathcal{A} \cup \mathcal{B}$ reunion of sets
$\mathbb{R}$ field of reals numbers
$\mathbb{C}$ field of complex numbers
$\mathcal{C}(z_c, r)$ circle centered at z_c with radius r
$\mathcal{B}(z_c, r)$ ball centered at z_c with radius r
$\mathcal{V}(z_c)$ Voronoï cell of z_c
$\mathcal{R}(z_c)$ convergence region of z_c
$\mathscr{C}$ modulation constellation

$\Re(z)$ real part of z
$\Im(z)$ imaginary part of z
z^* complex conjugate of z
$|z|$ modulus of z
$\mathrm{Arg}(z)$ argument of z

$h(t)$ time function
$\tilde{h}(f)$ Fourier Transform of h
$\delta(t)$ Diract delta function
$f(t) * g(t)$ convolution product

X, Y real random variable
Z complex random variable
$p_Z(z)$ probability density function
$F_Z(z)$ cumulative distribution function
$\Phi_Z(z)$ first characteristic function
$\Psi_Z(z)$ second characteristic function
$\mathbb{P}\left[\cdot\right]$ probability measure
$\mathbb{E}\left[\cdot\right]$ expectation operator
$\mathbb{V}\left[\cdot\right]$ variance operator
$\mathbb{J}\left[\cdot\right]$ pseudo-variance operator
$\mu_p^q(Z)$ moment of order (p, q)
$\kappa_p^q(Z)$ cumulant of order (p, q)
$\mathcal{CN}(\cdot, \cdot, \cdot)$ complex normal distribution
$\boldsymbol{\theta}$ distribution parameter vector
$\boldsymbol{\Theta}$ parameter set
$\widehat{\boldsymbol{\theta}}$ parameter vector
$\bar{\mu}_p^q$ sample estimator of $\mu_p^q(Z)$
$\bar{\kappa}_p^q$ sample estimator of $\kappa_p^q(Z)$
$\mathrm{B}(\widehat{\boldsymbol{\theta}})$ estimation bias
$\mathrm{MSE}(\widehat{\boldsymbol{\theta}})$ mean square error
$\mathbb{L}\left[\boldsymbol{\theta}; \mathbf{z}\right]$ log-likelihood function

$\succeq$ complex generalized inequality
$\simeq$ approximate equality
$\sim$ distribution law
$\equiv$ equivalence
$\mathcal{O}$ complexity order

Résumé

Introduction

Cette thèse s'inscrit dans des problématiques de traitement du signal, et plus particulièrement des signaux issus des télécommunications. Le modèle de communication considéré fait intervenir une station de base (BS), qui consiste en une collection d'antennes couvrant une certaine zone géographique, schématisée par un hexagone sur la figure 1, et plusieurs équipements utilisateurs (UE) ou sources, typiquement des téléphones cellulaires. Ces utilisateurs communiquent vers la station de base par ondes électromagnétiques.

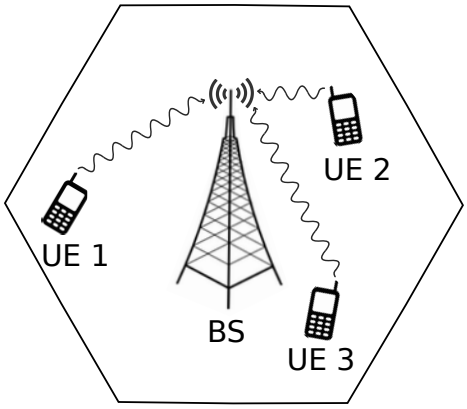

Figure 1 – *Communication entre une station de base (BS) et trois utilisateurs (UE).*

La bonne réception de signaux ainsi émis par plusieurs utilisateurs implique deux difficultés majeures. Premièrement, les signaux de chaque utilisateur interfèrent au niveau de la station de base, ce qui génère de l'interférence inter-utilisateur (IUI) et complexifie sensiblement le décodage du signal. De plus, ces signaux subissent lors de leur propagation l'influence de leur environnement, modélisée par le canal de propagation. Ces canaux sont inconnus du récepteur, mais leur estimation est cruciale pour garantir une transmission fiable : c'est le problème d'estimation du canal. Dans les réseaux actuels, le traitement de l'interférence inter-utilisateur est le plus souvent réalisé par de l'accès multiple dit orthogonal. Par exemple, l'accès orthogonal en temps consiste en ce que les utilisateurs transmettent leur signal à tour de rôle dans des intervalles de temps successifs, tandis que l'accès orthogonal en fréquence attribue aux utilisateurs des bandes de fréquence séparées. Cela permet ainsi de prévenir l'interférence, les contributions des différentes sources ne se recouvrant pas. L'estimation du canal se fait quant à elle via des symboles "pilotes" c'est-à-dire des séquences prédéterminées connues du récepteur, qui lui permettent par comparaison avec le signal réellement reçu d'en déduire une estimation du canal. Ces séquences pilotes ne portent en revanche aucune information sur le signal en lui-même.

Bien qu'efficaces, ces techniques induisent une raréfaction de la bande passante et une réduction du débit utile qui deviennent de plus en plus difficile à concilier avec les applications sans fil modernes telles que l'Internet des Objets (IoT), lesquelles exigent des débits toujours plus élevés sur des réseaux de plus en plus denses en utilisateurs. Dans la perspective des prochaines générations de réseaux il est donc crucial de pouvoir aller au-delà de ces limitations en considérant d'une part de l'accès multiple non orthogonal (NOMA), permettant ainsi à plusieurs utilisateurs d'émettre dans les mêmes ressources, qu'elles soient temporelles, fréquentielles ou autres, et l'estimation aveugle de canal, qui s'affranchit des séquences pilotes et n'utilise que le signal utile pour estimer le canal de propagation.

Modélisation

La communication entre un utilisateur et sa station de base est modélisée de la manière suivante : tout d'abord, le signal émis par l'utilisateur consiste en une séquence de N nombres complexes s_n nommés symboles, qui prennent leur valeur uniformément dans un ensemble fini $\mathscr{C}$ appelé constellation. Les symboles d'une constellation, génériquement notés c, représentent l'amplitude et la phase d'un signal de référence, la porteuse, qui consiste en une simple sinusoïde de fréquence supposée connue du récepteur et qui sert de support à la transmission des symboles – on parle alors de modulation linéaire. On peut distinguer trois grandes familles de telles modulations, à savoir les modulation en amplitude (ASK), dont la constellation associée consiste en des points régulièrement espacés sur l'axe réel, les modulations en phase (PSK), pour lesquelles les symboles sont disposés en cercle, et les modulations en quadrature (QAM), dont les symboles sont répartis selon une grille carrée (voir Fig.2 ou Fig.I.3 pour des exemples).

Lors de sa propagation, le signal émis subit un certain nombre de modifications dues à son environnement. Ces modifications sont représentées par le canal de propagation, qui en général est une fonction complexe du temps et de la fréquence. Une approximation forte faite dans cette thèse est celle du canal "plat", dont la réponse en fréquence est constante sur la bande passante du signal émis. Un tel canal est alors modélisé par un simple nombre complexe h. Le signal est de plus perturbé par des fluctuations aléatoires modélisées par un bruit complexe additif w de distribution gaussienne circulaire de variance N_0.

Au niveau de la station de base, le signal reçu consiste alors en une série de N symboles notés r_n donnés par

$$r_n = hs_n + w_n \tag{1}$$

où w_n est une réalisation du bruit. Du fait de ce dernier, les symboles reçus ne coïncident pas avec les symboles de la constellation d'où ils ont été émis. Pour estimer les symboles qui lui ont été envoyés, le récepteur utilise alors le principe de la détection à seuils, qui consiste à associer à chaque symbole reçu le symbole de la constellation qui lui est le plus proche. Il a pour ce faire besoin au préalable de compenser l'influence du canal, ce qui nécessite donc une estimation de h, notée $\widehat{h}$. L'imprécision de cette estimation ainsi que le bruit impliquent

que certains symboles estimés par la détection à seuils différent des symboles réellement émis. La qualité de la transmission est alors mesurée par le taux d'erreur symboles (SER), qui donne la probabilité qu'un symbole émis soit incorrectement estimé au récepteur. Des informations plus détaillées relatives au modèle et aux hypothèses de travail dans lequel cette étude se place peuvent être consultées au chapitre I.

Si l'on considère à présent plusieurs utilisateurs émettant simultanément et de manière synchrone vers une même station de base, on utilise le modèle du canal à accès multiple (MAC), qui donne le signal reçu comme une combinaison linéaire des signaux sources de chaque émetteur, chaque coefficient représentant le canal (plat) d'un utilisateur spécifique.

$$r = \sum_{k=1}^{K} h_k s_k + w \tag{2}$$

Chaque utilisateur transmet donc une sequence de symboles selon une constellation qui lui est propre, lesquels subissent l'influence de leur canal associé. Les contributions de chaque utilisateur se somment au niveau de la station de base, et le signal reçu est alors obtenu par addition du bruit gaussien, comme illustré sur la figure 2. L'ensemble des symboles obtenus par combinaison linéaire des symboles de chaque constellation source définit la constellation mélange.

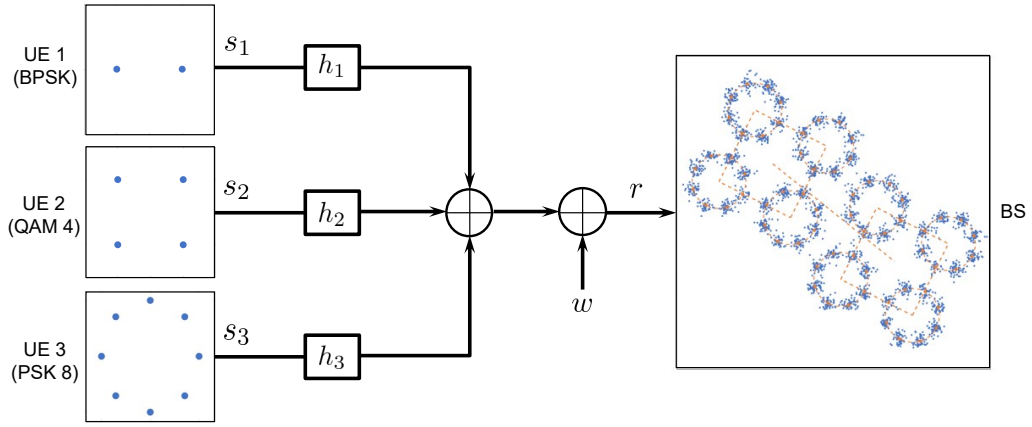

Figure 2 – *Représentation schématique d'une transmission à trois utilisateurs avec le modèle du canal à accès multiple. Les points en orange forment la constellation mélange.*

En supposant que les utilisateurs émettent chacun N symboles, le vecteur des symboles reçus $\mathbf{r}$ s'écrit comme $\mathbf{r} = \mathbf{hS} + \mathbf{w}$, avec $\mathbf{h}$ le vecteur canal, qui contient les coefficients de canal de chaque source, $\mathbf{S}$ la matrice des symboles émis, dont chaque ligne représente les symboles émis par un utilisateur donné, et $\mathbf{w}$ le vecteur des réalisations du bruit. La récupération des symboles émis par chaque source implique donc un double problème d'estimation, à savoir estimer le vecteur canal $\mathbf{h}$ et la matrice des symboles émis $\mathbf{S}$. Ce type de problème est connu dans la littérature sous le nom de séparation de sources aveugle (BSS). Le travail présenté dans cette thèse se place en réalité dans un cas limite de ce

problème puisque les transmissions considérées sont mono-antennaires, c'est-à-dire que la station de base et les utilisateurs ne sont pourvus chacun que d'une seule antenne. Du fait de sa complexité, cette instance du problème de séparation de sources est relativement peu traitée dans la littérature, comparativement aux cas à plusieurs antennes.

Méthodes et objectifs

Une approche particulièrement répandue pour résoudre ce double problème d'estimation $(\mathbf{h}, \mathbf{S})$ est celle de l'annulation successive d'interférence (SIC) [32], qui repose sur l'hypothèse que les contributions de chaque source à la puissance totale du signal reçu sont très différentes. Cela permet de décoder le signal source par source, par ordre de puissance reçue décroissante, en assimilant les signaux issus des sources de moindre puissance à du bruit. Lorsque cette hypothèse est vérifiée, l'annulation successive d'interférence fournit en effet une méthode peu coûteuse et performante pour séparer les signaux d'utilisateurs en accès non orthogonal. En revanche, dès que plusieurs sources ont des puissance comparables à la réception, les conséquences en termes de taux d'erreur s'avèrent la plupart du temps dramatiques. Les erreurs commises se propagent de plus à l'estimation des sources restantes, pénalisant ainsi doublement les sources les moins puissantes : étant décodées en dernier, elles souffrent d'une latence de traitement plus élevée, et sont les plus à même d'être l'objet d'une mauvaise estimation. Ainsi ce type d'approche n'est pas adapté aux cas où l'interférence entre les sources est prédominante, et on préfèrera dès lors se tourner vers des méthodes de détection conjointe.

L'algorithme au cœur de cette thèse, connu sous le nom d'Iterative Least Squares with Enumeration (ILSE) [5], constitue une alternative pertinente au SIC en ceci qu'elle propose une estimation conjointe du vecteur canal et des symboles émis. L'approche utilisée est celle dite du maximum de vraisemblance, qui consiste à chercher les paramètres du mélange les plus vraisemblables compte tenu des symboles observés. Dans le cas du mélange linéaire gaussien, la fonction à minimiser, notée J, revêt la forme particulièrement simple d'un problème des moindres carrés :

$$J(\mathbf{h}, \mathbf{S}) \triangleq \| \mathbf{r} - \mathbf{hS} \|^2 \tag{3}$$

La minimisation directe de cette fonction n'étant pour autant pas accessible, l'algorithme ILSE propose une procédure itérative basée sur l'alternance entre la minimisation de J par rapport à $\mathbf{h}$, la variable $\mathbf{S}$ étant alors fixée, et la minimisation de J par rapport à $\mathbf{S}$ à canal fixé. Ainsi, partant d'une estimation initiale $\widehat{\mathbf{h}}_0$ du canal, l'algorithme en déduit une première estimation de la matrice des symboles émis, qui à son tour est utilisée pour obtenir une estimation affinée du canal, et ainsi de suite jusqu'à ce que l'algorithme atteigne un point fixe, qui correspond à un minimum de la fonction J. L'estimation du canal à une itération donnée, $\widehat{\mathbf{h}}_t$, compte tenu des symboles estimés à l'étape précédente $\widehat{\mathbf{S}}_{t-1}$ est donnée par l'estimateur ordinaire des moindres carrés :

$$\widehat{\mathbf{h}}_t^T = \mathbf{r}\widehat{\mathbf{S}}_{t-1}^\dagger \left(\widehat{\mathbf{S}}_{t-1} \widehat{\mathbf{S}}_{t-1}^\dagger \right)^{-1} \tag{4}$$

L'estimation de la matrice des symboles émis à partir de l'estimation du canal se fait quant à elle en associant chaque symbole reçu au symbole de la constellation estimée qui lui est le plus proche. Il s'agit donc d'une détection à seuils effectuée sur la constellation mélange estimée, appelée dans le cadre de cet algorithme l'étape d'énumération :

$$\widehat{\mathbf{S}}_t = \underset{\mathbf{S}\in(\mathscr{C}_1\times\cdots\times\mathscr{C}_K)^N}{\operatorname{argmin}} \| \mathbf{r} - \widehat{\mathbf{h}}_t^T \mathbf{S} \|^2 \tag{5}$$

La figure 3 illustre la constellation mélange estimée à convergence de l'algorithme dans le cas d'un mélange de deux QAM 4 pour deux estimations initiales différentes du vecteur canal. Dans le premier cas (à gauche) on constate une estimation quasi-parfaite du canal et des symboles émis, qui correspond au minimum global de la fonction J. On comprend ainsi l'intérêt des méthodes d'estimation conjointes, qui ne sont pas limitées par le niveau d'interférence entre les utilisateurs. En revanche, la fonction de coût exhibe la plupart du temps de nombreux minima locaux, et les constellations mélange qui leur sont associées diffèrent radicalement du mélange réel, comme l'illustre le second cas de figure, à droite. La nature du point fixe vers lequel l'algorithme converge est uniquement déterminée par l'estimation initiale du vecteur canal. La stratégie habituelle consiste donc à initialiser l'algorithme plusieurs fois jusqu'à ce que le minimum global ait été atteint. Cette approche naïve soulève néanmoins deux problèmes, à savoir celui du critère à adopter pour déterminer si une solution donnée est optimale ou non, ainsi que le nombre d'itérations requis pour atteindre ce minimum global. Ces limitations, en plus d'une complexité relativement élevée due à la phase d'énumération, font de l'algorithme ILSE une méthode peu utilisée en pratique. La question de l'initialisation est donc fondamentale pour la mise en application réelle de cet algorithme, et plus généralement des méthodes d'estimation basées sur le maximum de vraisemblance.

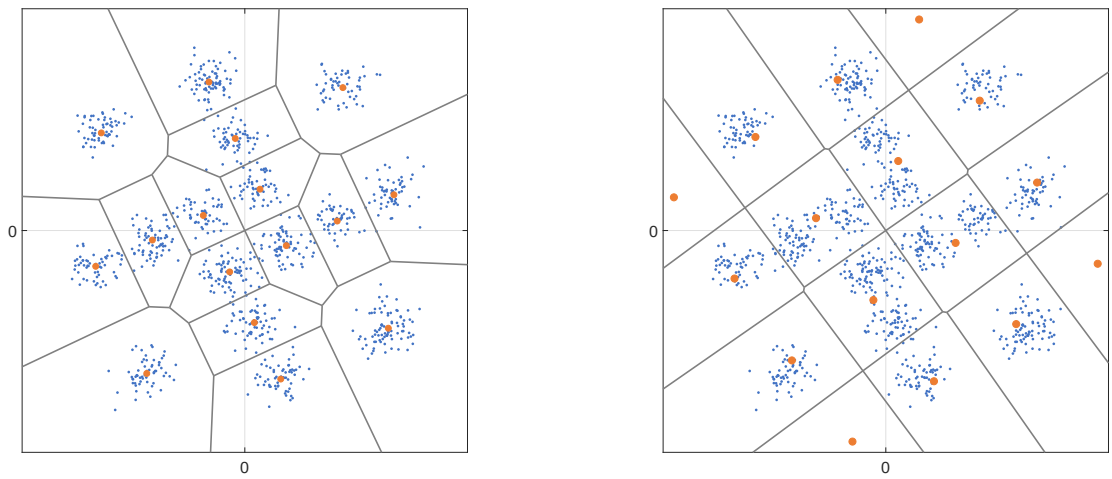

Figure 3 – *Observations d'un mélange de deux QAM 4 (points bleus) et constellation mélange estimée à convergence de l'algorithme ILSE (points oranges) avec les seuils associés (traits noirs). Gauche : cas du minimum global. Droite : cas d'un minimum local.*

Le travail présenté dans cette thèse affiche donc un double objectif : élaborer d'une part

des stratégies d'initialisation qui permettent à la fois d'améliorer la fiabilité de l'algorithme ILSE et d'en réduire la complexité ; d'autre part, explorer la capacité de ces algorithmes à fournir une bonne estimation du canal et des symboles émis dans le cas particulièrement défavorable de transmissions monoantennaires dominées par l'interférence inter-utilisateur. Ces problématiques sont abordées selon trois axes de complexité croissante, à commencer par la restriction à des transmissions à une seule source, au chapitre II. Le cas de plusieurs sources est traité dans le chapitre III, et une généralisation à des modèles de canaux plus réalistes est effectuée au chapitre IV dans le cadre des transmissions multiporteuses. Le chapitre V porte quant à lui sur des considérations plus générales relatives aux algorithmes de classification dans le cas de données partiellement superposées.

Points fixes et stratégies d'initialisation à un utilisateur

La caractérisation précise des points fixes d'un algorithme tel qu'ILSE, même dans le cas d'un seul utilisateur, constitue un problème difficile, on se restreint donc dans un premier temps à une approche asymptotique, en considérant le bruit comme nul et un nombre de symboles reçus infini. Dans ces conditions, les symboles reçus coïncident exactement avec la constellation mélange. L'objectif est ici de trouver des points (des canaux) invariants par l'application successive de la phase d'énumération et de la phase d'estimation du canal de l'algorithme ILSE, ceci afin d'en extraire des conclusions générales sur le comportement de l'algorithme et en déduire des stratégies d'initialisation adaptées. Une première approche pour guider cette recherche est de considérer les propriétés géométriques des constellations étudiées, dont on s'attend à ce qu'elles impliquent une certaine structure sur les points fixes. En particulier, les modulations en quadrature régulières exhibent une propriété structurelle remarquable appelée structure hiérarchique : toute constellation QAM à 4^m symboles, notée ici $\mathscr{C}_m$, peut être décomposée de manière non unique en une combinaison linéaire de deux QAM de taille inférieure selon l'équation ensembliste suivante :

$$\mathscr{C}_m = 2^{m-m'}\mathscr{C}_{m'} + \mathscr{C}_{m-m'} \tag{6}$$

Pour une QAM de taille 4^m, on dénombre ainsi $m-1$ décompositions hiérarchiques non triviales. Si on prend le cas d'une QAM 64 par exemple, on vérifie que n'importe quel symbole c de la constellation associée peut être obtenu par combinaison linéaire d'un symbole de QAM 4, c_1, multiplié par 4, et d'un symbole de QAM 16, noté c_2, ou de manière équivalente à partir d'un symbole de QAM 16 multiplié par 2 et d'un symbole de QAM 4, tel qu'illustré sur la figure 4.

On montre alors que ces décompositions induisent un ensemble de points fixes situés en $\{h, 2h, 4h, \cdots 2^{m-1}h\}$, que l'on appelle points fixes hiérarchiques. La phase d'énumération associée à ces points particuliers peut être vue comme une projection de la constellation observée sur la constellation dont le préfacteur est le plus grand dans la décomposition hiérarchique correspondante. En reprenant le cas de la QAM 64 l'étape d'énumération associée au point $4h$ ramène chaque symbole c sur le symbole c_1 de sa QAM 16 sous-jacente. On obtient ainsi un sous-ensemble de points fixes, commun dans sa construction à toutes les

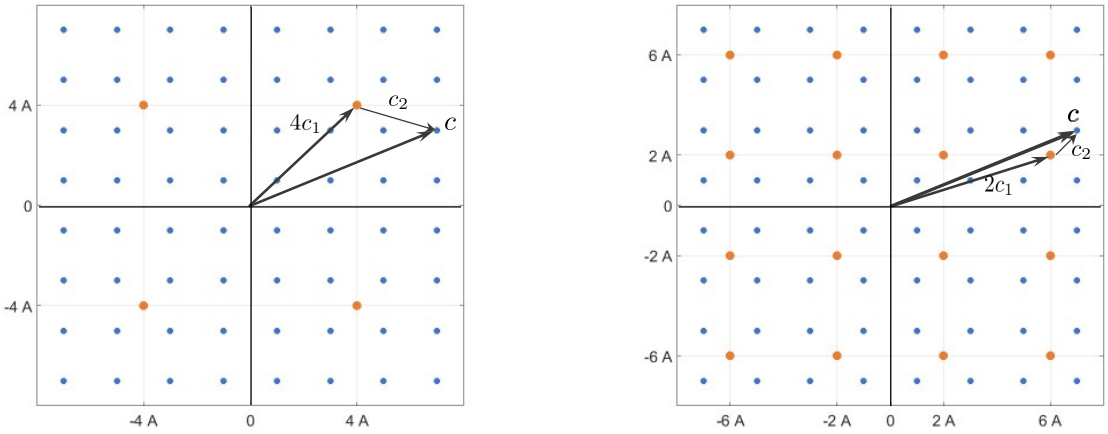

Figure 4 – *Décomposition hiérarchique de la QAM64 (points bleus) en une QAM4 et une QAM16 (gauche) et en une QAM16 et une QAM4 (droite).*

QAM et plus généralement à toute constellation basée sur une structure hiérarchique. En particulier, ces résultats s'appliquent directement aux modulations en amplitude (ASK), qui sont les homologues réels des constellations QAM.

On peut également obtenir une cartographie complète des points fixes dans le régime asymptotique par simulation, en initialisant l'algorithme ILSE sur un nombre suffisant de points dans le plan complexe. Le résultat obtenu pour la QAM 16 avec un canal pris égal à 1 est représenté sur la figure 5, à gauche. Cet exemple constitue le cas non trivial le plus simple à considérer, étant donné que la QAM 4, et plus généralement les modulations en phase (PSK), n'admettent qu'un seul point fixe dans le régime asymptotique à certaines rotations près, comme montré à la section II.3.1. Outre la position des points fixes on accède également à leur région de convergence, c'est-à-dire l'ensemble des points du plan complexe tel que l'algorithme ILSE converge vers un point fixe donné. La couleur associée à chacune de ces régions est représentative de la valeur de la fonction de coût à convergence de l'algorithme, les zones plus sombres correspondant à des minima locaux plus "profonds". On vérifie la présence des deux points fixes hiérarchiques prévus par la théorie, situés en h et $2h$, auxquels viennent s'ajoutent quatre autres points fixes, spécifiques à la QAM 16, dont l'expression exacte est donnée dans le tableau II.1 et qui n'ont pas d'interprétation géométrique évidente vis-à-vis du minimum global h. On relève également la symétrie de l'ensemble par rapport à la première bissectrice, conséquence de la symétrie par rotation et par conjugaison complexe de la constellation.

La procédure peut être réitérée pour des QAM d'ordre supérieur. La partie droite de la figure 5 montre le résultat obtenu pour la QAM 256, et le cas de la QAM 64 peut être visualisé sur la figure II.11. Le nombre de points fixes augmente drastiquement avec la taille de la constellation : sans compter les répliques obtenues par symétrie, on en dénombre une

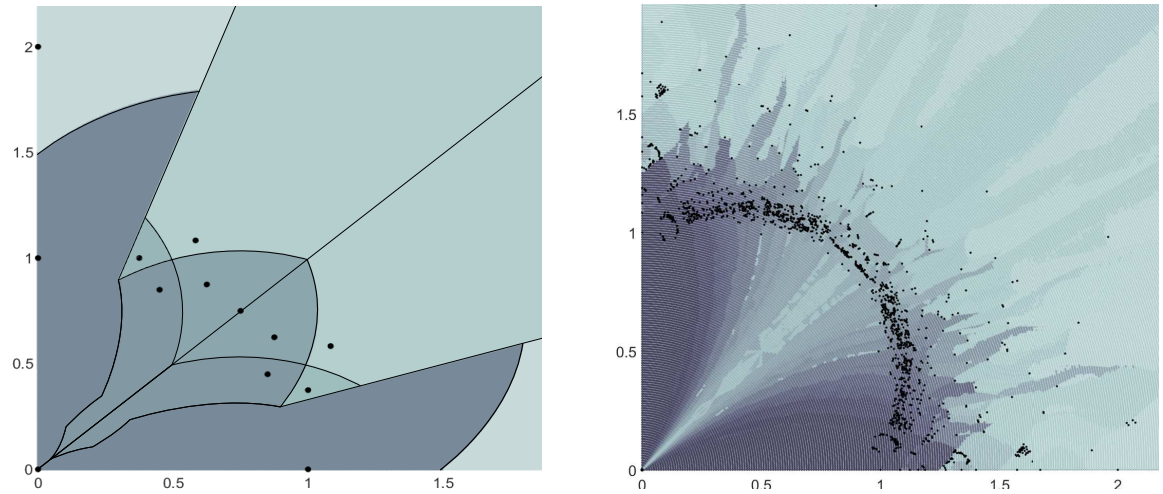

Figure 5 – *Positions des points fixes et régions de convergence de l'algorithme ILSE pour la QAM 16 (gauche) et la QAM 256 (droite).*

centaine pour la QAM 64 et environ 800 pour la QAM 256. La caractérisation exacte de ces points, à l'instar de ce qui a été fait pour la QAM 16, reste théoriquement accessible, mais néanmoins laborieuse. On peut en revanche relever une certaine similarité dans la répartition globale des points fixes entre ces deux exemples, avec notamment la présence d'un récif dense de points fixes de module grossièrement égal au module de h. Dans la perspective d'une stratégie d'initialisation aléatoire, telle que souvent utilisée dans ce genre d'algorithmes, il est clair que cette zone constitue un obstacle majeur à la possibilité de converger vers le minimum global h, et il convient donc d'empêcher l'algorithme de s'en approcher.

On peut alors envisager essentiellement deux stratégies d'initialisation : choisir un point initial h_0 extrêmement loin en module du véritable canal, ce que l'on nomme l'approche "lointaine" , ou à l'inverse choisir un point initial de module très faible, que l'on appelle approche "perturbative". Dans le premier cas, la recherche du minimum global s'effectue de manière détournée, en faisant converger l'algorithme vers le point fixe hiérarchique de module le plus élevé, c'est-à-dire $2^{m-1}h$, et dont on peut directement déduire le canal h. Ce point présente en effet le double avantage d'être commun à toutes les QAM et remarquablement bien isolé des autres points fixes. Le vecteur des symboles émis qui lui est associé, obtenu via la phase d'énumération, a de plus la particularité de n'être constitué que de quatre symboles distincts contre 4^m pour l'ensemble de la constellation, ce qui le rend aisément détectable. Pour ce qui est de l'approche perturbative, l'objectif est de converger directement vers le minimum global, h. Compte tenu de la forme des régions de convergence au voisinage de l'origine, la meilleure stratégie consiste à choisir un point arbitrairement proche de 0, l'envergure en angle de la région de convergence associée au minimum global (zone la plus sombre) augmentant à mesure que l'on s'approche de l'origine. Dans les deux cas, le canal étant inconnu il n'est pas possible de savoir à l'avance quelle phase choisir pour que le point initial appartienne à la zone de convergence du point fixe désiré. En pratique

l'algorithme doit donc être testé sur plusieurs points initiaux avec des phases différentes, qu'on peut choisir régulièrement espacées, et garder la solution qui atteint la plus petite valeur en termes de fonction de coût.

La question est maintenant de savoir si les stratégies d'initialisation proposées sont applicables hors du cas asymptotique, c'est-à-dire à nombre de symboles reçus fini et bruit non nul. On effectue donc des simulations Monte Carlo sur des QAM 16 et QAM 64 en moyennant sur un grand nombre de canaux tirés aléatoirement le taux d'erreur symbole obtenu en initialisant l'algorithme ILSE via la méthode lointaine et perturbative. Les résultats sont présentés section II.5.2 en fonction du rapport $E_b/N0$ qui donne le rapport signal à bruit. De manière générale, la méthode perturbative se révèle plus fiable que l'approche lointaine. Ce résultat peut s'expliquer par le fait que l'introduction du bruit dans le mélange a pour effets de déplacer, masquer ou ajouter certains minima locaux. Ce phénomène est d'autant plus marqué sur les minima locaux les plus superficiels, et en particulier le point hiérarchique vers lequel la stratégie lointaine repose. Il est alors extrêmement difficile de prévoir vers quel point fixe l'algorithme converge. Les deux méthodes se révèlent néanmoins supérieures à la stratégie d'initialisation naïve, notamment dans le cas de la QAM 16 pour lequel l'approche perturbative donne des résultats identiques à la situation idéale avec un canal parfaitement connu du récepteur. La raison pour laquelle la méthode perturbative est moins performante pour la QAM 64 tient au fait que l'espacement en angle utilisé entre les différents essais d'initialisation est le même que pour la QAM 16, là où les régions de convergence de la QAM 64 sont plus resserrées en angle les unes des autres. Il est donc possible d'obtenir de meilleures performances en utilisant une résolution angulaire plus élevée, au prix d'un nombre d'essais plus important. On constate également un gain significatif par rapport à la stratégie naïve en termes du nombre d'itérations avant convergence de l'algorithme ILSE, cumulé sur les différentes initialisations. Le nombre d'itérations moyen reste cependant assez élevé, les méthodes d'initialisation considérées étant aléatoires et ne se basant pas sur le signal reçu pour en extraire une estimation initiale du canal.

Outre ces stratégies d'initialisation aléatoire, on peut également initialiser l'algorithme ILSE en utilisant directement le signal reçu. Deux méthodes sont ainsi proposées : la première est basée sur un algorithme de classification appelé k-produits [37]. L'algorithme original étant inutilisable hors des modulations PSK, une généralisation tirant parti de la structure hiérarchique des QAM et des ASK est effectuée, appelée k-produits hiérarchiques, et permet à la fois un gain en précision et une baisse de complexité. L'algorithme produit une classification initiale des symboles émis que l'on peut ainsi utiliser via l'étape d'estimation du canal, Eq.(4), pour obtenir une estimation initiale de h. La seconde méthode consiste à utiliser les statistiques du signal reçu, et plus particulièrement ses moments, pour en déduire une expression théorique du canal. Ces deux méthodes se révèlent par simulation extrêmement efficaces en termes de précision et de complexité et surpassent assez largement les méthodes d'initialisation aléatoire précédentes.

À un utilisateur, il est donc possible de mettre en évidence un certain nombre de propriétés des points fixes de l'algorithme ILSE, en se basant sur la structure géométrique des constel-

lations considérées, et plus particulièrement la structure hiérarchique des QAM régulières. L'étude et l'utilisation de ces points fixes permettent d'élaborer des méthodes d'initialisation aléatoires améliorées par rapport à la stratégie naïve traditionnelle. En particulier, la stratégie perturbative se présente comme la plus fiable du fait de sa grande robustesse aux effets du bruit sur les points fixes, et également la moins coûteuse. Ces approches restent néanmoins assez sophistiquées, et sous-optimales dans le sens où elles ne tirent pas avantage de l'information contenue dans le signal reçu. Ceci amène à considérer d'autres stratégies d'initialisation pour traiter le cas de plusieurs utilisateurs.

Détection aveugle à plusieurs sources

Une approche générale pour l'initialisation de problèmes d'optimisation connus comme étant non convexes, consiste à chercher un initialiseur statistiquement moins "performant" que l'estimateur du maximum de vraisemblance, mais plus facilement accessible. L'idée sous-jacente étant que la méthode d'initialisation choisie fournisse un estimateur suffisamment fiable pour appartenir à la région de convergence du minimum global. La stratégie adoptée consiste donc à obtenir, à partir du signal reçu r, un premier estimateur $\widehat{\mathbf{h}}_0$ du vecteur canal, qui servira ensuite comme point initial pour l'algorithme ILSE. La méthode d'estimation retenue est celle de la méthode des moments, qui repose sur le fait que les quantités statistiques déduites du signal reçu, exprimées comme une fonction vectorielle $\mathbf{T}$ des moments μ_n de r, dépendent explicitement des paramètres du modèle, ici le vecteur canal $\mathbf{h}$, via une certaine fonction $\mathbf{g}$. L'estimateur de la méthode des moments, $\widehat{\mathbf{h}}_0$, est alors obtenu en inversant cette dépendance et en substituant aux moments théoriques de la variable r leur équivalent empirique $\overline{\mu}_n(r)$:

$$\mathbf{T}\left(\mu_1(r), \mu_2(r), \cdots, \mu_n(r)\right)) = \mathbf{g}(\mathbf{h}) \Rightarrow \widehat{\mathbf{h}_0} = \mathbf{g}^{-1}\left(\mathbf{T}(\overline{\mu}_1(r), \overline{\mu}_2(r)), \cdots, \overline{\mu}_n(r)\right) \tag{7}$$

Les sources s_k étant indépendantes, un choix naturel pour les quantités statistiques à considérer réside dans les cumulants $\kappa_n(r)$ du signal reçu, qui s'expriment comme des polynômes particuliers des moments, et ont l'avantage d'être additifs sur des sommes de variables aléatoires indépendantes. On se limite ici aux pseudo-cumulants, c'est-à-dire aux cumulants qui ne font pas intervenir la conjuguée complexe de r.

$$\kappa_n(r) = \sum_{k=1}^{K} h_k^n \kappa_n(s_k) + \kappa_n(w) \tag{8}$$

L'expression du n-ième cumulant peut être simplifiée en invoquant d'une part la symétrie circulaire continue du bruit, qui implique que tous les cumulants non-circulaires de w sont nuls, permettant ainsi de s'affranchir d'une dépendance explicite de l'estimateur vis-à-vis du bruit. D'autre part la symétrie de rotation discrète de chaque source s_k, caractérisée par un entier q_k appelé cyclicité, implique que seuls les cumulants de la source s_k d'ordres multiples de q_k peuvent être non nuls. On obtient ainsi une équation polynomiale faisant intervenir les coefficients du canal mis à la puissance q_k, notés η_k, des coefficients combinatoires définis par

$\alpha_{p,q} \triangleq \frac{(p_k q_k)!}{p_k (q_k!)^{p_k}}$ et les moments des sources mises à la puissance q_k, notées χ_k :

$$\kappa_n(r) = \sum_{k \in \mathscr{D}_{\mathbf{q}}(n)} \eta_k^{p_k} \alpha_{p_k,q_k} \kappa_{p_k} \left(\frac{\mu_1(\chi_k)}{\alpha_{1,q_k}}, \frac{\mu_2(\chi_k)}{\alpha_{2,q_k}}, \cdots, \frac{\mu_{p_k}(\chi_k)}{\alpha_{p_k,q_k}} \right) \tag{9}$$

L'estimateur des moments $\widehat{\mathbf{h}}_0$ est alors obtenu en choisissant un ensemble de cumulants d'ordres appropriés et en résolvant le système associé.

De manière générale, il n'existe pas de solution exacte au problème des moments (9) pour un nombre de sources quelconque. Le choix du nombre de cumulants à considérer et de leur ordre dépend du nombre de sources et des relations arithmétiques entre leur cyclicité. Le tableau 1 présente un certain nombre de mélanges pour lesquels une expression théorique de l'estimateur du vecteur canal a été obtenue avec les cyclicités associées aux constellations considérées et les ordres des cumulants utilisés. Au-delà de trois ou quatre sources le problème devient en général insoluble analytiquement, et l'application à un nombre arbitraire de sources nécessite donc de recourir à des méthodes numériques. On montre néanmoins qu'il est toujours possible, par un choix approprié de cumulants, d'obtenir un système triangulaire par blocs, ce qui permet dans certains cas une résolution exacte. En particulier, lorsque les cyclicités des constellations du mélange sont toutes différentes, le système devient triangulaire, ce qui permet une résolution par récurrence pour un nombre arbitraire de sources.

Mélange	QAM M_1, QAM M_2	3×QAM M	2×ASK M_1, 2×ASK M_2
Cyclicité	$(4, 4)$	$(4, 4, 4)$	$(2, 2, 4, 4)$
Ordre	$(4, 8)$	$(4, 8, 12)$	$(2, 4, 6, 8)$

Table 1 – *Exemples de mélanges résolus analytiquement par la méthode des moments.*

Parmi les mélanges considérés le cas de deux QAM régulières de taille respective M_1 et M_2 constitue un exemple récurrent dans cette thèse. Toutes les QAM ayant la symétrie du carré, leur cyclicité est égale à 4. Les cumulants d'ordre 4 et 8 du signal reçu permettent alors d'exprimer les coefficients du canal mis à la puissance 4 en fonction du nombre de symboles de chaque QAM et de la valeur moyenne et pseudo-variance empiriques du signal mis à la puissance quatrième :

$$\widehat{\eta_1}^{(m)} = \frac{-15/8}{M_1^2 M_2^2 - 1} \cdot \left((M_2^2 + 1)\bar{\rho} + (-1)^{m+1} \sqrt{\frac{M_2^2 - 1}{M_1^2 - 1}} \tilde{\gamma}(\mu_\rho, \sigma_\rho^2) \right) \tag{10a}$$

$$\widehat{\eta_2}^{(m)} = \frac{-15/8}{M_2^2 M_1^2 - 1} \cdot \left((M_1^2 + 1)\bar{\rho} + (-1)^{m+1} \sqrt{\frac{M_1^2 - 1}{M_2^2 - 1}} \tilde{\gamma}(\mu_\rho, \sigma_\rho^2) \right) \tag{10b}$$

Si les deux QAM ont des tailles différentes, on obtient deux solutions distinctes pour l'estimateur du vecteur canal. Se pose alors la question du critère à utiliser afin de déterminer le choix qui fera converger l'algorithme Iterative Least Squares with Enumeration (ILSE) vers la meilleure solution. Si en revanche les deux QAM sont identiques les deux solutions sont permutation l'une de l'autre, ce qui correspond au fait que le modèle de

mélange linéaire ne permet pas de distinguer des sources utilisant la même constellation. De la même manière, il existe une ambiguïté de phase de $\pi/2$ sur chacun des deux coefficients du canal estimé, qui correspond à la symétrie de rotation discrète de $\pi/2$ des constellations QAM. En pratique, ces ambiguïtés de phase et de permutation, qui sont inhérentes au modèle, doivent être levées explicitement par l'ajout d'informations extrinsèques.

Les performances de l'algorithme ILSE initialisé au moyen de la méthode des moments sont évaluées par simulations Monte Carlo, et comparées à celles obtenues par une approche de type SIC et une stratégie d'initialisation naïve. Les canaux sont tirés de manière aléatoire avec la même amplitude moyenne, ce qui signifie que l'interférence entre utilisateurs, mesurée par le rapport signal sur interférence, est maximale. Les mesures considérées sont l'erreur quadratique moyenne normalisée des canaux estimés et le taux d'erreur symbole conjoint, défini comme la probabilité de commettre une erreur de décision sur l'estimation du symbole d'au moins un utilisateur. Les résultats, présentés section III.4.2, attestent un gain très appréciable vis-à-vis de la stratégie d'initialisation aléatoire d'une part, mais également du SIC qui se trouve ici hors de son point de fonctionnement idéal. La stratégie consistant à initialiser l'algorithme ILSE avec l'estimateur fourni par le SIC ne suffit pas par ailleurs à compenser la faiblesse de cet algorithme en situation d'interférence forte. Les taux d'erreur obtenus pour des mélanges de deux QAM pour l'algorithme proposé sont extrêmement satisfaisants compte tenu du fait qu'il s'agit des taux d'erreur non codés, c'est-à-dire sans codage de canal préalable. On observe néanmoins un plancher d'erreur dans la limite de bruit faible, d'autant plus élevé que la complexité des constellations impliquées dans le mélange augmente et qui correspond à la convergence de l'algorithme vers des minima locaux. On mesure finalement le nombre moyen d'itérations requis par l'algorithme pour converger. Celui-ci augmente naturellement avec la taille de la constellation mélange, mais reste raisonnable même à fort bruit et à quatre utilisateurs. À fort bruit l'algorithme converge très rapidement, en une dizaine d'itérations tout au plus.

On peut fournir une analyse plus poussée du plancher d'erreur observé dans les simulations dans le cas simplifié de deux utilisateurs, pour lequel la structure globale de la constellation mélange est caractérisée par le rapport h_r des coefficients du vecteur canal. Si on se restreint aux réalisations des canaux telles que le taux d'erreur obtenu à l'issue de l'initialisation par la méthode des moments et l'algorithme ILSE est non nul, on constate que les quotients correspondants sont concentrés autour de points bien spécifiques, comme illustré sur la figure 6. Les constellations mélange associées sont telles que certains symboles sont quasiment confondus. A l'extrême, on atteint une condition de non identifiabilité [47], c'est-à-dire qu'on peut trouver plusieurs jeux de symboles distincts (s_1, s_2) et (s'_1, s'_2) qui par combinaison linéaire donnent le même symbole dans la constellation mélange :

$$h_1 s_1 + h_2 s_2 = h_1 s'_1 + h_2 s'_2 \tag{11}$$

Cette caractéristique induit la présence de points fixes proches du minimum global de l'algorithme ILSE, ce qui le rend extrêmement sensible à son initialisation pour ce type de mélange. On peut vérifier sur des mélanges plus complexes que ce critère de non identifiabilité prédit en effet la plupart des quotients de canaux pour lesquels l'algorithme

ne converge pas vers son minimum global. Le nombre de mélanges "non identifiables" augmentant avec le nombre de sources et la taille des constellations, leur contribution au taux d'erreur asymptotique s'en trouve renforcée. On peut néanmoins noter que dans le cas du mélange QAM 4–QAM 16, un quotient de canal problématique n'est pas prévu par le critère de non identifiabilité, et qui correspond en réalité à une constellation de QAM 64. On retrouve ainsi la décomposition hiérarchique de la QAM 64 en une QAM 16 et une QAM 4, ce qui donne un critère additionnel pour prédire les réalisations de canaux pour lesquelles l'algorithme ILSE a plus de difficultés à converger vers son minimum global.

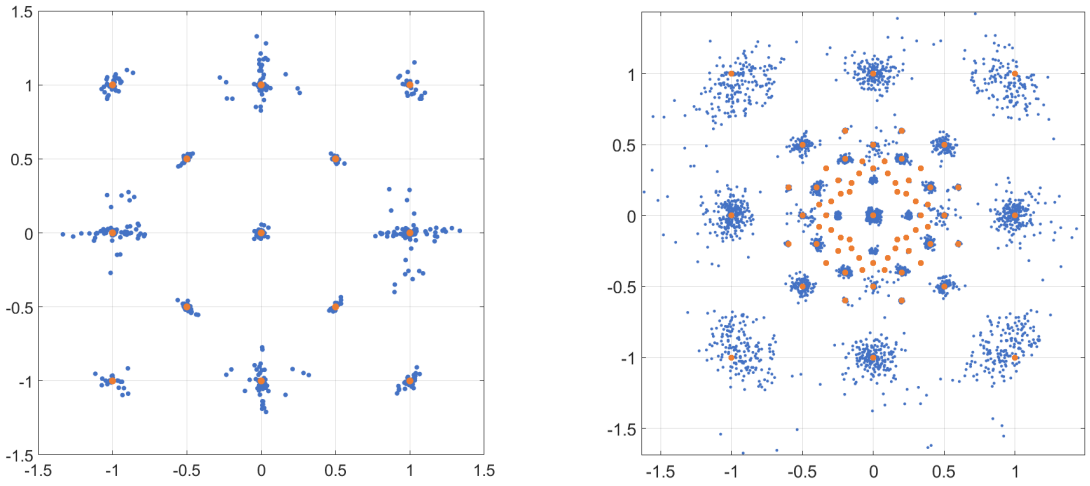

Figure 6 – *Réalisations du vecteur canal pour lesquelles le taux d'erreur obtenu après convergence d'ILSE est non nul (points bleus) et solutions théoriques du critère de non identifiabilité (points oranges) pour un mélange de deux QAM 4 (gauche) et un mélange QAM 4–QAM 16. (droite).*

À partir de cette analyse on peut considérer deux approches afin d'améliorer le taux d'erreur asymptotique de l'algorithme. La première est une stratégie dite "préventive", qui consiste à systématiquement associer au rapport des coefficients du canal estimé par la méthode des moments le quotient de canal prédit comme problématique qui lui est le plus proche. On construit alors d'autres estimations du vecteur canal avec lesquelles on initialise également l'algorithme, et on retient la meilleure solution au sens de la valeur de la fonction de coût atteinte à convergence. Cette stratégie, testée sur un mélange de deux QAM 4, permet de sensiblement baisser le taux d'erreur asymptotique et de retarder l'effet de plancher, mais se révèle assez coûteuse puisqu'elle implique de lancer l'algorithme plusieurs fois même dans des situations où la solution donnée par la méthode des moments est suffisante pour converger vers le minimum global. On peut également partir directement de l'estimation du vecteur canal donnée par l'algorithme selon une approche "corrective" : l'objectif est alors de déterminer si la solution considérée est mauvaise, en regardant notamment sa conformité vis-à-vis des hypothèses du modèle de communication.

En particulier, les situations dans lesquelles certains symboles n'apparaissent pas où sont très faiblement représentés constituent une violation de l'hypothèse d'indépendance des sources, ce qui permet de détecter efficacement un certain nombre de minima locaux. Plus largement, la comparaison de la distribution empirique des symboles estimés avec celle des symboles émis, supposée uniforme, constitue un autre critère de discrimination des mauvaises solutions. L'approche corrective reste toutefois moins efficace que la stratégie perturbative, et plus subtile à mettre en œuvre, ce qui encourage une utilisation conjointe des deux méthodes.

Ainsi, dans les scénarios d'interférence forte, pour lesquels les techniques traditionnelles basées sur l'annulation successive d'interférence ou les stratégies d'initialisation naïves ne sont pas suffisantes pour garantir une estimation fiable des symboles émis, la méthode des moments se pose en une alternative relativement simple sur le plan technique et qui démontre son efficacité dans un certain nombre de configurations de mélange. Par ailleurs, l'analyse de l'origine du plancher d'erreur, et en particulier le critère de non identifiabilité, permettent de prédire, dans un mélange donné, les réalisations de canaux les plus à même de mener l'algorithme vers des minima locaux, et ouvrent la voie vers l'élaboration de stratégies visant à améliorer la robustesse d'ILSE quant à de ces points fixes indésirables. L'extension des résultats présentés à des mélanges de plus grande envergure constitue une étape cruciale dans la perspective de faire de l'algorithme d'ILSE un outil de choix parmi les techniques de détection aveugles monoantennaires.

Extension aux transmissions multiporteuses

La dernière étape de ce travail autour de l'algorithme ILSE consiste à généraliser les résultats précédents au cas plus réaliste de canaux sélectifs en fréquence, c'est-à-dire dont la réponse en fréquence n'est pas constante. Dans le domaine temporel, on obtient un canal dit à trajets multiples, qui correspond à une situation dans laquelle le signal émis par un utilisateur arrive selon plusieurs chemins à la stations de base, suite à des phénomènes de réflexion ou de diffraction sur des obstacles tels que des habitations ou des véhicules, comme on peut le voir sur la figure 7. Le canal est alors modélisé par un vecteur de taille L, où L représente le nombre de trajets et est appelé mémoire, dont chaque coefficient modélise le canal de propagation d'un des chemins :

$$r_n = \sum_{\ell=1}^{L} h_{\tau_\ell} s_{n-\tau_\ell} + w_n \tag{12}$$

Les trajets multiples empruntés par le signal introduisent de l'interférence inter-symboles (ISI) : à chaque temps symbole, le récepteur observe une superposition de symboles transmis à des temps différents, ce qui rend l'application directe des techniques de détection vues jusqu'ici désastreuse en termes de taux d'erreur. Une solution pour prévenir ce phénomène est de passer à des transmissions dites multiporteuses, qui consistent à transmettre le signal par blocs de P symboles, chaque symbole d'un bloc donné étant modulé par une porteuse de fréquence différente appelée sous-porteuse. En particulier, dans le cas de l'Orthogonal

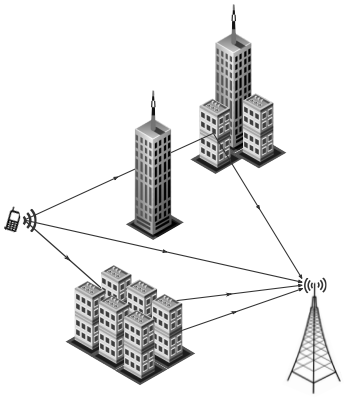

Figure 7 – *Canal à trajets multiples avec* $L = 4$.

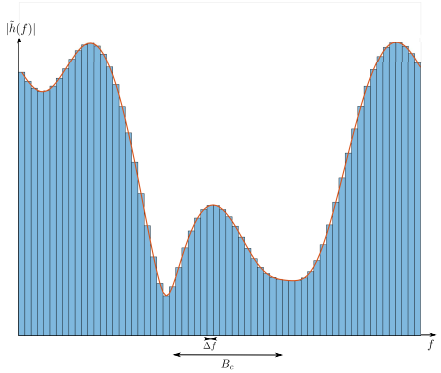

Figure 8 – *Approximation d'un canal de bande de cohérence* B_c *par* P *sous-canaux plats de largeur* Δf.

Frequency Division Multiplexing (OFDM) [82] considéré ici, les fréquences des sous-porteuses sont régulièrement espacées d'une quantité Δf choisie petite devant la bande de cohérence du canal B_c, qui caractérise l'échelle de variation en fréquence du canal. Cela revient à découper la réponse en fréquence du canal en P sous-bandes de largeur Δf, de telle sorte à ce qu'à l'échelle d'une sous-bande le canal puisse être considéré comme plat, voir figure 8. Ainsi, au niveau du récepteur, tout se passe comme si on recevait P séquences de symboles en parallèle, chacune ayant subi son propre canal plat, dont les coefficient $\tilde{h}_p$ sont donnés par la transformée de Fourier Discrète (DFT) du canal temporel:

$$\tilde{r}_p = \tilde{h}_p \tilde{s}_p + \tilde{w}_p \tag{13}$$

On fait également l'hypothèse d'un canal à mémoire courte, à savoir que le nombre de trajets est petit devant le nombre de sous-porteuses, $L \ll P$, ce qui est souvent le cas en pratique.

Dans le cas d'un signal OFDM à plusieurs utilisateurs, on se ramène sur chaque sous porteuse au modèle du canal à accès multiple et à canaux plats de l'équation (2), la différence étant que toutes les quantités considérées sont dans le domaine fréquentiel. Étant donné que le but premier du récepteur est de retrouver les symboles qui lui ont été transmis, la stratégie naturelle pour décoder ce type de signaux est d'estimer les canaux en fréquentiel. Cela reviendrait donc ici à appliquer l'algorithme ILSE indépendamment sur chaque sous-porteuse. Cette stratégie peut néanmoins être critiquée à deux égards : premièrement, le modèle de mélange linéaire induit des ambiguïtés de phase et de permutation sur l'estimation des canaux de chaque sous-porteuse. Traiter les sous-porteuses indépendamment augmente donc de façon exponentielle le nombre de ces ambiguïtés et par conséquent la probabilité d'une mauvaise estimation. Deuxièmement, en multipliant les appels à l'algorithme ILSE la probabilité de converger vers un minimum local sur au moins l'une des sous-porteuses se trouve augmentée. Pour ces raisons il semble donc davantage pertinent d'estimer le canal directement dans le domaine temporel, en exploitant le fait que les vecteurs canaux fréquentiels de chaque utilisateur, rassemblés dans la matrice $\tilde{\mathbf{H}}$ de taille $P \times K$, sont obtenus à partir de leur

équivalent temporel par transformée de Fourier :

$$\tilde{\mathbf{H}} = \mathbf{F}_L \mathbf{H} \tag{14}$$

avec $\mathbf{H}$ la matrice $P \times L$ des canaux temporels et $\mathbf{F}_L$ la restriction de la matrice de Fourier de taille P à ses L premières colonnes. Cette approche est d'autant plus justifiée que le nombre de sous-porteuses P est généralement grand devant la mémoire L des canaux. En estimant le canal directement en temps, on diminue ainsi considérablement le nombre de paramètres effectifs du modèle par la même occasion.

On procède donc à la généralisation de l'algorithme ILSE aux transmissions OFDM, que l'on appelle simplement ILSE-OFDM. La fonction de coût à minimiser est donnée par la somme sur les sous-porteuses des fonctions de coût de l'algorithme d'origine, en remplaçant de plus les canaux fréquentiels $\tilde{h}_p$ par leur expression en termes de la matrice des canaux temporels $\mathbf{H}$:

$$J_P(\mathbf{H}, \{\tilde{\mathbf{S}}_p\}; \tilde{\mathbf{R}}) = \sum_{p=1}^{P} \parallel \tilde{\mathbf{r}}_p - \mathbf{f}_p \mathbf{H} \tilde{\mathbf{S}}_p \parallel^2 = \sum_{p=1}^{P} J(\mathbf{f}_p \mathbf{H}, \tilde{\mathbf{S}}_p; \tilde{\mathbf{r}}_p) \tag{15}$$

avec $\mathbf{f}_p$ la p-ième ligne de la matrice $\mathbf{F}_L$. Les symboles entre chaque sous-porteuse étant indépendants, l'étape d'énumération consiste simplement en P étapes d'énumérations en parallèle qui donnent la matrice des symboles émis relative à chaque sous-porteuse. La principale différence tient à l'étape d'estimation du canal, qui implique la minimisation de J par rapport à la matrice $\mathbf{H}$:

$$\mathbf{vec}\,(\mathbf{H}) = \left(\sum_{p=1}^{P} (\tilde{\mathbf{S}}_p^T \otimes \mathbf{f}_p)^\dagger (\tilde{\mathbf{S}}_p^T \otimes \mathbf{f}_p) \right)^{-1} \mathbf{vec} \left(\sum_{p=1}^{P} \mathbf{f}_p^\dagger \tilde{\mathbf{r}}_p \tilde{\mathbf{S}}_p^\dagger \right) \tag{16}$$

avec $\mathbf{vec}\,(\mathbf{H})$ le vecteur de taille LK obtenu en superposant les colonnes de $\mathbf{H}$.

Reste à considérer le problème de l'initialisation de l'algorithme, qui nécessite une estimation temporelle initiale du canal. L'application de la méthode des moments sur chaque sous-porteuse p donne un vecteur $\tilde{\boldsymbol{\eta}}_p$ qui contient les estimations du p-ième coefficient fréquentiel du canal de chaque utilisateur mis à la puissance sa cyclicité. On construit ainsi une matrice $\tilde{\boldsymbol{\Xi}}_0$ dont chaque colonne $\tilde{\boldsymbol{\xi}}_k$ donne une estimation du canal en fréquence d'un utilisateur donné, mis à la puissance sa cyclicité q_k. On dispose ensuite d'un algorithme connu sous le nom d'autodéconvolution, qui utilise le fait que la transformée de Fourier discrete inverse de la puissance q-ième du vecteur canal fréquentiel d'un utilisateur donne la convolution cyclique du canal temporel avec lui même q fois :

$$\tilde{\boldsymbol{\xi}} = \tilde{\mathbf{h}}^{\mathbf{q}} \Rightarrow \boldsymbol{\xi} = \mathbf{h}^{\circledast q} \triangleq \underbrace{\mathbf{h} \circledast \mathbf{h} \circledast \cdots \circledast \mathbf{h}}_{q \text{ fois}} \tag{17}$$

En développant l'expression de cette autoconvolution, il est alors possible d'exprimer $\mathbf{h}$ comme la solution d'un problème linéaire dont les coefficients dépendent du vecteur $\boldsymbol{\xi}$. Étant

donné que l'estimation $\tilde{\boldsymbol{\xi}}_0$ du vecteur $\boldsymbol{\xi}$ obtenu par la méthode des moments est imparfaite, l'estimation initiale du canal temporel de l'utilisateur considéré est en pratique définie comme la solution de moindre norme du système, obtenue par une décomposition en valeurs singulières.

Pour que la méthode de l'autodéconvolution soit réellement pertinente il est néanmoins nécessaire que les coefficients du vecteur colonne $\tilde{\boldsymbol{\xi}}$ correspondent bien à un même utilisateur, ce qui n'est pas garanti compte tenu des ambiguïtés de permutation introduites par la méthode des moments sur chaque sous-ensemble de sources utilisant la même constellation. Lorsque tel est le cas pour chaque colonne de $\tilde{\boldsymbol{\Xi}}$, la matrice $\boldsymbol{\Xi}$ obtenue par transformée de Fourier inverse a sa partie inférieure nulle. Partant de l'estimation $\tilde{\boldsymbol{\Xi}}_0$ de la méthode des moments on cherche donc à permuter les coefficients sur chaque ligne afin d'identifier, par transformée de Fourier inverse, ce sous-bloc de zéros. L'estimation étant imparfaite, la permutation retenue est plus précisément celle qui minimise la norme du sous-bloc inférieur. Néanmoins, le nombre de sous-porteuses utilisé en pratique ne permet pas en général de tester toutes les permutations possibles, et on est donc contraint de se limiter à une recherche partielle, illustrée sur la figure 9 pour le cas simplifié de deux utilisateurs et six sous-porteuses. La matrice $\tilde{\boldsymbol{\Xi}}_0$ est ainsi constituée de deux colonnes notées $\boldsymbol{\zeta}$ et $\boldsymbol{\xi}$. L'ensemble des matrices obtenues en permutant les coefficients de chaque ligne est représenté sous forme d'un arbre dont chaque niveau de profondeur correspond à une sous-porteuse donnée. Partant d'un nœud, la branche supérieure et inférieure correspondent au fait de permuter ou non les coefficients de la sous-porteuse suivante.

La recherche partielle consiste à baser le choix de permuter ou non les coefficients d'une sous-porteuse donnée en se basant uniquement sur un nombre limité de sous-porteuses situées en aval, appelé "horizon". Dans l'exemple présenté, l'horizon a été choisi égal à trois, ce qui signifie que l'on teste l'ensemble des permutations portant sur les deux sous-porteuses subséquentes à la sous-porteuse considérée. Cela revient à explorer le sous-graphe de profondeur 3 ayant pour racine la dernière sous-porteuse traitée. On extrait alors de ce sous-graphe la solution qui donne le bloc inférieur le plus faible par transformée de Fourier inverse de la matrice associée, représentée sur la figure de gauche par le chemin en gras. La première branche de ce chemin indique si la sous-porteuse considérée doit être permutée ou non. Ici en l'occurrence, l'algorithme préconise de ne pas permuter les coefficients de la troisième sous-porteuse. La procédure est ensuite réitérée sur la sous-porteuse suivante. On avance ainsi sous-porteuse par sous-porteuse jusqu'à avoir traversé l'ensemble du graphe. Il est clair, par construction, que la solution obtenue est sous-optimale, et peut radicalement différer de celle que l'on obtiendrait en explorant l'intégralité du graphe, c'est-à-dire en testant toutes les permutations.

L'ensemble de l'algorithme proposé peut-être décliné en deux variantes, en fonction de si certaines sources utilisent la même constellation ou non. Dans le premier cas, l'estimation de $\tilde{\boldsymbol{\Xi}}_0$ issue de la méthode des moments est suivie d'une recherche partielle sur chaque sous-ensemble de sources ayant la même constellation afin de corriger les ambiguïtés de permutations. La méthode d'autodéconvolution est ensuite appliquée en parallèle à chaque

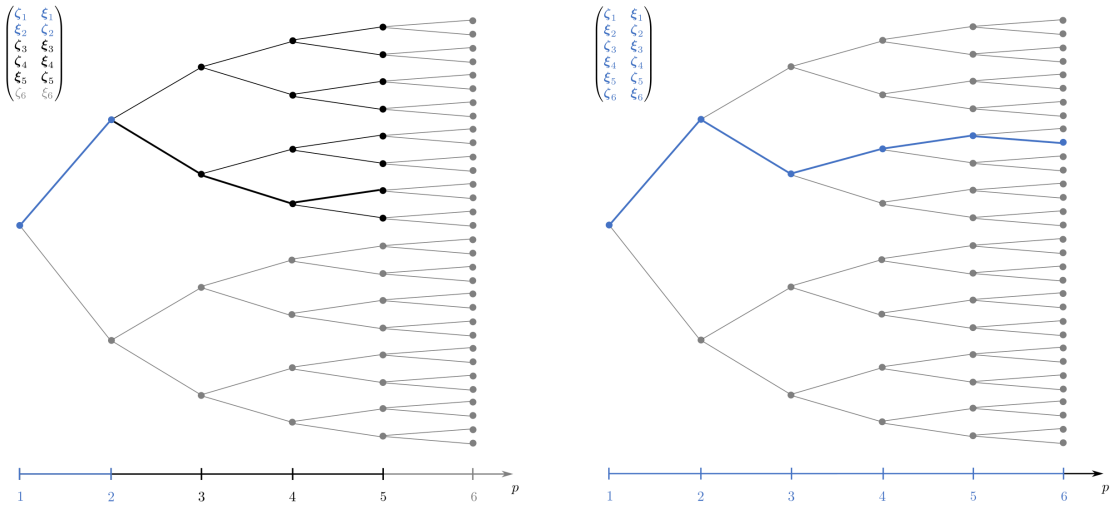

Figure 9 – *Illustration sous forme de graphe de l'algorithme de recherche partielle pour $K = 2$ sources et $P = 6$ sous-porteuses. Les chemins en bleu correspondent aux sous-porteuses déjà traitées, et les parties en gris clair à celles qui ne sont pas considérées pour la sous-porteuse en cours. Le chemin en gras représente la solution de moindre coût pour la sous-porteuse considérée. La figure de droite montre le résultat final de l'algorithme.*

utilisateur, ce qui donne une estimation initiale de la matrice des canaux temporels que l'on utilise comme point de départ pour l'algorithme ILSE-OFDM. Dans le cas ou les constellations sont différentes, il n'y a pas d'ambiguïté de permutation mais la méthode des moments donne généralement plusieurs solutions pour chaque sous-porteuse. On applique alors pour chaque sous-porteuse l'algorithme ILSE monoporteuse sur ces différentes solutions, et on retient celle qui donne le meilleur résultat au sens de la fonction de coût.

Les résultats en termes de taux d'erreur symbole conjoint de ces deux séquences d'algorithmes ont été mesurés sur un mélange de deux QAM 4 pour le cas de constellations identiques et sur un mélange QAM 4–QAM 16 pour le cas de constellations distinctes. Les résultats obtenus, présentés en section IV.4.2, ne sont en l'état pas satisfaisants. On vérifie cependant que dans l'hypothèse où les ambiguïtés de phase et de permutation ont été parfaitement résolues, l'algorithme ILSE-OFDM atteint des taux d'erreurs comparables à ceux obtenus en supposant une connaissance parfaite du canal, ce qui suggère que les méthodes de recherche partielle et d'autodéconvolution ne sont pas suffisamment performantes. Il n'en reste pas moins que l'algorithme ILSE-OFDM montre de meilleures performances que l'application sur chaque sous-porteuse de l'algorithme ILSE pour estimer les canaux en fréquentiels. On en conclut que l'algorithme proposé constitue une approche pertinente et prometteuse du problème d'estimation aveugle de sources dans les transmissions multi-porteuses par rapport aux méthodes d'estimation conjointes purement fréquentielles, mais qu'elle nécessite en amont des méthodes qui soient à même de lever les ambiguïtés de phase

et de permutation de l'estimation initiale, sans quoi la convergence de l'algorithme vers son minimum global ne peut être garantie.

Classification de données partiellement intriquées

La dernière partie de cette thèse rompt quelque peu avec les considérations précédentes en s'intéressant aux techniques de classification de données. Plus particulièrement, le problème abordé est celui de la capacité des algorithmes de classification a produire des résultats fiables lorsque certaines classes de données se recouvrent partiellement. Ce problème touche à la notion même de "classe", et peut donc être envisagé sous différents angles.

L'approche proposée repose sur la représentation des données comme réalisations d'un mélange de distributions de probabilités ayant des modes distincts. Considérant N données réelles de dimension D, la densité de probabilité empirique $\rho_{\mathbf{w}}(\mathbf{x})$ des observations est modélisée par le biais de fonctions "noyaux", ici choisies comme des tangents hyperboliques, centrées autour de chaque observation :

$$\rho_{\mathbf{w}}(\mathbf{x}) = \frac{1}{\sum_{n=1}^{N} w_n} \sum_{n=1}^{N} w_n \left(1 - \tanh\left(\| \mathbf{x_n} - \mathbf{x} \|^2\right)\right) \tag{18}$$

où les $\mathbf{x}_n$ sont les observations et $\mathbf{w}$ un vecteur de poids de taille N. Les minima de cette fonction constituent des estimations des modes de la distribution mélange sous-jacente, qui correspondent aux centroïdes des classes. Le principe de la méthode de classification proposée consiste à alterner l'estimation d'un centroïde par minimisation de la fonction densité, et l'estimation de la classe associée. L'étape de minimisation se fait selon un algorithme itératif initialisé sur une observation aléatoire non-encore classée. La classe associée $\mathcal{C}$ est ensuite déterminée en construisant un ellipsoïde centré autour de ce mode et en sélectionnant les observations qui y appartiennent. L'extension de l'ellipsoïde, caractérisée par ses demi-axes, dépend d'un paramètre T_h choisi de telle sorte à limiter la taille de l'ellipsoïde et ainsi éviter d'absorber les éventuelles classes proches. La mise à jour du vecteur poids $\mathbf{w}$ permet par ailleurs de supprimer la contribution des points nouvellement classés au profil de densité global, favorisant la détection des classes de moindre importance aux itérations suivantes. L'algorithme se poursuit jusqu'à ce que tout ou une proportion suffisante d'observations aient été classées.

Par construction, cet algorithme de classification dit "elliptique" produit un recouvrement de l'ensemble des observations par des structures ellipsoïdales. Le nombre de classes trouvé se révèle en général supérieur au nombre réel de classes, l'introduction du vecteur poids favorisant également l'apparition de classes résiduelles. Pour palier à ce problème une seconde phase est ajoutée à l'algorithme, qui consiste à identifier parmi chaque sous-ensemble de classes partageant une intersection non vide les moins signifiantes, et à en redistribuer le contenu parmi les classes restantes. Cette seconde phase s'arrête lorsque le nombre de

classes restantes coïncide avec le nombre attendu.

L'algorithme proposé est testé sur des mélanges gaussiens aléatoires avec des nombres de composantes croissants et comparé à quelques méthodes de classification de la littérature. La qualité des classifications produites est mesurée selon deux critères, à savoir l'indice de Myrkin normalisé et la Variation d'Information [133]. De manière générale, l'algorithme elliptique produit de meilleurs – sinon comparables – résultats que la plupart des autres méthodes testées. Seul l'algorithme Espérance-Maximisation [26], spécifiquement adapté aux mélanges gaussiens, atteint des performances légèrement supérieures. Ceci encourage de futurs développements et améliorations de l'algorithme elliptique ainsi que des simulations plus poussées faisant intervenir d'autres méthodes de classification.

Conclusion

L'ensemble des résultats présentés dans cette thèse, obtenus pour des hypothèses de transmission particulièrement défavorables en termes d'interférence et de nombre d'antennes à disposition, contribuent à mieux comprendre l'algorithme ILSE et constituent une base de travail pour rendre ce type d'algorithmes plus à même d'être appliqués dans des systèmes réels. Les différentes approches proposées ouvrent la voie vers de nombreuses extensions et améliorations, à commencer par la généralisation de ces méthodes à un nombre de sources plus important et à des mélanges plus complexes. La relaxation de certaines hypothèses du modèle constitue également un axe de recherche pertinent, notamment en ce qui concerne la synchronicité des sources.

Introduction

Background

With the recent densification of networks and the fast-increasing volumes of data conveyed by modern mobile applications, wireless communication systems are faced with upcoming challenges in terms of resources allocation, achieved data rates and reliability constraints. In that respect, Non Orthogonal Multiple Access (NOMA) techniques have received considerable interest in recent years from both the research and industrial fields as a promising alternative to the traditional Orthogonal Multiple Access (OMA) schemes, compatible with the massive connectivity and spectral efficiency requirements of Fifth Generation (5G) networks and of the Internet of Things (IoT) functionalities [1]. As opposed to Frequency Division Multiple Access (FDMA),Time Division Multiple Access (TDMA), Code Division Multiple Access (CDMA) and Orthogonal Frequency Division with Multiple Access (OFDMA) [2], all based on a mutually exclusive allocation of the overall radio resource between User Equipments (UE) through the use of distinct time slots, frequency bands or spreading codes, NOMA allows multiple users to simultaneously share the same resources, thus increasing by large the achievable capacity of reception devices.

Allowing several UE to use the same resources for their transmissions introduces Inter-User Interference (IUI), a major source of impairment in wireless communication systems. Actually, the motivation for use of OMA in previous networks generations is largely accountable by the fact that they provide simple, low-complexity solutions to efficiently suppress interference. The counterpart for imposing orthogonality between users is however a scarcity in the available resources, substantially limiting the number of distinct users that can be simultaneously dealt with. On the other hand, ensuring reliable communications while maintaining high data rates in interfering scenarios comes at the expense of an increasing complexity in the detection schemes employed by wireless receivers and of their embedded hardware. Typical NOMA strategies for addressing IUI exploit power diversity and allocate different power levels to the users according to the quality of their propagation environment [3]. At the receiver these differences in power can be used to extract each users's signal based on Successive Interference Cancellation (SIC) techniques. Such strategies are efficient in many situations, but their performances are strongly limited in low received Signal to Interference Ratio (SIR) levels scenarios.

The second central concern of both orthogonal and non-orthogonal multiple access wireless communications relates to the propagation environment of the transmitted signals, known as the channel. The performances of any detection scheme are entirely dependent on its ability to compensate the undesirable effects introduced during signal propagation. Hence, robust strategies to acquire the Channel State Information (CSI) are of foremost importance in the design of reliable detectors. In most cases this estimation process is carried out by means of reference signals, called pilots, which are known at both sides of the transmission and sent to

the receiver prior to the actual signal of interest. Such data-aided strategies however require a regular reacquisition of the pilot sequences to account for the temporal evolution of the propagation environment. This, in turn, results in a loss of the actual datarate achieved by the transmission. On the other hand, blind channel estimation methods aim at estimating the channel directly from the received signal, without resorting to any training sequence. At the expense of an increased complexity, these techniques make efficient use of all available information about the data. In regard to the increasing volumes of data required by modern wireless applications, these methods stand as a serious alternative to the traditional pilot-based schemes.

Thesis objectives

This thesis addresses the above issues by considering the two-fold problem of blind channel estimation and multiuser signal detection in scenarios where interference is predominant, and with the additional constraint that only one antenna is available at the receiver. Blind estimation of channel and sources have received considerable interest in the past decades, and have led to the development of a wide diversity of techniques in the context of Blind Source Separation (BSS) [4]. Of particular interest are the estimation methods based on the Maximum Likelihood (ML) approach, which exhibit very interesting statistical properties. However, these methods most often involve resolution of non-convex optimization problems. As a consequence, these algorithms have the undesirable property of converging to spurious solutions depending on the initial point they are provided with, which stronly limits their practical use.

The main objective of the presented work is to understand under which conditions convergence of the above approaches towards spurious solutions can be prevented, and to propose optimization strategies for making them more likely to converge to their global minimum in a single try. In particular our study will be centered around the ILSE algorithm [5], an iterative method initially proposed in the framework of overdetermined linear mixtures. Our motivation is to show that, within reasonable assumptions about the incoming signals, information on the potential fixed points of the algorithm and initialization strategies can be jointly used to achieve low detection error rates even in the worst-case scenario of a single-sensor and maximal degree of interference.

Outline

The thesis is divided into five chapters with an increasing order of complexity in the considered transmission models. The first chapter is designed as an introductory part to the basic tools and fundamental concepts pertaining to wireless communications. The main assumptions that constitute the basis for the forthcoming developments are exposed at the end of the chapter, in light of the notions reviewed therein.

The second chapter considers one of the simplest conceivable communication model, namely the point-to-point transmission in a flat-fading propagation environment. The clustering approach to the joint ML channel estimation and symbol detection is presented along with the core algorithm of our study, ILSE. We show that, in the simple case of a single source, it is possible to infer information about the location of the fixed points based on the geometric properties of the source constellations. Consequently, some blind strategies taking into account this information are proposed so as to ensure convergence of the algorithm towards its global minimum even starting from a totally random initial state. Two simple initialization techniques derived from the received data are discussed as well and tested through simulations. The results reveal that in this oversimplified case it is indeed possible to make the algorithm converge to its global minimum with a single try.

The third chapter stands as the cornerstone of the presented work and introduces IUI by considering the flat-fading multiple access channel transmission with an arbitrary number of users and one single sensor. Based on the connection of the model to BSS, we propose general channel estimators to be used as initial states for ILSE derived from the cumulants of the received signal and the method of moments. Explicit expressions for the channel estimators are derived in diverse mixture settings. The proposed initialization scheme is compared to the traditional SIC techniques and demonstrates both the pertinence of the ML approach and the necessity to find good initial states for the algorithm. A further analysis of the obtained results shows that the situations in which ILSE is likely to converge to a local fixed point are restricted to a predictable subset of channel realizations, and that some of the corresponding outcomes of the algorithm can be identified, thus allowing the design of possible corrective strategies.

In the fourth chapter we consider the more realistic model of a frequency-selective multiple access channel. In the framework of multicarrier transmissions, this problem can be casted as several parallel flat-fading multiuser transmissions. Based on the assumption of a short impulse response in comparison to the number of subcarriers, an extension of ILSE allowing for a temporal estimation of the channel is derived. Several initialization strategies addressing the phase and permutation ambiguities inherent to the BSS problem are discussed, and the overall scheme is evaluated by simulations. The method is shown to have the potential to perfectly estimate the channel provided that all phase and source ordering ambiguities can be reliably solved.

The fifth and last chapter is devoted to an enlarged discussion around cluster analysis, and in particular the ability of clustering algorithms to detect and appropriately deal with clusters that are partially merged or entangled. A two-step algorithm based on a density representation of the dataset is proposed as a first solution to this problem. Comparative simulations with other clusterings techniques show promising results and suggest further developments of the method.

Finally, the thesis concludes by a summary of its main contributions and elaborates on future work perspectives.

Chapter I

Technical background

Contents

This first chapter is devoted to an introduction of the key fundamental concepts used troughout this thesis. Its content is divided in three parts, namely theory of complex random variables, statistical estimation and wireless communication principles. The objective is to provide the reader with the minimal material required for this work to be accessible, hence the addressed topics are not intended to be exhaustive. References to classical books from the literature are provided all along the chapter for the reader interested in more technical details and advanced considerations.

I.1 Generalities on complex random variables

Signal processing, in particular when applied to wireless communications, is mostly concerned with complex-valued random signals. Complex random variables thus stand as the natural framework for modeling such processes. Yet, fundamentals results from probability

theory expressed in the complex formalism are seldom encountered in the literature. This introductory part makes a good opportunity to review well-known elementary notions of probabilities in the complex field framework.

I.1.1 Basic definitions and functions

Most of the probabilistic results on complex random variables readily follows from the theory of two-dimensional random vectors. Let X and Y be two real random variables, supposedly continuous for simplicity. The scalar complex random variable Z, defined by $Z \triangleq X + iY$ with i the square root of -1, is entirely described by its probability density function (pdf) $p_Z(z)$, which is a real-valued function defined on (a part of) the complex plane $\mathbb{C}$. The natural isomorphism between Z and the bivariate random vector (X, Y) allows $p_Z(z)$ to be defined by

$$p_Z(z) \triangleq p_{(X,Y)}\left(\Re(z), \Im(z)\right) \tag{I.1}$$

where $\Re(z) \triangleq \frac{z+z^*}{2}$ and $\Im(z) \triangleq \frac{z-z^*}{2i}$ denote the real and imaginary parts of z respectively, and $p_{(X,Y)}(x, y)$ is the joint pdf of (X, Y). The summability condition of p_Z can be written

$$\int_{z\in\mathbb{C}} p_Z(z)\mathrm{d}z = 1 \tag{I.2}$$

with $\mathrm{d}z \triangleq \mathrm{d}x\mathrm{d}y$. Alternatively, Z can be written in polar coordinates as $Z = R\exp(i\Theta)$, with $R \triangleq |Z| = \sqrt{X^2+Y^2}$ and $\Theta \triangleq \operatorname{Arg} Z = \arctan(Y/X)$ the modulus and (principal determination of) the argument of Z, respectively. The corresponding expression of $p_Z(z)$ in terms of the joint pdf of (R, Θ) then reads

$$p_Z(z) = \frac{1}{|z|} p_{(R,\Theta)}\left(|z|, \operatorname{Arg} z\right) \tag{I.3}$$

From (I.3) the pdf of the modulus of Z can be expressed as a contour integral of $p_Z(z)$,

$$p_R(r) = \frac{1}{i}\oint_{\mathcal{C}(0,r)} p_Z(z)\frac{|z|}{z}\mathrm{d}z = \int_0^{2\pi} p_Z(re^{i\theta})r\mathrm{d}\theta \tag{I.4}$$

where $\mathcal{C}(0, r)$ denotes the circle of radius r centered at the origin of the complex plane.

Closely related to the pdf is the cumulative distribution function (cdf) of Z, denoted by $F_Z(z)$ and defined by

$$F_Z(z) \triangleq \mathbb{P}\left(Z \preccurlyeq z\right) = \mathbb{P}\left(X \leq \Re(z) \cup Y \leq \Im(z)\right) = F_{(X,Y)}(\Re(z), \Im(z)) \tag{I.5}$$

where $F_{(X,Y)}$ is the joint cdf of (X, Y) and $\preccurlyeq$ is the partial order on $\mathbb{C}$ induced by the non-negative, component-wise generalized inequality on $\mathbb{R}^2$ [6]. The relation between $F_Z(z)$ and $p_Z(z)$ can then be written [7]

$$p_Z(z) = 2i\left(\frac{\partial^2 F_Z(z)}{\partial z^2} - \frac{\partial^2 F_Z(z)}{\partial z^{*2}}\right) \tag{I.6}$$

where $\frac{\partial}{\partial z} \triangleq \frac{1}{2}\left(\frac{\partial}{\partial x} - i\frac{\partial}{\partial y}\right)$ and $\frac{\partial}{\partial z^*} \triangleq \frac{1}{2}\left(\frac{\partial}{\partial x} + i\frac{\partial}{\partial y}\right)$ are the Wirtinger differential operators [8].

A third way of describing a complex random variable Z is by means of the first characteristic function (cf) $\Phi_Z(z)$, defined by

$$\Phi_Z(z) \triangleq \mathbb{E}\left[\exp\left(\frac{i}{2}(zZ^* + z^*Z\right)\right] = \Phi_{(X,Y)}\left(\Re(z), \Im(z)\right) \tag{I.7}$$

where $\Phi_{(X,Y)}(x,y)$ is the usual characteristic function of the real random vector (X,Y). The cf $\Phi_Z(z)$ is closely related to the moments of Z, as shown in the next section.

I.1.2 Moments of complex random variables

The moments of a complex random variable Z are defined directly from those of real random variables by linearity of the expectation operator $\mathbb{E}$ on the complex field. That is, the mean of Z, $\mathbb{E}[Z]$ simply reads

$$\mathbb{E}[Z] \triangleq \mathbb{E}[X] + i\mathbb{E}[Y] \tag{I.8}$$

provided $\mathbb{E}[X]$ and $\mathbb{E}[Y]$ are well-defined. The major difference with respect to real random variables is that both Z and its conjugate Z^* can be used in the definition of moments. For instance, there are two distinct second-order moments, given by $\mathbb{E}\left[Z^2\right]$ and $\mathbb{E}\left[|Z|^2\right]$ (the third possibility being $\mathbb{E}\left[(Z^*)^2\right] = \mathbb{E}\left[Z^2\right]^*$ which is redundant with $\mathbb{E}\left[Z^2\right]$). For a given integer n there are $\lfloor \frac{n}{2} \rfloor + 1$ essentially distinct n-th order moments, where $\lfloor \cdot \rfloor$ is the floor function. In order to account for this multiplicity the following compact notation is often used in the literature

$$\mu_p^q(Z) \triangleq \mathbb{E}\left[Z^p (Z^q)^*\right] \tag{I.9}$$

Equivalently, the moments of Z can be obtained from the first cf (I.7) as

$$\mu_p^q(Z) = \left(\frac{2}{i}\right)^{p+q} \frac{\partial^p}{\partial z^p} \frac{\partial^q}{\partial z^{*q}} (\Phi_Z(0)) \tag{I.10}$$

In the rest of this thesis we will mainly be interested in the pure (*i.e.* non-mixed) moments of Z. Thus we will simply drop the exponent in (I.9), so that $\mu_n(Z) \equiv \mu_n^0(Z) = \mathbb{E}[Z^n]$.

Similarly to the case of real random variables, the central moments of Z are defined as the moments of the centered variable $Z - \mathbb{E}[Z]$. Of particlar interest are the central moments of order 2, respectively known as the variance $\mathbb{V}[Z]$ and pseudo-variance $\mathbb{J}[Z]$ and given by

$$\mathbb{V}[Z] \triangleq \mathbb{E}\left[|Z - \mathbb{E}[Z]|^2\right] = \mathbb{E}\left[|Z|^2\right] - |\mathbb{E}[Z]|^2 = \mathbb{V}[X] + \mathbb{V}[Y] \tag{I.11a}$$

$$\mathbb{J}[Z] \triangleq \mathbb{E}\left[(Z - \mathbb{E}[Z])^2\right] = \mathbb{E}\left[Z^2\right] - \mathbb{E}[Z]^2 = \mathbb{V}[X] - \mathbb{V}[Y] + 2i\,\mathrm{Cov}(X,Y) \tag{I.11b}$$

where $\mathbb{V}[X]$ and $\mathbb{V}[Y]$ respectively denote the usual variance of X and Y and $\mathrm{Cov}(X,Y) \triangleq \mathbb{E}[(X - \mathbb{E}[X])(Y - \mathbb{E}[Y])]$ is the covariance between X and Y. A complex random variable having a zero variance is equivalent to a deterministic complex number. On the other hand, a random variable having zero pseudo-variance implies for its real and imaginary parts to have the same variance and be uncorrelated. If, in addition to $\mathbb{J}[Z] = 0$ we have $\mathbb{E}[Z] = 0$, then Z is called a *proper* random variable [9].

I.1.3 Circularly-symmetric complex random variables

A complex random variable Z is called circular-symmetric if, for any $\varphi \in [0\,;\,2\pi[$, Z and $e^{i\varphi}Z$ have the same distribution [10]. The pdf of such variable is spherical with respect to the origin, *i.e.* $p_Z(z) = g(|z|)$ for a given real-positive function g. From (I.3) the pdf of the modulus of Z simply reads

$$p_R(r) = 2\pi r g(r) \tag{I.12}$$

It also follows from the definition that *all* non-absolute ($p \neq q$) moments $\mu_p^q(Z)$ of a circularly-symmetric random variables are null. This is easily seen by imposing Z and $e^{i\varphi}Z$ to have the same moments for any φ, so

$$\mu_p^q(Z) = \mu_p^q(e^{i\varphi}Z) = e^{i\varphi(p-q)}\mathbb{E}\left[Z^p(Z^q)^*\right] = e^{i\varphi(p-q)}\mu_p^q(Z) \tag{I.13}$$

hence $\mu_p^q(Z) = 0$ whenever $p \neq q$. In particular, all pure moments $\mu_n(Z)$ with $n > 0$ are null.

A sufficient condition for a random variable Z to be circular-symmetric is for its argument to be uniformly distributed in $[0\,;\,2\pi[$ and decorrelated from $|Z|$. The most well-known example of such variable is the circularly-symmetric normal distribution, whose distribution is given as [11]

$$p_Z(z) \triangleq \frac{1}{\pi\sigma^2} e^{-\frac{|z|^2}{\sigma^2}} \tag{I.14}$$

where the parameter σ^2 gives the variance of Z, $\mathbb{V}[Z] = \sigma^2$. Eq.(I.14) is equivalent to the bivariate real gaussian distribution with zero mean and covariance matrix $\frac{\sigma^2}{2}\mathbf{1}$, with $\mathbf{1}$ the identity matrix of dimension 2. The particular case $\sigma = 1$ corresponds to the standard complex normal distribution, which is the complex analog of the standard normal distribution.

From (I.12) the pdf of the modulus of a circularly-symmetric normal variable is given by

$$p_R(r) = \frac{2r}{\sigma^2} e^{-\frac{r^2}{\sigma^2}}, \quad r \geq 0 \tag{I.15}$$

which is a Rayleigh distribution with parameter $\frac{\sigma}{\sqrt{2}}$ [12]. The moments of R (the absolute moments of Z) read

$$\mathbb{E}\left[R^n\right] = \sigma^n \frac{n}{2}\Gamma\left(\frac{n}{2}\right) \tag{I.16}$$

with $\Gamma(x)$ the gamma function [13].

I.1.4 Cumulants

Cumulant are statistical quantitites alternative to moments and central moments. They are formally defined as the derivatives at the origin of the second characteristic function, $\Psi_Z(z) \triangleq \mathrm{Log}(\Phi_Z(z))$, where $\mathrm{Log}(z)$ denotes the principal determination of the complex logarithm

$$\kappa_p^q(Z) \triangleq \left(\frac{2}{i}\right)^{p+q} \frac{\partial^p}{\partial z^p}\frac{\partial^q}{\partial z^{*q}}(\Psi_Z(0)) \tag{I.17}$$

Similarly to the moments we have $\kappa_p^q(Z) = \kappa_q^p(Z)^*$, so for a given integer n there are $\lfloor \frac{n}{2} \rfloor + 1$ distinct cumulants. The only cumulant of order 1 is the mean of Z, and the two cumulants of order two are the variance and pseudo-variance of Z. For real random variables, the third and fourth-order cumulants are involved in the skewness and kurtosis of the pdf, respectively. More generally, higher order cumulants can be thought of as measures of deviation of Z from the complex normal distribution, for which all cumulants of order higher than two vanish [14].

Cumulants of order n can be expressed as polynomials of degree n in the moments of Z and their conjugates. Restricting to the specific case of pure cumulants, we can write

$$\kappa_n(Z) = P_n(\mu_1(Z), \mu_2(Z), \cdots, \mu_n(Z)) \tag{I.18}$$

where P_n is a n-variate polynomial of degree n and the same simplified notation as for pure moments was used. The first polynomials $P_n(z_1, \cdots, z_n)$ read [15]

$$P_1(z_1) = z_1 \tag{I.19a}$$
$$P_2(z_1, z_2) = z_2 - z_1^2 \tag{I.19b}$$
$$P_3(z_1, z_2, z_3) = z_3 - 3z_2z_1 + 2z_1^2 \tag{I.19c}$$
$$P_4(z_1, z_2, z_3, z_4) = z_4 - 4z_3z_1 - 3z_2^2 + 12z_2z_1^2 - 6z_1^4 \tag{I.19d}$$

In the following, to avoid dealing with multiple notations we will most often write the n-th pure cumulant $\kappa_n(Z)$ and its polynomial expression in terms of its moments alike. Additionally, when the context makes it clear we will also drop the explicit dependency of the moments in their underlying variable Z, making the three following notations equivalent

$$\kappa_n(Z) \equiv \kappa_n(\mu_1(Z), \mu_2(Z), \cdots, \mu_n(Z)) \equiv \kappa_n(\mu_1, \mu_2, \cdots, \mu_n) \tag{I.20}$$

One of the principal motivations for use of cumulants is their additivity property for mutually independent random variables. That is, if $(Z_1, Z_2, \cdots Z_n)$ denotes a set of n mutually independent complex random variables, then

$$\kappa_p^q(Z_1 + Z_2 + \cdots + Z_n) = \kappa_p^q(Z_1) + \kappa_p^q(Z_2) + \cdots + \kappa_p^q(Z_n) \tag{I.21}$$

This is essentially a consequence of the additivity of the complex logarithm and the factorization of the characteristic function of a random vector with independent components into the product of the characteristic function of each component. Additionally, the n-th pure cumulant is a complex-homogeneous function of degree n in the complex random variable Z, meaning that

$$\kappa_n(cZ) = c^n \kappa_n(Z) \tag{I.22}$$

for any complex number c. More generally, all n-th order cumulants are real-homogeneous functions of degree n in Z.

I.1.5 Convergence of random variables

Convergence modes of complex random variables do not formally differ from their real counterparts. Given a sequence Z_n, $n \in \mathbb{N}$, of complex random variables, there are four usual

notions of convergence of Z_n towards a complex random variable Z:

$$\textbf{Almost sure convergence: } Z_n \xrightarrow{a.s.} Z \Leftrightarrow \mathbb{P}\left(Z_n(\omega) \underset{n\to\infty}{\to} Z(\omega)\right) = 1 \tag{I.23a}$$

$$\textbf{Convergence in probability: } Z_n \xrightarrow{p} Z \Leftrightarrow \forall \varepsilon > 0,\ \mathbb{P}\left(|Z_n - Z| > \varepsilon\right) \underset{n\to\infty}{\to} = 0 \tag{I.23b}$$

$$\textbf{Convergence in distribution: } Z_n \xrightarrow{d} Z \Leftrightarrow F_{Z_n}(z) \underset{n\to\infty}{\to} F_Z(z) \tag{I.23c}$$

$$\textbf{Convergence in } r\textbf{-th mean: } Z_n \xrightarrow{r} Z \Leftrightarrow \mathbb{E}\left[|Z_n - Z|^r\right] \underset{n\to\infty}{\to} 0 \tag{I.23d}$$

As is well-known [16], almost sure convergence implies convergence in probability, which itself implies convergence in distribution. Convergence in r-th mean implies convergence in probability but generally share a direct relation with the other convergence modes. The most common occurrences of the convergence in r-th mean are the convergence in mean ($r = 1$) and the mean square convergence ($r = 2$).

From definitions (I.23a)–(I.23d) many properties on the convergence of operations on random variables can be derived. We only retain the so-called *continuous mapping theorem* [17], which states that almost sure convergence, convergence in probability and convergence in distribution are preserved under continuous functions. Formally,

$$Z_n \xrightarrow{a.s./p/d} Z \Rightarrow g(Z_n) \xrightarrow{a.s./p/d} g(Z) \tag{I.24}$$

for any complex function g continuous everywhere except possibly on a set with probability zero for the probability measure of Z.

The above convergence modes find a direct application in the most fundamental limit theorems of statistics: the almost sure convergence and convergence in probability are respectively involved in the strong and weak law of large numbers, while convergence in distribution is at the core of the *Central Limit Theorem*. For scalar complex variables the latter reads

$$\frac{1}{N}\sum_{n=1}^{N} Z_n \xrightarrow{d} \mathcal{NC}(\mu, \sigma^2/N, \gamma^2/N) \tag{I.25}$$

for any sequence Z_n of independent and identically distributed complex random variables with mean $\mathbb{E}[Z] = \mu$, variance $\mathbb{V}[Z] = \sigma^2$ and pseudo-variance $\mathbb{J}[Z] = \gamma^2$, and where $\mathcal{NC}(\mu, \sigma^2, \gamma^2)$ denotes the complex normal distribution

$$Z \sim \mathcal{NC}(\mu, \sigma^2, \gamma^2) \Leftrightarrow p_Z(z) = \frac{1}{\pi\sqrt{\sigma^4 - |\gamma|^4}} \exp\left(\frac{|z-\mu|^2\,\sigma^2 - \Re(\gamma^2(z^* - \mu^*)^2)}{\sigma^4 - |\gamma|^4}\right) \tag{I.26}$$

with $\mathbb{V}[Z] = \sigma^2$ and $\mathbb{J}[Z] = \gamma^2$. The circularly-symmetric complex normal variable (I.14) is obtained as a special case of (I.26) for $\gamma = 0$.

I.2 Estimation theory

Estimation theory is concerned with infering properties of an unknown random process with only a limited amount of information available. More specifically, given a sample of N observations of the process under consideration, as well as some possible prior information on its statistical properties, one aims at drawing the most accurate conclusions on the process so as to characterize or predict its behavior within as small uncertainty as possible. Typical examples include meteorological forecast, poll-based electoral strategies or stock market prices predictions, among countless others [18].

I.2.1 Definitions

Formally speaking, the unknown random process is modeled by a complex random variable (or vector, or function) Z, and the sample consists in N realizations $(Z_1, \cdots, Z_N)$ of Z, usually assumed – but not necessarily – independent. A priori partial knowledge on Z can be of many kinds, including constraints on its value range, statistical independence of its components for a vector, ergodicity or stationarity for a time series, and so on. In the framework of parametric estimation, the random variable Z is known to belong to a family of probability distributions $p_{\boldsymbol{\theta}}(z)$ parametrized by a parameter vector $\boldsymbol{\theta}$ taking its values in a set $\boldsymbol{\Theta}$. In this context the aim of estimation theory is to find from the observed sample the actual value $\boldsymbol{\theta}_0$ of $\boldsymbol{\Theta}$ taken by Z. Alternatively one may be more interested in statistical quantities derived from the distribution of Z, typically the mean or the variance, which are functions of $\boldsymbol{\theta}_0$. Estimation methods then consist in deriving functions of the observations $T(Z_1, \cdots, Z_N)$, called *statistics*, such that whatever value $\boldsymbol{\theta}_0$ the actual distribution of Z may have, $T(Z_1, \cdots, Z_N)$ yields a good approximation of $\boldsymbol{\theta}_0$ or the function $g(\boldsymbol{\theta}_0)$ of interest. The resulting rule is called an *estimator* of $\boldsymbol{\theta}_0$ (or $g(\boldsymbol{\theta}_0)$), and is denoted by $\widehat{\boldsymbol{\theta}}$, *i.e.* $\widehat{\boldsymbol{\theta}} \triangleq T(Z_1, \cdots, Z_N)$. The estimator is itself a random variable, as it depends on the random observations through the statistics T. A particular realization of $\widehat{\boldsymbol{\theta}}$ is called an *estimate* of $\boldsymbol{\theta}_0$, and the quantity of interest ($\boldsymbol{\theta}_0$) the estimand. The distribution parameter is usually considered as deterministic, but may also be considered random so as to model the uncertainty or lack of information about the underlying statistical data model. The latter case corresponds to the Bayesian inference philosophy [19]. From a more general perspective, it is not always possible, nor relevant, to assume an a priori parametric model for the estimation problem under consideration. Non-parametric estimation refers to this class of methods which do not imply a full parameter characterization, or do not rely on a specific type of distribution at all. Latter approaches are also termed distribution-free [20].

In the next parts of the thesis we will occasionnally make the following distinction on estimators depending on the nature of the quantity they aim at finding:

- we will call *estimator* a statistics or a rule which aims at finding a deterministic quantity. This is the most-encountered case and corresponds to the above definition for parametric models;
- we will call *predictor* a statistics for which the estimated quantity is itself random.

> Typically, given a random variable Z a predictor $\widehat{Z}$ aims at producing an instantaneous value which is as close as possible as the current realization of Z.

The notion of predictor encompasses that of estimator, in the sense that the latter is obtained from the former by simply imposing the predicted random variale to be deterministic. For this reason in the literature the term estimator is often found to refer to both notions alike. It is also worth mentioning that despite being apparently close, the notions of predictor and Bayesian inference are fundamentally different in that the interpretation of randomness is not the same: in the Bayesian framework the use of a probability distribution for the estimand stems from a degree of incertitude in the assumed data model. On the other hand, the variable estimated by a predictor is the result of an actual random process, to which the observed data are subsequent.

I.2.2 Properties of estimators

Once an estimator (or a predictor) has been derived, the fundamental question to address is that of its quality. Loosely speaking, a good estimator $\widehat{\boldsymbol{\theta}}$ is one that tends to produce estimates close to the actual value $\boldsymbol{\theta}_0$. There are several ways of formally defining this notion of accuracy. The most intuitive one is to check whether the estimates of $\widehat{\boldsymbol{\theta}}$ are on average close to the estimand $\boldsymbol{\theta}_0$. This is measured by the bias $B(\widehat{\boldsymbol{\theta}})$:

$$B(\widehat{\boldsymbol{\theta}}) \triangleq \boldsymbol{\theta}_0 - \widehat{\boldsymbol{\theta}} \tag{I.27}$$

An estimator achieving a null bias is said to be unbiased: the realizations produced are on average identical to the estimated quantity. The simplest example of an unbiased estimator is the sample mean of a random variable Z, denoted by $\overline{Z}$:

$$\overline{Z} = \frac{1}{N}\sum_{n=1}^{N} Z_n \tag{I.28}$$

for which we have trivially $\mathbb{E}\left[\overline{Z}\right] = \mathbb{E}\left[Z\right]$. On the opposite, the uncorrected sample variance and pseudo-variance are respectively biased estimators of the variance and pseudo-variance of Z. For the variance we have indeed

$$\overline{\sigma}^2 \triangleq \frac{1}{N}\sum_{n=1}^{N} |Z_n - \overline{Z}|^2 \Rightarrow \mathbb{E}\left[\overline{\sigma}^2\right] = \frac{N-1}{N}\mathbb{V}\left[Z\right] \tag{I.29}$$

so that $B(\overline{\sigma}^2) = \frac{\mathbb{V}[Z]}{N}$, and similarly for $\mathbb{J}\left[Z\right]$. The uncorrected sample variance and pseudo-variance are however asymptotically unbiased, meaning that their bias goes to 0 as the sample size N tends to infinity.

Another way of assessing how close a given estimator is from its estimand is by measuring its mean square deviation, known as the Mean Square Error (MSE) and defined by

$$\mathrm{MSE}(\widehat{\boldsymbol{\theta}}) \triangleq \mathbb{E}\left[|\widehat{\boldsymbol{\theta}} - \boldsymbol{\theta}_0|^2\right] = |B(\widehat{\boldsymbol{\theta}})|^2 + \mathbb{V}\left[\widehat{\boldsymbol{\theta}}\right] \tag{I.30}$$

Estimators minimizing the MSE are called Minimum Mean Square Error (MMSE) estimators. Such estimators are endowed with better statistical properties than unbiased ones. Yet exact derivation of the MMSE is often unachievable. A reasonable compromise then consists in restricting oneself to the class of Minimum Variance Unbiased Estimators (MVUE). As can be seen from the decomposition of the MSE as the sum of the squared-modulus bias and the variance of $\widehat{\boldsymbol{\theta}}$ Eq.(I.30), MVUE are usually suboptimal compared to MMSE estimators, as the latter are not necessarily unbiased. However the study of MVUEs is easier than that of MMSE, and several statistical tools, such as the Cramer-Rao Lower Bound (CRLB) exist to help achieving or at least approaching the MVUE [18]. A further suboptimal class of estimators is provided by the Best Linear Unbiased Estimators (BLUE), which consists in estimators that are linear in the observations, unbiased and whose variance is minimal compared to any other linear unbiased estimator. Except for some specific cases, the BLUE does not generally coincide with the MVUE.

Several other quality properties of estimators can be defined. One of the most important is consistency, which means that an estimator converges in probability to its estimand, *i.e.* $\widehat{\boldsymbol{\theta}} \xrightarrow{p} \boldsymbol{\theta}_0$. If convergence holds almost surely, we say that the estimator is strongly consistent. Other useful properties of estimators include efficiency, asymptotic normality and robustness [21]. In the remaining sections we briefly review some of the most well-known classes of estimators.

I.2.3 Least Squares Estimators

Least Squares Estimators (LSE) refer to a wide class of estimators that are built upon minimizing the squared deviation between an observed sample $Z_1, \cdots Z_N$ and a set of predicted data $\widehat{Z}_1, \cdots \widehat{Z}_N$. More specifically, the observations Z_n are assumed to originate from a predefined data model depending on the parameter $\boldsymbol{\theta}_0$ to be estimated, and are corrupted by additive noise:

$$Z_n = f(\mathbf{s}_n, \boldsymbol{\theta}_0) + B_n \tag{I.31}$$

where f is a known function, $\mathbf{s}_n$ a deterministic known m-th dimensonal vector and B_n is a random variable modeling the noise, usually assumed to have zero mean. The LSE is then obtained by searching the estimated data according to the same model, $\widehat{Z_n} = f(\mathbf{s}_n, \widehat{\boldsymbol{\theta}}))$, and minimizing the sum of squared residuals between the observed and estimated samples with respect to $\widehat{\boldsymbol{\theta}}$:

$$J_{LS} \triangleq \sum_{n=1}^{N} |Z_n - f(\mathbf{s}_n, \widehat{\boldsymbol{\theta}})|^2 \tag{I.32}$$

The different least-squares approaches depend on the form of the function f. In the simplest setting, the data is supposed to depend linearly on $\boldsymbol{\theta}_0$, so that $f(\mathbf{s}, \boldsymbol{\theta}_0) = \mathbf{s}^T \boldsymbol{\theta}_0$, where $\mathbf{s}^T$ is the transpose of $\mathbf{s}$, *i.e.* a row vector of dimension m. This is called the Linear Least Squares (LLS) problem, and the minimum of (I.32) is then given by the so-called normal equation

$$\widehat{\boldsymbol{\theta}} = (\mathbf{S}\mathbf{S}^\dagger)^{-1}\mathbf{S}^\dagger\mathbf{Z} \tag{I.33}$$

where $\mathbf{S} \triangleq (\mathbf{s}_1, \cdots \mathbf{s}_N)$ is the $M \times N$ matrix obtained by concatenating the vectors $\mathbf{s}_n$, $\dagger$ denotes the hermitian transpose and $\mathbf{Z} \triangleq (Z_1, \cdots Z_N)$. The resulting estimator $\widehat{\boldsymbol{\theta}}$ is known as the Ordinary Least Squares (OLS) estimator.

Generally, neither the OLS estimator nor LSE exhibit any optimality condition as is the case for the MMSE or MVUE estimators. This is because the least-squares cost function does not take into account the full random nature of Z but only specific realizations. One can notably see that (I.32) is merely a sampled version of the MSE, Eq.(I.30). The very same reason accounts for the ubiquity of least-squares methods in practical applications, as they do not require any probabilistic assumption on the noise B_n (the zero-mean assumption is not an actual requirement for use of least-squares methods). There are cases however where the LSE can be related to other classes of estimators. The most well-known such example is given by the Gauss-Markov theorem [22], which states that under the assumptions that the noise realizations B_n are uncorrelated, zero-mean and homoscedastic (*i.e.* with identical variance), the OLS estimator coincides with the BLUE. Furthermore, with the additional assumption that the B_n's are distributed according to a circular-symmetric complex normal variable (Eq.(I.14)), the OLS estimator can be shown to be the MVUE.

Least squares methods are extensively used in a wide variety of problems such as curve-fitting and regression analysis [23], to name a few. Extensions of the LLS model to less restrictive hypotheses include the Weighted Least Squares (WLS) problem, which assumes the noise variables have different variances (heteroscedasticity), the Generalized Least Squares (GLS) problem, which further accounts for correlation between the noise realizations, and Non Linear Least Squares (NLLS) which considers non linear function-based data models [24].

I.2.4 The method of moments

The method of moments [18] provides a quite easy and general way of estimating the parameters $\boldsymbol{\theta}_0$ of an unknown parametric distribution $p_{\boldsymbol{\theta}_0}(z)$. The fundamental idea of the method is that statistical quantities derived from $p_{\boldsymbol{\theta}_0}(z)$ almost always depend on $\boldsymbol{\theta}_0$. The most natural example of such quantities are the moments of Z, $\mu_p^q(Z)$, but other possibilities such as cumulants may be considered as well. Restricting to pure moments only for simplicity we can thus write

$$\mu_p(Z) = f_p(\boldsymbol{\theta}_0) \tag{I.34}$$

for a given known function $f_p(\boldsymbol{\theta})$. Consequently, if P is the number of parameters θ_p in $\boldsymbol{\theta}$, then by considering an appropriate choice of P moments of Z one obtains a set of equations which, if invertible, directly yield the desired actual parameters $\boldsymbol{\theta}_0$ as functions of the chosen moments. The choice of which moments to consider is in general not unique. Now, because the distribution of Z is precisely unknown, the actual moments of Z cannot be observed. The method of moments then suggests to replace them with their sample counterpart. That is, denoting $\bar{\mu}_p$ the sample estimator of $\mu_p(Z)$, the moment method estimator components $\widehat{\theta}_p$ are given by

$$\widehat{\theta}_p \triangleq g_p\left(\bar{\mu}_1, \cdots \bar{\mu}_P\right) \tag{I.35}$$

for $p \in \{1, \cdots, P\}$, where g_p is a function derived from the inversion of the system of equations induced by the chosen moments, which for simplicity have been here assumed to consist in the first P moments of Z.

The estimators provided by the moment method are most often consistent, as long as their derivation involves continuous functions. This is essentially a consequence of the fact that all sample moments are consistent and of the continuous mapping theorem (I.24). On the opposite, the moment method estimators are generally biased, even though all sample moments are unbiased. For some classes of functions however, corrections may be applied to turn these estimators into unbiased ones. This is notably the case for any estimator expressed as a polynomial of the sample moments, the simplest example being the Bessel's correction to the sample variance (I.29). This holds in particular for all sample cumulants and central moments, the unbiased versions of which are sometimes referred to as k-statistics and h-statistics, respectively [23].

The formal simplicity underlying the method of moments makes it applicable to many problems where an exact derivation of more optimal estimators is impossible. At least, the method provides a convenient basis for obtaining consistent estimators that can then be refined using more advanced techniques. An extension of the method is the Generalized Moment Method (GMM) [25], which relies on more general moment constraints and is applicable even when an exact solution to the traditional moment problem does not exist. Not only the GMM extends the original moment method, but it actually encompasses several other families of estimators, including the OLS discussed previously and the maximum likelihood estimators, that we now introduce.

I.2.5 Maximum Likelihood Estimators

We conclude our overview of state of the art parametric estimation methods by the most well-known of them, namely Maximum Likelihood Estimators (MLE) [21]. Contrary to the method of moments, which relies on statistical quantities derived from actual underlying distribution p_{θ_0} of the data, maximum-likelihood methods are directly based on the joint distribution of the observed sample $p_{\theta_0}(\mathbf{z})$, where $\mathbf{z} = (z_1, \cdots, z_N)$. More precisely, in this approach the joint pdf is seen only as a function of the parameter $\boldsymbol{\theta} \in \boldsymbol{\Theta}$, the variable $\mathbf{z}$ being fixed, and is called the *likelihood*. Equivalently, the *log-likelihood* is defined as the logarithm of $p_{\theta_0}(\mathbf{z})$ viewed as a function of $\boldsymbol{\theta}$:

$$\mathbb{L}\left[\boldsymbol{\theta}; \mathbf{z}\right] \triangleq \log\left(p_{\boldsymbol{\theta}}(\mathbf{z})\right). \tag{I.36}$$

The MLE $\widehat{\boldsymbol{\theta}}$ is then obtained by maximizing the (log)-likelihood and replacing $\mathbf{z}$ with the random observed sample $\mathbf{Z} \triangleq (Z_1, \cdots, Z_N)$. Conceptually, the MLE corresponds to the value of the parameter $\boldsymbol{\theta}$ which best accounts for the observed data sample $\mathbf{Z}$. The motivation for use of the log-likelihood instead of the likelihood is first because for independent observations, $\mathbb{L}\left[\boldsymbol{\theta}; \mathbf{z}\right]$ simply decomposes as the sum of the log-likelihood of each observation

$$\mathbb{L}\left[\boldsymbol{\theta}; \mathbf{z}\right] = \sum_{n=1}^{N} \mathbb{L}\left[\boldsymbol{\theta}; z_n\right] \tag{I.37}$$

which is easier to handle than the corresponding product of likelihoods. Besides, the expectation of the Hessian matrix (= matrix of second derivatives) of $\mathbb{L}[\boldsymbol{\theta}; \mathbf{Z}]$ with respect to the data, known as the Fisher information matrix, also has a strong conceptual meaning in terms of the minimum variance achievable by any unbiased estimator.

One of the simplest example of explicit derivation of the MLE is for a circularly-symmetric complex normal variable with known variance σ^2, translated by a unknown complex constant c_0. The resulting variable Z has the following distribution

$$p_Z(z) = \frac{1}{\pi\sigma^2} e^{-\frac{|z-c_0|^2}{\sigma^2}} \tag{I.38}$$

and $\mathbb{E}[Z] = c_0$. Here we have a single parameter to estimate, namely $c_0 \in \mathbb{C}$. The log-likelihood of N independent realizations of Z reads

$$\mathbb{L}[c; \mathbf{z}] = -N\log(\pi) - 2N\log(\sigma) - \sum_{n=1}^{N} \frac{|z_n - c|^2}{\sigma^2} \tag{I.39}$$

Ignoring the irrelevant known constants, the maximization of (I.39) here reduces to the LLS minimization problem (I.32). The resulting estimator is simply given by the sample mean (I.28), *i.e.* $\widehat{c} = \overline{Z}$. In this particular case, the MLE, the LSE and the moment method estimator all coincide and achieve the minimal possible variance among all other unbiased estimators.

Under weak conditions, the MLE is shown to be consistent, unbiased, and asymptotically efficient, meaning that its variance tends to the CRLB with the sample size N. For large enough samples, the MLE is thus a good approximation to the MVUE, making it a relevant choice in most situations. The maximization of the log-likelihod may represent in itself a challenging problem, and theoretical solutions such as the one presented above are not often achievable in more advanced, practical applications. Iterative optimization methods such as gradient descents or Newton-Raphson based algorithms are possible alternatives to find the MLE in such cases. Among the manifold applications of the maximum likelihood approach to estimation, let us mention the well-known Expectation-Maximization (EM) algorithm, a data clustering technique which essentially consists in finding the MLE of a linear mixture of parametric probability distributions [26].

I.3 Introduction to wireless communications

With the far-reaching success of cellular telephony, wireless communications have garnered considerable interest and experienced major developments in the past few decades. This last part of our introductory chapter is devoted to an overview of the very basic concepts underlying digital wireless transmissions. The fundamental notions and terminology developed in the subsequent sections will be extensively used all along the thesis.

I.3.1 Basic model of a wireless transmission

Wireless communications allow transmission of information on long distances and between a large number of users without dependency on full-wired networks. The information is encoded in electromagnetic waves radiating in the air instead of electric signals transiting through wires, making communication possible even between mobile devices. In the cellular telephony framework, the basic model for wireless transmission involves several User Equipments (UE), such as mobile phones or laptop computers, emitting signals to a reception device called a Base Station (BS), as shown on Fig.I.1. The BS consists essentially in one or several antennas covering a certain space area, here represented as an hexagon, called a *cell*. A wireless network is composed of several such interconnected BS, each receiving from and transmitting to devices belonging to their cell. Interconnection between BS allows communication between users located in different cells. Several devices can simultaneously transmit to the same BS and, conversely, the BS can send individual signals to each user or broadcast the same signal to all users in its cell. In the telecommunication terminology, a transmission between one or several UE to a given BS is called an *uplink* transmission, and the reverse communication is referred to as *downlink*.

An important feature of wireless communications is that they efficiently take advantage of the frequency spectrum to allow multiple simultaneous transmissions without interference. The signals involved in a wireless system are band-limited, meaning that their spectral (= frequency) content is limited to a bounded region of the spectrum. Formally speaking, the Fourier transform of a band-limited signal vanishes outside of a positive frequency interval whose length B is called the *bandwidth*. A signal whose spectral band contains the zero frequency is called a *baseband* signal, and a *passband* signal otherwise. Each wireless application relies on its own frequency range, allowing for signals intended to different systems to be superposed in time and still be separately recovered based on their frequency content. In Fig.I.1 for instance, adjacent BS may operate in different frequency bands so as to avoid interference from neighbouring cells transmissions.

A simplified representation of an overall wireless transmission is depicted on Fig.I.2. At the emitter side, the information takes the form of a digital stream. The input bits are mapped to binary codewords through a source encoder, so as to remove the inherent correlation between the initial bits due to the informative content of the transmitted message. The resulting binary stream can then be approximated by a sequence of independent and equally likely random bits. Another encoding, named channel encoding, adds a structured redundancy to the emitted sequence which acts as a safeguard against errors that may occur during signal propagation. The coded binary sequence is next transformed into an analog signal by a modulator. Due to the propagation medium and the environment, the transmitted wave experiences various sources of impairment. The channel models signal distortions related to the propagation environment, while noise refers to undesirable and totally unpredictable residual radiations, stemming for instance from internal thermal noise of electronic components. The equalizer aims at mitigating the effects of these transformations at the receiver. As for the rest of the reception steps they are by and large

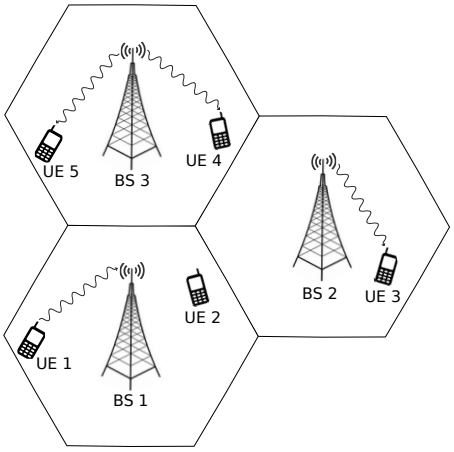

Figure I.1 – *Basic wireless network model with 3 base stations and 5 user equipments.*

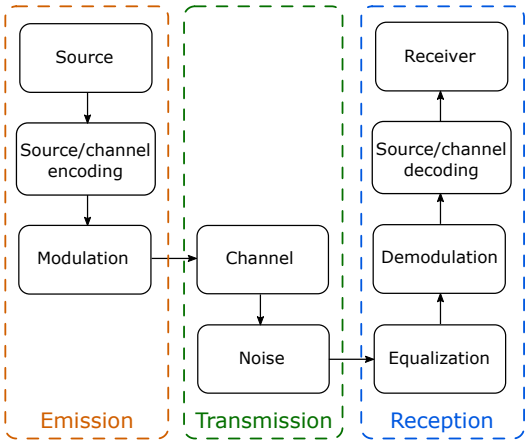

Figure I.2 – *Simplified functional block diagram of a wireless transmission.*

the reverse of their emission counterparts: demodulation allows to convert the received signal back to a binary sequence. The channel decoder can detect and in some extent correct errors contained in the received sequence. The source decoder finally recovers the message in its initial form and transmits it to the receiver.

In the rest of the thesis we will only be interested in the part of the transmission that takes place between the modulator and the demodulator. The following sections describe in more detail the involved functional blocks.

I.3.2 Modulation

The aim of the modulator is to convert the input binary sequence into a continuous signal suited to the application requirements. Obviously the analog signal must be adaptative and in one-to-one correspondance with the input sequence. To do so the modulator segments the incoming sequence in binary words of fixed size d, and maps the set of 2^d possible binary words to a set of M predefined waveforms $\psi_m(t; c_m)$, $m \in \{1, \cdots, M\}$. The numbers c_m are called the modulation symbols and take their values in a given finite alphabet $\mathscr{C}$. Each incoming binary word is associated with one of the M signals, which is emitted for a fixed duration T called the symbol period or time epoch. The transmitted signal consists then in the concatenation of these reference signals. In a general setting, the choice of the modulation symbol at a given time epoch depends both on the current binary word and on the preceding output symbols. In the case where the symbols are solely determined by the binary words the modulator is defined as *memoryless* [27]. The modulation alphabet $\mathscr{C}$ is then in one-to-one correspondance with the set of binary words, and $M = 2^d$. Furthermore, if the functions $\psi_m(t; c_m)$ are linear in the modulations symbols, *i.e.* $\psi_m(t) = c_m\ \phi_m(t)$ for a given function $\phi_m(t)$, the modulation is said to be *linear*. This is the case we will consider in the following.

In most wireless communications, the modulated signals are obtained by modification of the amplitude and phase of the same reference waveform called a *carrier*. The carrier is a pure sinusoid of frequency f_c. In the complex representation of signals the m-th modulated waveform simply reads $\psi_m(t) = c_m e^{2i\pi f_c t}$. Hence the modulation is fully characterized by the carrier frequency f_c and the M complex numbers c_m whose amplitude and argument respectively give the amplitude and phase to apply to the carrier. The corresponding alphabet $\mathscr{C}$ is called the *constellation*. Linear wireless modulation schemes can be declined in three main classes [28]:

- Amplitude Shift Keying (ASK) modulations, also called Pulse Amplitude Modulation (PAM), only affect the amplitude of the carrier. The corresponding symbols are real and of the form $c_m = A(2m-1-M)$, where A is a real coefficient which gives the reference amplitude of the transmitted waveforms. The special case $M = 2$ is known as the Binary Phase Shift Keying (BPSK) modulation and is the simplest of all linear modulation schemes, with transmitted signals that are simply antipodal, $s_m(t) = (-1)^m A e^{2i\pi f_c t}$, with $m \in \{1, 2\}$. An example of the resulting waveform $s(t)$ is shown in Fig.I.5;
- Phase Shift Keying (PSK) modulations only affect the phase of the carrier. The symbols are equally distributed over a circle of radius A, $c_m = A e^{\frac{2i\pi(m-1)}{M}}$. For $M = 2$ we recover the BPSK, and the case $M = 4$ is also given the specific name of Quadratic Phase Shift Keying (QPSK);
- Quadrature Amplitude Modulation (QAM) modulations affect the carrier in both amplitude and phase. A QAM M with $M = 4^n$ symbols for a given integer n is called regular. The constellation of a regular QAM M is obtained from two independent ASK of size $\sqrt{M}$, one on the real axis and the other on the imaginary axis. The resulting symbols can be written $c_m = a_{m_r} + i a_{m_i} = A(2m_r - 1 - \sqrt{M} + i(2m_i - 1 - \sqrt{M}))$, where a_{m_r} and a_{m_i} belong to an ASK $\sqrt{M}$ and $m \in \{1, \cdots, M\}$ is specified by the couple of integers $(m_r, m_i) \in \{1, \cdots, \sqrt{M}\}^2$ as $m \triangleq \sqrt{M}(m_r - 1) + m_i$. The simplest example of a QAM constellation is obtained for $M = 4$, and is equivalent, up to a complex multiplication, to the QPSK modulation. For M not a power of 4 there are several ways of defining a QAM constellation [27]. In the following we will only be interested in regular QAM, that we will simply call QAM for short.

Representative examples of the three types of modulations described above are presented on Fig.I.3. As can be seen all three constellations exhibit several geometrical symmetries. The first one is the complex conjugate invariance: the constellation $\mathscr{C}$ is stable under complex conjugation, meaning that for each symbol c in $\mathscr{C}$, we have $c^* \in \mathscr{C}$. The second symmetry is the discrete rotational invariance: for each constellation, we can find a minimal, non-zero integer q such that $e^{\frac{2i\pi}{q}}\mathscr{C} = \mathscr{C}$, where $c_0\mathscr{C} \triangleq \{c_0\, c \mid c \in \mathscr{C}\}$ for any $c_0 \in \mathbb{C}$. The integer q is called the *rotational order* of the constellation $\mathscr{C}$. From the previous definitions and Fig.I.3 we find that for ASK modulations $q = 2$, for PSK $q = M$ and for QAM $q = 4$.

The energy of a constellation $\mathscr{C}$ is defined as the mean energy of its symbols. Since the bits in the input sequence are close from being equally likely, we can consider that the

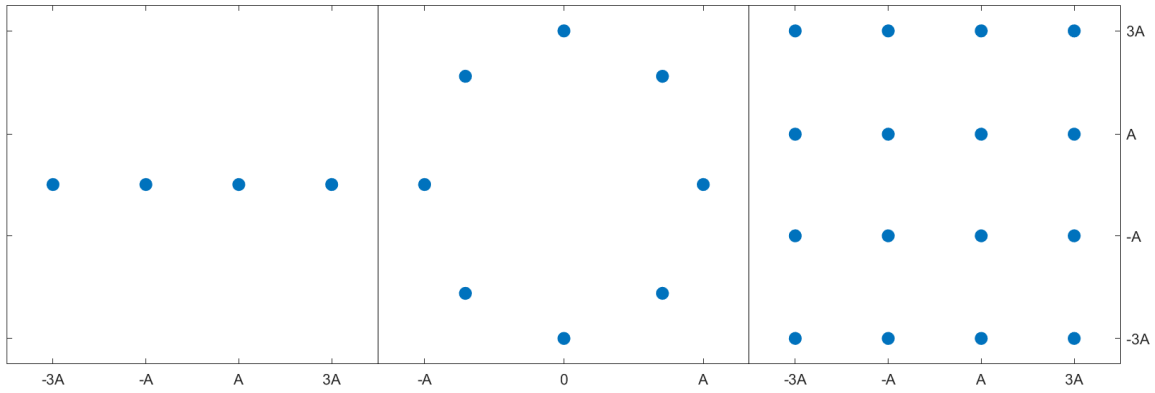

Figure I.3 – *Three representative examples of linear modulations. From left to right: ASK* 4*, PSK* 8 *and QAM* 16*.*

modulation symbols have a discrete uniform distribution, so the energy E_s of $\mathscr{C}$ is simply given by

$$E_s \triangleq \frac{1}{M}\sum_{m=1}^{M} |c_m|^2 \tag{I.40}$$

The energy of the above three families of modulations can be computed for a general M and read [29]:

$$\textbf{ASK: } E_s = \frac{1}{3}(M^2-1)A^2 \tag{I.41a}$$

$$\textbf{PSK: } E_s = A^2 \tag{I.41b}$$

$$\textbf{QAM: } E_s = \frac{2}{3}(M-1)A^2 \tag{I.41c}$$

One can also define the energy per bit E_b of the modulation, defined as the average energy needed to modulate one bit of signal and given by $E_b \triangleq E_s/\log_2(M)$.

Within the assumption of a linear carrier-based modulation scheme, the transmitted waveform at the output of the modulator can be written as the real part of

$$s(t) = \sum_{n=-\infty}^{+\infty} s_n e^{2i\pi f_c t} g(t-nT) \tag{I.42}$$

where $s_n \in \mathscr{C}$ are independent realizations of the constellation symbols and $g(t)$ is a baseband function referred to as the pulse-shaping filter. The simplest choice for $g(t)$ is a rectangular window of duration T the symbol period, so that signals associated with consecutive symbols do not overlap. The latter phenomenon is called Inter-Symbol Interference (ISI). In practice, due to spectral constraints smoother choices of waveforms may be preferable. A popular choice is the raised-cosine filter, defined by [29]

$$g_\alpha(t) \triangleq \frac{\sin(\pi t/T)}{\pi t/T}\frac{\cos(\alpha\pi t/T)}{1-4\alpha^2t^2/T^2} \tag{I.43}$$

where $\alpha \in [0\ ;\ 1]$ is called the roll-off factor. The advantage of the raised cosine filter is that it is stricly band-limited and still prevents ISI, while the rectanglar pulse has a theoretically infinite bandwidth, as can be seen on Fig.I.4. Yet for conceptual simplicity we will consider in the following the simpler model provided by the rectangular window.

It is worth mentioning that in addition to the linear modulations presented here, many non-linear modulations schemes also exist for wireless systems. These modulations may introduce memory in the choice of the reference waveforms, meaning that the signal emitted by the modulator in a given symbol period depends both on its current input (the binary word) and on its previous outputs. The interest of such methods is an increased flexibility for designing an overall waveform with good temporal and spectral properties. For instance, signals emitted from linear modulators exhibit phase jumps, as can be seen on Fig.I.5 for the BPSK modulation. The resulting discontinuities in the time domain have undesirable effects on the signal spectral content. By resorting to non-linear modulation schemes such problems can be circumvented, at the price of a higher implementation complexity. Frequency Shift Keying (FSK), Gaussian Minimum Shift Keying (GMSK), Continuous Phase Modulation (CPM) or Offset Quadrature Amplitude Modulation (OQAM) are a few well-known examples of non-linear modulations used in many wireless systems [27].

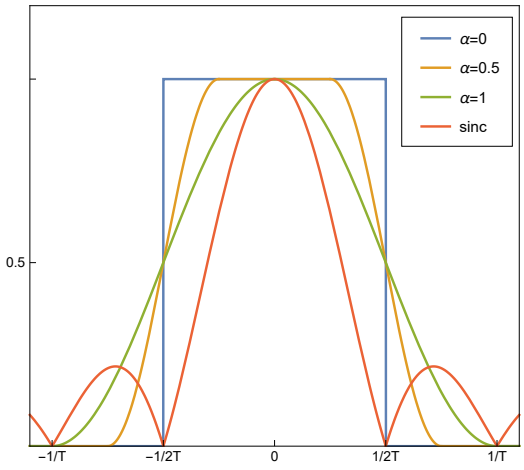

Figure I.4 – *Frequency response of the rectangular pulse and of the raised cosine filter for several roll-offs factors.*

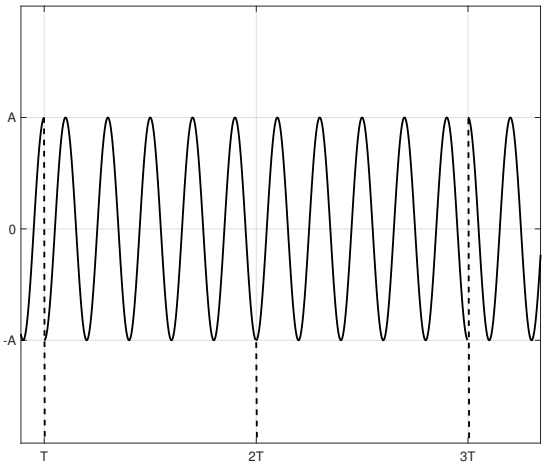

Figure I.5 – *Transmitted waveform from a BPSK modulator on several symbol periods.*

I.3.3 Propagation channel and noise

Due to interactions with its environment, the transmitted waveform is subject to various physical processes that alter its temporal and spectral content. Reflection on obstacles such as buildings, scattering by small objects or particles, diffraction, motion of the transmitter and/or the receiver are as many typical examples of phenomena inducing transformations of the signal such as attenuation, delay, dephasing or frequency shifts. The state of the propagation environment is encapsulated in what is called the *channel*. Formally, the channel

is modeled as a linear, time-invariant or slowly time-variant system fully characterized by its impulse response function $h(t)$. The received signal $r(t)$ can thus be written as the convolution product of the input signal $s(t)$ and the channel impulse response $h(t)$:

$$r(t) = h(t) * s(t) \triangleq \int_{-\infty}^{\infty} h(u)s(t-u)\mathrm{d}u \tag{I.44}$$

Equivalently one can consider the channel transfer function $\tilde{h}(f)$, defined as the Fourier transform of $h(t)$, which gives the attenuation and dephasing induced by the environment for every frequency component.

A quite simple but reasonable channel model extensively used in wireless communications is the multipath fading channel: due to the presence of obstacles that deflect or scatter the input signal, the observed signal $r(t)$ at the receiver is composed of a sum of scaled and delayed replicas of $s(t)$ coming from several paths, each having its own length, dephasing and attenuation. The impulse response of such channels have the following form [30]:

$$h(t) = \sum_{\ell=1}^{L} h_\ell(t)\delta(t-\tau_l(t)) \tag{I.45}$$

where the integer $\ell \in \{1, \cdots, L\}$ indexes the different paths, $h_\ell(t)$ is a complex number accounting both for attenuation and dephasing, $\tau_\ell(t)$ is the time propagation delay of the ℓ-th path and $\delta(t)$ is the Dirac delta function. The coefficients $h_\ell(t)$ are called the channel taps, and $h(t)$ is said to be a L-taps channel. An illustrative example of a multipath propagation with 5 paths/taps is presented on Fig.I.6. Both attenuation and delay are generally functions of time, as the position or properties of obstacles involved in a given path may evolve during the transmission. For instance, a reflector moving at constant velocity introduces a linear time delay, which corresponds to a global frequency shift in the spectrum known as the Doppler shift. Temporal variations of the complex amplitudes $h_\ell(t)$ are generically called *fading*. The time scale on which the channel taps and delays change significantly is measured by the channel coherence time T_c. A channel with a small, respectively large, coherence time is categorized as fast-fading, respectively slow-fading. In the latter case the paths characteristics can be considered as approximately constants for several time symbol periods T [31].

Another useful temporal quantity is the delayspread T_d of the multipath channel, defined as the difference between the maximum and minimum path delays

$$T_d \triangleq \max_{1\leq\ell\leq L}(\tau_l) - \min_{1\leq\ell\leq L}(\tau_l) \tag{I.46}$$

For an homogeneous enough propagation medium this is equivalent to the delay between the longest and shortest paths. The delayspread allows to characterize two central channel properties, namely ISI and coherence bandwith. In a multipath propagation, ISI occurs when the propagation delay of some of the paths is longer than that of the shortest path by more than a symbol period T. Thus in order to prevent ISI one needs to make sure that

$T > T_d$. This way all the relevant information about a given symbol is contained in a single symbol period of the received signal. A related property of the channel is provided by the coherence bandwidth B_c, which is the spectral counterpart of the coherence time T_c. That is, B_c is a measure of how fast the spectral content of the channel significantly changes with frequency. It is roughly given by the inverse of the delayspread, $B_c \simeq 1/T_d$. Comparing the bandwidth $B = 1/T$ of the input signal $s(t)$ to the channel coherence bandwidth B_c leads to the following useful characterization of channels: a channel is referred to as *flat-fading* if the input signal bandwidth is small compared to the channel coherence bandwidth, *i.e.* $B \ll B_c$. The name stems from the fact that the transfer function $H(f)$ of a flat-fading channel can be approximated as constant over a frequency range B. In the time domain this means the impulse response $h(t)$ is essentially composed of a single tap, or equivalently that all signal replicas arrive at approximately the same time relatively to a symbol period, $T_d \ll T$. In the opposite case where B and B_c are of the same order, the channel is said to be frequency-selective.

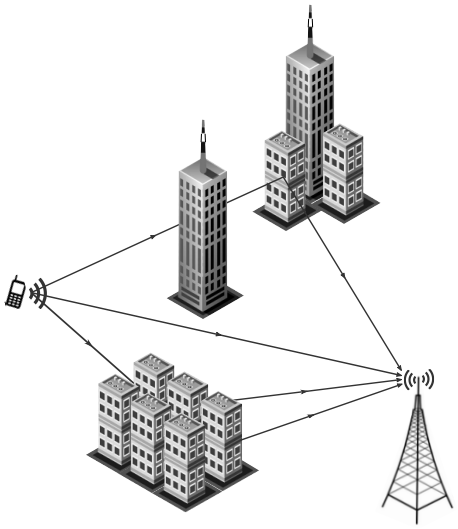

Figure I.6 – *Multipath channel propagation ($L = 4$)*

The tremendous number of degrees of freedom involved in a typical channel propagation, such as the density of obstacles, their position and velocity, makes an exact characterization of the channel variations out of reach. Most often fading is then modeled as a random process, and the coefficients h_ℓ are considered as random variables. Several statistical models can be used, depending on the spatial scale at which the fading takes place. In particular, multipath fading accounts for the small-scale variations of the channel amplitudes due to the interference of signal replicas coming from many different paths. The simplest statistical approach to multipath fading stems from Rayleigh scattering, a well-known physical phenomenon which arises when a propagating wave is scattered by a high density of objects with typical size far lower than the signal wavelength. The effect of each scatterer on the incoming wave is modeled as a random attenuation and dephasing. According to

the central limit theorem (I.25), the sum of the contributions from each scatterer follows a complex gaussian distribution. Provided there is no line of sight between the transmitter and the receiver the limiting distribution can be assumed circular-symmetric complex normal, so $h_\ell \propto \mathcal{CN}(0,1,0)$, and $|h_\ell|$ follows a Rayleigh distribution (I.15). More refined probabilistic models of multipath fading exist, such as the Nakagami distribution or the Rician fading, which occurs when a direct path exists between the emitter and the receiver [32].

The channel accounts for the input signal transformations related to the propagation conditions. Another source of impairment must be considered on the receiver side: due to impredictable radiations coming from thermal fluctuations or residual interference with other transmissions, the received signal is corrupted by a background noise, usually modeled by an additive white gaussian random process $w(t)$. Loosely speaking, $w(t)$ can be thought of as a continuous sequence of independent and identically distributed complex, circularly-symmetric normal variables. It is characterized by its power spectral density, that is the power of the background noise per unit bandwidth, which is constant and often denoted by N_0[1]. Integrating this noise model to the channel results in the Additive White Gaussian Noise (AWGN) channel model. In the case of a flat-fading channel, $h(t) = h\delta(t)$, the received signal $r(t)$ is thus given by

$$r(t) = hs(t) + w(t) \tag{I.47}$$

This model is the one we will adopt almost all along the thesis. The more realistic frequency-selective channels will be considered in Chapter IV in the context of multicarrier transmissions.

I.3.4 Demodulation

We can now turn to the crucial part of the wireless transmission, that is, recovering the input binary sequence from the received signal $r(t)$. Let us consider an input signal $s(t)$ consisting of N modulated waveforms, with N chosen so that the channel amplitude h is approximately constant over the time interval NT, *i.e.* $NT < T_c$. Equations (I.42) and (I.47) give $r(t)$ as

$$r(t) = h \sum_{n=0}^{N-1} s_n e^{2i\pi f_c t} g_T(t - nT) + w(t) \tag{I.48}$$

where $g_T(t)$ denotes the normalized rectangular pulse of duration T and amplitude $1/\sqrt{T}$. The role of demodulation is to recover the symbols c_n from $r(t)$. For the time being, let us consider that there is no channel, *i.e.* $h = 1$. The information relative to a given c_n is entirely contained in the restriction of $r(t)$ to the interval $[nT\,;\,(n+1)T[$. The irrelevant contribution of the carrier $e^{2i\pi f_c t}$ can also be removed by applying a correlator to $r(t)$, or equivalently an adaptive matched filter [29]. This results in an observed symbol r_n defined as

$$r_n \triangleq \langle g_T(t - nT)e^{2i\pi t f_c} | r(t) \rangle = \frac{1}{\sqrt{T}} \int_{nT}^{(n+1)T} r(t) e^{-2i\pi t f_c} \mathrm{d}t = s_n + w_n \tag{I.49}$$

[1] Actually the spectral power density of the white noise is constant over the bandwidth B of the emitted signal, which is assumed to be normalized to one at the receiver.

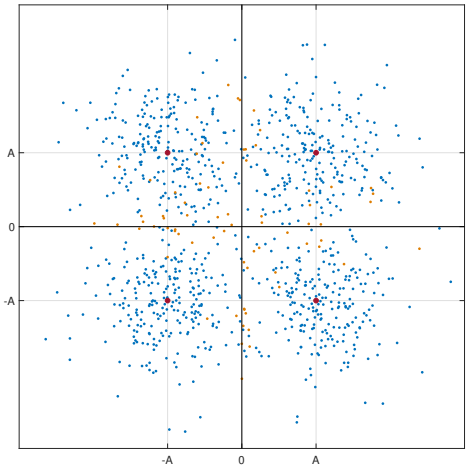

Figure I.7 – *Threshold demodulation of the QAM4. Red dots show the constellation symbols, blue dots the correctly estimated received symbols and orange dots the misdetections. Decision boundaries are indicated by the black lines.*

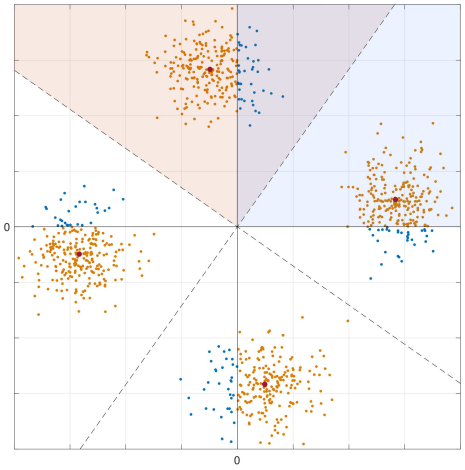

Figure I.8 – *Non equalized demodulation of a QAM4. Dashed lines represent the decisions boundaries of the transformed constellation $h\mathscr{C}$. The orange and blue shaded regions respectively show the Voronoï cells of symbols $A(1+i)$ and $hA(1+i)$.*

where $w_n \triangleq \langle g_T(t-nT)e^{2i\pi t f_c}|w(t)\rangle$ is a random variable than can be shown to follow a circular-symmetric complex normal distribution with variance N_0. Hence the observed symbols r_n are noisy realizations of the source symbols s_n, as illustrated on Fig.I.7 for a QAM4 modulation. Demodulation consists then in an estimation problem: given an observed symbol r_n, we must find an estimate $\widehat{s}_n \in \mathscr{C}$ of the actual transmitted symbol s_n. Note also that in order to apply (I.49) the receiver needs the carrier frequency f_c. We define as *coherent* modulation the situation where f_c is perfectly known at the receiver. Otherwise the modulation is referred to as *non-coherent*: the carrier frequency must be estimated by the receiver, and other types of correlators or filters can be applied to the received signal so as to account for the uncertainty of the resulting estimator. In the following we will always consider a coherent demodulation.

A natural approach for estimating s_n is to look for the MLE estimator. Because the emitted symbols are equally likely and the noise is complex normal, it can be shown that in this case the MLE is simply given by

$$\widehat{s}_n = \underset{c\in\mathscr{C}}{\operatorname{argmin}}(|r_n - c|^2) \tag{I.50}$$

Eq.(I.50) has a simple geometrical meaning: the estimate of s_n is given by the constellation symbol which is the closest to the noisy received symbol r_n. The demodulation then comes down to assigning each r_n to the closest symbol in the constellation. This is tantamount to considering for each c in $\mathscr{C}$ the region $\mathcal{V}(c)$ such that any point belonging to $\mathcal{V}(c)$ is closest to c than to any other constellation symbol. This set of regions form a partition of the complex

plane better known as a Voronoï tessellation [33]. The regions $\mathcal{V}(c)$ are called Voronoï cells, and their boundaries define the decision thresholds for assigning r_n to a given c. For this reason the demodulation defined by (I.50) is called a threshold detection or decoding. The decision thresholds of the QAM 4 are shown on Fig.I.7. In this simple case the estimation of s_n is simply based on the sign of the real and imaginary parts of r_n, and the Voronoï cells are the four principal orthants of $\mathbb{R}^2 \equiv \mathbb{C}$, so for instance $\mathcal{V}(A(1+i)) = \{z \in \mathbb{C} | z \succcurlyeq 0\}$. More generally the shape of the decision regions is determined by the geometrical structure of the constellation $\mathscr{C}$.

Because of the additive gaussian noise, the received symbol r_n may not lie in the Voronoï region of their corresponding emitted symbol s_n, *i.e.* $r_n \notin \mathcal{V}(s_n)$. This results in a misdetection, as the estimated symbol $\widehat{s}_n$ differs from the actual one. This corresponds to the orange dots in Fig.I.7. Quite intuitively, higher power noise levels are expected to result in more frequent detection errors. The quality of the demodulation is measured by the Symbol Error Rate (SER), namely the probability $P_s \triangleq \mathbb{P}(\widehat{s} \neq s)$ of a symbol misdetection. For a circularly-symmetric complex normal noise with variance N_0 and equally likely modulation symbols, P_s can be written as

$$P_s = 1 - \frac{1}{M}\sum_{m=1}^{M} \mathbb{P}(r \in \mathcal{V}(c_m) | s = c_m) = 1 - \frac{1}{M}\sum_{m=1}^{M} \int_{\mathcal{V}(c_m)} e^{-|z-c_m|^2/N_0} \frac{\mathrm{d}z}{\pi N_0} \tag{I.51}$$

where we used the law of total probability on the discrete random variable s. In general P_s does not admit a closed-form expression, except for some specific constellations such as the regular QAMs. In this case Eq.(I.51) reads

$$P_s = \frac{2(\sqrt{M}-1)}{\sqrt{M}} \operatorname{erfc}\left(\sqrt{\frac{3\log_2(M)}{2(M-1)}\frac{E_b}{N_0}}\right)\left[1 - \frac{1}{2}\frac{(\sqrt{M}-1)}{\sqrt{M}} \operatorname{erfc}\left(\sqrt{\frac{3\log_2(M)}{2(M-1)}\frac{E_b}{N_0}}\right)\right] \tag{I.52}$$

The result of P_s is often expressed in terms of the ratio E_b/N_0, which mesures the received Signal to Noise Ratio (SNR) per bit, that is the relative proportion of informative signal compared to the background noise. The theoretical SER curves of several regular QAMs are presented on Fig.I.52. As can be seen, larger constellations result in a higher symbol error probability. This is the counterpart of the higher transmission rate gain achieved by these constellations, since they encode longer binary words in the same duration T.

The modulation symbols being coded representations of binary words, one can also measure the Bit Error Rate (BER), or probability P_b of a wrong bit detection. There is in general no exact formula relating P_b and P_s, as the number of misdetected bits for a given symbol error depends on the precise relation between the symbols and the binary words. There is one particular coding however that allows to minimize the BER in most circumstances, namely the Gray coding. It consists in mapping the binary words to the constellation symbols in such a way that, between any pair of neighbouring symbols, the associated binary words differ by only one bit. As in case of a wrong symbol estimation the actual and estimated symbols are more likely to be neighbours of each other, we can then reasonably expect that

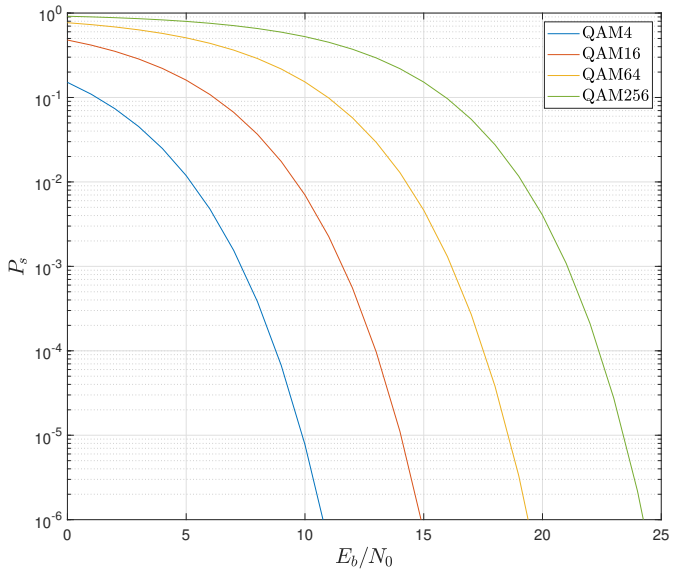

Figure I.9 – *Probability of symbol error for several regular QAM constellations.*

for a moderate noise power, a symbol misdetection most often results in a single bit error. The probability of a bit misdetection is then approximately given by

$$P_b \simeq \frac{P_s}{\log_2(M)} \tag{I.53}$$

All the previous discussion was based on a transmission without any channel. Introduction of the channel has a determinant impact on the demodulation scheme, as the received symbols now read

$$r_n = hs_n + w_n \tag{I.54}$$

Compared to (I.49), the observed symbols are centered around the complex-scaled constellation $h\mathscr{C}$. The effect of h on $\mathscr{C}$ is a scaling by $|h|$ and a rotation by $\mathrm{Arg}(h)$. Applying without any modification the previous threshold detection will result in a catastrophic misdetection probability. This can be seen on Fig.I.8, with most of the symbols being incorrectly estimated. This is because the Voronoï cells of the transformed constellation are given by $\mathcal{V}(hc) = h\mathcal{V}(c)$, so only the received symbols belonging to the intersection sets $\mathcal{V}(c) \cap \mathcal{V}(hc)$ are mapped to the correct symbol c. Consequently, in order for the threshold detection to apply the receiver must compensate the effect of h on the received signal. This is called signal equalization, and the knowledge of the channel is called the Channel State Information (CSI). Unlike information relative to the emitted signal, such as the carrier frequency or the modulation scheme, that can be considered as shared by both the transmitter and receiver, the channel is unknown at both sides of the transmission, so there is no other choice for the receiver but to estimate it. There are essentially two classes of estimation methods to acquire the CSI:

- pilot-based estimation strategies rely on the transmission of a predefined sequence of symbols, called pilots, prior to the actual signal. The pilot sequence is known by the

receiver, so it can be demodulated and compared to the expected sequence to derive an estimation of the channel coefficients. Other pilots are regularly transmitted so as to account for the temporal variation of the channel. By an appropriate design of the pilots, this method can result in accurate estimation of the CSI. It implies however a loss in the useful data rate as the pilots do not carry any information on the transmitted signal.

- blind estimation methods on the opposite only rely on the received signal to estimate the channel. Prior information on the channel statistics, when available, may be used as well to improve the accuracy of the resulting estimators.

I.4 Conclusion and main assumptions

In this introductory chapter the essential statistical tools underlying wireless communications were reviewed, and fundamentals of modulations, channel fading and symbol detection were presented. At this stage and before proceeding any further, it is worthwhile to summarize the assumptions made on the transmissions that will be considered all along the thesis:

- the input waveform consists in a sequence of N independent and identically distributed source symbols s_n linearly modulating a carrier of known frequency f_c, and transmitted at the known symbol period T;
- the common distribution of the source symbols s_n is discrete uniform, of support the modulator constellation $\mathscr{C}$ with M symbols, so $\mathbb{P}(s_n = c) = \frac{1}{M}$ for all $c \in \mathscr{C}$. The constellation is known at the receiver and can be either an ASK, a PSK or a regular QAM. $\mathscr{C}$ exhibits the complex conjugate symmetry and discrete rotational invariance of order q;
- the propagation channel is assumed to be flat-fading and to vary slowly enough with time to be considered as constant over the whole transmission, *i.e.* $NT < T_c$. Within these assumptions the channel is modeled by a single coefficient h. When neccessary, the statistical model considered for h is the Rayleigh fading: h then follows a zero-mean, circularly-symmetric complex normal distribution with unknown variance σ_h^2;
- the signal is corrupted by an additive white gaussian noise $w(t)$ with power spectal density N_0. N_0 is not supposed to be known by the receiver;
- the unknown channel h is blindly estimated at the receiver: no pilot symbols are transmitted;
- the received signal is coherently demodulated by threshold detection of the observed corrupted symbols r_n given by (I.54). The noise samples w_n follow a circularly-symmetric complex normal distribution with variance N_0.

Blind channel estimation stands at the core of this thesis. It will first be discussed in the context of single-user transmissions in the next chapter. The results and methods derived therein will be then extended to multiuser blind detection in Chapter III, and to multicarrier transmissions in Chapter IV.

Chapter II

Single-user blind detection

Contents

II.1 Introduction

II.1.1 Point-to-point transmission

We begin our study with the simplest wireless transmission model, namely the Single-Input Single-Output (SISO) transmission in a flat-fading environment. In this model, the channel h is reduced to a single complex coefficient which multiplies the incoming symbols. Addition of a cicularly-symmetric complex normal noise with variance N_0 leads to the following expression for the n-th received symbol r_n:

$$r_n = hs_n + w_n \tag{II.1}$$

where s_n are the source symbols, assumed to belong to a finite constellation $\mathscr{C}$ with discrete uniform distribution over its M symbols. As we have seen in the previous chapter, applying a threshold decoding to (II.1) without taking into account the channel results in catastrophic error rates, making channel estimation necessary. Actually, estimating the channel in such a simple case as (II.1) is of little interest, as blind identification of the more general SISO frequency-selective channel is already well-covered in the literature [34]. In Section II.4 we will see an example of a very simple estimator of the SISO flat-fading channel derived from the method of moments.

Our objective in this chapter is more related to the study of the algorithm that will serve as the very basis for the later multiuser blind detection problem. Specifically, the general approach we will adopt for channel and symbol estimation is that of Maximum Likelihood (ML). As we have seen in Chapter I, for equally likely constellation symbols the ML estimation of the emitted symbols comes down to the Voronoï classification of the received symbols. This step is actually reminiscent of a reference clustering algorithm known as k-means [35][1]. More precisely, it appears that the joint ML estimation of h and $\mathbf{s} \triangleq (s_1, \cdots, s_N)$ can be seen as a constrained k-means clustering problem, as is explained in the following.

II.1.2 Blind channel estimation by the k-means algorithm

In [36] a clustering approach to blind channel estimation was proposed in the context of distributed co-phasing transmissions, consisting in a geometrically constrained version of the well-known k-means algorithm. Specifically, while in the original algorithm the centroïds (= centers of the data clusters) can be anywhere in the data space, here the symbols belong by definition to a given constellation with a specific structure. Accounting for this constraint leads to the following modified cost function

$$J(h, \mathbf{s}) = \sum_{n=1}^{N} |r_n - h s_n|^2 = \| \mathbf{r} - h\mathbf{s} \|^2 \tag{II.2}$$

with $h \in \mathbb{C}$ and $\mathbf{s} \in \mathscr{C}^N$ (here h and $\mathbf{s}$ are dummy variables and are not to be confused with the actual channel and actual emitted symbols). The k-means algorithm iteratively minimizes (II.2) by alternating two steps, namely estimation of the centroïds location and assignment of the data points to clusters by Voronoï tessellation. In its constrained variant the former step is readily obtained as

$$\widehat{h}_t = \frac{\sum_{n=1}^{N} (\widehat{s}_n)_{t-1}^* r_n}{\sum_{n=1}^{N} |(\widehat{s}_n)_{t-1})|^2} = \frac{\langle \widehat{\mathbf{s}}_t | \mathbf{r} \rangle}{\| \widehat{\mathbf{s}}_t \|^2} \tag{II.3}$$

where $\widehat{h}_t$ and $\widehat{\mathbf{s}}_{t-1}$ respectively denote the estimated channel and emitted symbols at iteration t and $t-1$. The assignment step comes down to the usual threshold demodulation (I.50) based on the current channel estimator $\widehat{h}_t$

$$(s_n)_t = \underset{c \in \mathscr{C}}{\operatorname{argmin}} \left(|r_n - \widehat{h}_t c| \right) \tag{II.4}$$

[1] In this thesis, "the" k-means algorithm actually refers to the iterative procedure proposed in [35] to solve the k-means problem. While this approach is not the only one it is certainly the most widespread, hence this misuse of language is very comon in the literature.

It turns out that the proposed constrained k-means algorithm is actually a particular case of a more general blind estimation multiuser technique known as Iterative Least Squares with Enumeration (ILSE) [5]. This algorithm will be at the core of the next chapter, so we will not present it here, but as it encompasses the algorithm presented in [36] it seems more appropriate for consistency to use the name of the more general method. To emphasize that we are here in the particular case of a single source signal and a single receiver, we will refer to this algorithm as the SISO-ILSE algorithm.

As a variant of k-means, the SISO-ILSE approach exhibits the same general features. In particular, the sequence $(\widehat{h}_t, \widehat{\mathbf{s}}_t)$ can be shown to systematically converge to a fixed point of the algorithm: that is, from a given t_* the channel estimation step (II.3) maps $\widehat{h}_{t_*}$ to $\widehat{\mathbf{s}}_{t_*}$ and similarly the threshold decoding (II.4) maps $\widehat{\mathbf{s}}_{t_*}$ to $\widehat{h}_{t_*}$. The couple $(\widehat{h}_{t_*}, \widehat{\mathbf{s}}_{t_*})$ is a minimum of the cost function (II.2). The main limitation of the k-means approach is that most often there are several such fixed points, and only one or a few of them achieve the global minimum of J. In other words the function is not jointly convex in $(\mathbf{h}, \mathbf{s})$ and the algorithm may converge to spurious local minima. Forasmuch as the final fixed point entirely depends on the initial state h_0 or $\mathbf{s}_0$ provided to the algorithm, the usual way of circumventing this indesirable behavior is to test the algorithm on several, usually random, initial points, and retain the solution achieving the lowest cost function at convergence, $J(\widehat{h}_{t_*}, \widehat{\mathbf{s}}_{t_*})$. This naïve strategy is often considered as sufficient in many applications, but has in general no guarantee of succeeding and induces a computational loss. Consequently, in situations where the number of fixed points makes the random strategy unfruitful or the delay requirements of the application are prohibitive, it becomes crucial to provide k-means with appropriate initialization techniques or prior information about potential spurious fixed points.

This chapter is devoted to the design of such initialization strategies in the reduced-complexity framework provided by the point-to-point transmission. In this simple setting the degrees of freedom of the symbol locations, or centroïds, reduce to a single complex coefficient, namely the channel h. We can thus expect reliable methods for ensuring convergence of the SISO-ILSE algorithm towards its global minimum to exist. We will be interested in two types of initializations:

- methods based on the data and designed to provide the algorithm with a suitable initial state, whether it be a channel estimate or an initial symbol assignment;
- methods based on a priori knowledge of the structure and position of particular local minima.

II.2 Hierarchical k-products algorithm

II.2.1 The k-products algorithm

In [37], an alternative approach to the traditional k-means clustering algorithm was introduced. The method, called k-products, aims at estimating the means c_m of a mixture of

M unspecified complex distributions based on an observation sample $\mathbf{z}$ of size N. This is achieved by minimizing the following positive cost function

$$J_{KP}(\mathbf{u};\mathbf{z}) \triangleq \sum_{n=1}^{N}\prod_{m=1}^{M}|z_n-u_m|^2 \tag{II.5}$$

where $\mathbf{u}\in\mathbb{C}^M$. The name k-products stems from the fact that J_{KP} is formally identical to the k-means cost function with the sum over the centroïds replaced by products. The motivation for this choice is that, for a noiseless mixture, there is necessarily one integer m such that $z_n = c_m$, so at $\mathbf{u}=\mathbf{c}$ all products in (II.5) are exactly zero and $J_{KP}=0$. For non-zero noises one can thus expect that at $\mathbf{u}=\mathbf{c}$ each product has one of its factor very close to zero so $J_{KP}(\mathbf{c};\mathbf{z})$ should be close to its minimum.

The core interest of the k-products approach is that it can be turned into a convex optimization problem on the set of equivalence classes $\mathbb{C}^M/\mathcal{S}_M$, where $\mathcal{S}_M$ denotes the set of permutations of M elements. More specifically, the authors showed that minimization of J_{KP} reduces to finding the roots of a complex polynomial of degree M, whose coefficients $(v_1,\cdots,v_M)\triangleq\mathbf{v}$ are the solution to

$$\mathbf{M}\mathbf{v}=\mathbf{m} \tag{II.6}$$

where $\mathbf{M}$ and $\mathbf{m}$ are the $M\times M$ matrix and $M\times 1$ vector of sample moments of the random mixture variable Z, respectively defined by $\mathbf{M}_{jk}\triangleq\overline{\mu}_k^j(Z)$ and $\mathbf{m}_j\triangleq\overline{\mu}_K^j(Z)$ with the moment notations introduced in Section I.1.2. The matrix $\mathbf{M}$ can be shown to be non-singular (see apendix A of [37]), so the solution to (II.6) is unique, and the roots of the resulting polynomial provide, up to permutations, the estimation of the mixture components means $\mathbf{c}$. The computational complexity of the algorithm is in $\mathcal{O}(NM)$.

Convexity of the k-products represents a very appealing feature for a clustering algorithm. The cost for this property, however, is that the mimimum of J_{KP} yields a biased estimator of the mixture components means, *i.e.* $\mathbb{E}[\widehat{\mathbf{c}}]\neq\mathbb{E}[\mathbf{c}]$. Loosely speaking, the value of each product in (II.5) is the result of a balance between the contribution from the closest mixture component of z_n, for which the distance is minimal, and the other components, which may lie far from z_n. Hence the minimum of the overall product is not necessarily achieved next to the closest component, as it is "attracted", so to speak, by the other components.

In regard to these two properties, the k-products algorithm can be thought of as the counterpart of the k-means approach: the unbiasedness and non-global nature of the latter transpose to biasedness and convexity for the former. This makes k-products, in addition to its reduced complexity, a natural candidate to use as an initial estimation step for k-means. We can thus reasonably expect the same strategy to apply to the SISO-ILSE algorithm. It turns out that, while for free clusters the biased centroïds provided by k-products are in many cases close enough to the actual ones, introducing symmetry and regularity in the centroïds locations generally has a catastrophic impact on the bias.

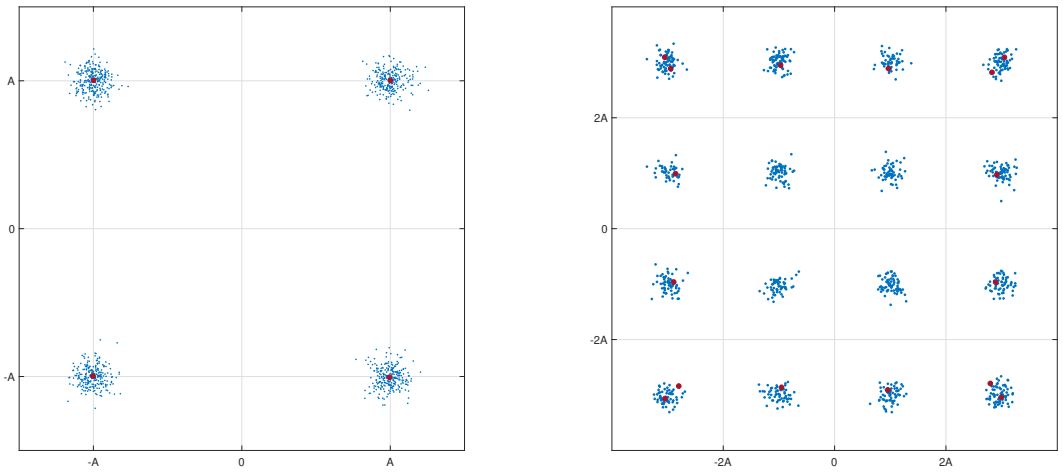

Figure II.1 – *Representative outcome of k-products on a QAM 4 (left) and a QAM 16 (right). Blue dots correspond to the received symbols and red dots to the estimated centroïds.*

As a manifest illustration of this statement, we consider on Fig.II.1 the result of the k-products on a QAM 4 and a QAM 16, respectively. In the first case we see that the estimated constellation symbols coincide almost perfectly with the actual ones. More generally, it appears that for PSK modulations the k-products algorithm performs quite well in finding the symbols location. The situation is radically different in the QAM 16 case: the resulting estimators are all located close to the outer square symbols of the constellation. In particular, the algorithm places two centroïds for each corner symbol, so that the inner square symbols are completely ignored. With the qualitative argument provided earlier to account for the bias, in this case the outer symbols attract the centroïds to the point of leaving the inner clusters empty. Note that this phenomenon is not due to a particularly unfavorable observed sample, and is characteristic of the algorithm for this constellation. Applying k-products to a QAM 64 results in an even worse estimation, with less than half of the centroïds correctly estimated. A similar behavior can also be observed on ASK modulations, with the outmost symbols exercing more and more attraction on inner symbols as the size of the constellation increases. This is a quite expectable resemblance, as QAM are constructed from ASK constellations. As a consequence, except for PSK modulations, straight application of the k-products algorithm is not a reasonable initialization strategy for the SISO-ILSE, and modifications of the original method are necessary to make this approach relevant for constellations associated with linear modulations.

II.2.2 The hierarchical k-products algorithm

QAM constellations, or equivalently ASK, exhibit an interesting structural property in addition to conjugation and rotational symmetry in that they are recursively built from a single PSK constellation. Specifically, a (regular) QAM with $M = 4^p$ symbols can be decomposed into a QAM with $4^{(p-1)}$ symbols and a QAM 4. This can be shown directly from the generic expression of the QAM symbols c_m, see I.3.2. Assuming $A = 1$ for simplicity we

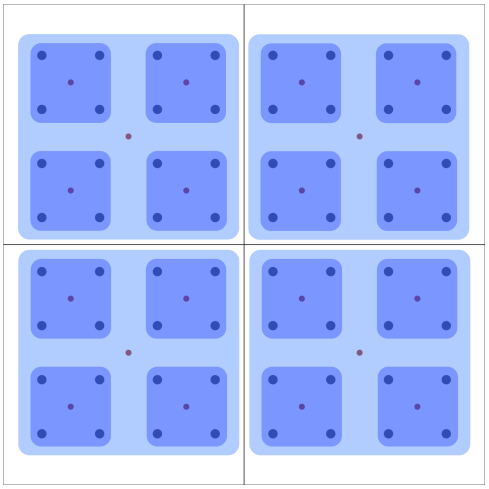

Figure II.2 – *Recursive decomposition of a QAM 64 as four QAM 16 or sixteen QAM 4. Smaller dots indicate the origin of each sub-constellation.*

have

$$\begin{aligned} c_m &= (2m_1 + 1 - 2^p) + i(2m_2 + 1 - 2^p) \\ &= 2\underbrace{\left[(2a_1 + 1 - 2^{p-1}) + i(2a_2 + 1 - 2^{p-1})\right]}_{\in \mathrm{QAM}\, 4^{p-1}} + 2^{p-1}\underbrace{\left[(2b_1 - 1) + i(2b_2 - 1)\right]}_{\in \mathrm{QAM}\, 4} \end{aligned} \tag{II.7}$$

where $a_j \in \{0, \cdots, 2^{p-1}\}$ and $b_j \in \{0, 1\}$ respectively denote the quotient and remainder of the Euclidean division of m_j by 2, *i.e.* $m_j = 2a_j + b_j$. Hence, recursively applying (II.7) shows that a QAM 4^p is given by a linear combination of p independent QAM 4 constellations as

$$\mathscr{C} = \sum_{j=1}^{p} 2^{p-j}\mathscr{C}_4 = \{\textstyle\sum_{j=1}^{p} 2^{p-j} c_{m_j} | c_{m_j} \in \mathscr{C}_4\} \tag{II.8}$$

where $\mathscr{C}_4$ denotes the QAM 4 constellation. As an immediate consequence of (II.8), any QAM 4^p can be decomposed into two independent QAM with 4^{p_1} and 4^{p_2} symbols, with $p = p_1 + p_2$. For instance, a QAM 64 can be decomposed as the sum of a QAM 16 with scaling factor 2 and a QAM 4, or as the sum of a QAM 4 with scaling factor 4 and a QAM 16, as illustrated on Fig.II.2. The same results readily apply to the ASK constellations with BPSK replacing the QAM 4 in (II.8).

The recursive property of QAM constellations suggests the following modification to the k-products algorithm: since the method yields good results on PSK modulations, we can expect that, by applying it to a dataset of received QAM M symbols with $M = 4^p$ *as if* it was a QAM 4, the estimated centroïds will be close to the centers of the four QAM 4^{p-1} in the decomposition (II.7). In other words we cluster the data in four coarse clusters according to a QAM 4, ignoring their internal structure. Then, we can repeat the same procedure to cluster each of the four obtained QAM 4^{p-1} constellations in four QAM with 4^{p-2} symbols, and so forth until the full decomposition (II.8) in p QAM 4 has been achieved. The clustering

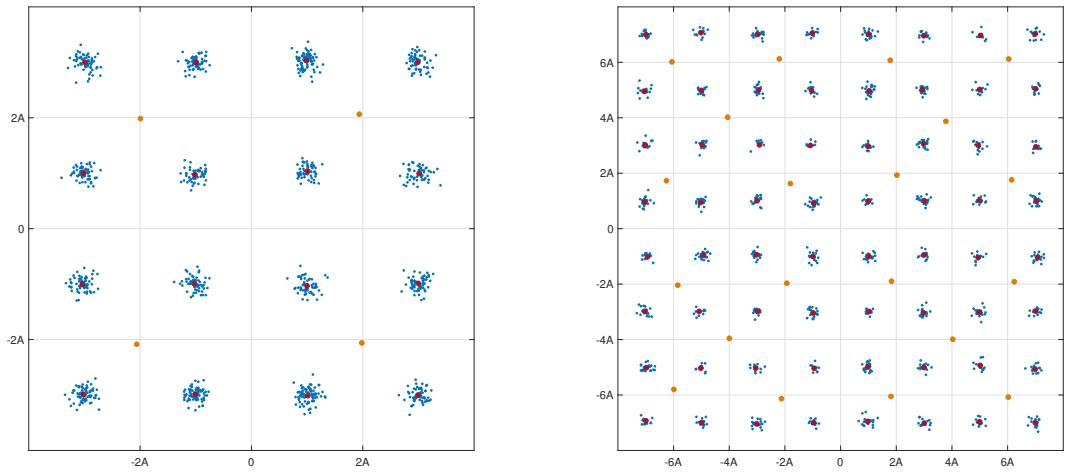

Figure II.3 – *Outcome of the hierarchical k-products algorithm on a QAM16 (left) and a QAM64 (right). Red dots indicate the final centroïds and orange dots the result of the intermediary steps.*

itself at a given step is done by a threshold detection of the data based on the estimated centers of the current sub-constellations. We call this modified k-products algorithm the hierarchical k-products, as a reference to the class of divisive hierarchical clustering algorithms, which iteratively split clusters into smaller ones starting from a single global cluster.

Fig.II.3 shows the results of applying the hierarchical k-products clustering to a QAM16 and a QAM64. As can be seen in both cases all the centroïds are now close to the actual constellations symbols. We notice that the intermediary centers returned by the algorithm do not always coincide very well with the expected ones. Yet, as long as the threshold detection is able to correctly cluster most of the data, this bias has a negligible impact on subsequent iterations.

The complexity of the hierarchical k-products algorithm can be obtained as follows: at the first step, we perform a single k-products on the full dataset with 4 clusters, so the complexity is in $\mathcal{O}(4N)$. The subsequent threshold decoding requires computations of the distances between each data point and each centroïd, which results in a complexity in $\mathcal{O}(4N)$ as well. For the second step, 4 k-products are applied to the four data clusters obtained in step 1, the size of which can be considered as $N/4$ (this hypothesis has no consequence on the final result). The computational load of the centroïd estimation step is then $4\mathcal{O}(4N/4) = \mathcal{O}(4N)$. The clustering step, being carried out on the same data subsets, is also in $\mathcal{O}(4N)$. Iterating in this fashion we see that each recursion has the same complexity $\mathcal{O}(8N)$, so the overall cost of the algorithm is given by $p\mathcal{O}(8N) = \mathcal{O}(Np)$. This is to be compared with the complexity $\mathcal{O}(N4^p)$ of a single k-products with 4^p clusters. Hence, making use of the special recursive structure of QAM contellations in the k-products approach both allows a fairly accurate estimation of all the symbols and a reduction in the overall computational load.

We have successfully modified the k-products algorithm to provide a meaningful, low computational initial estimation of the constellation symbols. From there, by threshold decoding a first estimation of the emitted symbols is obtained, which can be used as an initial state of the SISO-ILSE algorithm for refinement. Finally, although all the above discussion and presented figures made the assumption of no propagation channel, $h = 1$, introduction of an unknown channel does not require any modification of the algorithm since

$$J_{KP}(\mathbf{u};\mathbf{r}) = h^M \sum_{n=1}^{N} \prod_{m=1}^{M} |s_n + w_n/h - u_m/h|^2 = h^M J_{KP}(\mathbf{u}';\mathbf{s}') \tag{II.9}$$

with $u'_m \triangleq u_m/h$ and $s'_n \triangleq s_n + w_n/h$.

II.3 Local minima of the SISO-ILSE algorithm

The study of the fixed points of the general k-means algorithm is made extremely difficult by the fact that the centroïds are completely unconstrained, so the number of degrees of freedom is large. Several seeding strategies for the initial points to provide to the algorithm have been studied, the most well-known being the k-means++ algorithm, [38]. In the case of the SISO-ILSE, the location of the centroïds only depends on a complex parameter – the channel h –, and the geometrical structure of the constellation $\mathscr{C}$. As the most commonly used constellations are of only three types, in this simplified framework it may be possible to infer the location of some potential fixed points. This prior information is of great interest, as it can be used to design strategies for preventing the algorithm from converging to spurious solutions.

II.3.1 General results

All three types of constellations commonly used in wireless modulations exhibit some symmetries. It is thus natural to expect the fixed points of the SISO-ILSE algorithm to observe a regular structure as well. In the following we give a first insight of how symmetry of the constellation and symmetry of the fixed points are related. To do so it is first useful to rewrite the SISO-ILSE cost function as

$$J(h,\mathbf{s}) = \sum_{n=1}^{N} \left|r_n - hc_{I(n)}\right|^2 \equiv J(h,\mathbf{I}) \tag{II.10}$$

where $I(n) \in \{1,\cdots,M\}$ is a random variable indicating the label of the constellation symbol corresponding to s_n, *i.e.* $s_n = c_{I(n)}$. The cost function J is equivalently described by the variables $(h,\mathbf{s})$ or $(h,\mathbf{I})$. From now on, the actual channel and emitted symbols indicator function will be respectively denoted by h and I, so that $r_n = hc_{I(n)} + w_n$.

Most of the discussion on the SISO-ILSE fixed points will be made for zero noise and in the limit of large sample sizes. The former assumption implies that all received symbols

emitted from the same constellation symbol, say c_m, are mapped to a same given symbol c'_m by threshold decoding. The corresponding indicator function $I'(n)$ is then fully characterized by a mapping $g : \mathscr{C} \mapsto \mathscr{C}$ such that $c_{I'(n)} = g(c_{I(n)})$, or, equivalently, by a mapping $g' : \{1, \cdots, M\} \mapsto \{1, \cdots, M\}$ such that $c_{I'(n)} = c_{g'(I(n))}$. For simplicity we denote both mappings with the same notation g, *i.e.* $g(c_{I(n)}) \equiv c_{g(I(n))}$. In the limit $N \to \infty$, the channel estimation step (II.4) then reads

$$\widehat{h} = \frac{\sum_{n=1}^{N} c^*_{I'(n)} h c_{I(n)}}{\sum_{n=1}^{N} |c_{I'(n)}|^2} = h \frac{\sum_{m=1}^{M} f_m c^*_{g(m)} c_m}{\sum_{m=1}^{M} f_m |c_{g(m)}|^2} \underset{N\to\infty}{\to} h \frac{\mathbb{E}\left[g^*(C)C\right]}{\mathbb{E}\left[|g(C)|^2\right]} \tag{II.11}$$

where C is the random variable from which the emitted symbols c_n are drawn, $\mathscr{C}$ being the support of its pdf, and $f_m \triangleq \frac{|I^{-1}(\{m\})|}{N}$ is the empirical frequency of symbol c_m, which by the law of large number converges in probability to $\mathbb{P}(C = c_m) = \frac{1}{M}$, since the symbols are assumed equally likely. In the following we examine (II.11) for several mappings g induced by the symmetries of the constellation.

Discrete rotational symmetry

The simplest symmetry to consider is the discrete rotational invariance of $\mathscr{C}$ of order q. In this case we do not need to assume a zero noise, neither a uniform distribution for the emitted symbols. Let us assume that h_1, defines a fixed point of the SISO-ILSE algorithm, with associated indicator function I_1, and consider the channel predictor defined by $h_2 \triangleq e^{\frac{2i\pi k}{q}} h_1$, with $k \in \{1, \cdots, q\}$. Then h_2 is also a fixed point of the algorithm, with indicator function I_2 defined by $c_{I_2(n)} \triangleq e^{\frac{-2i\pi k}{q}} c_{I_1(n)}$. First, given I_2 we have

$$\widehat{h} = \frac{\sum_{n=1}^{N} c^*_{I_2(n)} r_n}{\sum_{n=1}^{N} |c_{I_2(n)}|^2} = \frac{\sum_{n=1}^{N} e^{\frac{2i\pi k}{q}} c^*_{I_1(n)} r_n}{\sum_{n=1}^{N} |c_{I_2(n)}|^2} = e^{\frac{2i\pi k}{q}} \frac{\sum_{n=1}^{N} c^*_{I_1(n)} r_n}{\sum_{n=1}^{N} |c_{I_1(n)}|^2} = e^{\frac{2i\pi k}{q}} h_1 = h_2 \tag{II.12}$$

so the channel estimation based on the indicator function I_2 indeed yields h_2. Now, it is easy to see that threshold decoding of the received symbols based on the transformed constellation $h_2\mathscr{C}$ gives the indicator function I_2 since

$$c_{I_2(n)} = \underset{c\in\mathscr{C}}{\arg\min} \left(|r_n - c\, h_2|\right) = \underset{c\in\mathscr{C}}{\arg\min} \left(|r_n - c\, e^{\frac{2i\pi k}{q}} h_1|\right) = c_{I_1(n)} e^{\frac{-2i\pi k}{q}} \tag{II.13}$$

By definition, I_2, equivalently h_2, is then a fixed point of the algorithm. Consequently, for any constellation with discrete rotational symmetry the set of fixed points exhibits the same invariance. It actually turns out that, for PSK modulations with zero-noise, the set generated by h and the discrete rotational symmetry is the only equivalence class of fixed points of the algorithm. This is because, for any initial point h_0, the threshold decoding and channel estimation necessarily result in $\widehat{h} = e^{\frac{2i\pi k_0}{q}} h$ with $k_0 \in \{1, \cdots, q\}$ the integer minimizing $|h - e^{\frac{2i\pi k_0}{q}} h_0|$. Consequently, for any PSK modulation, up to permutations and in the noise-free case, the SISO-ILSE algorithm has a single fixed point. This has a strong implication since it means the algorithm will always converge to one of its equivalent global

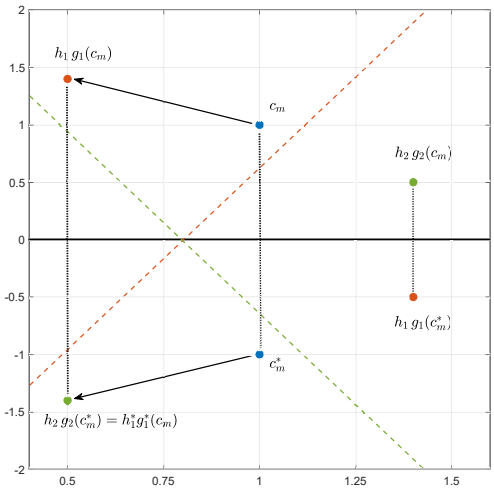

Figure II.4 – *Illustration of the conjugate mapping. Dashed lines represent decision boundaries.*

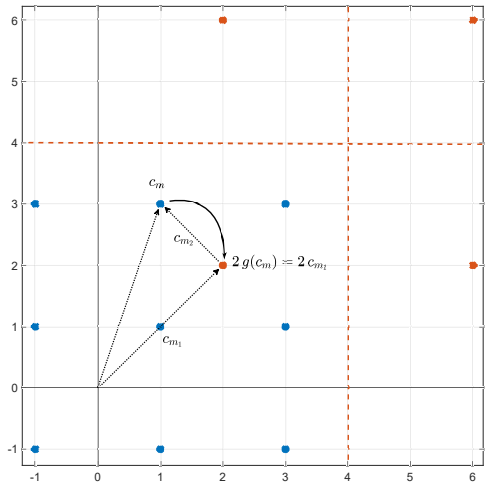

Figure II.5 – *Illustration of the recursive mapping for the QAM16.*

minima, regardless of the initial state. A sufficient condition for this property to hold in non-zero noise scenarios would be for the noise not to influence the assignment of the received symbols to the constellation symbols, so that $c_{I'(n)} = g(c_{I(n)})$ for any $n \in \{1, \cdots, N\}$ as in the zero-noise case.

Symmetry by complex conjugation

A similar, yet more restrictive result can be obtained for complex conjugation symmetry. It requires C and C^* to have the same pdf, *i.e.* $\mathbb{P}(C = c_m) = \mathbb{P}(C = c_m^*)$ for any $m \in \{1, \cdots, M\}$, which is in particular verified for uniformly distributed symbols. Then, if h_1 is a fixed point of the SISO-ILSE algorithm with indicator function characterized by mapping g_1, $h_2 \triangleq h\frac{h_1^*}{h^*}$ is also a fixed point of the algorithm with associated mapping g_2 defined by $g_2(C) \triangleq g_1^*(C^*)$. From (II.11) we have indeed

$$\widehat{h} = h\frac{\mathbb{E}\left[g_2^*(C)C\right]}{\mathbb{E}\left[|g_2(C)|^2\right]} = h\frac{\mathbb{E}\left[g_1(C^*)C\right]}{\mathbb{E}\left[|g_1^*(C^*)|^2\right]} = h\frac{\mathbb{E}\left[g_1^*(C)C\right]^*}{\mathbb{E}\left[|g_1(C)|^2\right]} = h\frac{h_1^*}{h^*} \tag{II.14}$$

It is then not difficult to check that threshold decoding with $\widehat{h} = h_2$ results in the indicator function induced by mapping g_2, as is schematized on Fig.II.4. Unlike the previous case here the result only holds in probability: given a fixed point h_1, the probability that $h\frac{h_1^*}{h^*}$ is also a fixed point tends to 1 as the sample size N grows.

Recursive symmetry

In the previous section we have seen that any QAM constellation with $M = 4^p$ symbols can be decomposed as p QAM 4 with scaling factors given by powers of two, Eq.(II.8). This decomposition affects the support $\mathscr{C}$ of the pdf of C. Now, in the case of equally likely

symbols, the recursive property of QAM holds for the variable C itself. That is, if C is distributed according to a discrete uniform distribution with support a QAM M and $M = 4^p$, then C can be decomposed as

$$C = \sum_{j=1}^{p} 2^{p-j} C_j \tag{II.15}$$

where the C_j's are independent random variables following a discrete uniform distribution with support a QAM 4. This is a consequence of the fact that the sum of independent and uniform random variables with disjoint supports is also uniform. From (II.15) C can also be expressed as

$$C = 2^{p_1} C_1 + C_2 \tag{II.16}$$

where C_1 and C_2 are independent variables following a uniform QAM 4^{p_1} and QAM 4^{p-p_1} distribution, respectively. Let us consider then the mapping g defined by $g(C) = C_1$. Eq.(II.11) thus reads

$$\widehat{h} = h \frac{\mathbb{E}\left[C_1^*(2^{p_1} C_1 + C_2)\right]}{\mathbb{E}\left[|C_1|^2\right]} = h \frac{2^{p_1}\mathbb{E}\left[|C_1|^2\right] + \mathbb{E}\left[C_1^* C_2\right]}{\mathbb{E}\left[|C_1|^2\right]} = 2^{p_1} h \tag{II.17}$$

since C_1 and C_2 are independent and have zero-mean. One can also check that threshold decoding based on $2^{p_1}h$ results in mapping g, *i.e.* $g(c_m) = g(2^{p_1} c_{m_1} + c_{m_2}) = c_{m_1}$ with $m_1 \in \{1, \cdots, 4^{p_1}\}$ and $m_2 \in \{1, \cdots, 4^{p-p_1}\}$. Fig.II.5 provides an illustration for the QAM 16 case. We have thus shown that for QAM constellations, $2^p h$ with $p \in \left\{1, \cdots, \frac{\log_2(M)}{2}\right\}$ defines a set of fixed points of the SISO-ILSE algorithm in the noise-free case and in the limit of large sample sizes. The same result holds for ASK modulations with $p \in \{1, \cdots, \log_2(M)\}$.

II.3.2 Case study: the QAM 16

Let us illustrate the previous results on a specific example. Among the three usual linear modulation schemes, QAM constellations have the richer structure. Besides we have seen that for PSK modulations there is essentially one single fixed point. Hence the simplest non trivial constellation we can consider is the QAM 16. In this case it is possible to completely characterize the set of fixed points in the large samples limit and zero-noise assumption. First, the rotational symmetry of order $q = 4$ and complex conjugation invariance allow us to restrict our search to the subset $\mathcal{S} \triangleq \{z \in \mathbb{C} | 0 \leq \mathrm{Arg}(z) \leq \pi/4\}$. We also know from the constellation recursive structure that h and $2h$ are fixed points of the SISO-ILSE algorithm. In addition to these we can find four other fixed points given in Table II.1 along with their associated mapping g.

$g(\mathscr{C})$	$\frac{7+5i}{8}h$	$\frac{17+9i}{20}h$	$\frac{8+3i}{8}h$	$\frac{13+7i}{12}h$
$g(1+i)$	$1+i$	$1+i$	$1+i$	$1+i$
$g(1+3i)$	$3+i$	$3+3i$	$1+3i$	$1+i$
$g(3+i)$	$3-i$	$3-i$	$3-i$	$3-i$
$g(3+3i)$	$3+i$	$3+i$	$3+i$	$3+i$

Table II.1 – *Non trivial fixed points of SISO-ILSE for a QAM* 16.

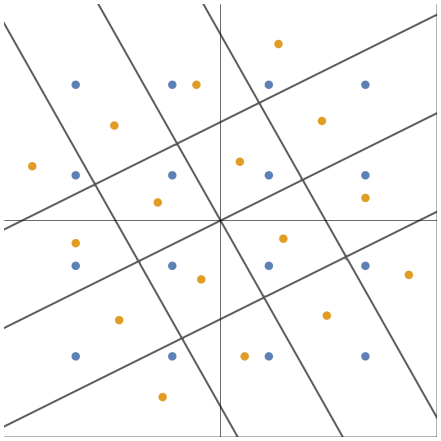

Figure II.6 – *Threshold detection of a QAM16 with* $h' = \frac{17+9i}{20}$ *(*$h = 1$*).*

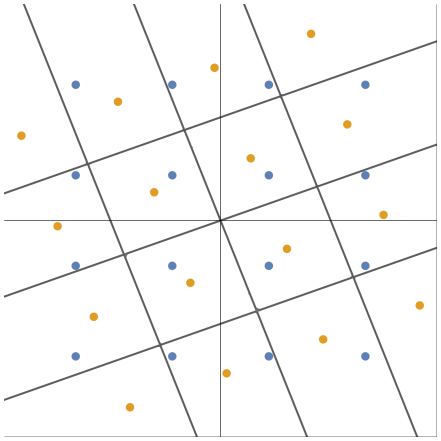

Figure II.7 – *Threshold detection of a QAM16 with* $h' = \frac{8+3i}{8}$ *(*$h = 1$*)*

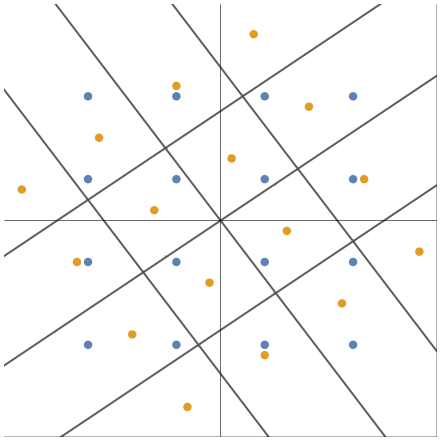

Figure II.8 – *Threshold detection of a QAM16 with* $h' = \frac{7+5i}{8}$ *(*$h = 1$*)*

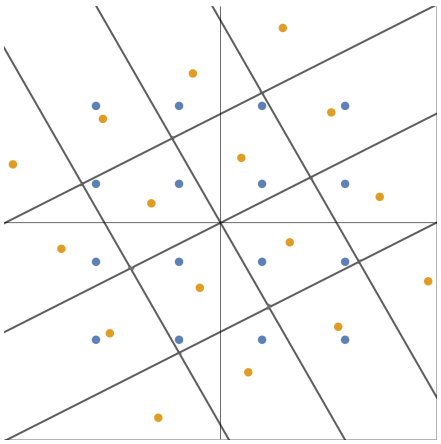

Figure II.9 – *Threshold detection of a QAM16 with* $h' = \frac{13+7i}{12}$ *(*$h = 1$*)*

The mappings for constellation symbols $c_m \not\simeq 0$ are deduced by rotational symmetry, $g(e^{\frac{ik\pi}{2}}c) = e^{\frac{ik\pi}{2}}g(c)$ for $k \in \{0, \cdots, 3\}$. That the points in II.1 are indeed fixed points of the algorithm is not difficult to prove. Consider for instance $h' = \frac{17+9i}{20}h$. Then from (II.11) we have

$$\begin{aligned}\widehat{h} = h\frac{\sum_{m=1}^{M} g^*(c_m)c_m}{\sum_{m=1}^{M} |g(c_m)|^2} &= \frac{|1+i|^2 + (1-i)(1+3i) + (3+i)^2 + (3-i)(3+3i)}{|1+i|^2 + |1+i|^2 + |3-i|^2 + |3+i|^2}h \\ &= \frac{17+9i}{20}h \end{aligned} \tag{II.18}$$

Besides, we can see from Fig.II.6 (with $h = 1$ for simplicity) that the threshold decoding of the actual constellation (blue dots) with respect to the estimated one (orange dots) indeed results in the mapping g of II.1. The proof is similar for the three other fixed points, whose respective mappings are illustrated on II.7, II.8 and II.9.

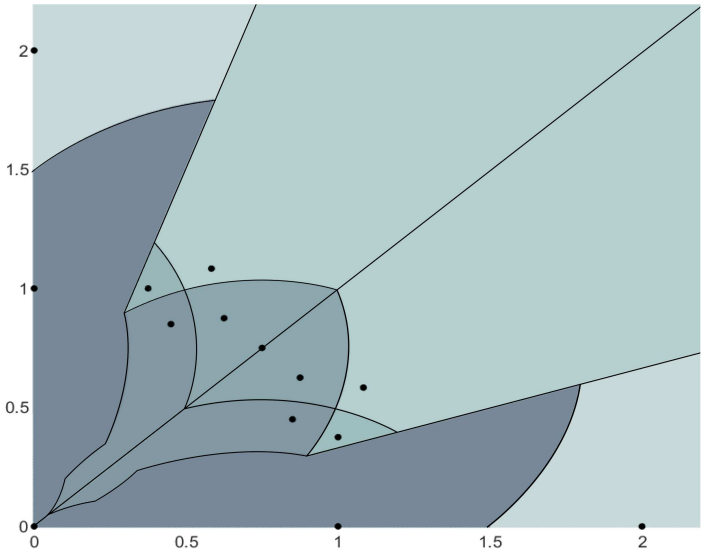

Figure II.10 – *Fixed points of SISO-ILSE and associated convergence regions for the QAM*16, $h = 1$. *Darker colors indicate lower values for the cost function at convergence.*

We have shown that the set constituted of h, $2h$ and the points in II.1 defines fixed points of the SISO-ILSE algorithm for the QAM 16. In order to theoretically find all potential fixed points, one would test all mappings g from $\mathscr{C}$ to $\mathscr{C}$ compatible with the constellation geometrical constraints and check if they are preserved at the next iteration. In practice the complete set of fixed points can be reliably obtained through numerical simulation, by initializing SISO-ILSE on a lattice of complex numbers. Not only this method allows to recover the fixed points with good precision, provided the lattice is tight enough, but most of all it gives us access to the convergence or attraction region $\mathcal{R}(h')$ of each fixed point h', namely the subset of $\mathbb{C}$ for which the algorithm converges to h'. In order to achieve the large sample size limit each constellation symbol is used the same number of times to generate the received symbols. The position of the resulting fixed point in the positive orthant ($z \succcurlyeq 0$) and their associated attraction region are depicted on Fig.II.10, where we have taken $h = 1$.

Despite the relative simplicity of the constellation under consideration, we observe that the convergence regions exhibit non trivial geometrical shapes. In the set $\mathcal{S}$ we can identify 8 fixed points, among which the four points of II.1, the two points induced by the hierarchical symmetry, plus two unpredicted points located at 0 and $\frac{3}{4}(1+i)$. Their convergence region is reduced to a single point, *i.e.* $\mathcal{R}(0) = \{0\}$ and likewise for $\frac{3}{4}(1+i)$. Such points are referred to as unstable, in the sense that they are not observable in non-zero noise cases. They arise from the fact that at those precise locations some of the constellation symbols are equidistant to some subset of symbols of the transformed constellation, so there is an ambiguity in the threshold decoding. Such situations never occur for non-zero noise, so these points are of no practical interest, as we are only concerned with fixed points that can survive non-zero noises. This means that the 6 fixed points given by Table II.1 and the recursive symmetry are

the only relevant fixed points of the SISO-ILSE algorithm, and fully characterize its possible outcomes in the noise-free and asymptotic sample size limit.

II.3.3 Initialization strategies for higher order QAM

The above simulation for finding the fixed points and their convergence region can be readily applied to higher order QAM constellations. The results are presented on Fig.II.11 for the QAM 64 and Fig.II.12 for the QAM 256. As is evident from the figures, the number of fixed points drastically increases with the constellation size. Compared to the QAM 16, restricting to $\mathcal{S}$ and including unstable fixed points 113 points are identified for the QAM 64, and 806 for the QAM 256. Most of fixed points are concentrated around a circle with radius slightly greater than 1, or $|h|$ in the general case. Despite being quite isolated from its neighbouring points, it seems increasingly unlikely to find the global minimum h with only one or even several completely random initializations. Yet, a closer look at the fixed points structure for these three constellations actually reveals two common features that can be used to ease the convergence of the algorithm towards its global minimum.

The first observation is that the fixed points induced by the recursive structure of QAM are well separated from the others, and have a rather large convergence region. In particular, for a QAM with $M = 4^p$ symbols, the largest (in the modulus sense) of these local minima is located at $h' = 2^{p-1}h$ and is completely isolated. One can be quite easily convinced that this fixed point is actually the furthest local minimum admissible by the QAM constellation, at least in the zero-noise limit. Another special property of these fixed points is that, by definition, their associated mapping is such that some constellation symbols are not represented, resulting in empty clusters. Specifically, for $h_j \triangleq 2^{j-1}h$ with $j \in \{1, \cdots, p\}$, the number of non-empty clusters (the cardinal of the image set of the associated mapping g_j) is given by 4^{p+1-j}. This makes these local minima very easy to detect, even for non-zero noises. In particular, the point $h_p = 2^{p-1}h$ has only 4 non-empty clusters.

The second feature concerns the convergence region structure of the global minimum h. As can be seen from figures II.10–II.12, inside the principal ring of fixed points the convergence regions have a strong dependency in the argument of the initial point provided to the algorithm. As we get closer from the origin we see that the angular range spanned by $\mathcal{R}(h)$ increases, suggesting that we are more likely to converge to h with a initial point very close to zero. As far as our simulations can tell, this feature also holds for non-zero noises, as h is always a global minimum of the algorithm.

These two special properties of QAM constellations provide us with two possible complementary intialization strategies for the SISO-ILSE algorithm:

far-off initialization: the initial point is chosen with an arbitrary large modulus so as for the algorithm to converge to $h_p = 2^{p-1}h$. Then dividing by 2^{p-1} an estimation of h can be obtained and refined by a second run of the algorithm at this point;

perturbative initialization: here the objective is to directly converge to the global min-

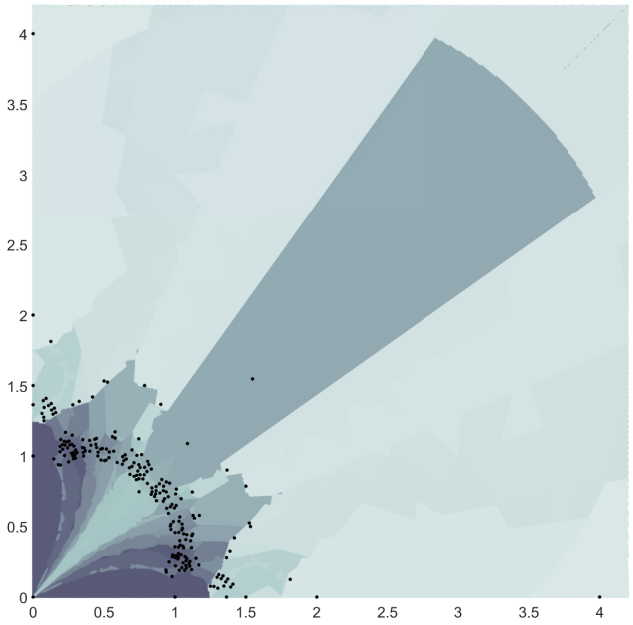

Figure II.11 – *Fixed points of SISO-ILSE and associated convergence regions for the QAM64.*

imum h. The optimal strategy is to choose an initial point arbitrary close from the origin so as to benefit for the maximum angular spread of $\mathcal{R}(h)$.

The proposed initializations can be considered as dual, both in their very definition but also in their advantages and limits. The local minimum aimed by the far-off initialization has the advantage of being very easily identifiable, since all but four of its clusters are empty or almost empty. On the opposite, the global minimum h is not the only fixed point having all constellations symbols equally represented, even in the zero-noise case. For instance, in the QAM 16 case both h and $\frac{17+9i}{20}h$ have an uniform repartition of classes. Reliable distinction between such fixed points requires examination of the cost function at convergence and taking the point achieving the minimum cost. In any case, the success of either strategy is conditioned by the angle of the initial point provided to the algorithm. In practice one would test the algorithm on several initial points in the positive orthant, equally separated in angle so as to ensure one of them lies in the proper angular range. From figures II.10–II.12 one can see that the angular spread of $\mathcal{R}(h)$ is larger than that of $\mathcal{R}(2^{p-1}h)$, so the number of initializations is expected to be lower for the perturbative strategy than for the far-off intialization. As we can also see that the angular range of $\mathcal{R}(h)$ decreases as the size of the constellation increases, for higher order QAM the angular spacing between consecutive initializations may be reduced, resulting in an increased number of initializations.

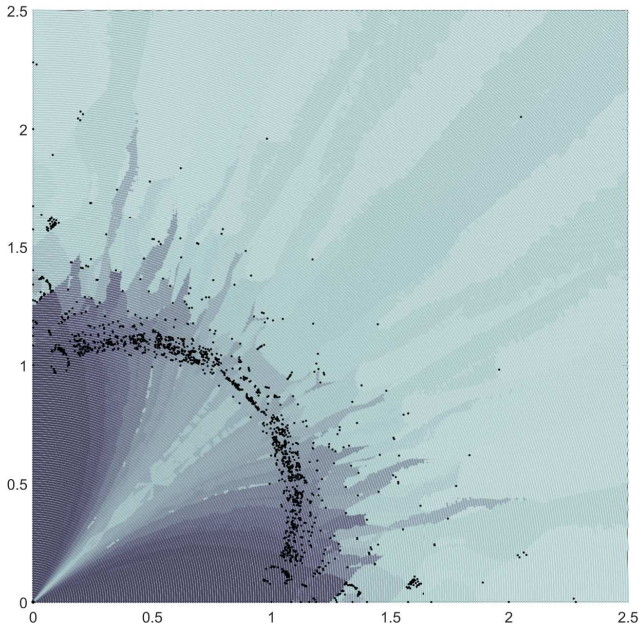

Figure II.12 – *Fixed points of SISO-ILSE and associated convergence regions for the QAM256.*

II.3.4 Influence of the noise

Most of our analysis on the SISO-ILSE fixed points was conducted in the noise-free case and in the asymptotic sample size limit. This allowed exact derivations but is of limited practical interest. A precise characterization of how relaxing these assumptions affect the position and structure of the fixed points is difficult, so we limit ourselves to a qualitative discussion. Note that more advanced results on the effects of noise have been carried out in the scope of Constant Modulus Algorithms (CMA) and can be found in [39]. In our case, it was observed that introducing noise has the effect of masking some of the fixed points, in addition to shifting the location of the remaining ones. Quite intuitively, fixed points with lower cost function at convergence tend to better survive noise than shallow costs fixed points, as small perturbations to a function with a "deep" minimum is unlikely to significantly alter its overall behavior. In that respect, introducing noise is at the advantage of the algorithm since it has statistically fewer possible local minima to converge to.

On the other hand, joint effect of noise and deviation from the uniform symbol distribution may occasionnally result in the emergence of fixed points non predicted by the asymptotic analysis. While in most cases the conditions for these additional local minima to appear seem too stringent to significantly alter the algorithm outcome, they have a negative impact on the seeding strategies introduced in the previous section, which heavily rely on the properties and relations between fixed points. In particular, it was observed for the QAM 16 an unpre-

dicted fixed point located at $\frac{14+6i}{8}\,h$, also having only 4 non-empty clusters as the point $2h$. Forasmuch as the far-off seeding strategy is solely based on this empty-cluster property, not taking into account this additional fixed point is likely to result in spurious solutions. A possible strategy for the QAM 16 will be exposed in a later simulation. Noise and non-uniform induced fixed points may also affect the perturbative seeding technique, but according to our simulations it is globally more resilient to this phenomenon, as it involves deeper local minima which are more robust against noise, and make little place for additional fixed points.

II.4 Initialization by channel prediction

II.4.1 Moment method channel predictor

The two previous sections were respectively concerned with providing the SISO-ILSE algorithm with an initial symbol estimation, achieved by the k-products algorithm, and proposing optimization strategies to improve the probability of converging to the global minimum with random initializations. A third possibility not yet addressed is to provide SISO-ILSE with an initial channel estimate. That is, we search for a channel predictor accurate enough to ensure that the algorithm converges to the actual channel with high reliability. A straightforward way of obtaining such predictor is given by the method of moments, I.2.4. Here the only parameter is the channel h, so we just need one single statistical quantity. The moments of the received symbols r_n are the natural choice to consider. Denoting r the random variable from which the r_n's are drawn, the m-th pure moment of r, $\mu_m(r)$, reads

$$\mu_m(r) = \mathbb{E}\left[r^m\right] = \sum_{p=1}^{m} \binom{m}{p} h^p \mathbb{E}\left[s^p\right] \mathbb{E}\left[w^{m-p}\right] = h^m \mathbb{E}\left[s^m\right] \tag{II.19}$$

where we have used the fact that all pure moments of a circularly-symmetric complex random variable are zero, Eq.(I.13). Hence considering pure moments makes unnecessary to estimate the unknown noise variance N_0. Now, because the constellation $\mathscr{C}$ observes the discrete rotational symmetry of order q and the emitted symbols are equiprobable, the random variable s is itself discrete circularly-symmetric, meaning that s and $e^{\frac{2i\pi k}{q}} s$ have the same distribution. As a consequence, all pure moments of s must verify

$$\mathbb{E}\left[s^m\right] = \mathbb{E}\left[\exp\left(\frac{2i\pi m}{q}\right) s^m\right] = \exp\left(\frac{2i\pi m}{q}\right) \mathbb{E}\left[s^m\right] \tag{II.20}$$

which implies $\mathbb{E}\left[s^m\right] = 0$ for all integers m which are not a multiple of q. From (II.19) the smallest non zero moment of r is thus $\mu_q(r)$. Finally replacing the actual, unobservable moment by its sample counterpart $\overline{\mu}_q(r)$ yields the following simple moment method predictor $\widehat{h}$:

$$\widehat{h} \triangleq \left(\frac{\overline{\mu}_q(r)}{\mu_q(s)}\right)^{\frac{1}{q}} \tag{II.21}$$

It should be noted that because the complex q-th root is not uniquely defined the obtained predictor is not unique. Also, the fact that (II.19) does not depend on the noise variance N_0 does not imply that $\widehat{h}$ is independent on the noise, as the sample moment statistics usually depend on N_0.

II.4.2 Statistics of the channel predictor

Let us consider the q-th power of the channel predictor given by (II.21). Then by the Central Limit Theorem, Eq.(I.25), $\widehat{h}^q$ approximates the following complex normal distribution for large sample sizes

$$\widehat{h}^q \sim \mathcal{NC}\left(h^q, \frac{\mathbb{V}\left[r^q|h\right]}{A^2N\left|\mathbb{E}\left[s^q\right]\right|^2}, \frac{\mathbb{J}\left[r^q|h\right]}{A^2N\mathbb{E}\left[s^q\right]^2}\right) \tag{II.22}$$

where A is the reference amplitude of the constellation $\mathscr{C}$, that we suppose equal to 1 for simplicity. From (II.19) the pseudo-variance of r^q can be readily expressed as $\mathbb{J}\left[r^q|h\right] = h^{2q}\mathbb{J}\left[s^q\right]$. Besides, because $\mathscr{C}$ is invariant under complex conjugation and the symbols are equally likely, s and s^* follow the same distribution, so $\mathbb{J}\left[s^q\right] = \mathbb{J}\left[s^q\right]^*$ and the pseudo-variance is real. By Eq.(I.11b) this implies that the real and imaginary parts of $\widehat{h}^q$ are uncorrelated, which under the complex normal assumption is equivalent to statistical independence.

Computing $\mathbb{J}\left[s^q\right]$ is a straighforward task for PSK modulations as $\mathbb{E}\left[s^{p\,q}\right] = 1$ for any integer p, so $\mathbb{J}\left[s^q\right] = 0$. In this particular case the distribution of $\widehat{h}$ is asymptotically circularly-symmetric complex normal, Eq.(I.26). The situation is different for QAM constellations, for which $q = 4$. The fourth and eighth moments of s^4 can be computed by decomposing the QAM M symbols into two independent ASK$\sqrt{M}$ symbols, $s = a_1 + ia_2$ with $(a_j)_m = 2m - 1 - \sqrt{M}$. This yields

$$\mathbb{E}\left[s^4\right] = 2\mathbb{E}\left[a^4\right] - 2\mathbb{E}\left[a^2\right]^2 = \frac{2}{\sqrt{M}}\sum_{m=1}^{\sqrt{M}} a_m^4 - 2\left(\sum_{m=1}^{\sqrt{M}} a_m^2\right)^2 = -\frac{4}{15}(M^2-1) \tag{II.23a}$$

$$\mathbb{E}\left[s^8\right] = 2\mathbb{E}\left[a^8\right] - 56\mathbb{E}\left[a^2\right]\mathbb{E}\left[a^6\right] + 70\mathbb{E}\left[a^2\right]^2 = \frac{16}{45}(M^2-1)(M^2-13) \tag{II.23b}$$

where derivation of the moments of the ASK involves computation of Bernoulli numbers [40]. Consequently the conditional pseudo-variance of the predictor $\widehat{h}^4$ reads

$$\mathbb{J}\left[\widehat{h}^4\middle|h\right] = \frac{h^8}{N}\frac{\mathbb{J}\left[s^4\right]}{\mathbb{E}\left[s^4\right]^2} = 4\frac{h^8}{N}\frac{M^2-16}{M^2-1} \tag{II.24}$$

As for the variance of r^q, using the independence of the noise with respect to the source symbols and the noise circular symmetry it is given by

$$\mathbb{E}\left[|r^{2q}|\middle|h\right] = \sum_{j=1}^{q}\binom{q}{j}^2 |h|^{2j}\mathbb{E}\left[|s|^{2j}\right]\mathbb{E}\left[|w|^{2(q-j)}\right] \tag{II.25}$$

where from Eq.(I.16) $\mathbb{E}\left[|w|^{2m}\right] = N_0^{2m}m!$. Hence computation of the variance of $\widehat{h}$ requires computation of the even absolute moments of s. In the case of PSK modulations we have again $\mathbb{E}\left[|s|^p\right] = 1$ for any integer p so (II.25) can be simplified as

$$\mathbb{E}\left[|r^{2q}|\middle|h\right] = q!N_0^q\sum_{j=1}^{q}\binom{q}{j}\frac{1}{j!}\left(\frac{|h|^2}{N_0}\right)^j = N_0^q q! L_n\left(-\tfrac{|h|^2}{N_0}\right) \tag{II.26}$$

with $L_n(x)$ the n-th Laguerre polynomial [13]. For QAM constellations the even absolute moments can be derived with the same procedure as the pure moments

$$\mathbb{E}\left[|s|^2\right] = 2\mathbb{E}\left[a^2\right] = \frac{2}{3}(M-1) \tag{II.27a}$$

$$\mathbb{E}\left[|s|^4\right] = 2\mathbb{E}\left[a^4\right] + 2\mathbb{E}\left[a^2\right]^2 = \frac{4}{45}(M-1)(7M-13) \tag{II.27b}$$

$$\mathbb{E}\left[|s|^6\right] = 2\mathbb{E}\left[a^6\right] + 6\mathbb{E}\left[a^2\right]\mathbb{E}\left[a^4\right] = \frac{8}{105}(M-1)(9M^2-40M+51) \tag{II.27c}$$

$$\mathbb{E}\left[|s|^8\right] = \frac{16}{1575}(M-1)(83M^3-637M^2+1897M-2183) \tag{II.27d}$$

As can be seen from Eq.(II.27) the p-th moment of $|s|^2$ is essentially given by M^p, with $M \geq 4$. In most settings it is safe to assume that $N_0 < 1 < M$, so we can reasonably reduce the sum in (II.25) to its dominant term $|h^8|\mathbb{E}\left[|s|^8\right]$. The variance of $\widehat{h}^4$ is then approximated by

$$\mathbb{V}\left[\widehat{h}^4\middle|h\right] \simeq \frac{|h|^8}{N}\frac{\mathbb{V}\left[s^4\right]}{\mathbb{E}\left[s^4\right]^2} = \frac{|h|^8}{N}\frac{4}{7}\frac{(M-4)(19M^2-85M+136)}{(M^2-1)(M+1)} \tag{II.28}$$

II.4.3 Outage probability

In order for the SISO-ILSE algorithm to converge to its global minimum, the initial channel predictor must lie in the convergence region of h, $\mathcal{R}(h)$. A natural way of measuring how good the moment method predictor is would consist in evaluating the conditional outage probability $p \triangleq \mathbb{P}\left(\widehat{h} \notin \mathcal{R}(h)\middle|h\right)$. Even for a rather simple case such as the QAM 16, due to the complicated shape of $\mathcal{R}(h)$ it may be difficult to compute exactly p. We can however find an upperbound on p by considering a real number α such that the complex ball of radius α centered at h is included in the convergence region of h, *i.e.* $\mathcal{B}(h,\alpha) \in \mathcal{R}(h)$. Then, by Chebyshev's inequality we have

$$p = \mathbb{P}\left(\widehat{h} \notin \mathcal{R}(h)\middle|h\right) \leq \mathbb{P}\left(\widehat{h} \notin \mathcal{B}(h,\alpha)\middle|h\right) = \mathbb{P}\left(|\widehat{h}-h| > \alpha\middle|h\right) \leq \frac{\mathbb{E}\left[|h-\widehat{h}|^2\middle|h\right]}{\alpha^2} \tag{II.29}$$

We recognize on the right-hand side of Eq.(II.29) the conditional MSE of predictor $\widehat{h}$ given a channel h. Similarly to (I.30) we can decompose the conditional MSE in terms of conditional bias and variance as follows:

$$\mathbb{E}\left[|h-\widehat{h}|^2\middle|h\right] = \mathbb{E}\left[|h-\mathbb{E}\left[\widehat{h}\middle|h\right]|^2\middle|h\right] + \mathbb{E}\left[|\widehat{h}-\mathbb{E}\left[\widehat{h}\middle|h\right]|^2\middle|h\right] \tag{II.30}$$

so to compute the conditional MSE we need the conditional means of $\widehat{h}$ and $|\widehat{h}|^2$. An exact computation would require the distribution of $\widehat{h}$, which for QAM is not easy to derive even assuming $\widehat{h}^4$ to be complex normal. We can resort to approximate moments by Taylor expansion of Z^γ and $|Z|^{2\gamma}$ around $\mathbb{E}[Z]$, with Z a complex random variable and $\gamma \in \mathbb{R}$. At

second order this yields

$$\mathbb{E}\left[Z^{\gamma}\right] \simeq \mathbb{E}\left[Z\right]^{\gamma}\left(1+\frac{\gamma(\gamma-1)}{2}\frac{\mathbb{J}\left[Z\right]}{\mathbb{E}\left[Z\right]^{2}}\right) \tag{II.31a}$$

$$\mathbb{E}\left[|Z|^{2\gamma}\right] \simeq |\mathbb{E}\left[Z\right]|^{2\gamma}\left(1+\gamma^{2}\frac{\mathbb{V}\left[Z\right]}{|\mathbb{E}\left[Z\right]|^{2}}+\frac{\gamma(\gamma-1)}{2}\left(\frac{\mathbb{J}\left[Z\right]}{\mathbb{E}\left[Z\right]^{2}}+\frac{\mathbb{J}\left[Z\right]^{*}}{\mathbb{E}\left[Z\right]^{*2}}\right)\right) \tag{II.31b}$$

Applying (II.31) to $Z=\widehat{h}^{4}$ and $\gamma=\frac{1}{4}$ we have then

$$\mathbb{E}\left[\widehat{h}\middle|h\right] \simeq h\left(1-\frac{3}{32N}\frac{\mathbb{J}\left[s^{4}\right]}{\mathbb{E}\left[s^{4}\right]^{2}}\right) \tag{II.32a}$$

$$\mathbb{E}\left[|\widehat{h}|^{2}\middle|h\right] \simeq |h|^{2}\left(1+\frac{1}{16N}\frac{\mathbb{V}\left[s^{4}\right]}{\mathbb{E}\left[s^{4}\right]^{2}}-\frac{3}{16N}\frac{\mathbb{J}\left[s^{4}\right]}{\mathbb{E}\left[s^{4}\right]^{2}}\right) \tag{II.32b}$$

which provides the following approximate expression for the conditional MSE

$$\mathbb{E}\left[|h-\widehat{h}|^{2}\middle|h\right] \simeq \frac{|h|^{2}}{16N}\left(\frac{\mathbb{V}\left[s^{4}\right]}{\mathbb{E}\left[s^{4}\right]^{2}}\right) = \frac{|h|^{2}}{28N}\frac{(M-4)(19M^{2}-85M+136)}{(M^{2}-1)(M+1)} \tag{II.33}$$

We are now left with the choice of α to compute the upper bound on p. Ideally α should be as large as possible, so that $\mathcal{B}(h,\alpha)$ is the largest complex ball included in $\mathcal{R}(h)$. As this requires to know the boundaries of $\mathcal{R}(h)$, it may be difficult to derive an exact expression of α for a generic QAM. In the case of the QAM 16 however, the number of fixed points and the structure of their convergence regions allow a precise characterization of α. For simplicity we assume here that $h=1$. Denoting h_{ℓ} the point in $\mathbb{C}$ lying on the boundary of $\mathcal{R}(1)$ and such that $|h_{\ell}-1|=\alpha$, *i.e.* $h_{\ell}\triangleq\mathcal{R}(h)\cap\mathcal{C}(h,\alpha)$ a first condition h_{ℓ} must fulfill is given by

$$|h_{\ell}(3+i)-(3+i)|^{2} = |h_{\ell}(3-i)-(3+i)|^{2} \tag{II.34}$$

which yields $\mathrm{Arg}\left(h_{\ell}\right)=\arctan\left(1/3\right)$, or $h_{\ell}=\lambda\frac{3+i}{\sqrt{10}}$, with $\lambda\in\mathbb{R}$. This corresponds to the straight line boundary of $\mathcal{R}(1)$, as seen on Fig.II.13. Minimizing then $|h_{\ell}-1|^{2}$ with respect to λ we find $\lambda=\frac{3}{\sqrt{10}}$, so $h_{\ell}=\frac{9+3i}{10}$, or $h_{\ell}=\frac{9+3i}{10}\,h$ in the general case. The location of h_{ℓ} is shown on Fig.II.13. The maximal radius α_{ℓ} is thus given by $\frac{|h|}{\sqrt{10}}$, which combined with (II.33) yields the following bound for the QAM 16 outage probability

$$p \leq \frac{10}{|h|^{2}}\mathbb{E}\left[|h-\widehat{h}|^{2}\middle|h\right] \simeq \frac{5}{7N}\frac{(M-4)(19M^{2}-85M+136)}{(M^{2}-1)(M+1)} \simeq \frac{7.20}{N} \tag{II.35}$$

The upper bound provided by (II.35) is actually very loose: simulations performed with $N=50$ QAM 16 symbols result in a measured probability of $\widehat{h}$ lying out of $\mathcal{B}(h,|h|/\sqrt{10})$ of order 10^{-3} for a noise power of order 10dB, while (II.35) only gives $p\leq 0.14$. It seems Chebyshev's bound is not a fully appropriate choice to accurately approximate the outage probability, so other bounds should be considered to get closer to the actual result. Apart from very low values of N ($N\simeq 10$), the simulated outage probabilities are extremely low, so we can expect the moment channel predictor to perform very well in most practical situations.

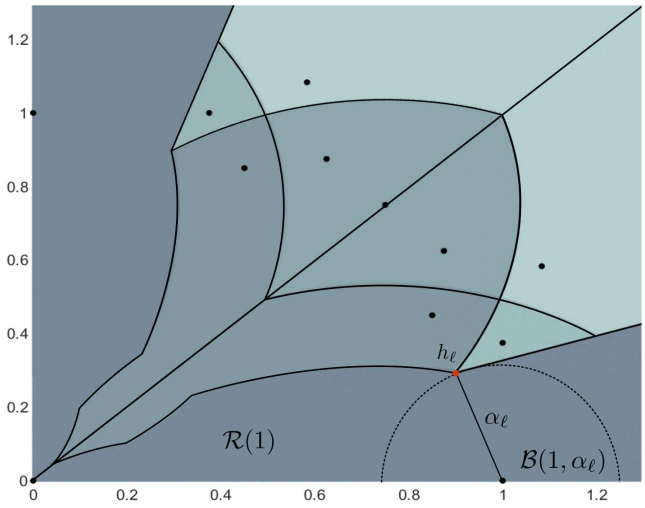

Figure II.13 – *Largest complex ball with center h lying in $\mathcal{R}(h)$ for the QAM16 ($h = 1$). The orange dot shows the intersecting point h_ℓ between the boundaries of $\mathcal{R}(h)$ and $\mathcal{B}(h, \alpha_\ell)$.*

II.5 Comparative simulations

II.5.1 Simulation settings

Now having several possible initialization strategies for the SISO-ILSE algorithm at our disposal we can address the central question of the gain one may benefit from using them compared to the naïve random strategy, and how they compare to each other. In wireless communication systems there are two essential measures of performance we can think of: the first one is the averaged SER (I.51), which evaluates the quality or reliability of the transmission. The second is the computational complexity, which provides an appreciation of whether a practical implementation of the considered method is feasible with respect to the delay requirements of the application at hand. As we are here concerned with an iterative procedure, a natural basis for comparison is the mean number of iterations required for the algorithm to converge. To be more accurate we should account for the fact that some of the presented strategies require multiple runs of the algorithm. We thus define N_{ite} as the mean number of iterations of SISO-ILSE cumulated over the different runs needed for a given strategy to yield its final channel predictor.

The above figures of merit are computed through Monte-Carlo simulations. The channel fading statistical model considered is the Rayleigh fading: h follows a circularly-symmetric complex normal distribution with variance $\sigma^2 = 1$, Eq.(I.14) (meaning that $|h|$ is Rayleigh-distributed with parameter $\frac{1}{\sqrt{2}}$). For each channel realization, $N = 1000$ symbols are generated from a regular QAM source with M equally likely symbols. The noise is circularly-symmetric complex normal with power N_0. The reference amplitude of the constellation A is chosen so that the energy per bit E_b is equal to one. The channel is estimated by the SISO-ILSE algorithm and the received sequence is demodulated accordingly by threshold

detection. For comparison we also perform the ideally equalized demodulation, in which the channel is perfectly known. The different tested strategies are summarized below:

perfect CSI: threshold detection based on the actual value of the channel;

random initialization: the naïve SISO-ILSE algorithm initialized with several random channels drawn from the same distribution as that of the actual channel. The number of initializations is fixed to four, and the retained solution is the one that achieves the lowest cost function;

moment method predictor: the SISO-ILSE algorithm is initialized with the channel predictor provided by the method of moments, Eq.(II.21);

hierarchical k-products: the channel-transformed constellation symbols are estimated by the hierarchical k-products algorithm introduced in Section II.2. The obtained centroïds are used to demodulate the received symbols by threshold detection, and the result is provided as an initial symbol estimation state for the SISO-ILSE algorithm;

far-off initialization: the initial channel is first chosen at random with an arbitrary large modulus to drive the algorithm to one of its outer local minima. The resulting fixed point is then rescaled so as to serve as a basis for better initial states. The scaling modulus is chosen according to the number of empty clusters resulting from a threshold decoding based on the fixed point, Section II.3.3, and the three phase values $\{-\frac{\pi}{8}, 0, \frac{\pi}{8}\}$ are tested. The final channel estimate is then chosen as the one which minimizes the final cost of the algorithm. The overall procedure thus requires four entire runs of the algorithm, which motivates the choice made for the random initialization strategy;

perturbative initialization: the initial channel is chosen at random with an arbitrary small modulus and three different phases $\{-\frac{\pi}{8}, 0, \frac{\pi}{8}\}$ so as to converge to one of the inner fixed points of the algorithm. The one achieving the lowest cost is then retained as the global minimum. The algorithm is thus performed thrice.

II.5.2 Results

The averaged SER and mean total number of iterations of the algorithm are provided on Fig.II.14 for the QAM 16. As can be seen, except for the random initialization all tested strategies almost perfectly coincide with the known channel case. As for the complexity, obviously the moment method and hierarchical k-products strategies require significantly lower iterations for convergence of SISO-ILSE, first because they both require only a single run of the algorithm and also because the initial state is most often already close to the global minimum. At high E_b/N_0 values the algorithm usually converges in no more than two iterations. Conversely the number of iterations achieved by the far-off and perturbative initializations is more than four times higher than the latter methods since the initial point is chosen at random, and may consequently lie far from any fixed point of the algorithm. Still, for low noise powers and considering their disadvantage compared to data-driven initialization strategies the total, cumulated number of iterations is quite reasonable – of

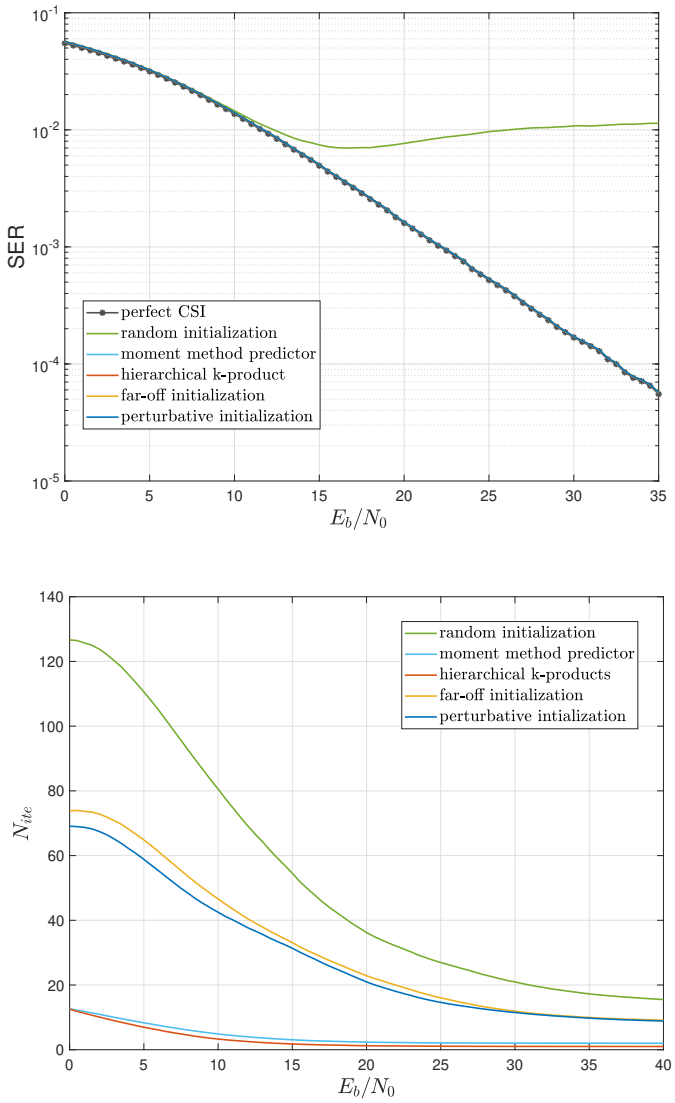

Figure II.14 – *Performances of the SISO-ILSE algorithm for the QAM* 16 *with several initialization strategies: average SER (top) and mean cumulated number of iterations (bottom).*

the order ten –, and is in any case far lower than that of the naïve strategy. This shows the relevance of using the fixed points structure to both improve and fasten the outcome of the algorithm in this simple case.

Similar simulations were carried out for a QAM 64 modulation scheme, whose results are presented on Fig.II.15. Again the channel and symbol initial estimation procedures reveal extremely efficient and almost achieve the lower performance bound provided by the perfect CSI demodulation, within the same order of iterations as in the previous case. Despite being still globally better than the naïve strategy, the far-off and perturbative initializations encounter difficulty in finding the global minimum of the SISO-ILSE algorithm. In particular

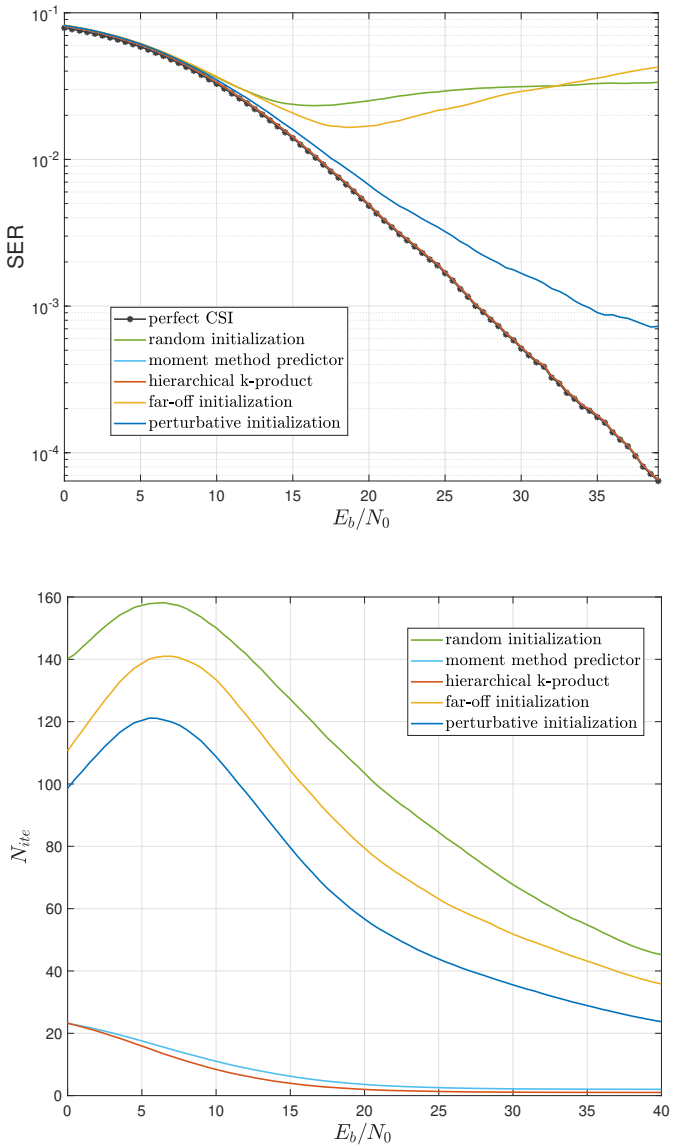

Figure II.15 – *Performances of the SISO-ILSE algorithm for the QAM64 with several initialization strategies: average SER (top) and mean cumulated number of iterations (bottom).*

the far-off strategy is no longer monotonically decreasing and is even outperformed by the fully-random strategy at high E_b/N_0 levels. This is the result of the increase in the number of fixed points with the constellation size, and the related decrease in the angle spread of the convergence regions of interest. In that respect the perturbative scheme is more reliably transposable to higher order QAM as it is essentially immune to the emergence of additional local minima. In order to improve the performance of the blind strategies a tighter angular resolution than the $\pi/8$ one can be considered, but at the evident cost of an increase in the total number of iterations. Alternatively a finer characterization of the local minima of the

QAM 64 could be performed so as to design more elaborate seeding strategies. In the light of this second simulation the k-products and moment method channel predictor appear as equivalently appropriate initialization strategies for the SISO-ILSE algorithm.

II.6 Conclusion

The blind estimation of the flat-fading SISO channel was addressed in the ML sense by means of the SISO-ILSE algorithm, a geometrically constrained version of the k-means clustering technique. Because the centroïds are fully characterized by a single complex parameter and the constellation's geometry, some general results on the location of fixed points of the algorithm were derived in the noise-free case, based on the inherent symmetries of usual linear wireless modulations. In particular, it was shown that for PSK constellations there was essentially a single fixed point, thus making a preliminary initialization of the algorithm unnecessary. The situation is radically different for regular QAM, for which two seeding strategies to find the global minimum from a fully random initialization were proposed, based on the location and convergence regions of the fixed points. Two initialization strategies for the SISO-ILSE algorithm were also presented, equally suitable for any constellation type. The first one consists in a modification of the k-products algorithm to address constellations with recursive structure, and the second consists in a simple moment method channel prediction. Simulations revealed first the relevance of our fixed point analysis in mitigating the convergence of the algorithm towards spurious solution, and emphasized the effectiveness of the proposed blind initialization procedures in successfully estimating the channel. While in this simplified framework the latter strategies clearly outperform the former both in achieved error rates and complexity, making practical use of seeding techniques unnecessary, we will see in the next chapter that for multiuser transmissions both kinds of techniques are relevant in their own right.

Chapter III

Multiuser blind detection

Contents

Part of this work has been published in the following letter:

S. Smith, M. Pischella, M. Terre. "A moment-based estimation strategy for underdetermined single-sensor blind source separation", IEEE Signal Processing Letters, vol. 26(6), pp. 1-5, 2019, (doi:10.1109/LSP.2019.2909968)

III.1 Introduction

III.1.1 Multiple access channel

This chapter constitutes the core of the work presented in this thesis, namely blind channel estimation in multiuser transmissions. We consider K users simultaneously transmitting their source signal to the same receiver. This situation can occur for instance in an uplink communication where several devices located in the same cell are emitting to the same Base Station (BS), as is represented on Fig.III.1. At the BS, a superposition of the signals coming from each user is observed, hindering the identification of each individual source: this is called Multiuser Interference (MUI) or Inter-User Interference (IUI). Let us denote the symbols emitted from user k by s_k, with $k \in \{1, \cdots, K\}$. Each source signal experiences a different propagation environment that we model by a flat-fading channel h_k. We also assume that the users have the same symbol period T and that they are all time-synchronized. That is, at a given time epoch the BS receives exactly one symbol from each user during the symbol duration T. At the receiver, an additive background noise modeled as a circularly-symmetric complex normal variable with variance N_0 further impinges on the observed signal. Within these assumptions, at a given time epoch the observed symbol resulting from the superposition of the symbols from each user transformed by the channel and the background noise is given by the following instantaneous, linear mixture model:

$$r = \sum_{k=1}^{K} h_k s_k + w = \langle \mathbf{h} | \mathbf{s} \rangle + w \tag{III.1}$$

where $\langle \cdot | \cdot \rangle$ denotes the hermitian scalar product on $\mathbb{C}^K$. The sources s_k can reasonably be assumed mutually independent and independent of the noise w. Moreover, each source is assumed to be uniformly distributed over its constellation, denoted by $\mathscr{C}_k$, with a corresponding rotational order q_k. We refer to the joint (mixed) constellation and denote by $\mathscr{C}_{\mathbf{h}}$ the set of all symbols observable from the mixture without any noise, *i.e.* $\mathscr{C}_{\mathbf{h}} \triangleq \sum_{k=1}^{K} h_k \mathscr{C}_k$. An example of received symbols from $K = 3$ users is presented on Fig.III.2. The objective of the receiver is to blindly recover the emitted symbols from each user. In the following we will call Eq.(III.1) the Multiple-Input Single-Output (MISO) transmission model to indicate that there is a single sensor at the receiver. Note that in general the term MISO actually refers to communications scenarios where the emitter uses several antennas to transmit its input signal. Since here only one antenna is assumed for each source it would be more appropriate to speak of a multiuser SISO transmission. Yet, as all considered transmissions in the thesis involve only one antenna at both the transmitter and receiver sides, we will use the MISO denomination for convenience.

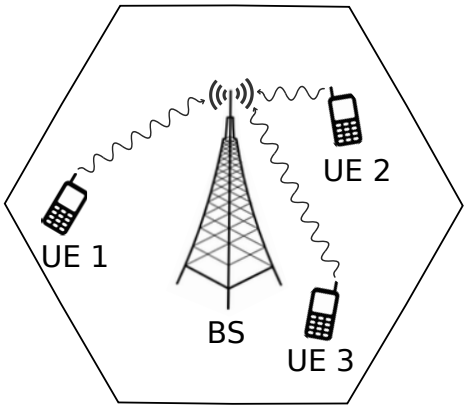

Figure III.1 – *Illustration of a multiuser uplink transmission ($K = 3$).*

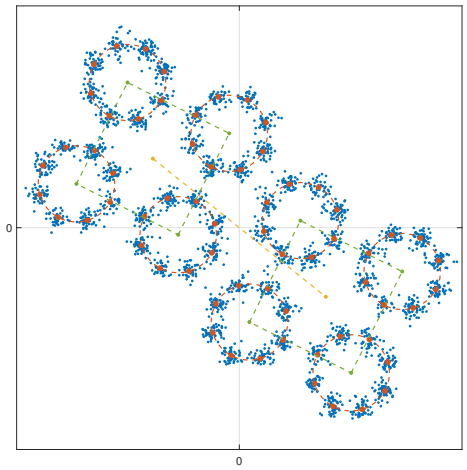

Figure III.2 – *Received symbols from three sources using a BPSK, a QAM4 and a PSK8. The red dots constitute the joint mixed constellation $\mathscr{C}_{\mathbf{h}}$.*

III.1.2 Blind Source Separation

The model described by Eq.(III.1) can actually be seen as a particular instance of a general signal processing problem known as Blind Source Separation (BSS) [4]. In the scope of instantaneous and linear mixtures, it is based on the following matrix model

$$\mathbf{r} = \mathbf{AS} + \mathbf{w} \tag{III.2}$$

where:

- $\mathbf{r}$ is the D-dimensional vector of received signals with D the number of sensors or *diversity* of the mixture;
- $\mathbf{s}$ is a vector of K unknown mutually independent source signals;
- $\mathbf{A}$ is an unknown $D \times K$ matrix known as the mixing matrix;
- $\mathbf{w}$ is a D-dimensional noise vector, usually assumed to be independent of the sources.

The aim of BSS is two-fold: from a set of N realizations of $\mathbf{r}$, identify the mixing matrix $\mathbf{H}$ and recover the N realizations of the source vector $\mathbf{s}$. A typical application of (III.2) is the estimation of directions of arrival in signal array processing [41]: in this framework the columns of $\mathbf{A}$ are also known as steering vectors. Other popular applications of BSS include medical bioengineering, audio or speech signal processing and statistical data analysis, among many others [42], [14].

The main difficulty of this problem stems from the fact that both $\mathbf{s}$ and $\mathbf{H}$ are unkown to the receiver. As a consequence, solutions to the BSS problem are generally not unique and

can only be defined up to some ambiguities [43]. It is indeed easy to check that given any solution $(\mathbf{A}, \mathbf{s})$ of (III.2), then for any permutation matrix $\mathbf{P}$ and any non-singular diagonal matrix $\mathbf{D}$, $(\mathbf{APD}, \mathbf{D}^{-1}\mathbf{P}^{-1}\mathbf{s})$ is also a solution to the BSS problem, thus resulting in a scaling and ordering ambiguity of the solution. Such matrices formed by the combination of a permutation and a scaling are sometimes called generalized permutation matrices. The conditions under which, up to these fundamental model invariances, the mixing matrix and the sources can be recovered are known as the identifiability and separability conditions. Several works have been devoted to the theoretical study of these conditions and can be found in [44] and [45] for real-valued mixtures, in [46] for complex mixtures, and more recently in [47] in the scope of finite-alphabet sources.

The most well-known framework for addressing the BSS problem is probably the Independent Component Analysis (ICA) [48], which aims at finding a transformation of the received signal so as to obtain the most statistically independent components. ICA techniques usually involve minimization of contrast functions based on the cumulants of the received signal as well as joint diagonalization methods [49,50]. Additional assumptions on the sources can be used to further constrain the problem, such as constant modulus [51,52], time-frequency signatures [53,54] or finite-alphabet property of the sources [5,55,56]. More recently, Bounded Component Analysis (BCA) has been proposed as an alternative technique based on the assumption that the sources are bounded and on the geometry of their joint support [57]. This can be thought as a generalization of ICA inasmuch the assumption of mutual independence is relaxed. BCA can thus be applied to the separation on independent and dependent sources [58], in underdetermined and overdetermined mixtures alike [59] as well as convolutive mixtures [60].

Whenever the number of sources exceeds the number of sensors ($K > L$), the mixture model of Eq.(III.2) is referred to as an Underdetermined Mixtures (UDM) and traditional ICA techniques no longer apply as the mixing matrix $\mathbf{A}$ is rank-deficient. This led to the development of other strategies to address the BSS problem, most of which are based on the cumulants of the received signal [61] and symmetric tensor decompositions [62, 63]. FOOBI [64], FOBIUM [65], BIOME [66] or BIRTH [67] are a few names of such algorithms that exploit the so-called covariance (second order), quadricovariance (fourth-order) or hexacovariance (sixth-order) of the received signal. For a given number of sensors D these methods are usually characterized by an upper bound on the number of sources they can deal with. Another possible approach to underdetermined BSS is also provided by Sparse Component Analysis (SCA), which relies on the assumption that only a small number of sources are simultaneously active, resulting in a sparse representation of the source realizations vectors [68–71].

The MISO channel model introduced in (III.1) represents a limiting case of underdetermined BSS in that the receiver has only one sensor ($D = 1$) at his disposal to estimate both the incoming sources and the mixing vector $\mathbf{h}$. This situation represents the worst scenario in terms of available information, and is not covered by the above algorithms, as their operating upper bound on the number of users reduces to 1 in this

specific case. Moreover, since the symbols come from discrete modulations the sources exhibit the finite-alphabet property, which constitutes a precious information in this highly unfavorable framework. Despite having received less treatment, the BSS of finite-alphabet sources with a single sensor has been addressed in several works. In [72] the case of balanced binary sources was addressed by an iterative learning procedure. A deterministic approach for ASK constellations with arbitrary symbol probabilities in a noiseless environment was proposed in [73], and a geometric approach based on the distribution of differences between the mixed symbols was discussed in [74] for ASK modulations. Generalizations to non-linear and convolutive mixtures can be found in [75] and [76], respectively.

There are two main limitations to the above algorithms: first, they are restricted to real-mixtures, while the channels in our model are complex-valued. More importantly, though it is true that the proposed approaches are based on the geometrical structure induced by the users constellations and the channels, in the noisy case they rely on techniques such as the EM scheme to estimate the location of the mixed joint constellation symbols. Such algorithms, in their original formulation, do not impose any constraint on the centroïds structure. Consequently their parameter space is by far larger than that of the mixture. Forasmuch as these algorithms are known to have local minima, not taking into account the reduced dimension of the actual parameter space makes them more likely to fail at successively finding the mixed symbols. On the opposite, the Iterative Least Squares with Enumeration (ILSE) algorithm proposed in [5] in the framework of overdetermined mixtures fully accounts for the special structure of the joint constellation. ILSE seems then a more appropriate algorithm to consider for addressing noisy mixtures of finite-alphabet sources, provided it can be applied to the underdetermined case.

On the basis of these observations and the results of the previous chapter, our objectives can be summarized as follows:

- in a first part we will present the ILSE algorithm in the MISO framework, along with a classical procedure from wireless communications allowing the recovery of interfering sources in low interference scenarios, known as Successive Interference Cancellation (SIC). The justification for use of ILSE to our problem will be further discussed and made clear in light of our model assumptions;

- the main part of the chapter will be devoted to the initialization of ILSE. The method of moments will serve as a basis for providing the algorithm with appropriate initial channel estimates. Explicit formulas for the derived predictors will be given for various mixture settings;

- simulations will be carried out to evaluate the proposed initialization strategies. Contrary to what is usually done in the literature, our results will account for the overall ability of the algorithm to converge in a single try to its global minimum, and will not restrict to specific channel realizations. In particular, our simulations will assume maximum interference levels between the users.

III.2 Blind multiuser detection algorithms

III.2.1 Successive Interference Cancellation

Successive Interference Cancellation [32] is a well-known iterative method which allows to sequentially retrieve multiple simultaneous interfering source signals based on their relative powers. More specifically, given K linearly mixed independent source signals s_k and a background noise w, the averaged received power is given from (III.1) by the sum of the received powers from each user, plus the noise power. Now, if one of the sources, say s_1, has a substantially stronger received power relative to all other sources and noise, *i.e.* $|h_1|^2 \mathbb{E}\left[|s_1|^2\right] \gg |h_k|^2 \mathbb{E}\left[|s_k|^2\right]$ for $k \neq 1$ and $|h_1|^2 \mathbb{E}\left[|s_1|^2\right] \gg \mathbb{E}\left[|w|\right]^2$, then we can write

$$\mathbb{E}\left[|r|^2\right] = \sum_{k=1}^{K} |h_k|^2 \mathbb{E}\left[|s_k|^2\right] + \mathbb{E}\left[|w|^2\right] = |h_1|^2 \mathbb{E}\left[|s_1|^2\right] + \varepsilon \tag{III.3}$$

where ε, the sum of the received powers from the remaining sources and the noise, is small compared to $|h_1|^2 \mathbb{E}\left[|s_1|^2\right]$. In words, from the perspective of the strongest source, the contributions from all other users and the background noise are tantamount to a single, global noise. Consequently, the statistics of the received signal can be used to estimate h_1 within small imprecision. Should one be solely interested in the square modulus of h_1 for instance, then from (III.3) the following estimator could be reasonably used

$$|h_1|^2 \simeq \frac{\overline{\mu}(|r|^2)}{\mathbb{E}\left[|s_1|^2\right]} \tag{III.4}$$

where $\overline{\mu}(|r|^2)$ denotes the sample averaged received power. Hence the source signal s_1 can be separately estimated using a standard threshold detection scheme, allowing its contribution to the total received signal to be compensated. The same procedure can then be applied to the residual received signal to decode the strongest remaining sources, and so forth until all the sources have been estimated. Assuming for simplicity that the sources are sorted by decreasing received power, the overall SIC procedure basically consists in iterating over the following steps

$$\widehat{h}_k = T\left(\widehat{r}_k\right) \tag{III.5a}$$

$$\widehat{s}_k = \underset{s \in \mathscr{C}_k}{\operatorname{argmin}} |\widehat{r}_k - \widehat{h}_k s|^2 \tag{III.5b}$$

$$\widehat{r}_{k+1} = \widehat{r}_k - \widehat{h}_k \widehat{s}_k \tag{III.5c}$$

with $k \in \{1, \cdots, K\}$, $\widehat{r}_1 \triangleq r$ and $T(r)$ is a given statistics of the received signal used to estimate the channels. If the number of sources K is known, then SIC stops after K iterations. Otherwise, one can define a lower power bound on the residual signal under which it is considered that all signals of interest have been estimated and only noise remains. This requires however all sources to have significantly higher power than the noise, as well as an estimation of the noise power.

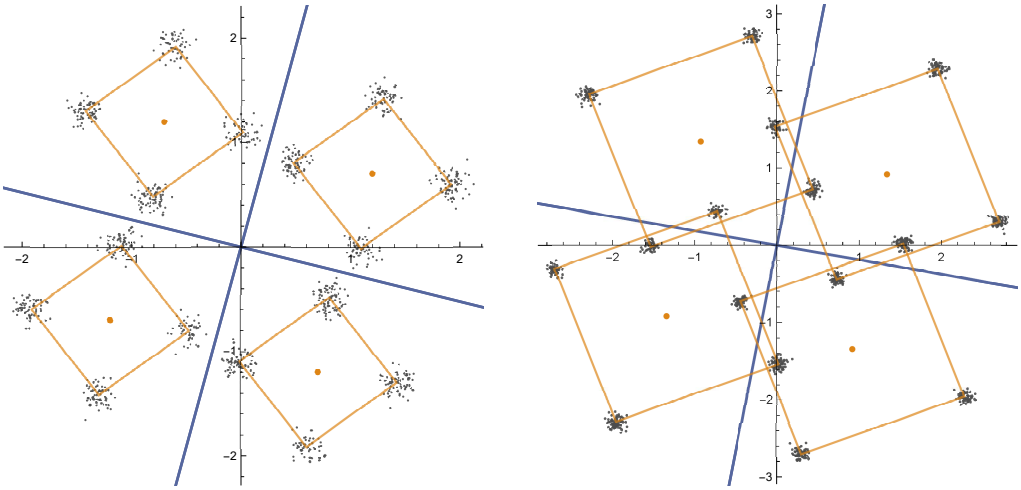

Figure III.3 – *First source decoding step of a two-users mixture with SIC in weak (left) and strong (right) interference regimes. The blue lines represent the decision regions associated with the channel estimation.*

The fundamental underlying assumption of SIC is that the received contributions from each user have a strong power diversity. If this condition is not fullfilled, (III.5a) essentially results in an estimation of a mixture of channel powers corresponding to subsets of source signals with similar powers. Consequently, the associated decoding step yields a poor estimation of the source under consideration, which is likely to considerably hinder the estimation of the remaining sources in subsequent iterations through the residual received signal. This is illustrated on Fig.III.3 for two users using QAM modulation schemes. In the left configuration, the channel coefficients are such that the received powers are well separated from each other and from the noise, allowing an almost perfect estimation of the first source. In the second setting, the received powers are of the same order, hence despite an appreciably low noise power level only half of the first user transmitted symbols are correctly estimated. All in all, SIC provides a simple and low-computational estimation of linear mixtures involving weakly interfering sources, but is not adapted beyond this framework, as will be demonstrated in later simulations.

III.2.2 Iterative Least Squares with Enumeration

One possible approach to solve the linear BSS problem lies in ML estimation. That is, given a set of N independent observations of the received signal, we aim at maximizing the (log)-likelihood function with respect to the mixture parameters, namely the channel vector $\mathbf{h}$ and the emitted source symbols. Denoting by $\mathbf{r}$ the (row) vector of realizations of r and by $\mathbf{S}$ the $K \times N$ matrix whose columns are the realizations of the source vector $\mathbf{s}$, Eq.(III.1) yields

$$\mathbf{r} = \mathbf{hS} + \mathbf{w} \tag{III.6}$$

with $\mathbf{w}$ a vector of N independent realizations of w. Since the background noise is circularly-symmetric complex normal with variance N_0, the conditional probability distribution of the

received signal given $\mathbf{h}$ and $\mathbf{S}$ is complex normal with the same variance and mean $\mathbf{hS}$. Hence, maximizing the log-likelihood function $\mathbb{L}[\mathbf{h}, \mathbf{S}; \mathbf{r}]$ amounts to minimizing the following least squares cost function:

$$J(\mathbf{h}, \mathbf{S}) \triangleq \| \mathbf{r} - \mathbf{hS} \|^2 \tag{III.7}$$

Despite being merely quadratic, the joint minimization of (III.7) in $\mathbf{h}$ and $\mathbf{S}$ is a non-trivial problem, especially since it involves both a continuous variable (the channel vector) and a discrete one (the transmitted symbols matrix). The Iterative Least Squares with Enumeration method [5] proposes an iterative procedure to minimize J in an alternating least squares fashion: at each step of the algorithm, the cost function is first minimized with respect to one of its variales $\mathbf{h}$ or $\mathbf{S}$, the other being fixed. The resulting optimum is then used to minimize J with respect to the remaining variable, and the overall procedure is iterated until convergence of the algorithm.

In the single-sensor BSS model setting, the minimization of J with respect to the continuous channel vector $\mathbf{h}$ at iteration t yields the usual OLS estimator $\widehat{\mathbf{h}}_t$ given by Eq.(I.33)

$$\widehat{\mathbf{h}}_t^T = \mathbf{r}\widehat{\mathbf{S}}_{t-1}^\dagger \left(\widehat{\mathbf{S}}_{t-1} \widehat{\mathbf{S}}_{t-1}^\dagger \right)^{-1} \tag{III.8}$$

where $\widehat{\mathbf{S}}_{t-1}$ is the estimation of the transmitted symbols matrix at iteration $t-1$. Obviously equation (III.8) is meaningful only if $\widehat{\mathbf{S}}_{t-1}$ has independent rows. Otherwise the channel estimator is obtained by taking the minimum norm solution of (III.7). The authors have shown that a sufficient condition for the K rows of $\widehat{\mathbf{S}}_{t-1}$ to be linearly independent is that every combination of symbols from each user appears at least once. In particular this result holds regardless of the underdetermined or overdetermined nature of the mixture. Let us note however that independence of the rows of $\widehat{\mathbf{S}}_t$ at a given iteration t is not necessarily preserved under subsequent iterations.

As for the transmitted symbols matrix estimation step, given an estimation of the channel vector $\widehat{\mathbf{h}}_t$ ILSE proceeds by enumerating all combinations of symbols from each user, and selecting one which minimizes the squared residual

$$\widehat{\mathbf{S}}_t = \underset{\mathbf{S} \in (\mathscr{C}_1 \times \cdots \times \mathscr{C}_K)^N}{\operatorname{argmin}} \| \mathbf{r} - \widehat{\mathbf{h}}_t^T \mathbf{S} \|^2 \tag{III.9}$$

It is shown in [5] that the sequence of joint estimators $(\widehat{\mathbf{h}}_t, \widehat{\mathbf{S}}_t)$ produced by the algorithm belongs to a finite set, and that the corresponding sequence of costs $J(\widehat{\mathbf{h}}_t, \widehat{\mathbf{S}}_t)$ is decreasing and stationary. Consequently, the algorithm converges to a fixed point in a finite number of steps. The overall complexity of the method is dominated by the enumeration step (III.9) and is in $\mathcal{O}(NKD)$ per iteration, where here the dimension of the mixture D is one. Additional performance analyses such as bounds on the error rates achievable by the proposed method were provided in [77].

As in the SISO case, the ILSE algorithm can be thought of as a particular case of the k-means clustering algorithm, in which the position of the centroïds are constrained

to lie on a predefined stucture determined by the mixed constellation $\mathscr{C}_{\mathbf{h}}$. As such, many of the well-established properties of k-means readily apply to ILSE. Foremost is that the cost function (III.7) generally has several local minima, so the minimization iterative procedure presented above does not necessarily converge to the actual minimum of J. As a deterministic process, the fixed point towards which the method converges is, for a given mixture, solely determined by the initial point provided to the algorithm. It is thus customary to test the algorithm on several random initial states, either until the global minimum has been achieved, or for a fixed number of times and retaining the solution with minimal final cost. Note that in the former strategy the appreciation of whether the fixed point under consideration is a local or global minimum may require additional information such as for instance an estimation of the background noise power, as well as careful lower threshold design for the cost function. In any case, randomly repeating over the algorithm has in general no guarantee of succeeding in finding the true minimum of J, and can besides reveal computationnally prohibitive as the number of sources and dimension of the mixture grow.

In [5] an alternative initialization strategy for ILSE was proposed, namely Iterative Least Squares with Projection (ILSP). In this variant of the initial procedure, the source matrix $\mathbf{S}$ is first considered as a continuous variable. Minimizing (III.7) with respect to $\mathbf{S}$ then reduces to an OLS problem similar to (III.8). The (continuous) resulting estimator is then projected back onto the joint discrete constellation in the minimum distance sense. The mixing matrix estimation step is left unchanged. Despite a decreased complexity compared to the original ILSE, the ILSP procedure suffers from two major drawbacks:

- due to the projection step, the sequence of estimators produced does not necessarily decrease the cost function J. Hence the algorithm does not always converge, or can exhibit cyclic behavior, as reported in [56];
- since based on the same cost function and the same alternating least squares process, the previous discussion on the presence of local minima and the choice of the initial state also applies to ILSP.

This motivated the use of ILSP as an initialization procedure for ILSE rather than a self-consistent algorithm. Additionally, in the case of single-sensor mixtures, the mixing matrix reduces to a row vector, hence the matrix inversion in the computation of the OLS continuous source matrix estimator is never possible. One can of course always consider the pseudo-inverse solution instead, but in all likelihood the use of ILSP does not seem appropriate to address this particular setting.

Despite being originally presented as a solution to the overdetermined linear BSS problem, the ILSE approach is not limited to this setting, as neither the enumeration nor the channel vector estimation steps have any requirement regarding the mixture dimension. Hence ILSE can be applied to underdetermined problems as well. Moreover, as a special case of k-means, the same underlying assumptions on the statistical mixtures under consideration can be made, namely:

- mixture components have nearly the same variances;
- mixture components are equally likely.

Note that the above properties rather define an ideal framework for use of k-means based algorithms than actual requirements. In other words, k-means or ILSE can also be used on non homogeneous mixtures with unequal weights, but at the expense of an expected decrease in overall performance. Within our assumptions of a complex circular noise and the uniformity of each source's distribution however, the ILSE indeed appears to be a particularly relevant candidate, shall one provides it with a good enough initialization strategy. This is the main objective of this chapter and the object of the next section.

III.3 Proposed channel predictor

III.3.1 Problem Formulation

In order to make ILSE more likely to converge to its global minimum, we propose to initialize it with a channel vector predictor based on the method of moments and the cumulants of the received signal. Due to the mutual independence of the sources and their independence with respect to the noise, the n-order pure cumulant of r conditioned on the realization of the channel vector, simply denoted by $\kappa_n(r)$, reads

$$\kappa_n(r) = \sum_{k=1}^{K} (A_k h_k)^n \kappa_n(s_k) + \kappa_n(w) \tag{III.10}$$

where we used the homogeneity property of cumulants on the channel coefficients, Eq.(I.22), and A_k is the reference amplitude of constellation $\mathscr{C}_k$. Eq.(III.10) can be simplified as follows : first, because of the circular symmetry of the noise, all the pure moments, and consequently all the pure cumulants of w, are zero. Besides, as was seen in Section II.4, Eq.(II.20), the uniform assumption of each source's distribution combined with the discrete rotational symmetry of their support $\mathscr{C}_k$, implies that all (pure) moments of source s_k of order non-multiple of q_k are zero as well. Likewise, the n-th order (pure) cumulant of s_k, as an homogeneous polynomial of degree n in the variable s_k, is necessarily zero if n is not a multiple of q_k. In the case q_k divides n, we can express the n-th order cumulant of source s_k as

$$\kappa_n(s_k) = \alpha_{p_k,q_k} \kappa_{p_k}\left(\frac{\mu_{q_k}(s_k)}{\alpha_{1,q_k}}, \frac{\mu_{2q_k}(s_k)}{\alpha_{2,q_k}}, \cdots, \frac{\mu_{p_k q_k}(s_k)}{\alpha_{p_k,q_k}}\right) \tag{III.11}$$

with p_k the quotient of the division of n by q_k and $\alpha_{p,q} \triangleq \frac{(pq)!}{p!(q!)^p}$. Let us recall that the right-hand side of (III.11) is to be understood as the polynomial associated with the general pure cumulant of order p_k, and not as a cumulant of s_k, as was explained in Section I.1.4. A proof of (III.11) is provided in Appendix A.1. Further defining $\mathbf{q} \triangleq (q_1, \cdots q_K)$, $\chi_k \triangleq s_k^{q_k}$ and $\eta_k \triangleq (A_k h_k)^{q_k}$, (III.10) simplifies to

$$\kappa_n(r) = \sum_{k \in \mathscr{D}_{\mathbf{q}}(n)} \eta_k^{p_k} \alpha_{p_k,q_k} \kappa_{p_k}\left(\frac{\mu_1(\chi_k)}{\alpha_{1,q_k}}, \frac{\mu_2(\chi_k)}{\alpha_{2,q_k}}, \cdots, \frac{\mu_{p_k}(\chi_k)}{\alpha_{p_k,q_k}}\right) \tag{III.12}$$

where $\mathscr{D}_{\mathbf{q}}(n)$ is the subset of $\{1,\cdots,K\}$ such that q_k divides n, with quotient p_k. Thus, by an appropriate choice of cumulants of the received signal to be estimated, one obtains a polynomial system in the channels q_k-th power predictors. As for arbitrary rotational orders q_k (III.12) does not generally have an analytical solution, in the following we will mainly restrict to two opposite special cases: all rotational orders are distinct, and all are equal.

III.3.2 Distinct rotational orders

The linear BSS problem being defined up to permutation of the sources, we can without loss of generality assume that the q_k's are sorted in ascending order, $q_k < q_{k+1}$ with $k \in \{1,\cdots,K-1\}$. Then, from (III.12) we see that $\mathbb{E}[r^{q_k}]$ can only depend on the first k sources, *i.e.* $\mathscr{D}_{\mathbf{q}}(q_k) \subseteq \{1,\cdots,k\}$. Further assuming that $\mathbb{E}[\chi_k] \neq 0$ for each source s_k, by considering the cumulants of r for each order q_k Eq.(III.12) reduces to a triangular system, whose solution is recursively given by

$$\begin{aligned}\eta_1 &= \mathbb{E}[r^{q_1}]/\mathbb{E}[\chi_1] \\ \eta_k &= \frac{1}{\mathbb{E}[\chi_k]}\left(\kappa_{q_k}(r) - \sum_{m\in\mathscr{D}_{\mathbf{q}}^{+}(q_k)} \eta_m^{p_m}\kappa_{p_m}(\chi_m)\right)\end{aligned} \tag{III.13}$$

where $\mathscr{D}_{\mathbf{q}}^{+}(q_k) \triangleq \mathscr{D}_{\mathbf{q}}(q_k)\backslash\{k\}$. The number of terms in the sum of (III.13) depends on the divisibility relations between the rotational orders. As a particular case, when all q_k's are mutually prime, the system is diagonal ($\mathscr{D}_{\mathbf{q}}(q_k) = \varnothing$), and the solution of each channel's power predictor simply reads

$$\eta_k = \frac{\mathbb{E}[r^{q_k}]}{\mathbb{E}[\chi_k]} \tag{III.14}$$

In the context of digital communications this setting is however quite unlikely to occur, as the modulation schemes employed are most often binary.

The computation of the channel predictors in (III.13) essentially requires to compute the K cumulant estimates of r from order q_1 to q_K. The precise number of distinct moments of r involved for this depends on the divisibility relations between the q_k's, but is in any case included in the integer set $\{q_1, q_1+1,\cdots,q_K\}$. The computational load of the n-th order sample moment is in $\mathcal{O}(Nn)$. Further neglecting the number of operations in the expression of each cumulant with respect to N, the overall complexity of the method is given by

$$\sum_{n=q_1}^{q_K}\mathcal{O}(nN) = \mathcal{O}\left(N\frac{q_1+q_K}{2}(q_K-q_1+1)\right) \simeq \mathcal{O}\left(N(q_K^2-q_1^2)\right) \tag{III.15}$$

In digital transmissions, practical choices of rotational orders are powers of 2 and typically range from 2 to 16, meaning that system (III.13) can basically estimate up to $K=4$ channel predictors. Beyond this bound it is likely that some users will share the same rotational orders. Let us give a practical example of (III.13) by considering a BPSK modulation, a QPSK and a PSK 8. Then $\mathbf{q}=(2,4,8)$ and $\mathbb{E}[\chi_k]=1$ for all k in $\{1,2,3\}$, so from (III.13)

we get

$$\eta_1 = \mathbb{E}[\rho] \tag{III.16a}$$
$$\eta_2 = \mathbb{J}[\rho] \tag{III.16b}$$
$$\eta_3 = \mathbb{J}\left[\rho^2\right] - 68\mathbb{E}[\rho]^2\,\mathbb{J}[\rho] \tag{III.16c}$$

where $\rho \triangleq r^2$ and we used the additional equation given by $\kappa_6(r)$ to simplify the expression of $\kappa_8(r)$ in (III.16c).

Finally, since the system is triangular there is only one predictor $\widehat{\boldsymbol{\eta}}$. However, for each $\widehat{\eta}_k$ there are q_k possible roots $\widehat{h}_k$, hence strictly speaking the moment channel predictor is not unique, and the number of possible channel predictors is given by $q_1 q_2 \cdots q_K$. Yet, as far as ILSE is concerned, the particular choice of a given predictor has in this case no influence on the output of the algorithm because of the rotational symmetry of the sources, and only results in global permutations in the estimated symbols for each user. Consequently for distinct rotational orders there is essentially only one possible initial channel predictor for ILSE, which makes the solution of the moment problem unique, in that respect.

III.3.3 Equal rotational orders

In the opposite case where all rotational orders are equal, *i.e.* $q_k = q$ for all k in $\{1, \cdots, K\}$, only moments of r that are multiple of q can be non-zero. The appropriate variable to consider is then $\rho \triangleq r^q$. Let us recall that having identical rotation orders does not imply having identical constellations. Especially, all QAM constellations are of rotational order $q = 4$ regardless of their size. Considering (III.12) for the n-th multiple of q yields

$$\kappa_n\left(\frac{\mu_1(\rho)}{\alpha_{1,q}}, \frac{\mu_2(\rho)}{\alpha_{2,q}}, \cdots, \frac{\mu_n(\rho)}{\alpha_{n,q}}\right) = \sum_{k=1}^{K} \kappa_n\left(\frac{\mu_1(\chi_k)}{\alpha_{1,q}}, \frac{\mu_2(\chi_k)}{\alpha_{2,q}}, \cdots, \frac{\mu_n(\chi_k)}{\alpha_{n,q}}\right)\eta_k^n \tag{III.17}$$

Hence, taking (III.17) for integers n from 1 to K results in a full polynomial set of equations. For an arbitrary number of sources K there is no analytical solution to this system, so in general solving the problem requires numerical algorithms. For $K \leq 4$ however, algebraic expressions for $\boldsymbol{\eta}$ can be derived. As for complexity, the computation of predictors from system (III.17) essentially consists in estimating the moments of ρ from order 1 to qK. Considering sample moment estimators and neglecting both the number of operations in the polynomials κ_n and the complexity of the root-finding algorithm needed in the general case, the overall complexity of the estimation process is approximately in $\mathcal{O}\left(NqK^2\right)$.

In the two next sections we give exact solutions to (III.17) for two and three sources, respectively. As we will often illustrate our results with QAM constellations, it is useful to note that in this case the polynomials κ_n involved in (III.17) have the following simplified expression

$$\kappa_n\left(\frac{\mu(\chi)}{\alpha_{1,4}}, \frac{\mu_2(\chi)}{\alpha_{2,4}}, \cdots, \frac{\mu_n(\chi)}{\alpha_{n,4}}\right) = 2\frac{M^{2n}-1}{4^{2n}-1}6^n\kappa_{2n}\left(\frac{1}{\alpha_{2,2}}, \frac{1}{\alpha_{4,2}}, \cdots, \frac{1}{\alpha_{2n,2}}\right) \tag{III.18}$$

where χ denotes the fourth power of a QAM source with M symbols. The first terms of (III.18) read

$$\kappa_1\left(\frac{\mu_1(\chi)}{\alpha_{1,4}}\right) = -\frac{4}{15}(M^2-1) \tag{III.19a}$$

$$\kappa_2\left(\frac{\mu_1(\chi)}{\alpha_{1,4}}, \frac{\mu_2(\chi)}{\alpha_{2,4}}\right) = -\frac{32}{525}(M^4-1) \tag{III.19b}$$

$$\kappa_3\left(\frac{\mu_1(\chi)}{\alpha_{1,4}}, \frac{\mu_2(\chi)}{\alpha_{2,4}}, \frac{\mu_3(\chi)}{\alpha_{3,4}}\right) = -\frac{707\,584}{23\,648\,625}(M^6-1) \tag{III.19c}$$

A similar expression can be derived for ASK constellations, and is provided in Appendix A.2 along with a proof of (III.18).

Two-sources case

When $K=2$, system (III.17) can be quite easily solved in the q-th power channel $\boldsymbol{\eta}$ for any choice of constellations with equal rotation order. The system to consider explicitely reads

$$\mathbb{E}[\rho] = \eta_1\mathbb{E}[\chi_1] + \eta_2\mathbb{E}[\chi_2] \tag{III.20a}$$

$$\mathbb{E}[\rho^2] - \alpha_{2,q}\mathbb{E}[\rho]^2 = \left(\mathbb{E}[\chi_1^2] - \alpha_{2,q}\mathbb{E}[\chi_1]^2\right)\eta_1^2 + \left(\mathbb{E}[\chi_2^2] - \alpha_{2,q}\mathbb{E}[\chi_2]^2\right)\eta_2^2 \tag{III.20b}$$

There are two solutions $\boldsymbol{\eta}^{(m)}$, $m\in\{1,2\}$ to this system. Defining $\mu_\rho \triangleq \mathbb{E}[\rho]$, $\sigma_\rho^2 \triangleq \mathbb{J}[\rho]$, $\mu_k \triangleq \mathbb{E}[\chi_k]$, $\sigma_k^2 \triangleq \mathbb{J}[\chi_k]$ and $\omega_k \triangleq \beta_q\mu_k^2 - \sigma_k^2$ with $\beta_q \triangleq \alpha_{2,q}-1 = \binom{2q-1}{q}-1$, the components of each vector solution are

$$\begin{aligned}
\eta_1^{(m)} &= \frac{\mu_1\mu_\rho(\sigma_2^2-\beta_q\mu_2^2) + (-1)^{m+1}\mu_2\gamma(\mu_\rho,\sigma_\rho^2)}{\mu_1^2(\sigma_2^2-\beta_q\mu_2^2) + \mu_2^2(\sigma_1^2-\beta_q\mu_1^2)} = \frac{\mu_1\omega_2\mu_\rho + (-1)^{m+1}\mu_2\gamma(\mu_\rho,\sigma_\rho^2)}{\mu_1^2\omega_2+\mu_2^2\omega_1} \\
\eta_2^{(m)} &= \frac{\mu_2\mu_\rho(\sigma_1^2-\beta_q\mu_1^2) - (-1)^{m+1}\mu_1\gamma(\mu_\rho,\sigma_\rho^2)}{\mu_1^2(\sigma_2^2-\beta_q\mu_2^2) + \mu_2^2(\sigma_1^2-\beta_q\mu_1^2)} = \frac{\mu_2\omega_1\mu_\rho - (-1)^{m+1}\mu_1\gamma(\mu_\rho,\sigma_\rho^2)}{\mu_1^2\omega_2+\mu_2^2\omega_1}
\end{aligned} \tag{III.21}$$

where $\gamma(\mu_\rho,\sigma_\rho^2)$ is the principal complex square root of

$$\Gamma(\mu_\rho,\sigma_\rho^2) = \omega_1(\mu_\rho^2\sigma_2^2 - \mu_2^2\sigma_\rho^2) + \omega_1\omega_2\mu_\rho^2 + \omega_2(\mu_\rho^2\sigma_1^2 - \mu_1^2\sigma_\rho^2) \tag{III.22}$$

Thus, we are basically left with two possible predictors $\widehat{\boldsymbol{\eta}}^{(1)}$ and $\widehat{\boldsymbol{\eta}}^{(2)}$. Although the choice of the q-th root of each component is irrelevant as pointed out in the previous section, each channel predictor $\hat{\eta}^{(m)}$ will generally make ILSE converge to different fixed points. Strategies regarding how to choose between both predictors are discussed in Section III.3.5. When both constellations are the same however, we have $(\widehat{\eta_1}^{(1)}, \widehat{\eta_2}^{(1)}) = (\widehat{\eta_2}^{(2)}, \widehat{\eta_1}^{(2)})$, so each solution is a permutation of the other and the predictor can be considered unique, as a consequence of the linear BSS model permutation invariance.

To illustrate the two-sources scenario let us consider two QAM constellations of respective size M_1 and M_2. Then we have $\mu_k = \frac{-4}{15}(M_k^2-1)$, $\sigma_k^2 = \frac{4^3}{15^2}(M_k^2-1)(M_k^2-16)$ and $\omega_k = \frac{4^3}{30}(M_k^4-1)$, so (III.21) reads

$$\widehat{\eta_k}^{(m)} = \frac{-15/8}{M_1^2M_2^2-1}\cdot\left((M_{\tau(k)}^2+1)\bar{\rho}+(-1)^{\tau(k)+m+1}\sqrt{\tfrac{M_{\tau(k)}^2-1}{M_k^2-1}}\tilde{\gamma}(\mu_\rho,\sigma_\rho^2)\right) \tag{III.23}$$

where $\tau(k)$ is the swap operator, *i.e.* $\tau(1)=2$ and $\tau(2)=1$, and $\tilde{\gamma}(\mu_\rho,\sigma_\rho^2)$ is the principal complex square root of

$$\tilde{\Gamma}(\mu_\rho,\sigma_\rho^2) \triangleq \frac{1}{15}(19\mu_\rho^2-\sigma_\rho^2)(M_1^2M_2^2-1)-\mu_\rho^2(M_1^2+M_2^2+2) \tag{III.24}$$

Three-sources case

In the three-sources case (III.17) can also be exactly solved for arbitrary source constellations. Yet to avoid unecessary cumbersome expressions we will restrict the derivation to the case where all three constellations are the same. System (III.17) can then be rewritten as

$$\Phi_n \triangleq \frac{P_n\left(\frac{\mu_1(\rho)}{\alpha_{1,q}},\ \frac{\mu_2(\rho)}{\alpha_{2,q}},\ \cdots,\ \frac{\mu_n(\rho)}{\alpha_{n,q}}\right)}{P_n\left(\frac{\mu_1}{\alpha_{1,q}},\ \frac{\mu_2}{\alpha_{1,q}},\ \cdots,\ \frac{\mu_n}{\alpha_{n,q}}\right)} = \eta_1^n+\eta_2^n+\eta_3^n, \quad n\in\{1,2,3\} \tag{III.25}$$

with $\mu_k \triangleq \mathbb{E}\left[\chi^k\right]$ and χ denotes any of the three statistically identical sources. By permutation symmetry we know that the solutions to this system are the three roots of the same cubic equation. We can thus search the components of $\boldsymbol{\eta}$ under the form $\eta_k = \frac{1}{3}\left(a+e^{ik\frac{2\pi}{3}}c+e^{-ik\frac{2\pi}{3}}\frac{b}{c}\right)$ with $(a,b,c)\in\mathbb{C}^3$. From (III.25) we obtain the equivalent system

$$\begin{cases}\Phi_1 &= a\\ \Phi_2 &= \frac{1}{3}\left(a^2+2b\right)\\ \Phi_3 &= \frac{1}{9}\left(a^3+c^3+\left(\frac{b}{c}\right)^3+6ab\right)\end{cases} \tag{III.26}$$

whose solution is

$$\begin{cases}a &= \Phi_1\\ b &= \frac{1}{2}\left(3\Phi_2-\Phi_1^2\right)\\ c &= \sqrt[3]{\frac{1}{2}\left(9\Phi_3+9\Phi_1\Phi_2-2\Phi_1^3+\sqrt{\left(9\Phi_3+9\Phi_1\Phi_2-2\Phi_1^3\right)^2-\frac{1}{2}(3\Phi_2-\Phi_1^2)^3}\right)}\end{cases} \tag{III.27}$$

where in the expression of c the choice of the cubic and square roots has no consequence on the solution $\boldsymbol{\eta}$, apart from permutation of its components. Similarly to the two-users case, for QAM constellations the coefficients a, b and c can be rewritten in terms of the constellation size M through equations (III.19a) - (III.19c). The resulting expressions are rather complicated and are omitted for the sake of simplicity.

III.3.4 Arbitrary rotational orders

In the general case of arbitrary rotational orders, there may be several approaches to solve the moment problem (III.11), depending on which cumulants one chooses to consider. An interesting fact is that we can always find an appropriate set of cumulants for which the resulting equation system displays a block-triangular structure. The number of blocks is then given by the number of distinct values in the rotational vector $\mathbf{q}$, and the number of equations in each block by the multiplicity m_k of the q_k associated to that block, *i.e.* the number of times the value taken by q_k appears in $\mathbf{q}$. For instance, in the all-distinct rotational orders case $m_k = 1$ for all k so the system is indeed triangular, while in the previous section we had $m_k = K$ for all k, resulting in a single-block structure of size K. Within each bock the number of distinct predictors (up to permutations) lies between 1, when all constellations associated to that block are the same, and $m_k!$, when all constellations are different. Hence the total number of distinct predictors is bounded by the products of the factorials of the multiplicities in $\mathbf{q}$.

To show how the orders of the cumulants in (III.11) can be chosen so as to obtain a block-triangular system, let us assume the q_k's to be sorted in ascending order. According to the previous section on equal rotational orders , the m_1 first cumulants of r of order multiple of q_1 form a set of equations in the channel vector power coefficients η_1 to η_{m_1}. Some of those equations may however also depend on other coefficients. This actually occurs for any integer $m \leq m_1$ such that $m\,q_1$ is a multiple of one of the (strictly) greater q_k's, $k > m_1$. So, in order to have a closed subset of equations for coefficients η_1 to η_{m_1} we can simply choose the m_1 smallest multiples of q_1 that are not multiples of any of the other distinct q_k. Applying the same reasoning to the second distinct rotational order, q_{m_1+1}, we see that taking the m_2 smallest cumulants of order multiple of q_{m_1+1} *and* not multiple of any of the remaining q_k's result in a subset of m_2 equations in the channels coefficients η_{m_1+1} to $\eta_{m_1+m_2}$, and possibly in the coefficients from η_1 to η_{m_1}, which have already been estimated. By recursion, we can build in this fashion subsets of m_k equations which depend on the m_k channel coefficients associated with the sources having the same rotational order q_k, and possibly on some of the coefficients derived from previous recursions. In particular, when all distinct rotational orders are mutually prime, the system is block-diagonal, meaning that each block forms a closed subset of equations.

Let us take a specific example to illustrate the above discussion by considering $K = 4$ sources, with $q_1 = q_2$ and $q_3 = q_4$ (so $m_1 = m_2 = 2$ and $m_3 = m_4 = 2$). The precise structure of the resulting system is determined by the divisibility relations between q_1 and q_3 and can be decomposed into three cases:

1. $q_1 < q_3 < 2q_1$: in this setting, q_3 cannot divide $2\,q_1$, since $q_3 > q_1$ so any multiple of q_3 is stricly greater than $2\,q_1$. Taking then the cumulants of r of order q_1 and $2\,q_1$ yields the closed subset of equations given by (III.20). Likewise, $2\,q_3$ is not a multiple of $2\,q_1$ (otherwise q_3 would be a multiple of q_1, which is impossible since the smallest multiple of q_1 is $2\,q_1 > q_3$), so taking the cumulants of order q_3 and $2\,q_3$ results in another closed subset of equations (III.20) which can be independently solved

from the first one. The system is block-diagonal, and the solutions are given by (III.21);

2. $2q_1 < q_3$: here the first subset of equations is obviously identical to that of the previous case. As for the second, if q_3 is not a multiple of q_1 then the system is block-diagonal. Otherwise, the cumulants of order q_3 and $2\,q_3$ depend on the coefficients η_1 and η_2. Using the solution from the first subset the second subset can be expressed in the same form as (III.20), and the solution is formally similar to (III.21);

3. the most interesting case occurs when $q_3 = 2\,q_1$. Considering equation (III.12) for $n = q_1, 2\,q_1, 3\,q_1$ and $4\,q_1$ results in the following system

$$\begin{cases} \kappa_1(\rho) = \kappa_1(\chi_1)\eta_1 + \kappa_1(\chi_2)\eta_2 \\ \kappa_2(\rho) = \kappa_2(\chi_1)\eta_1^2 + \kappa_1(\chi_2)\eta_2^2 + \dfrac{\alpha_{1,q_3}}{\alpha_{2,q_1}}\kappa_1(\chi_3)\eta_3 + \dfrac{\alpha_{1,q_3}}{\alpha_{2,q_1}}\kappa_1(\chi_4)\eta_4 \\ \kappa_3\left(\rho\right) = \kappa_3\left(\chi_1\right)\eta_1^3 + \kappa_3\left(\chi_2\right)\eta_2^3 \\ \kappa_4\left(\rho\right) = \kappa_4\left(\chi_1\right)\eta_1^4 + \kappa_4\left(\chi_2\right)\eta_2^4 + \dfrac{\alpha_{2,q_3}}{\alpha_{4,q_1}}\kappa_2\left(\chi_3\right)\eta_3^2 + \dfrac{\alpha_{2,q_3}}{\alpha_{4,q_1}}\kappa_2\left(\chi_4\right)\eta_4^2 \end{cases} \tag{III.28}$$

Here $\kappa_p(\chi_k)$ is just a shorthand notation for $\kappa_p\left(\frac{\mu_1(\chi_k)}{\alpha_{1,q_k}}, \cdots, \frac{\mu_p(\chi_k)}{\alpha_{p,q_k}}\right)$ and similarly for $\kappa_p(\rho)$ with $\rho \triangleq r^{q_1}$. As expected the second equation depends not only on η_1 and η_2, but also on η_3 and η_4. The third equation only involves η_1 and η_2 since $3\,q_1$ is not a mutiple of $q_3 = 2\,q_1$. Thus we can use the first and third equations of (III.28) to find predictors for η_1 and η_2, then solve the second and fourth equations in η_3 and η_4. To simplify the derivations, let us assume that constellations with equal rotational order are identical. Defining

$$\Phi_p \triangleq \frac{\kappa_p(\rho)}{\kappa_p(\chi_1)} = \frac{\kappa_p\left(\frac{\mu_1(\rho)}{\alpha_{1,q_1}}, \cdots, \frac{\mu_k(\rho)}{\alpha_{p,q_1}}\right)}{\kappa_p\left(\frac{\mu_1(\chi_1)}{\alpha_{1,q_1}}, \cdots, \frac{\mu_k(\chi_1)}{\alpha_{p,q_1}}\right)} \tag{III.29}$$

for $p \in \{1,2,3,4\}$, the (essentially unique) solution to system (III.28) is given by

$$\begin{cases} \eta_k = \dfrac{1}{2}\left(\Psi_1 + (-1)^k\sqrt{2\Psi_2 - \Psi_1^2}\right), & k \in \{1,2\} \\ \eta_k = \dfrac{1}{2}\left(\Psi_3 + (-1)^k\sqrt{2\Psi_4 - \Psi_3^2}\right), & k \in \{3,4\} \end{cases} \tag{III.30}$$

where the Ψ_p's, $p \in \{1,2,3,4\}$, are defined by

$$\Psi_1 \triangleq \Phi_1 \tag{III.31a}$$

$$\Psi_2 \triangleq \frac{1}{3}\left(2\frac{\Phi_3}{\Phi_1} + \Phi_1^2\right) \tag{III.31b}$$

$$\Psi_3 \triangleq \frac{1}{3}\,\frac{\alpha_{2,q_1}}{\alpha_{1,q_3}}\,\frac{\kappa_2(\chi_1)}{\kappa_1(\chi_3)}\left(3\Phi_2 - 2\frac{\Phi_3}{\Phi_1} - \Phi_1^2\right) \tag{III.31c}$$

$$\Psi_4 \triangleq \frac{1}{9}\,\frac{\alpha_{4,q_1}}{\alpha_{2,q_3}}\,\frac{\kappa_4(\chi_1)}{\kappa_2(\chi_3)}\left(9\Phi_4 - 2\frac{\Phi_3^2}{\Phi_1^2} - 8\Phi_1\Phi_3 + \Phi_1^4\right) \tag{III.31d}$$

As a practical application of (III.30) we can take for instance two ASK constellations of size M_1 and two QAM constellations of size M_2. Computing the first four polynomials $\kappa_n(\chi_1)$ (Eq.(A.12)),

$$\kappa_1(\chi_1) = \frac{1}{3}(M_1^2 - 1) \qquad \kappa_2(\chi_1) = -\frac{2}{45}(M_1^4 - 1) \tag{III.32a}$$

$$\kappa_3(\chi_1) = \frac{16}{945}(M_1^6 - 1) \qquad \kappa_4(\chi_1) = -\frac{16}{1575}(M_1^8 - 1) \tag{III.32b}$$

and using (III.19a) and (III.19b) for $\kappa_1(\chi_3)$ and $\kappa_2(\chi_3)$ the expression of the Ψ_p's are found to be

$$\Psi_1 = 3\varphi_1(\rho) \tag{III.33a}$$

$$\Psi_2 = \frac{105}{8}\frac{\varphi_3(\rho)}{\phi_1(\rho)} + 3\varphi_1^2(\rho) \tag{III.33b}$$

$$\Psi_3 = -\frac{1}{16}\frac{M_1^4 - 1}{M_2^2 - 1}\left(180\varphi_2(\rho) + 105\frac{\varphi_3(\rho)}{\varphi_1(\rho)} + 24\varphi_1^2(\rho)\right) \tag{III.33c}$$

$$\Psi_4 = -\frac{315}{4}\frac{M_1^8 - 1}{M_2^4 - 1}\left(\frac{5}{8}\varphi_4(\rho) + \frac{35}{64}\varphi_3(\rho)\varphi_1(\rho) + \frac{\varphi_3^2(\rho)}{\varphi_1^2(\rho)} - \frac{2}{35}\varphi_1^4(\rho)\right) \tag{III.33d}$$

with $\varphi_p(\rho) \triangleq \frac{\kappa_p(\rho)}{M_1^{2p}-1}$.

The block-triangular structure of the moment problem (III.11) has the theoretical interest of making possible derivation of analytical predictors for mixtures of more than four sources, the only constraint being for the size of each block (*i.e.* the multiplicities) to not exceed four. This strategy may however not be the best one in regards to computational complexity and overall quality of the derived predictors, as it requires computation of high-order cumulants, the estimation of which is known to be increasingly difficult due to higher variance and slower convergence properties. As a consequence, in practical implementations it may be more reliable to consider full sets of equations derived from cumulants of lower order. That is, for K sources we search for the K smallest cumulant orders such that the system is solvable with respect to all the channel coefficients. This may lead to an increased quality of the estimated quantitites, but generally requires as a counterpart the use of numerical algorithms to solve the system under consideration.

Let us also make clear that the block-triangular structure is a direct consequence of the discrete circular symmetry of the sources. Within our assumptions, this property is itself granted by the structure of the constellations and the uniformity assumption of the source distributions. Should the latter hypothesis be strongly violated, the constraints on the moments of the sources (II.20) will no longer hold. Consequently, any cumulant of the received signal is likely to be non zero and dependent on all the sources, resulting in systematically full equation system structures. The number of sources we can analytically address is then bounded by four, regardless of the considered modulation schemes. In digital communications however, the uniformity of sources is in general justified enough, so we can expect the proposed estimation procedure to provide channel predictors accurate enough to enhance robustness of the ILSE algorithm against convergence to spurious local minima.

III.3.5 Statistics of the cumulant-based predictors

In Section I.2.4 we stated that estimators provided by the methods of moments are generally consistent, as long as they involve continuous functions in the moments of the observed variables. In our case though this result must be considered with caution, because predictors derived from system (III.11) are generally not unique. In the case of distinct rotational orders, the predictor $\widehat{\boldsymbol{\eta}}$ is indeed unique. Moreover, as it only involves polynomial functions of the sample moments, it is always possible to find an unbiased, minimum-variance predictor. When the sample size is large, choice between an unbiased or biased predictor usually makes little difference in vertue of consistency. Besides, the channel predictor $\widehat{\boldsymbol{h}}$ is generally biased, regardless of whether $\widehat{\boldsymbol{\eta}}$ is unbiased or not. Consequently we will always only consider the non-corrected predictors obtained by simply replacing each moment by its sample counterpart.

The situation is more complicated for equal rotational orders, as the predictors are non unique. In Appendix A.3 we show that for two sources with circularly-symmetric channels, the asymptotic expected squared bias of both predictors $\widehat{\boldsymbol{\eta}}^{(m)}$ given in (III.21) is

$$\mathbb{E}\left[\left|B(\hat{\boldsymbol{\eta}}^{(m)}|\boldsymbol{\eta})\right|^2\right] \simeq \frac{1}{2}\left((|\varepsilon_1-1|^2+|\zeta_1|^2)\mathbb{E}\left[|\eta_1|^2\right]+(|\varepsilon_2-1|^2+|\zeta_2|^2)\mathbb{E}\left[|\eta_2|^2\right]\right) \tag{III.34}$$

where $\varepsilon_k \triangleq 1-\frac{2}{1+r_k/r_{\tau(k)}}$, $\zeta_k \triangleq \frac{2\mu_k/\mu_{\tau(k)}}{1+r_k/r_{\tau(k)}}$ and $r_k \triangleq \frac{\mu_k^2}{\omega_k}$. For QAM constellations we have $r_k = \frac{1}{30}\frac{M_k^2-1}{M_k^2+1} \in \left[\frac{1}{34}\,;\,\frac{1}{30}\right[$, so $\varepsilon_k \simeq 0$, $\zeta_k \simeq \mu_k/\mu_{\tau(k)} = \frac{M_k^2-1}{M_{\tau(k)}^2-1}$, and (III.34) simplifies to

$$\mathbb{E}\left[\left|B(\hat{\boldsymbol{\eta}}^{(m)}|\boldsymbol{\eta})\right|^2\right] \simeq \left(1+\left(\frac{M_1^2-1}{M_2^2-1}\right)^2\right)\frac{\mathbb{E}\left[|\eta_1|^2\right]}{2}+\left(1+\left(\frac{M_2^2-1}{M_1^2-1}\right)^2\right)\frac{\mathbb{E}\left[|\eta_2|^2\right]}{2} \tag{III.35}$$

Equations (III.34) and (III.35) show that none of the predictors $\widehat{\boldsymbol{\eta}}^{(m)}$ are consistent when considered independently. This is because, given a channel vector realisation $\mathbf{h}$, only one of the predictor in (III.21) is asymptotically unbiased. Consequently, in order to minimize the bias and the MSE, the choice of which predictor to use between $\widehat{\boldsymbol{\eta}}^{(1)}$ and $\widehat{\boldsymbol{\eta}}^{(2)}$ is of foremost importance. Obviously, the ideal strategy would consist in choosing the estimator which is the closest to the actual channel vector in the (conditional) MSE sense. In practice, we search for suboptimal strategies that should be as close as possible to the ideal one. Formally speaking, the choice between both $\widehat{\boldsymbol{\eta}}^{(m)}$ is conditioned on an event, say $\mathscr{A}$, such that denoting by $\widehat{\boldsymbol{\eta}}$ the retained predictor, we have for instance $\widehat{\boldsymbol{\eta}} = \widehat{\boldsymbol{\eta}}^{(1)}$ if $\mathscr{A}$ is realized and $\widehat{\boldsymbol{\eta}} = \widehat{\boldsymbol{\eta}}^{(2)}$ otherwise. Still assuming circular-symmetric channels, the expected, asymptotic squared bias of $\widehat{\boldsymbol{\eta}}$ can be obtained from the law of total expectation as

$$\mathbb{E}\left[|B(\hat{\boldsymbol{\eta}}|\boldsymbol{\eta})|^2\right] \simeq \frac{p}{2}\left((|\varepsilon_1-1|^2+|\phi_1|^2)\mathbb{E}\left[|\eta_1|^2\right]+(|\varepsilon_2-1|^2+|\phi_2|^2)\mathbb{E}\left[|\eta_2|^2\right]\right) \tag{III.36}$$

where p is the probability that the predictor chosen according to a given suboptimal strategy differs from the one obtained with the ideal strategy. For any $\mathscr{A}$-based strategy, p can always be considered less than $1/2$, since otherwise one just has to consider the inverse strategy

based on $\mathscr{A}^{\mathsf{c}}$ instead.

There may be several ways of defining an appropriate strategy such that p is small. Below are two possibilities:

- first, we can consider an additional moment or cumulant, say $\kappa_n(r)$, of the received signal. Applying (III.12) to both $\widehat{\boldsymbol{\eta}}^{(m)}$, the best predictor is defined as the one which is the closest, in the quadratic sense, to the sample cumulant $\bar{\kappa}_n$

$$\widehat{\boldsymbol{\eta}} \triangleq \underset{m\in\{1,2\}}{\operatorname{argmin}} \left(\left| \bar{\kappa}_n - \widehat{\kappa}_n^{(m)} \right|^2 \right) \tag{III.37}$$

  where $\widehat{\kappa}_n^{(m)}$ is the estimator of $\kappa_n(r)$ obtained by replacing $\boldsymbol{\eta}$ with $\widehat{\boldsymbol{\eta}}^{(m)}$ in (III.12)

- another possibility is to use the ILSE cost function (III.7) as a discrimination criterion

$$\widehat{\boldsymbol{\eta}} \triangleq \underset{m\in\{1,2\}}{\operatorname{argmin}} \left(J\left(\widehat{\mathbf{h}}^{(m)}, \widehat{\mathbf{S}}^{(m)} \right) \right) \tag{III.38}$$

  where $\widehat{\mathbf{S}}^{(m)}$ is an estimation of the emitted symbols matrix obtained from $\widehat{\mathbf{h}}^{(m)}$ by enumeration (III.9) and $\widehat{\mathbf{h}}^{(m)}$ denotes any q-th roots of $\widehat{\boldsymbol{\eta}}^{(m)}$. In the same fashion we can base the decision regarding which initial predictor to keep on a given iteration t rather than the first iteration. In particular, one can wait for ILSE to converge for both initial predictors and decide which one to discard based on the final cost function achieved by the algorithm.

Both strategies (III.37) and (III.38) naturally extend to an arbitrary number of sources: one has simply to consider as many additional moments or cumulants as needed in the first case, or compute the ILSE cost function for all possible distinct predictors, up to permutations within subsets of sources having equal rotational orders.

Fig.III.4 shows the MSE of channel predictors $\widehat{h}$ obtained with different strategies from a mixture of two sources using respectively a QAM 16 and a QAM 4, with circularly-symmetric channel coefficients drawn from the same Rayleigh distribution with parameter σ_r, and a ratio E_b/N_0 of 50 dB. For the additional moment/cumulant-based strategy the third cumulant of the fourth-power received signal was used, see (III.17) for $(n, K, q) = (3, 2, 4)$. Both additional moment (III.37) and the ILSE cost-driven (III.38) decision rules result in a substantial improvement of the quadratic error compared to the naïve, purely random strategy ($p = 1/2$). The probability of wrong decision against the ideal, actual channel-based strategy, p, was numerically computed for each Rayleigh parameter σ_r and found to tend very quickly to approximately 0.15 for the moment-based strategy and 0.11 for the ILSE one. Yet, only the full ILSE-based decision rule is able to compare to the ideal case in the whole range of Rayleigh parameters, with a misdecision probability of nearly 0.01. Quite intuitively, the best initial predictor, in the MSE sense, between $\widehat{\boldsymbol{\eta}}^{(1)}$ and $\widehat{\boldsymbol{\eta}}^{(2)}$, is most likely the one which converges to the best ILSE predictor at convergence of the algorithm.

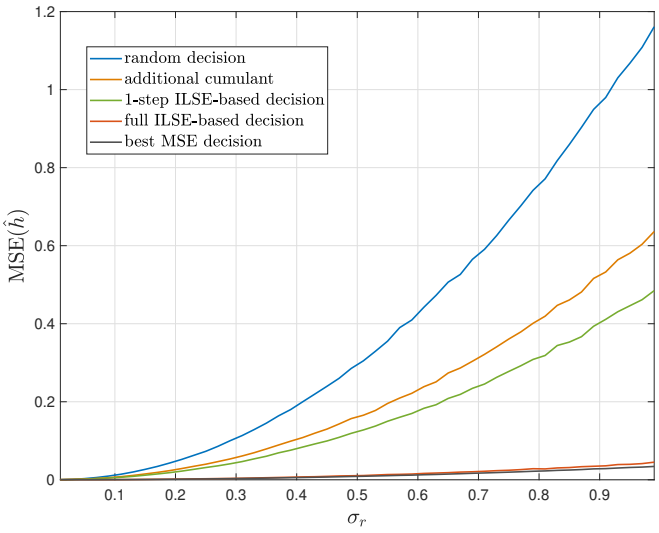

Figure III.4 – *Mean Square Error of different strategy-based channel predictors for two sources using a QAM16 and a QAM4*

It should be mentioned that when the constellations are identical, all the suboptimal strategies discussed above reduce to the random choice strategy, $p = \frac{1}{2}$. Because for identical sources the BSS problem is completely transparent to permutation, no blind strategy can distinguish between the several possible predictors provided by the moment problem.

The ILSE-based decision rule (III.38), when considered for more than one iteration, is actually little relevant, in the extent that the retained moment predictor is precisely to be used as an initial state for ILSE. Hence, after t iterations of ILSE one has not much of a reason to choose which $\widehat{\boldsymbol{\eta}}^{(m)}$ to discard and should directly consider instead the predictors $\widehat{\boldsymbol{\eta}}_t^{(m)}$ provided by ILSE at that iteration. A better strategy then consists in running ILSE in parallel for all initial predictors, and at a given iteration to stop all algorithms but the one achieving the lowest cost for that iteration. Likewise one can wait for ILSE to converge for all tested initial states and select the lowest, final cost solution. The latter possibility is obviously more computationnally demanding. Note however that in the framework of digital communications with binary modulation schemes, practical choices of constellations are such that the number of distinct solutions is in most cases reasonably small, so the additional computational load resulting from an exhaustive testing is not prohibitive. Consequently, in all the following we will always adopt this strategy whenever discriminating between distinct moment channel predictors is needed.

III.4 Performance analysis

III.4.1 Simulation settings

We now turn to the concrete application of the proposed initialization strategy to ILSE. Performances of the resulting algorithm are obtained through Monte Carlo simulations

conducted on several of the mixtures discussed in Section III.3. In all simulations, the channel vector coefficients are independently drawn from the same complex gaussian distribution with uniform variance $\sigma_h^2 = \frac{1}{\sqrt{2}}$ (so $\mathbb{E}\left[|h|\right]^2 = 1$). For each channel realization, the emitted signal consists in a sequence of $N = 1000$ symbol vectors $\mathbf{s}_n$ whose components are uniformly drawn from each source's constellation $\mathscr{C}_k$. Each constellation's reference amplitude A_k is defined so as to normalize the energy per bit, $E_b = 1$. This implies, in addition to the fact that the channels have the same distribution, that the averaged SIR equals one, meaning that the level of interference is maximal, and also accounts for the scaling invariance of the linear BSS model. The per-user emitted Signal to Noise Ratio (SNR) is expressed as the ratio E_b/N_0, with N_0 the complex noise variance.

The quality of the multiuser detector is measured in terms of the joint averaged SER, namely the sample probability of wrong symbol detection across all users

$$P_s \triangleq \mathbb{P}\left(\mathbf{s} \neq \widehat{\mathbf{s}}\right) = \mathbb{P}\left(\bigcup_{k=1}^{K} \{s_k \neq \widehat{s}_k\}\right) \tag{III.39}$$

where $\widehat{\mathbf{s}}$ is the estimator of the source vector resulting from a threshold decoding based on the channel predictor $\widehat{\mathbf{h}}$. Unlike the single-source case, there is no simple theoretical formula such as (I.52) for the averaged SER of the ideal (*i.e.* perfect CSI) threshold detection. This is because the Voronoï regions of the joint constellation $\mathscr{C}_{\mathbf{h}}$ have a non-trivial dependency in the channel vector $\mathbf{h}$, as shown on Fig.III.5. An exact expression for BPSK sources was actually derived in [28] but the resulting expression is already quite cumbersome to handle. Several upper and lower bounds on P_s can be derived, but as we are here only interested in the perfect CSI detection for comparative purposes, we will simply compute the corresponding SER by simulation. Addtionally we can measure the quality of the channel predictor by considering the (sample) Normalized Root Mean Square Error (NRMSE), which for multiuser transmissions is given by

$$\mathrm{NRMSE}(\widehat{\mathbf{h}}) \triangleq \frac{1}{\sqrt{K}} \frac{\sqrt{\mathbb{E}\left[\| \mathbf{h} - \widehat{\mathbf{h}} \|\right]^2}}{\sigma_h} \tag{III.40}$$

For comparison the performance of several blind multiuser detection methods is measured as well. The tested algorithms are listed below along with their denomination in the foregoing discussion.

perfect CSI: the ideal case where the channel is perfectly estimated;

r-ILSE: the ILSE algorithm with a fixed number of random initializations. In our simulations the number of trials was fixed to 10. The final predictor is obtained by choosing the one with the minimal cost value;

r-ILSE-ILSP: ILSE initialized with the ILSP algorithm for a fixed number of random initial states. The number of trials and selection of the final predictor are the same as for the previous method;

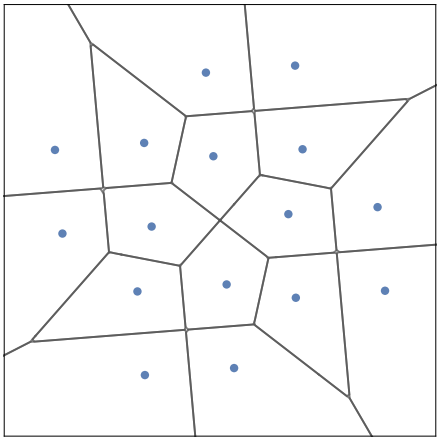

Figure III.5 – *Example of the decision regions for a mixture with two QAM4*

SIC: the SIC detection scheme presented in III.2.1. The estimation of the channels itself is based on the received signal cumulant, Eq.(III.12), with an appropriate choice for n, typically $n = q_K$;

SIC-ILSE: improvement attempt of the previous method by providing ILSE with the SIC channel predictors

MB (Moment-Based): joint channel predictors obtained from the moment method and used as a self-consistent strategy;

MB-ILSE: predictors obtained from ILSE initialized with the MB strategy.

In the following we will always assume any of the algorithms involved in the above strategies to have maximal partial information on the channels so as to achieve their best outcome. For instance, we provide SIC with a perfect estimation of the received powers from each user so that the source decoding order is optimized. Likewise, for the ILSE and ILSP-ILSE strategies, both based on random channel initalizations, the channels underlying probability density function is assumed to be known, so that the tested initial states are drawned according to the very same distribution. Finally, all indeterminacies affecting the channels predictors inherent to the symmetry of the BSS model or the sources are tackled by selecting the best solution with respect to the actual channel realization, in the squared error sense. Specifically, this amounts for the receiver to know

- the order in which each estimated source and channel are associated to their respective user (permutation invariance);
- the reference amplitude A_k of each constellation $\mathscr{C}_k$ (scaling invariance)
- which of the q_k's complex roots of $\widehat{\boldsymbol{\eta}}_k$ to consider (discrete-circular source invariance).

Obviously, in practical implementations the above information would have to be acquired through additional estimation procedures. Examples of suboptimal strategies based on partial

information on the channels will be discussed in Section III.6. In any case, a priori knowledge is always necessary for a meaningful solution of the BSS model to be retrieved.

III.4.2 Simulation results

Two sources

We first consider a two-users mixture simply composed of two QAM 4 sources. Fig.III.6 shows the SER and channel NRMSE of the algorithms presented above. Even in this quite simple case, 10 initializations of the random ILSE and ILSP-ILSE strategies are not enough to find the global minimum of their cost function. As expected, despite being provided with the perfect knowledge of the contributions of each source to the total received power, SIC is not able to yield reliable channel and source estimates, as the averaged SIR is 0dB. Likewise, the predictors derived from the moment method are in themselves not accurate enough to achieve satisfying error rates. Only ILSE initialized with either the moment method predictors or the SIC compares well to the ideal case for a wide range of noise power levels, yet with a clear advantage for the moment-based strategy. However, from approximately 20-25dB both algorithms seem to reach an error floor, close to 1.10^{-3} for the MB-ILSE scheme.

It is interesting to note that for very low values of E_b/N_0 (0-8dB), the self-consistent moment-based strategy performs better in terms of channel NRMSE than when used in conjonction with ILSE. This is because ILSE aims at jointly minimizing the likelihood with respect to the sources and the channels. For such high noise powers it appears indeed that the ILSE cost function J is not necessarily the best solution in the MSE sense. For moderate to high E_b/N_0 the predictors provided by ILSE are also the minimum NRMSE solutions among all other tested algorithms.

The most striking feature on Fig.III.6 is that the NRMSE of the MB-ILSE strategy is not monotonic decreasing, and achieves a minimum value around 26dB. Coincidentally, within the same range of E_b/N_0 the SER starts to considerably drift from the perfect CSI performance curve. A possible explanation accouting for this behavior is the global masking effect of the mixture's background noise with respect to local minima, which facilitates convergence of ILSE towards the global minimum of J. This has already been observed in Chapter II for the single-source case. Past a certain noise power level, thoses minima become more an more apparent to ILSE, hence making the global minimum more difficult to reach. The additional fact that the SER and the NRMSE seem to asymptotically tend to a fixed value can be explained by the residual occurence of those mixtures for which ILSE cannot easily avoid the local minima, even with a decent inital state. A more in-depth analysis of this hypothesis is proposed in the next section.

Fig.III.7 addresses a more complex case by considering a QAM 4 and a QAM 16. Essentially the same conclusions as in the previous case can be drawn, yet with an observed sensible loss in performance for all tested algorithms. In particular, compared to the previous

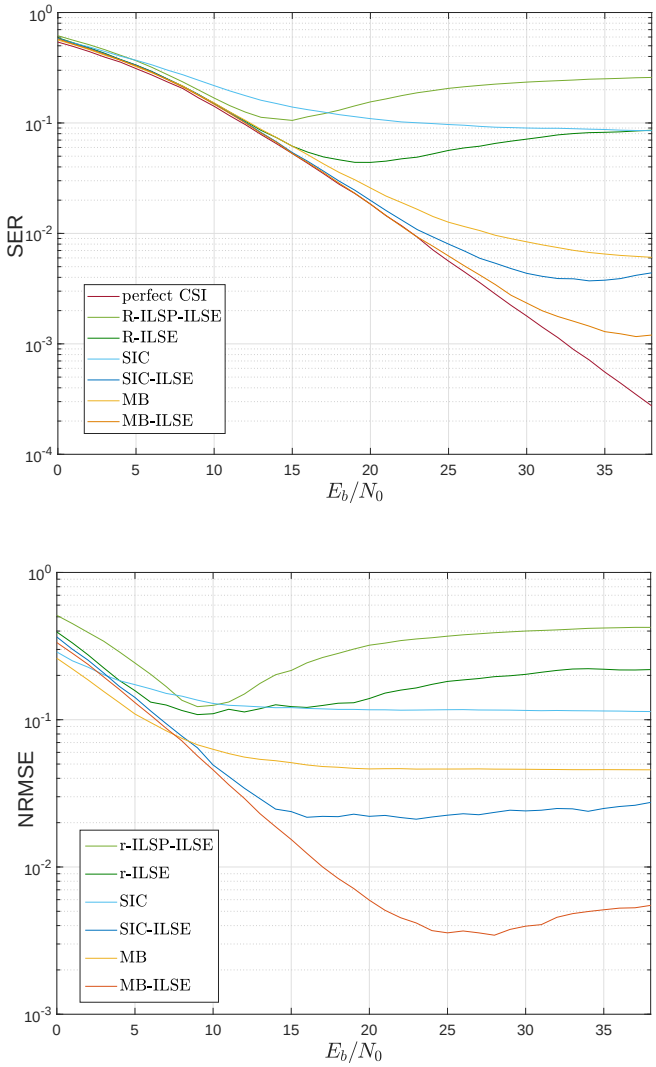

Figure III.6 – *Averaged SER (top) and NRMSE (bottom) of the two-QAM 4 mixture*

case SIC-ILSE no longer yields satisfying results, as the effects of the high interference regime intensify for higher order constellations. Here the asymptotic value reached by the MB-ILSE algorithm aproximately reads 3.10^{-2}, that is basically more than a factor ten compared to the previous mixture. The minimum of the NRMSE is achieved for a lower value than that of the two QAM 4 sources case, at approximately 18dB. Accordingly the range of E_b/N_0 for which the discrepancy betwen MB-ILSE and the perfect CSI decoding becomes manifest also occurs for lower noise powers. With an increase in the complexity and size of the overall constellation more spurious fixed points are to be expected. For high values of E_b/N_0 the Signal to Interference plus Noise Ratio (SINR) is dominated by interference, and the asymptotic error rate corresponds to those particularly strong interferent mixtures for which ILSE fails to converge to its global minimum.

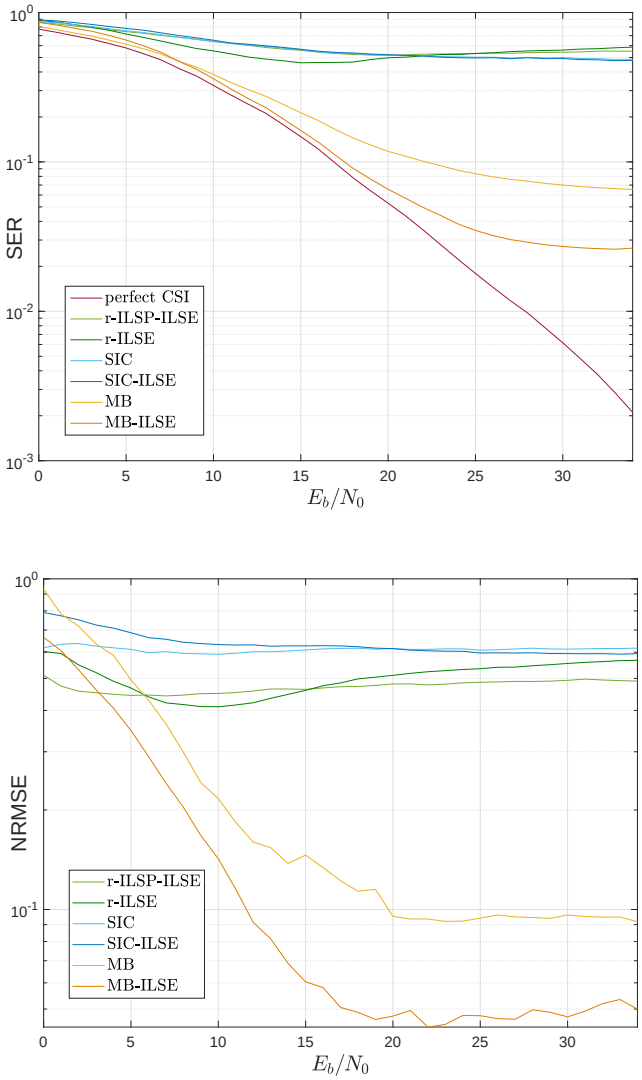

Figure III.7 – *Averaged SER (top) and NRMSE (bottom) of two-sources mixtures with one QAM4 and one QAM16*

Three sources

For the three-sources case we present the results obtained from a mixture consisting of three QAM4, Fig.III.8. All algorithms but MB-ILSE (and obviously the perfect CSI) fail to achieve error rates lower than 10^{-1}. Interestingly, despite the additional source the performances of MB-ILSE are quite similar to those of the QAM16-QAM4 mixture, and reach approximately for the same asymptotic error floor. Loosely speaking, the increased complexity of adding one simple QAM4 source compensates that of considering a higher order constellation in the two-sources scenario, both joint constellations having in the end 64 symbols.

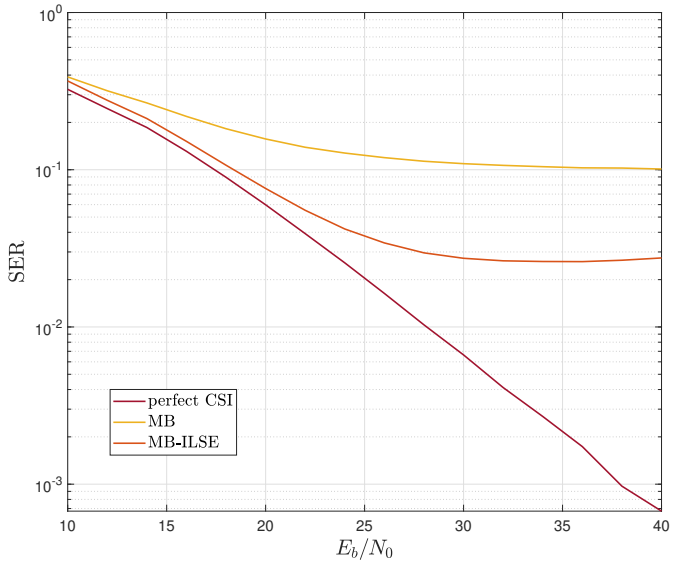

Figure III.8 – *Averaged SER of the three-QAM 4 mixture*

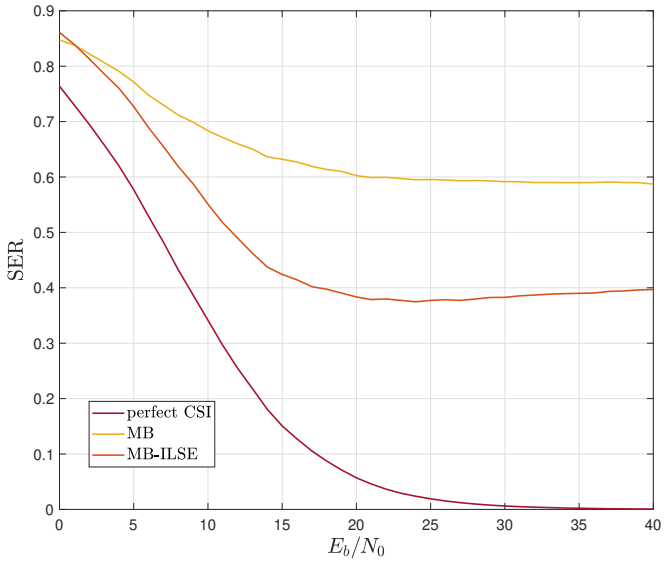

Figure III.9 – *Averaged SER of a four-sources mixture composed of two BPSK and two QAM 4*

Four sources

Let us finally consider the four-sources case addressed in III.3.4 with two BPSK and two QAM 4 constellations. From Fig.III.9 we clearly see the limits of the MB-ILSE strategy which quickly saturates at error rates of nearly 0.4. The loose argument used in the previous section to justify similar results from mixtures with the same total number of symbols does not hold here, the joint constellation being here of size 64 as well. It was actually observed trough additional simulations that the MB-ILSE algorithm has an increased overall difficulty to deal

with constellations having non equal rotational orders. For instance, a simulation performed on the three PSK example of III.3.2 also resulted in poor averaged error rates. Whether this is due to an overall increased number of local minima for such mixtures or to the moment problem estimation procedure itself has up to now not been clarified yet.

III.5 Optimization strategies

III.5.1 Origin of the error floor

We have seen that, for all mixtures considered above, the SER of the MB-ILSE algorithm always enters a saturation regime for low enough noise powers, and that the corresponding error floor increases drastically with the overall complexity (number of sources and geometry of the sources) of the mixture. This section aims at a better understanding of this phenomenon and some strategies to partially circumvent it. For this discussion the two-QAM 4 mixture will be mostly used as our reference model. Generalizations to more complex configurations will be carried out at the end of this section.

First, let us take a closer look at the SER of the two-QAM 4 mixture in the low noise power regime by considering its empirical probability function, restricted to cases where at least one symbol has been wrongly detected. This is represented on Fig.III.10 by means of the normalized histogram. The empirical pdf is clearly bimodal (trimodal if we include back the dominant mode consisting of the zero-error cases), with modes located at approximately 0.25 and 0.5 error rates. The number of modes, their position and their relative contribution to the overall density all depend on the size and structure of each source's constellation. Here the possible error rates at low noise powers are necessarily of the form $k/4$, with $k \in \{0, \cdots, 4\}$, so one could also expect additional modes located at 0.75 and 1. The pdf reveals that such scenarios have a negligible probability of occurrence. In other words, for the two-QAM 4, the minimum proportion of symbols the MB-ILSE algorithm can decode correctly is approximately 50%, regardless of the channel realizations. In the perspective of mitigating ILSE's residual error, study of the empirical pdf can thus help identify which mixture configurations contribute the most to the density profile and should be dealt with in priority.

The fundamental question we should address is whether the residual error rate of MB-ILSE originates from a subset of specific joint constellations structures, and hence is dependent on the channel realizations, or occurs regardless of the mixture. In the two-users setting, the joint constellation's geometry is entirely determined by the channel ratio $h_r \triangleq h_1/h_2$. We can then have a representation in the complex plane of the channel outputs for which the SER achieved by ILSE exceeds a given acceptable threshold value. For simplicity we take a threshold of zero, *i.e.* we consider all cases for which at least one symbol has been decoded wrong. The result is presented on Fig.III.11.

We clearly see that the channel ratios for which the SER is non zero are concentrated in several regions of the complex plane. The centroïds of these clusters exhibit a clear

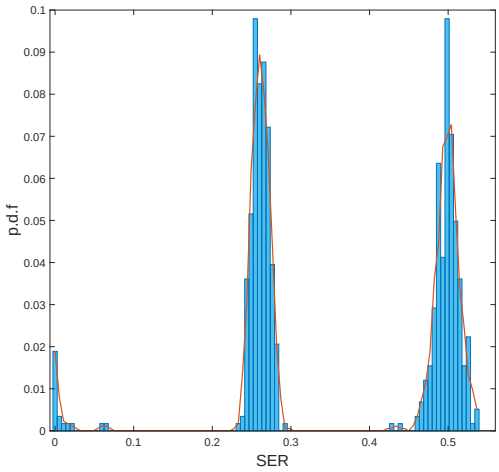

Figure III.10 – *Normalized histogram (blue) and empirical p.d.f. (orange) of the SER of the two-QAM4 mixture conditioned on non-perfect decoding cases* ($E_b/N_0 = 50dB$)

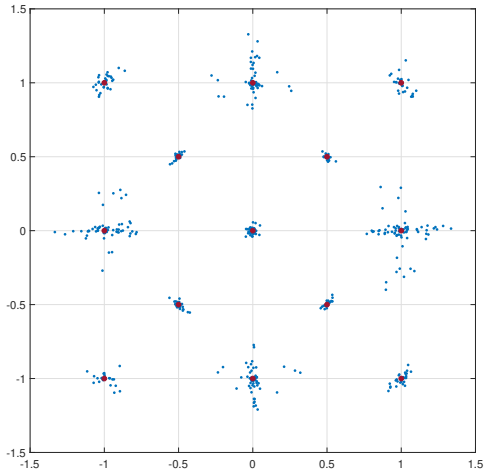

Figure III.11 – *Channel ratios distribution restricted to non-zero SER values (blue) and centroïds of the observed clusters (red)*

geometrical structure, suggesting a tight relation with respect to the constellations geometry. Restricting to the first quadrant ($h_r \succeq 0$), we have four centroïds approximately located at 0, $\frac{1+i}{2}$, 1 and $1+i$. Fig.III.12 shows the typical shapes of the joint constellations associated with each of these clusters. All have in common the fact that some symbols are very close to each other, to the point of completely fusing when approaching the exact location of the centroïds. We can then postulate that the channel coefficients for which the SER of MB-ILSE is non zero are the solutions to the equation

$$h_1 s_{11} + h_2 s_{12} = h_1 s_{21} + h_2 s_{22} \Rightarrow h_r = \frac{h_1}{h_2} = \frac{s_{22} - s_{12}}{s_{11} - s_{12}} \tag{III.41}$$

where $s_{ij} \in \mathscr{C}_j$, $(i,j) \in \{1,2\}^2$. Hence the centroïds belong to the finite support of the ratio of the random variables $s_1 - s_2$, where s_1 and s_2 are independent realizations of the same source. Considering the case of two QAM 4 we find that

$$\text{supp}(s_1 - s_2) = \{0, 1, i, -1, -i, 2+2i, -2+2i, -2-2i, 2-2i\} \tag{III.42}$$

so the support of the ratio, restricted to the first quadrant and assimilating the infinite quotient to zero, reads $\{0, 1, 1+i, \frac{1+i}{2}\}$. We indeed theoretically recover the empirical centroïds read from Fig.III.11.

Eq.(III.41) is actually a direct application of the non-identifiability conditions derived for finite-alphabet mixtures in noise-free scenarios in [47]. This provides a very intuitive and consistent explanation of ILSE's limitations in terms of the fundamental BSS concepts. Namely, ILSE is most likely to fail at solving the linear BSS model when the mixture is close to non-identifiability. Note however that in theory the involved mixtures are actually always

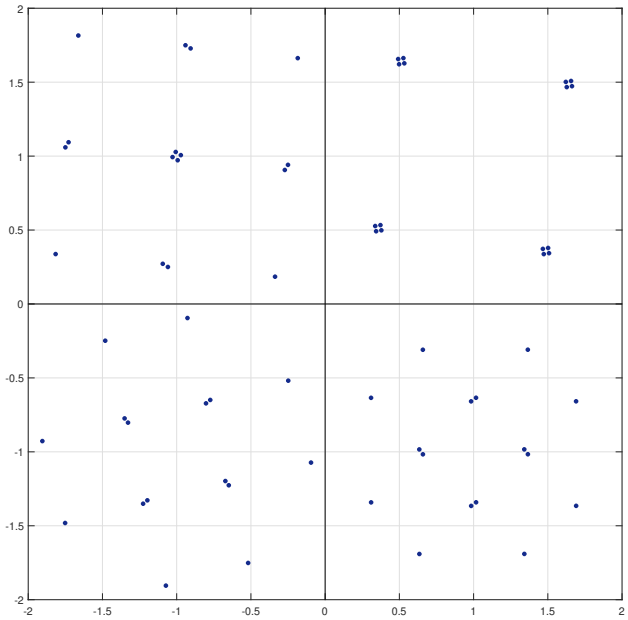

Figure III.12 – *Typical realizations of the four mixture configurations for which the SER is non-zero. From left to right and top to bottom:* $h_r \simeq 1$, $h_r \simeq 0$, $h_r \simeq \frac{1+i}{2}$ *and* $h_r \simeq 1+i$

identifiable, since the probability to have channel realizations such that (III.41) exactly holds is zero. We can then think of three main reasons accounting for ILSE to fail at perfectly decoding the received sequence in such scenarios:

1. the initial predictors provided by the moment method are statistically far from the actual channel;

2. the distribution of the local minima of the ILSE cost function for these mixtures makes it more difficult for the algorithm to converge to its global minimum, even with a good initial state;

3. the increased proximity of some of the symbols in these scenarios is such that the noise level makes it impossible to properly decode the symbols, even with a predictor close to the actual channel.

We can quite confidently discard the third hypothesis, as it would imply a similar error floor phenomenon for the perfect CSI decoding, which was not observed in any of our simulations. As for the first hypothesis, restricting the MSE of the moment method predictors to the channel realizations of Fig.III.11 indeed results in an higher score than for the global MSE. Additional specific simulations conducted on channel realizations representatives of the problematic mixtures also reveal the presence of fixed points close to the global minimum.

With these additional elements we now have a pretty good picture of the origin of the MB-ILSE error floor. Non optimal detections are essentially restricted to mixed constellations for which subsets of symbols are very close to each other. While for most

channel realizations the distribution of local minima is such that convergence of ILSE to the global minimum is not hindered by imprecision of the moment method predictors, for these subsets of constellations proximity of some spurious fixed points makes global convergence very sensitive to the initial predictor bias. From this analysis we can conclude that the main limitation of the MB-ILSE method is not interference, as otherwise any channel ratios with modulus close to 1 would be likely to result in non zero SER, but minimal inter-symbol distance in the joint constellation. Degradation of the performance of clustering-based algorithms for close or partially merged clusters is a quite general problem in statistical data analysis, that we will discuss in the last chapter of this thesis.

III.5.2 Detection of local minima

The next crucial point to address is whether the spurious solutions subsequent to non-global convergence of ILSE can be detected only with the limited information we have at disposal. We recall that ILSE, and more generally k-means, makes implicit assumptions on the underlying data distribution (see III.2.2), yet there is no guarantee all resulting solutions are actually consistent with these hypotheses. Hence a natural strategy for detecting sub-optimal solutions is to check whether the assumptions made on the mixture are observed, namely:

- the sources are independent;
- the sources are uniformly distributed.

Violation of the first condition has a strong implication: if some of the sources are fully correlated, then some combinations of symbols are impossible. Formally stated, the joint support of a linear combination (mixture) of correlated random variables is strictly included in the linear combination of the supports. This is simply the translation of k-means empty clusters solutions to geometrically constrained random variables. Consequently, if a solution of ILSE is such that some combinations of symbols are absent or extremely rare, most likely the algorithm has converged to a local minimum. Fully appropriate detection of empty classes would normally require design of a threshold value under which a given class is regarded as empty. For such low noise powers as those involved in the occurence of the SER floor, it is safe enough to simply consider a zero or infinitesimal threshold.

Fig.III.13 shows, for the two-QAM 4 mixture, which of the channel ratios resulting in an imperfect symbol decoding are such that some combinations of symbols never appear (a threshold value of 0.05 was used). Clearly the involved ratios are concentrated on the set $\{1, i, -1, -i\}$. Conditioning the SER on those solutions result in an averaged SER of approximately 0.5, which corresponds to the highest mode in the empirical error pdf of Fig.III.10. Quite intuitively solutions for which symbols are missing are the worst in terms of symbol detection errors. Identification and treatment of non-independent sources solutions hence present a triple advantage:

- its implementation is straightforward and does not require subtle threshold design;

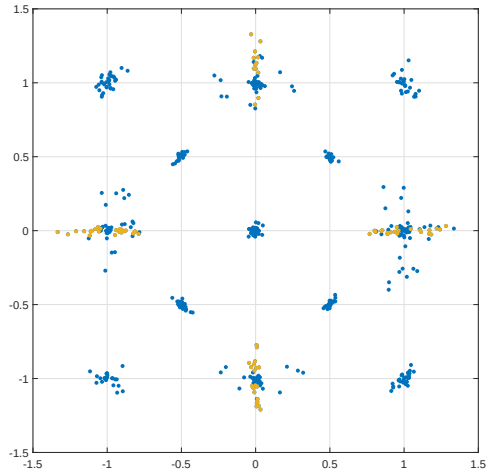

Figure III.13 – *Channel ratios leading to non-zero SER (blue) and non-independent sources ILSE solutions (yellow)*

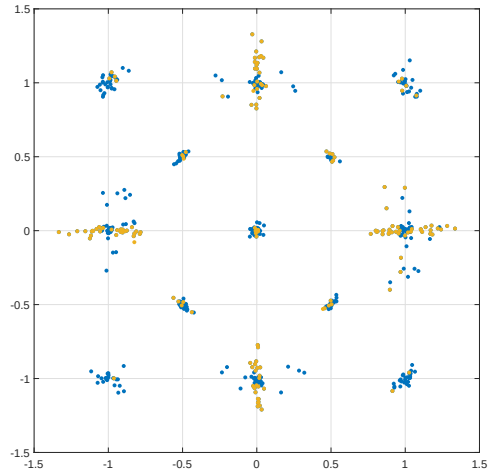

Figure III.14 – *Channel ratios leading to non-zero SER (blue) and non-uniform ILSE sources solutions (yellow)*

- it is valid for non-uniform sources as well;
- the involved spurious solutions highly contribute to the residual error floor.

However these solutions cannot entirely account for the residual error floor. To proceed further less restrictive hypotheses must be considered.

The second main assumption of our model is the discrete-uniform source distribution. Given an estimation of the mixed source symbols, exact uniformity implies for the population of each class to follow a binomial distribution with parameters N the number of received symbols and $p = M/N$ the probability of any class, with $M = \prod_k^K M_k$ the size of the joint constellation. We can then define a confidence interval for the population of each class within which we have a reasonable degree of confidence that the uniformity assumption is indeed observed. Specifically, for any estimated class $\widehat{\mathscr{C}}$ we design an interval I_ε of the form

$$I_\varepsilon \triangleq \left[\frac{N}{M}(1-\varepsilon)\,;\ \frac{N}{M}(1+\varepsilon)\right] \tag{III.43}$$

such that $\mathbb{P}\left(|\widehat{\mathscr{C}}| \in I_\varepsilon\right) \geq p_\varepsilon$, where p_ε is the so-called p-value representing the minimal confidence we have that a class with population contained in I_ε is indeed uniform. For the binomial distribution there is no convenient expression of ε as a function of p_ε. One can usually either compute ε numerically, or rely on bounds such as that provided by Hoeffding's inequality [78]

$$\mathbb{P}\left(|\widehat{\mathscr{C}}| \in I_\varepsilon\right) \geq p_H \triangleq 1 - 2\exp\left(-2\varepsilon^2 N\right) \Rightarrow \varepsilon = M\sqrt{-\frac{1}{2N}\log\left(\frac{1-p_H}{2}\right)} \tag{III.44}$$

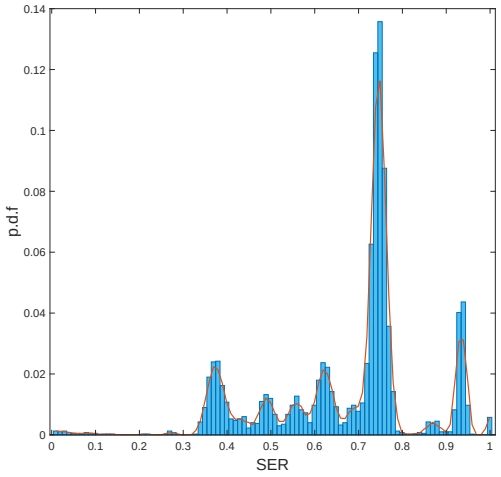

Figure III.15 – *Normalized histogram (blue) and empirical p.d.f. (orange) of the SER of the QAM16-QAM4 mixture conditioned on non-perfect decoding cases ($E_b/N_0 = 50dB$)*

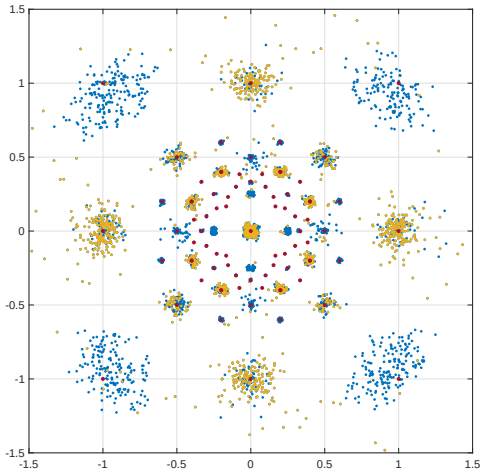

Figure III.16 – *Channel ratios leading to non-zero SER (blue) and non-independent ILSE sources solutions (yellow) for the QAM16-QAM4 mixture.*

Fig.III.14 displays the channel ratios for which ILSE solutions are regarded as non-uniform. For this simulation a threshold of 0.5 was used, meaning that we tolerate solutions having population up to 1.5 times the expected population of a truly uniform distribution. Obviously non-uniform cases include the non-independent sources cases of Fig.III.13. We see that the identified local solutions originate from the whole set of problematic channel ratios. Still a non negligible fraction of spurious fixed points remain undetected. The design of the confidence interval for identification of non-uniform solutions is in general a subtle problem. A too large threshold ε (high tolerance) results in most suboptimal solutions to be considered as uniform and not being detected. Conversely, if ε is chosen too small then good solutions are likely to be identified as spurious. This is not even mentioning that the optimal threshold may strongly depend on the sample size N. For these reasons, in the rest of the discussion we will focus on the non-independent sources solutions, whose detection appears more robust.

The above analysis conducted on the two-QAM4 mixtures holds for other two-users scenarios as well. Fig.III.15 and III.16 respectively show the empirical residual error pdf and the associated channel ratios for the QAM16-QAM4 mixture, along with the solutions detected as non consistent with the sources independence assumption. The position of the centroïds was derived from the same method as for the two-QAM4 case, Eq.(III.41). We see that all problematic ratio clusters but one are recovered in this way. The unpredicted clusters correspond to the set $h_r \in \{\frac{1}{4}, \frac{i}{4}, \frac{-1}{4}, \frac{-i}{4}\}$, and the related joint constellations appears to exhibit a structure very close to the single-user QAM64 constellation. This is reminiscent of the fact that for a QAM64 with channel h, the point $4h$ is a local minimum of the SISO-ILSE algorithm, as was demonstrated in Chapter II. Oddly enough though, the local minimum similarly induced by $2h$ is not observed, neither for the QAM16-QAM4 mixture nor for

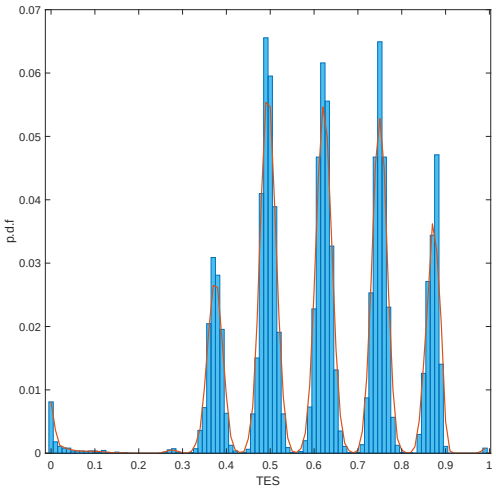

Figure III.17 – *Normalized histogram (blue) and empirical p.d.f. (orange) of the SER of the two-PSK 8 mixture conditioned on non-perfect decoding cases ($E_b/N_0 = 50dB$)*

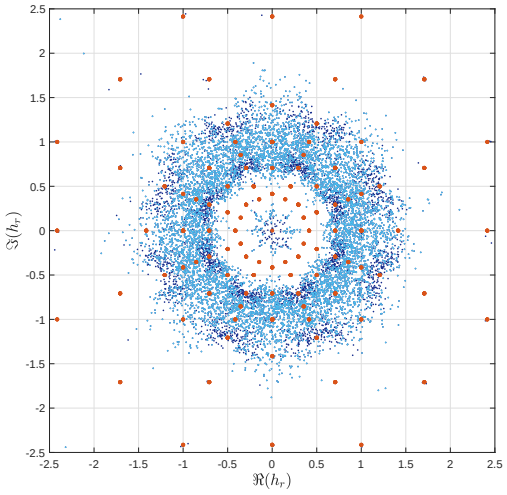

Figure III.18 – *Channel ratios leading to non-zero SER (blue) and non-independent ILSE sources solutions (yellow) for the two-PSK 8 mixture.*

the two-QAM 4 one. We also observe a substantial increase in both the proportion of non-independent sources solutions and their relative contribution to the residual error compared to the two-QAM 4 mixture: in the latter case these solutions were found to represent 29% of all suboptimal detections and their average SER was approximately 0.5, against 40% with an average error rate of 0.68 for the QAM 16-QAM 4. This phenomenon is even more visible for the two-PSK 8 mixture, Fig.III.18, for which 71.5% of suboptimal solutions were indentified as source-correlated, with an average SER of 0.65. Note here that the increased rotational symmetry order ($q = 8$) and the proximity of the centroïds makes it difficult to discern the different clusters. In any case, the predominance of non-independent sources solutions and their contribution to the asymptotic SER stresses the need and pertinence of giving particular care to their treatment.

III.5.3 Proposed solutions

Now that we dispose, at least for two-user mixtures, of a reliable way of both predicting for which channel realizations MB-ILSE is likely to result in a spurious solution, and detect those local fixed points for which independence and uniformity of the sources is not observed, we can think of several strategies to lower the asymptotic SER of the algorithm. At the very least, if a suboptimal solution is detected at the output of ILSE, the receiver can always ask for a retransmission of the current sequence in the hope that the next channel realization will be more favorable. This prudent strategy has however several drawbacks, the most obvious one being a loss in the useful data rate, and it does not exploit the predictable structure of the problematic channel ratios. Thus it should rather be used as a last resort solution, when attempts at correcting the output of the algorithm reveal ineffective.

Considering solely non-independent sources local minima, a possible strategy consists in providing ILSE with alternative initial channel predictors whose ratio are close to those predicted by (III.41) and known to result in the violation of the sources independence assumption. As an example, for the two-QAM 4 mixture there is essentially (modulo $\pi/2$-rotations symmetry) one single such point, namely $h_r = 1$ (Fig.III.13), and five for the QAM 16-QAM 4 mixture ($h_r \in \{0, 1, \frac{1+i}{2}, \}$, Fig.III.16). The new initial states may be chosen randomly or based on the moment method predictors $\widehat{\mathbf{h}}$. Of course, there is no guarantee to reach the global minimum with these initial states. Besides, if non-uniform sources solutions are to be included, this results in computing ILSE for the whole set of problematic channel ratios, which becomes large even for reasonably complex constellations, as can be seen for instance the two-PSK 8 case in Fig.III.18. As this whole analysis is fully relevant only in the low noise power regime, study of the ILSE cost function at convergence may here help to determine whether the global minimum has been achieved, possibly limiting the number of trials. Still for more complex mixtures this exhaustive testing procedure is likely to be too computationnally demanding for a practical use.

The strategy we will retain is somehow midway between systematic ask for retransmission and exhaustive testing. We will try additional initial states only for this channel ratio which is the closest, in the complex distance sense, to the one provided by the moment method predictors. In this fashion we limit the number of ILSE runs even for complex mixtures. In a fully preventive scheme, one can systematically compute the closest channel ratio from the estimated one and perform an additional run of ILSE to see which solution yields the minimum cost function, regardless of whether the solution achieved with the mere moment method predictors is detected as spurious or not. Otherwise the same possibilities as for the exhaustive testing strategy can be applied to determine if additional initial states should be tested: violation of the source independence/uniformity and examination of the cost function at convergence, among possible others.

Fig.III.19 shows the result of applying the above strategy to the two-QAM 4 mixture. The performance of the resulting enhanced MB-ILSE algorithm is labeled "MB-ILSE+". For this simulation the fully preventive correction scheme was used: given the moment method channel predictor $\widehat{\mathbf{h}}$ and its closest problematic ratio h_r the following three additional initializations were systematically tested on ILSE: $(h_r\widehat{h_1}, \widehat{h_1})$, $(\widehat{h_2}, \widehat{h_2}/h_r)$ and $(\frac{\widehat{h_1}+\widehat{h_2}/h_r}{2}, \frac{h_r\widehat{h_1}+\widehat{h_2}}{2})$. We observe a clear improvement of the final SER compared to the mere, non-corrected MB-ILSE, with error rates easily falling beyond the latter 10^{-3} asymptotic threshold. For very low noise powers the corrected MB-ILSE eventually loses to the perfect CSI detection. Regardless the achieved scores are very satisfying, given that they take into account any subsequent error control coding.

Let us conclude this section with a few words on higher-order mixtures. To this point, extension of the above strategies for more than two sources was not carried out. We can expect that channel realizations for which ILSE is more likely to converge to a local minimum still

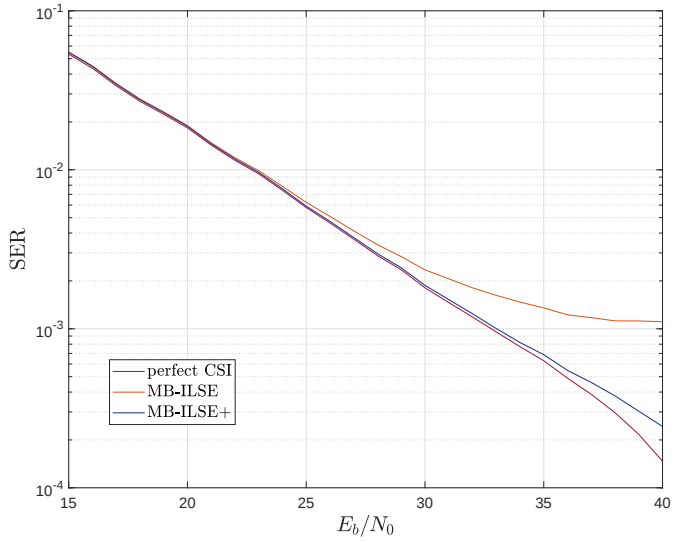

Figure III.19 – *Comparison of SER obtained for the two-QAM 4 mixture with perfect CSI (red), MB-ILSE (orange) and MB-ILSE with a preventive correction scheme (purple).*

result in joint constellations having closely grouped subsets of symbols. The equivalent of (III.41) to predict the position of these clusters would then be [47]

$$\langle \mathbf{h} | \mathbf{s}_1 - \mathbf{s}_2 \rangle = 0 \tag{III.45}$$

where $\mathbf{s}_1$ and $\mathbf{s}_2$ are two independent realizations of the random source vector $\mathbf{s}$. Note however that in regard to what was observed for the QAM 16-QAM 4 mixture, other problematic channels not covered by (III.45) may also exist. Applicability of the treatment strategies proposed for two-sources mixtures mostly depend if all solutions to (III.45) can be found. This matter is not covered by this work. As far as our simulations can tell, what still holds however is that non-independent sources spurious solutions highly contribute to the poor SER scores achieved by MB-ILSE for more than two-user mixtures. Fig.III.20 shows for instance, on the two-BPSK, two-QAM 4 mixture, the comparison between the raw MB-ILSE performance and the SER obtained by discarding solutions which do not observe source independence. Although the latter strategy is still clearly suboptimal with respect to the ideal, perfect CSI decoding, we see how significantly the non-independent sources fixed points account for the overall performance of MB-ILSE and how much can be gained by simply detecting them.

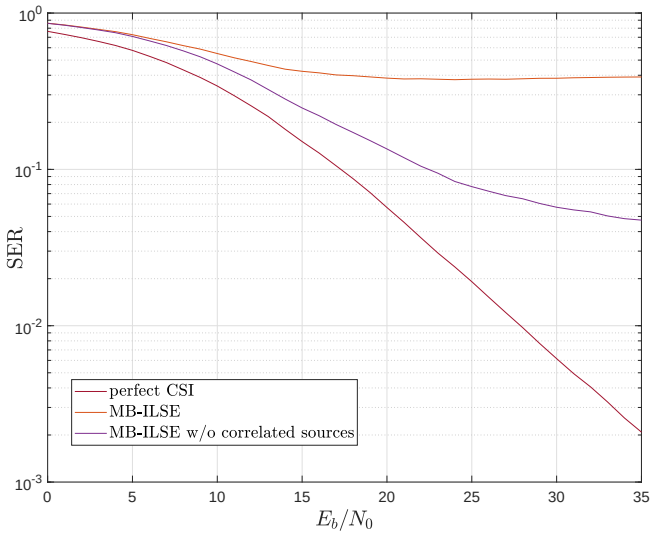

Figure III.20 – *Comparison of SER obtained with perfect CSI (red), non corrected MB-ILSE (orange) and MB-ILSE with rejection of non-independent source solutions (purple).*

III.6 Comments on practical implementation

All the performance curves presented so far assume that, within the equivalence class of predictors induced by the BSS model and source invariances, one can always identify the best representant with respect to the actual channel. It is legitimate to question whether this exact information can be well-approached with only partial information on the channels. First, it is not unrealistic to assume the receiver knows the reference amplitude of the constellations: the choice of amplitude may basically either depend solely on the transmitter, in which case the information could be sent to the receiver at the beginning of the whole transmission along with the used modulation scheme, or on the communication protocol, in which case the information can be accessed both by the receiver and the transmitter. Hence scaling invariance does not represent a fundamental problem in itself and can be considered as systematically resolved.

The situation is different for the permutation and discrete-circular phase invariances, for which neither the transmitters nor the receiver have generally any control on. As long as only different constellations are involved, the receiver can reliably associate each estimated symbol sequence to the right user based on the a priori knowledge of the modulation schemes used, except for very unlikely, strongly non-uniform scenarios in which the estimated symbols associated to a given user would be restricted to a subset included in the constellation from another user. When some of the constellations are identical however, the associated estimated symbol sequences can a priori come from any of the concerned users alike. A possible suboptimal strategy to recover the correct ordering would be then for the receiver to know or estimate the ordering of the channel powers. This again does not seem unfeasible in practice, as other multiuser detection techniques, such as SIC with the received powers,

require equivalent information.

To address the third problem, the receiver needs to have partial information on the channel's phase. This can be for instance the interval $\left[\frac{2p\pi}{q_k}\ ;\ \frac{2(p+1)\pi}{q_k}\right[$, $p \in \{0, \cdots, q_k - 1\}$, in which each channel's phase lies. This is indeed suboptimal compared to a direct use of the actual channel, because for channel's phase close to the bounds of the latter intervals the best channel predictor may actually belong to one of the adjacent intervals, due to estimation bias. The consequence of taking the wrong q_k-th root (*i.e.* the wrong interval) essentially consists in a global permutation for each of the estimated sequence symbols. This reveals dramatic for the SER as all subsequent estimated symbols are wrong. We can however expect that by appropriate error correction schemes such permutations can be detected, thus allowing phase correction to be performed past the symbol estimation step itself.

Fig.III.21 shows the SER curves obtained from the same mixtures as in Section III.4.2 by implementing the above suboptimal decision rules and comparing them to the optimal ones. We see that for most mixtures suboptimal and optimal strategies yield very close results. The relative gap is more pronounced for the two-QAM4 mixture, still the error rates achieved by the suboptimal strategy range in very satisfying values. This suggests that, by use of reliable estimation procedures for acquiring appropriate partial information about the channel realization, the performances obtained with a practical MB-ILSE are comparable to those of the ideal strategy.

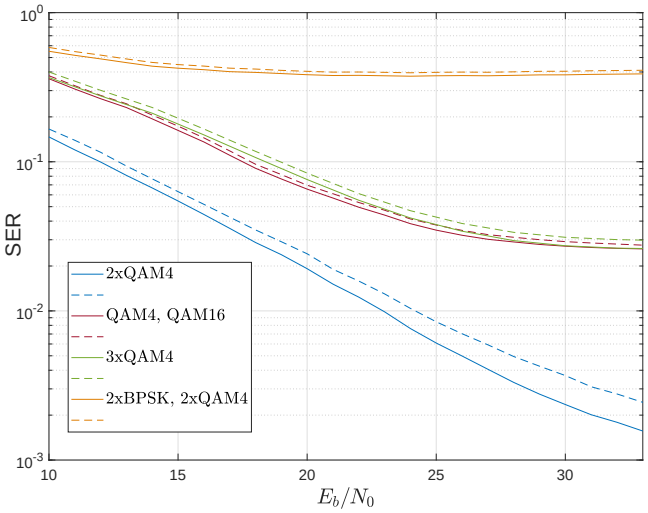

Figure III.21 – *Comparison of the SER between perfect decision (continuous lines) and suboptimal decision (dashed lines) among equivalent predictors*

Of practical interest is also the typical number of iterations needed for ILSE to converge to a fixed point, which combined with the known per iteration complexity provides an estimate of the overall computational load of the method. Fig.III.22 gives the mean number

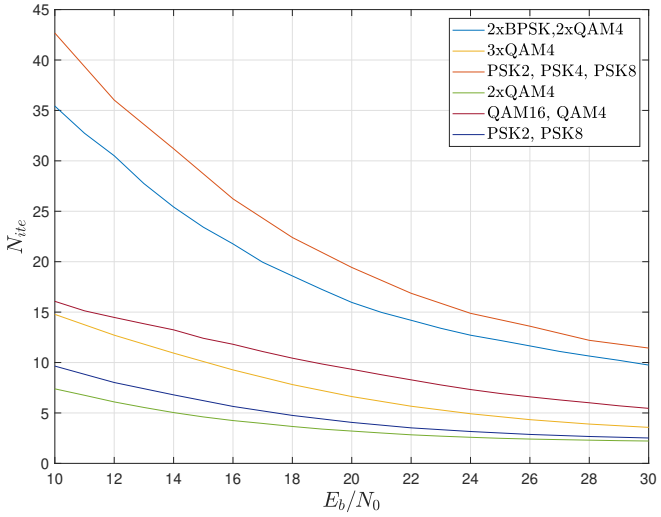

Figure III.22 – *Mean number of iterations for convergence of ILSE*

of iterations as a funtion of $\frac{E_b}{N_0}$. The number of steps obviously tends to increase with the number of sources and the joint contellation's size, yet is of order no more than 15 for most of the tested mixtures. For moderate noise power levels ($E_b/N_0 \simeq 18 - 20$dB) the convergence is on average achieved in less than 10 iterations. It is striking how for mixtures with distinct rotational orders the mean number of steps substantially increases, as is evident from the comparison of the three-PSK and three QAM 4 curves. In accordance with our previous observation concerning the SER scores achieved for such kind of mixtures, it seems indeed that the ILSE cost function has a more complex structure than for contellations with equal rotational orders. Let us finally recall that for distinct constellations with the same rotational order, several parallel, partial or full ILSE runs may be needed to extract a unique predictor depending on the chosen strategy, III.3.5. So, for the QAM 16 and QAM 4 mixture with an exhaustive cost-testing strategy for instance the mean number of iterations of the overall method should be doubled compared to the corresponding curve on Fig.III.22.

A last practical matter we should mention is the fact that the number of sources and the modulation schemes are supposed to be known at the receiver. In a more realistic implementation of the method such information should be acquired by the receiver as well. Estimation of the number and structure of the sources is out of the scope of this work, but we note that several methods for modulation classification and detection of the number of sources have been proposed in the literature, see for intance [79] or [80].

Algorithm 1 shows a global view of a possible complete MB-ILSE-based detection algorithm, taking into account the additional estimation steps discussed above. Strategies for detection and treatment of spurious fixed points have been included as well. We emphasize that all proposed procedures related to non uniqueness of the linear BSS model and convergence of ILSE to local minima are not intended to be exhaustive. Depending on the application and the computational resources at disposal, many other solutions may be designed, and the

Algorithm 1 Overall procedure illustration of the MB-ILSE blind multiuser detection

1)Preliminary steps
– estimation of the number of sources K
– estimation of the constellations $\mathscr{C}_k$ and their amplitude A_k, $k \in \{1, \cdots, K\}$

2)Channel prediction
– solve the moment problem (Eq. (III.12))
if solution to the moment problem is not unique (up to permutations) **then**
estimate which solution is the closest to the actual channel (Section III.3.5)
end if
– perform ILSE on the retained solution

3)Validity check
if ILSE solution detected as spurious **then**
– compute the closest expected problematic channel ratio (Eq.(III.45))
– try one or several initial states for this channel ratio
– select the best solution by comparison of the final cost function
if retained solution is still identified as spurious **then**
ask for a retransmission
end if
end if

4)Final decoding
– solve the BSS invariances for the retained solution (permutation and phase)
– estimate the emitted symbol sequence by threshold detection

structure of Algorithm 1 modified accordingly.

III.7 Conclusion

In this chapter the blind detection of multiuser tranmissions with a single receiver and in strong interference was addressed. The problem was formulated in the underdetermined linear BSS framework. We have seen through simulations how even for simple enough mixtures, traditional techniques such as SIC or randomly initialized ILSE fail at achieving acceptable error rates. In order to circumvent convergence of ILSE towards local fixed points we proposed an estimation strategy based on the cumulants of the received signal to be used as an initial state for ILSE. Exact solutions to various mixtures configurations were explicitely derived. The resulting algorithm has shown considerable performance gain compared to all other tested methods. Yet for complex mixtures the achieved error rates cannot ensure a reliable symbol decoding scheme. An in-depth analysis conducted on two-users mixtures in the low noise power regime revealed that the residual error rate originates from clusters of channel realizations for which the resulting mixed constellations are close to non-identifiability. In these configurations, the proximity of some local fixed

points to the global minimum of the ILSE cost function results in an increased sensibility to the initial state provided to the algorithm. Fortunately enough it also turns out that most of these spurious solutions can be easily detected, as they do not observe the source independence and uniformity assumptions. Based on these observations several strategies to improve the output of ILSE in these problematic mixture configurations were proposed, and successfully applied to the two-QAM 4 mixture. Extension of these strategies to more than two sources has not been carried out yet, but represents a foremost perspective for future work.

Appendix A

Proofs of Chapter III

A.1 Cumulants of a discrete-circular random variable

In this section we consider a complex random variable χ with discrete-circular invariance of order q. In Section III.3.1 we have already shown that the cumulants of χ of order n non multiple of q are necessarily zero. What is left to prove then is the expression (III.11) of $\kappa_n(\chi)$ when $n = pq$

$$\kappa_{pq}(\chi) = \alpha_{p,q}\kappa_p\left(\frac{\mu_q(\chi)}{\alpha_{1,q}}, \frac{\mu_{2q}(\chi)}{\alpha_{2,q}}, \cdots, \frac{\mu_{pq}(\chi)}{\alpha_{p,q}}\right) \tag{A.1}$$

with $\alpha_{p,q} \triangleq \frac{(pq)!}{p!(q!)^p}$ and $p \in \mathbb{N}$.

Let us proceed by recursion on p : for $p = 1$, the only non zero moment of χ from order 1 to q is $\mu_q(\chi)$, so $\kappa_q(\chi) = \kappa_q(0, \cdots, 0, \mu_q(\chi)) = \mu_q(\chi)$ and the result is verified, since $\alpha_{1,q} = 1$.

Now let us assume that (A.1) holds for all integers up to $p-1$. For arbitrary integer n, the n-th cumulant $\kappa_n(\chi)$ admits the following recursive formula in terms of lower order cumulants and moments

$$\kappa_n(\mu_1, \mu_2, \cdots, \mu_n) = \mu_n - \sum_{k=1}^{n-1}\binom{n-1}{k-1}\kappa_k(\mu_1, \mu_2, \cdots, \mu_k)\,\mu_{n-k} \tag{A.2}$$

where the dependency of the moments in the variable χ has been made implicit. Applying this formula for $n = pq$ and using the recursion hypothesis on the non-zero cumulants in the right-hand side yields

$$\kappa_{pq}(\mu_q, \mu_{2q}, \cdots, \mu_{pq}) = \mu_{pq} - \sum_{m=1}^{p-1}\binom{pq-1}{mq-1}\alpha_{m,q}\kappa_m\left(\frac{\mu_q}{\alpha_{1,q}}, \frac{\mu_{2q}}{\alpha_{2,q}}, \cdots, \frac{\mu_{mq}}{\alpha_{m,q}}\right)\mu_{(p-m)q} \tag{A.3}$$

For convenience only the non-zero moments of κ_{pq} have been explicitely written in the left-hand side of (A.3). The combinatorial prefactor of each P_m can be rewritten as

$$\binom{pq-1}{mq-1}\alpha_{m,q} = \frac{1}{\alpha_{p-m,q}}\frac{(pq)!}{(q!)^p}\frac{1}{p(m-1)!(p-m)!} = \frac{\alpha_{p,q}}{\alpha_{p-m,q}}\binom{p-1}{m-1} \tag{A.4}$$

so combining (A.4) and (A.3) we get

$$\kappa_{pq}(\mu_q, \mu_{2q}, \cdots, \mu_{pq}) = \alpha_{p,q}\left(\frac{\mu_{pq}}{\alpha_{p,q}} - \sum_{m=1}^{p-1}\binom{p-1}{m-1}\kappa_m\left(\frac{\mu_q}{\alpha_{1,q}}, \cdots, \frac{\mu_{mq}}{\alpha_{m,q}}\right)\frac{\mu_{(p-m)q}}{\alpha_{p-m,q}}\right) \tag{A.5}$$

Finally, using (A.2) again with $n = p$ and variables $\mu'_k \triangleq \frac{\mu_{kq}}{\alpha_{k,q}}$ yields the desired result (III.11).

A.2 Cumulants of uniform QAM and ASK sources

In this section we consider special cases of Eq.(III.11) for QAM ($q = 4$) and ASK ($q = 2$) sources, respectively. Let us denote S_M an uniform, regular QAM source with M symbols. Then S can be written as the linear combination of $K = \frac{1}{2}\log_2 M$ uniform, mutually independent QAM4 sources $S_4^{(k)}$, $k \in \{1, \cdots, K\}$.

$$S_M = \sum_{k=1}^{K} 2^{k-1} S_4^{(k)} \tag{A.6}$$

Applying the additivity of cumulants for independent variables and their homogeneity yields

$$\kappa_n(S_M) = \sum_{k=1}^{K} 2^{n(k-1)} \kappa_n(S_4^{(k)}) = \frac{M^{n/2}-1}{2^n - 1} \kappa_n(S_4) \tag{A.7}$$

The n-th cumulant of S_4 can be further simplified in a similar fashion by decomposing the QAM4 source S_4 in two independant, pure real and pure imaginary uniform BPSK sources, so that

$$\kappa_n(S_4) = (1 + i^n)\kappa_n(B) \tag{A.8}$$

where B denotes a BPSK source.

Considering now $n = 4p$ and the fact that for any PSKM modulation $\mu_{Mp} = 1$ we get from (III.11)

$$\kappa_{4p}(B) = \alpha_{2p,2}\kappa_{2p}\left(\frac{1}{\alpha_{1,2}}, \frac{1}{\alpha_{2,2}}, \cdots, \frac{1}{\alpha_{2p,2}}\right) \tag{A.9}$$

which combined with equations (A.8) and (A.7) gives

$$\kappa_{4p}(S_M) = 2\frac{M^{2p}-1}{4^{2p}-1}\kappa_{2p}\left(\frac{1}{\alpha_{1,2}}, \frac{1}{\alpha_{2,2}}, \cdots, \frac{1}{\alpha_{2p,2}}\right) \tag{A.10}$$

Applying again (III.11) on the left hand side of (A.10) finally yields

$$\kappa_p\left(\frac{\mu_4}{\alpha_{1,4}}, \frac{\mu_8}{\alpha_{2,4}}, \cdots, \frac{\mu_{4p}}{\alpha_{p,4}}\right) = 2.6^p \frac{M^{2p}-1}{4^{2p}-1}\frac{p!}{(2p)!}\kappa_{2p}\left(\frac{1}{\alpha_{1,2}}, \frac{1}{\alpha_{2,2}}, \cdots, \frac{1}{\alpha_{2p,2}}\right) \tag{A.11}$$

A very similar derivation can be made for ASK uniform sources and leads to

$$\kappa_p\left(\frac{\mu_2}{\alpha_{1,2}}, \frac{\mu_4}{\alpha_{2,2}}, \cdots, \frac{\mu_p}{\alpha_{p,2}}\right) = \frac{M^{2p}-1}{2^{2p}-1}\kappa_p\left(\frac{1}{\alpha_{1,2}}, \frac{1}{\alpha_{2,2}}, \cdots, \frac{1}{\alpha_{p,2}}\right) \tag{A.12}$$

A.3 Asymptotic bias of the two-sources q-th power channel predictor

In this section we derive an approximate bias and MSE for the fourth-power channel predictor $\hat{\boldsymbol{\eta}}$, valid in the large sample size limit. The predictor being non linear in the received signal statistics, we perform a Taylor expansion of $\gamma(\bar{\rho}, \bar{\rho_2})$ around its expected

value. At first order, we simply have $\mathbb{E}\left[\gamma(\bar{\rho},\bar{\rho_2})\right] \simeq \left(\mathbb{E}\left[\Gamma(\bar{\rho},\bar{\rho_2})\right]\right)^{1/2}$. Further assuming that $\mathbb{E}\left[\bar{\rho^2}\right] \simeq \mathbb{E}\left[\bar{\rho}\right]^2 = \mathbb{E}\left[\rho\right]^2$, we can show that

$$\mathbb{E}\left[\Gamma(\bar{\rho},\bar{\rho_2})\right] \simeq \left(\mu_2\omega_1\eta_1 - \mu_1\omega_2\eta_2\right)^2 \tag{A.13}$$

so at first order the conditionnal expectation $\mathbb{E}\left[\hat{\boldsymbol{\eta}}|\boldsymbol{\eta}\right]$ of the predictor given a realisation of the (q-th power) channel $\boldsymbol{\eta}$ is

$$\mathbb{E}\left[\hat{\boldsymbol{\eta}}^{(m)}\middle|\boldsymbol{\eta}\right] = \begin{cases} \boldsymbol{\eta} & \text{if} \quad \mathrm{Arg}\left(\mu_{\tau(m)}\omega_m\eta_m - \mu_m\omega_{\tau(m)}\eta_{\tau(m)}\right) \in \left]-\dfrac{\pi}{2}\,;\,\dfrac{\pi}{2}\right] \\ \begin{pmatrix} \varepsilon_1 & \zeta_2 \\ \zeta_1 & \varepsilon_2 \end{pmatrix}\boldsymbol{\eta} & \text{if} \quad \mathrm{Arg}\left(\mu_{\tau(m)}\omega_m\eta_m - \mu_m\omega_{\tau(m)}\eta_{\tau(m)}\right) \notin \left]-\dfrac{\pi}{2}\,;\,\dfrac{\pi}{2}\right] \end{cases} \tag{A.14}$$

with $\varepsilon_k \triangleq 1 - \frac{2}{1+r_k/r_{\tau(k))}}$, $\zeta_k \triangleq \frac{2\mu_k/\mu_{\tau(k)}}{1+r_k/r_{\tau(k)}}$ and $r_k \triangleq \frac{\mu_k^2}{\omega_k}$. We see that the bias of both predictors is conditioned by the event $\mathscr{B} \triangleq \left\{\mathrm{Arg}\left(\mu_2\omega_1\eta_1 - \mu_1\omega_2\eta_2\right) \in \left]-\frac{\pi}{2}\,;\,\frac{\pi}{2}\right]\right.$, whose outcome obviously depends on the unknown channel realization $\boldsymbol{\eta}$. Using the law of total expectation with the partition set induced by $\mathscr{B}$, the mean squared bias of $\hat{\boldsymbol{\eta}}^{(m)}$ is expressed as

$$\mathbb{E}\left[\left|B(\hat{\boldsymbol{\eta}}^{(m)}|\boldsymbol{\eta})\right|^2\right] = \mathbb{E}\left[\left|B(\hat{\boldsymbol{\eta}}^{(m)}|\boldsymbol{\eta})\right|^2\middle|\mathscr{B}\right]\mathbb{P}\left(\mathscr{B}\right) + \mathbb{E}\left[\left|B(\hat{\boldsymbol{\eta}}^{(m)}|\boldsymbol{\eta})\right|^2\middle|\mathscr{B}^{\mathsf{c}}\right]\mathbb{P}\left(\mathscr{B}^{\mathsf{c}}\right) \tag{A.15}$$

where $B(\hat{\boldsymbol{\eta}}^{(m)}|\boldsymbol{\eta}) \triangleq \mathbb{E}\left[\hat{\boldsymbol{\eta}}^{(m)}\middle|\boldsymbol{\eta}\right] - \boldsymbol{\eta}$ is the conditional bias of $\hat{\boldsymbol{\eta}}^{(m)}$ given $\boldsymbol{\eta}$. For circular-symmetric channels we can easily compute the probability of event $\mathscr{B}$. First, we can always write $\mathbb{P}\left(\mathscr{B}\right)$ as

$$\mathbb{P}\left(\mathscr{B}\right) = \mathbb{P}\left(\mathrm{Arg}\left(\tfrac{1}{c_1\eta_1 - c_2\eta_2}\right) \notin \left]-\tfrac{\pi}{2}\,;\,\tfrac{\pi}{2}\right]\right) = \mathbb{P}\left(\mathrm{Arg}\left((c_1\eta_1 - c_2\eta_2)^*\right) \notin \left]-\tfrac{\pi}{2}\,;\,\tfrac{\pi}{2}\right]\right) \tag{A.16}$$

Now if h_k is circular symmetric, then $c_k\eta_k$ is also circular-symmetric for any complex number c_k, so $c_k\eta_k$ and $c_k^*\eta_k^*$ have the same distribution. Hence we simply have $\mathbb{P}\left(\mathscr{B}\right) = \mathbb{P}\left(\mathscr{B}^{\mathsf{c}}\right) = \frac{1}{2}$, and the expected squared modulus bias of any of the predictors $\hat{\boldsymbol{\eta}}^{(m)}$ simplifies to

$$\mathbb{E}\left[\left|B(\hat{\boldsymbol{\eta}}^{(m)}|\boldsymbol{\eta})\right|^2\right] \simeq \frac{1}{2}\left(\left(|\varepsilon_1 - 1|^2 + |\zeta_1|^2\right)\mathbb{E}\left[|\eta_1|^2\right] + \left(|\varepsilon_2 - 1|^2 + |\zeta_2|^2\right)\mathbb{E}\left[|\eta_2|^2\right]\right) \tag{A.17}$$

for any circular-symmetric independent channels.

Chapter IV

Blind multiuser detection in OFDM transmissions

Contents

IV.1 Introduction

Heretofore we have been exclusively interested in narrowband transmissions, which allow to conveniently model the channel propagation as flat-fading. This framework is however quite restrictive and little realistic, as practical wireless communications involve signals whose spectral support is typically larger than the channel coherence bandwidth. The propagation channel is then selective in frequency over the total used bandwidth. In this chapter we will consider a particular class of transmission schemes suited to such frequency-selective environments, namely multicarrier transmissions.

IV.1.1 OFDM transmission

Modeling the propagation channel as flat-fading is tantamount to consider that the received signal comes from a single path, *i.e.* the channel impulse response reduces to a single coefficient h, Eq.(I.47). Conversely, introducing selectivity in frequency restores the multipath feature of wireless transmissions. That is, the observed signal is composed of several

scaled and delayed copies of the emitted waveform. Considering signals sampled at the symbol period T and a slow-fading multipath channel with AWGN noise $\mathbf{w}$, the received symbol r_n at time epoch n is given as

$$r_n = \sum_{\ell=1}^{L} h_\ell s_{n-\ell} + w_n \tag{IV.1}$$

where compared to time-continuous multipath channel fading model Eq.(I.45), each path delay has been quantized at the symbol period. The maximal length L on the channel impulse response is called the channel *memory*, and can be related to the channel delay spread T_d by $T_d \simeq TL$. From (IV.1) we see that the received symbol at period n not only contains the emitted symbol at time n (we neglect the first time delay by choosing an appropriate time origin for the receiver), but also replicas of previously emitted symbols due to the multipath propagation. This phenomenon is called the Inter-Symbol Interference (ISI), and is a highly undesirable effect is wireless communications.

The motivating idea behind multicarrier (more generally block) transmissions is to suppress ISI by emitting successive blocks of symbols instead of a fully serial time sequence [81]. To do so, the input sequence is segmented in blocks of P symbols, and each symbol in a block is transmitted during the period T according to a distinct carrier signal with frequency f_p, called a subcarrier. In the particular case of Orthogonal Frequency Division Multiplexing (OFDM) [82], the data blocks are referred to as OFDM symbols, and the subcarrier frequencies are equally spaced, in such a way that $f_p = f_c + (p-1)\Delta f$ with f_c the reference carrier frequency, and the frequency spacing Δf is chosen small compared to the channel coherence bandwidth, $\Delta f \ll B_c$. Because the subcarriers are ortogonal to eachother, each symbol in a block can be recovered without interference at the receiver by observing the signal in the appropriate subcarrier frequency band.

Emitting the symbols block-wise does actually not entirely prevent ISI, as symbols located at the end of a given block still interfer with the first symbols from the subsequent block. Interference between consecutive blocks is generically called Inter-Block Interference (IBI), and in the context of multicarrier transmissions is better known as Inter-Carrier Interference (ICI). The usual strategy to address ICI consists in introducing redundancy in each transmitted blocks by addition of the so-called Cyclic Prefix (CP). Denoting by $\mathbf{s}$ a generic OFDM symbol, the CP is composed of the N_{CP} first symbols of $\mathbf{s}$, and is appended to $\mathbf{s}$ to form an extended block of size $P + N_{CP}$. By doing so the last useful symbols in $\mathbf{s}$ are now transmitted free of interference, provided the size of the CP is larger that the channel memory L, *i.e.* $N_{CP} > L$. At the receiver, the CP is discarded from the observed signal, resulting in a block $\mathbf{r}$ of length P which from (IV.1) can be shown to have the following expression [83]:

$$\mathbf{r} = \mathbf{h} \circledast \mathbf{s} + \mathbf{w} \tag{IV.2}$$

where $\circledast$ denotes the cyclic convolution. The cyclic convolution is the discrete counterpart of the continuous convolution product, and in particular is mapped to a regular product under the Discrete Fourier Transform (DFT). Consequently, defining $\tilde{\mathbf{s}}$ to be the DFT of $\mathbf{s}$ and

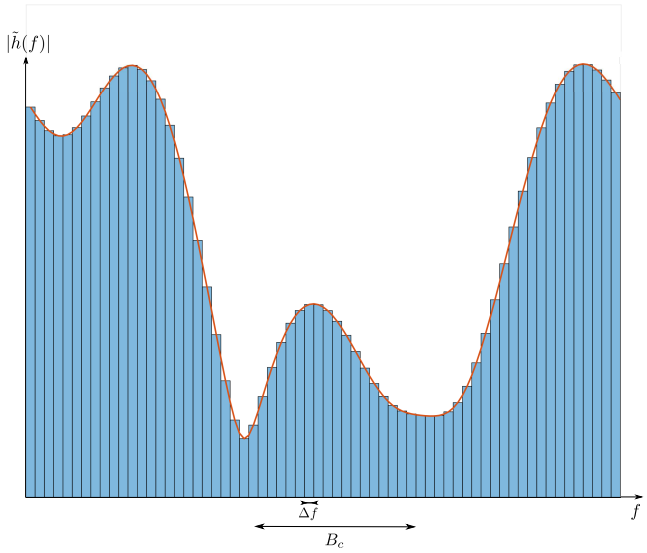

Figure IV.1 – *Division of a frequency-selective channel in $P = 64$ narrowband subcarriers.*

similarly for $\mathbf{r}$, $\mathbf{h}$ and $\mathbf{w}$, we find that

$$\tilde{\mathbf{r}} = \mathbf{F}\,\mathbf{r} = \tilde{\mathbf{h}} \cdot \tilde{\mathbf{s}} + \tilde{\mathbf{w}} \tag{IV.3}$$

where $\mathbf{F}$ is the $P \times P$ DFT matrix defined by $F_{p\ell} \triangleq \frac{1}{\sqrt{P}} \exp\left(\frac{-2i\pi\ell p}{P}\right)$, and the product in the right hand side applies component-wise. Because $\mathbf{F}$ is unitary, ($\mathbf{F}^\dagger = \mathbf{F}^{-1}$) and the components of $\mathbf{w}$ are independent circularly-symmetric complex normal, the distribution of the transformed noise $\tilde{\mathbf{w}}$ is left unchanged. Eq.(IV.3) is then nothing but a vectorized version of the received symbols in a flat-fading environment, Eq.(I.54), but with the emitted symbols in the frequency domain. The flat-fading feature of the frequency channel components is actually made possible by the fact that each subcarrier is narrowband, $\Delta f \ll B_c$, so over Δf the channel transfer function can be considered as constant, as illustrated on Fig.IV.1. The problem of symbol detection in a frequency-selective channel has then be turned in P symbol detection problems in the much simpler flat-fading model. Fig.IV.2 illustrates the different steps of the OFDM transmission scheme. The modulated symbols in the frequency domain $\tilde{s}_n$ are first assembled in blocks and transformed in the time domain by the Inverse Discrete Fourier Transform (IDFT). The CP is added on each block, and each resulting OFDM symbols $\mathbf{u}$ is converted back to a serial sequence to form the transmitted waveform. At the receiver the noisy and distorted OFDM symbols are recovered and the CP is removed. Equalization and symbol detection are done separately on each subcarrier, and the recovered time symbol block is transformed back to the frequency domain.

The conceptual simplicity of OFDM, in addition to its spectral efficiency and the low complexity pertaining to its practical implementation have considerably contributed to its popularity and spreading to various wireless applications, including radio and television broadcast [84], [85]. A wired counterpart of OFDM is also known as Discrete Multi-Tone (DMT)

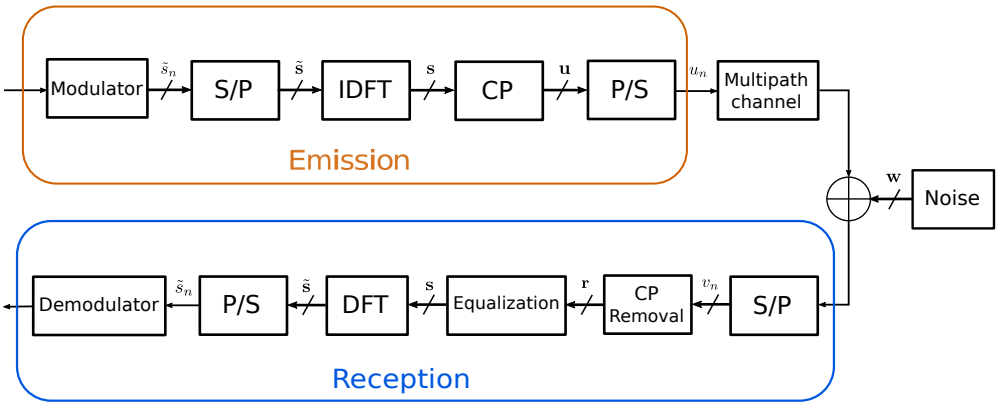

Figure IV.2 – *Functional block diagram of an OFDM transmission.*

and has application in hight-speed Digital Subscribe Line (DSL)-based transmissions [86]. While addition of the CP is the most encountered technique to suppress ICI in practice, other more recent techniques have been proposed, such as Zero-Padding (ZP)-OFDM, which consists in appending trailing zeros to each data block. The resulting scheme was shown to exhibit interesting properties over traditional CP-based strategies such as enhanced channel identifiability even in the presence of zero channel gains at the carrier frequencies [87]. The main limitation of OFDM is certainly its inherent dependency on the subcarriers frequency synchronisation: as suppression of ICI originates from the orthogonality between subcarriers, frequency offsets are a major source of impairment of OFDM, and requires the implementation of regular and reliable phase synchronization procedures [88].

IV.1.2 Channel estimation in OFDM

Channel estimation for SISO OFDM transmissions have been extensively studied in the literature. Blind procedures have attracted particular interest as they are free of any known pilot sequences, thus allowing to spare bandwidth. A general class of channel estimators is provided by the subspace methods, which rely on a matrix formulation of the received signal and its statistics, such as the autocorrelation. Based on distinct specificities introduced by the OFDM scheme several subspace procedures have been proposed. Some of them rely on the data redundancy inherent to the introduction of the CP [89], [90]. Virtual carriers, namely subcarriers left unmodulated in practical OFDM systems for spectral limitation purposes, provide another kind of diversity that is commonly exploited [91]. Some methods focus on minimizing the number of consecutive OFDM symbols required for the subspace problem to be well-conditioned [92], [93]. Subspace methods have also been proposed for the alternative ZP-OFDM scheme [87].

The special properties of OFDM have also led to the development of non-subspace estimation techniques. Oversampling was for instance used in [94] to derive a CP-free channel estimator. Of particular interest is also the finite alphabet property of the source symbols, which introduces additional constraints in the estimation problem. This was used

in [95] on PSK signals to propose a single-block based channel estimator. Joint use of virtual carriers and finite alphabets in [96] was proposed to estimate the channel directy in the time domain rather than in frequency. The resulting algorithm consists in an extension of the ILSP algorithm mentioned in Chapter III. Estimating the channel directly in time has the important advantage of circumventing the inherent phase ambiguities arising on each subcarrier due to the sources rotational symmetry. In general, this problem is solved through the use of training sequences. More generally, semi-blind channel estimation strategies are often used as a compromise between pilot-based and fully blind estimations [97], [98].

As for multiuser OFDM transmissions, much of the efforts have focused on Multiple-Input Multiple-Output (MIMO)-OFDM. In most cases the estimation problem has been addressed by the Stochastic Maximum Likelihood (SML) approach, based on a probabilistic representation of the emitted symbols. The EM algorithm is the most popular method to provide SML estimators and has been extensively used [99], [100], [101]. Alternative methods based on the SML approach include Information Geometric Identification (IGID) [102] and Majorize-Maximization (MM) [103] algorithms. Hard-decision ML estimation can be found in [104] where a tensor formulation of the MIMO-OFDM was proposed and the ILSE, ILSP algorithms as well as their recursive extensions were applied subcarrier-wise. Other BSS methods, and more particularly ICA have also been reported in [105] and [106], along with strategies to address the permutation ambiguities inherent to the problem formulation.

As far as we can tell, the study of underdetermined, and particularly single-sensor OFDM transmissions have been scarcely addressed in the literature. We can notably mention [107], in which several results on the identifiability conditions of the sources and the channels are derived for blind and non-blind scenarios, and the EM algorithm is applied in different settings. An adaptative EM algorithm is also proposed to track temporal channel variations in non-stationary environments. More generally, almost all MIMO-OFDM strategies presented above operate exclusively in the frequency domain. While this is well-motivated by the fact that symbol detection is indeed performed in frequency, this does not exploit the special structure of the channel frequency components as the DFT of an impulse response with a length often much shorter than the number of subcarriers. As EM-based or iterative least squares algorithms such as ILSE and ILSP are known to be very sensitive to their initialization, exploiting this additional information to reduce the parameter space of these methods can be determinant to prevent convergence towards local fixed points. In many cases the initialization is circumvented by use of training sequences, so the overall channel estimation is not completely blind. An additional advantage of estimating the channel in the time domain is that the phase ambiguities on each subcarrier are naturally solved, up to a global phase rotation. These two observations strongly motivate to extend the above algorithms to a direct, time domain channel estimation. On this basis, the main objectives of this chapter are the following:

- generalize the multiuser single receiver ILSE algorithm to the case of OFDM signals and with the channel estimated in the time domain. The resulting algorithm will be referred to as ILSE-OFDM;

- propose a channel initialization strategy for the ILSE-OFDM algorithm. The permutation and phase ambiguities will receive a particular attention.

The resulting channel estimation procedure will be simulated in several settings. Finally, in the following it will always be assumed that the channel memory L is much shorter than the number of subcarriers P, $L \ll P$. As a matter of fact, this assumption is not needed for the derivation of ILSE-OFDM, but will reveal useful when addressing the initialization of the algorithm, in addition to be a quite reasonable hypothesis in many practical transmission settings.

IV.2 The OFDM-ILSE algorithm

The single-sensor multiuser OFDM model can be readily obtained from the SISO-OFDM model of Eq.(IV.3). On each subcarrier the received signal is an instantaneous linear mixture of the emitted sources, as in Chapter III. Denoting by $\tilde{\mathbf{r}}_p$ the sequence of N received symbols from subcarrier p, we have

$$\tilde{\mathbf{r}}_p = \tilde{\mathbf{h}}_p \tilde{\mathbf{S}}_p + \tilde{\mathbf{w}}_p = \mathbf{f}_p \mathbf{H} \tilde{\mathbf{S}}_p + \tilde{\mathbf{w}}_p \tag{IV.4}$$

where:

- $\tilde{\mathbf{h}}_p$ is the $1 \times K$ row vector of the p-th frequency component of each user's channel;
- $\tilde{\mathbf{S}}_p$ is the $K \times N$ matrix whose columns represent the transmitted joint constellation symbols on subcarrier p;
- $\tilde{\mathbf{w}}_p$ is the $1 \times N$ row vector of complex normal noise on subcarrier p;
- $\mathbf{H}$ is the $L \times K$ matrix whose columns are the time channel vectors associated with each source;
- $\mathbf{f}_p$ is the p-th row of $F_{(P,L)}$, the submatrix obtained from the DFT matrix F by extraction of its L first columns.

We now proceed to the extension of the MISO-ILSE algorithm of Chapter III to OFDM signals. Let $\tilde{\mathbf{R}}$ denote the $P \times N$ received symbol matrix obtained by stacking the P row vectors $\tilde{\mathbf{r}}_p$. The (conditional) distribution of $\tilde{\mathbf{R}}$ is parametrized by the channel matrix $\mathbf{H}$ and the set of transmitted symbol matrices $\{\tilde{\mathbf{S}}_p\}$, $p \in \{1, \cdots, P\}$. Because the emitted symbols and the noise realizations are independent, the vectors $\tilde{\mathbf{r}}_p$ are independent so the conditional distribution of $\tilde{\mathbf{R}}$ factorizes as

$$p_{\tilde{\mathbf{R}}}(\mathbf{Z}) = \prod_{p=1}^{P} p_{\tilde{\mathbf{r}}_p}(\mathbf{z}_p) \tag{IV.5}$$

with $\mathbf{Z}$ a $P \times N$ complex matrix with rows $\mathbf{z}_p$. According to (IV.4) and the complex normal noise assumption, each $\tilde{\mathbf{r}}_p$ follows a shifted complex normal distribution with variance N_0 and mean $\mathbf{f}_p \mathbf{H} \tilde{\mathbf{S}}_p$. Maximizing the log-likelihood $\mathbb{L}\left[\mathbf{H}, \{\tilde{\mathbf{S}}_p\}; \tilde{\mathbf{R}}\right]$ reduces then to the minimization of

$$J_P(\mathbf{H}, \{\tilde{\mathbf{S}}_p\}; \tilde{\mathbf{R}}) = \sum_{p=1}^{P} \| \tilde{\mathbf{r}}_p - \mathbf{f}_p \mathbf{H} \tilde{\mathbf{S}}_p \|^2 = \sum_{p=1}^{P} J(\mathbf{f}_p \mathbf{H}, \tilde{\mathbf{S}}_p; \tilde{\mathbf{r}}_p) \tag{IV.6}$$

where $J(\mathbf{h}, \tilde{\mathbf{S}}; \tilde{\mathbf{r}})$ is the multiuser single sensor ILSE cost function defined in Chapter III, Eq.(III.7), and where we have reintroduced the received sequence as a parameter for clarity. From the above decomposition of the multicarrier cost function it directly follows that the enumeration step simply consists in P parallel single-carrier enumerations, Eq.(III.9):

$$\tilde{\mathbf{S}}_p = \underset{\tilde{\mathbf{S}} \in (\mathscr{C}_1 \times \cdots \times \mathscr{C}_K)^N}{\operatorname{argmin}} \| \tilde{\mathbf{r}}_p - \mathbf{f}_p \mathbf{H} \tilde{\mathbf{S}} \|^2 \tag{IV.7}$$

The minimization of J with respect to $\mathbf{H}$ given the set of symbol matrix estimates $\{\tilde{\mathbf{S}}_p\}$ can be carried out exactly as follows. First, it is straightforward to check that J_P is a convex function of $\mathbf{H}$, as a sum of convex functions of the linearly transformed variable $\mathbf{f}_p \mathbf{H}$ [6]. To find the minimum we have to differentiate J_P with respect to the complex matrix $\mathbf{H}$. Without entering into the technical details, the differential of J_P is obtained by expressing $\Delta J_P(\mathbf{dH}) \triangleq J_P(\mathbf{H} + \mathbf{dH}) - J_P(\mathbf{H})$ as

$$\Delta J_P(\mathbf{dH}) = \langle \frac{\partial J_P}{\partial \mathbf{H}} | \mathbf{dH} \rangle + \langle \frac{\partial J_P}{\partial \mathbf{H}^\dagger} | \mathbf{dH}^\dagger \rangle \tag{IV.8}$$

with $\langle \mathbf{A} | \mathbf{B} \rangle_F \triangleq \operatorname{Tr}\left[\mathbf{A}^\dagger \mathbf{B}\right]$ the hermitian scalar product of matrices induced by the Frobenius norm [108] with $\operatorname{Tr}[\cdot]$ the trace operator, and $\frac{\partial J_P}{\partial \mathbf{H}}$ is a $P \times L$ matrix called the matrix gradient of J_P with respect to $\mathbf{H}$. The minimum of J_P is achieved when either $\frac{\partial J_P}{\partial \mathbf{H}}$ or $\frac{\partial J_P}{\partial \mathbf{H}^\dagger}$ are zero. From the definition of J_P and after a few classic matrix manipulations we obtain

$$\Delta J_P(\mathbf{dH}) = \sum_{p=1}^{P} \operatorname{Tr}\left[\left(\tilde{\mathbf{S}}_p \tilde{\mathbf{S}}_p^\dagger \mathbf{H}^\dagger \mathbf{f}_p^\dagger \mathbf{f}_p - \tilde{\mathbf{S}}_p \tilde{\mathbf{r}}_p^\dagger \mathbf{f}_p \right) \mathbf{dH} \right] + \text{h.c.} \tag{IV.9}$$

where h.c. denotes the hermitian conjugate of the sum in the right hand side of (IV.9). By linearity of the Trace operator and identification with (IV.8) we thus have

$$\frac{\partial J_P}{\partial \mathbf{H}} = \sum_{p=1}^{P} \left(\tilde{\mathbf{S}}_p \tilde{\mathbf{S}}_p^\dagger \mathbf{H}^\dagger \mathbf{f}_p^\dagger \mathbf{f}_p - \tilde{\mathbf{S}}_p \tilde{\mathbf{r}}_p^\dagger \mathbf{f}_p \right)^\dagger = \sum_{p=1}^{P} \left(\mathbf{f}_p^\dagger \mathbf{f}_p \mathbf{H} \tilde{\mathbf{S}}_p \tilde{\mathbf{S}}_p^\dagger - \mathbf{f}_p^\dagger \tilde{\mathbf{r}}_p \tilde{\mathbf{S}}_p^\dagger \right) \tag{IV.10}$$

Now, in order to solve $\frac{\partial J_P}{\partial \mathbf{H}} = 0$ for $\mathbf{H}$ the following useful matrix identity is used [109]: let us denote $\mathbf{M}$ an arbitrary complex matrix such that $\mathbf{M}$ factorizes in three matrices $(\mathbf{U}, \mathbf{Z}, \mathbf{V})$ as

$$\mathbf{UZV} = \mathbf{M} \tag{IV.11}$$

Then it can be easily shown that

$$\left(\mathbf{V}^T \otimes \mathbf{U} \right) \mathbf{vec}\left(\mathbf{Z} \right) = \mathbf{vec}\left(\mathbf{M} \right) \tag{IV.12}$$

where $\otimes$ denotes the tensor or Kronecker product and $\mathbf{vec}\left(\cdot\right)$ is the vectorization operation that concatenates the columns of a given matrix in a single column vector. Applying (IV.12)

to $\mathbf{Z} = \mathbf{H}$, $\mathbf{U} = \tilde{\mathbf{S}}_p\tilde{\mathbf{S}}_p^\dagger$, $\mathbf{V} = \mathbf{f}_p\mathbf{f}_p^\dagger$ and $\mathbf{M} = \tilde{\mathbf{r}_p}\tilde{\mathbf{S}}_p^\dagger$, Eq.(IV.10) is equal to zero for

$$\mathbf{vec}\,(\mathbf{H}) = \left(\sum_{p=1}^{P}(\tilde{\mathbf{S}}_p^T \otimes \mathbf{f}_p)^\dagger(\tilde{\mathbf{S}}_p^T \otimes \mathbf{f}_p)\right)^{-1}\mathbf{vec}\left(\sum_{p=1}^{P}\mathbf{f}_p^\dagger\tilde{\mathbf{r}}_p\tilde{\mathbf{S}}_p^\dagger\right) \tag{IV.13}$$

and the matrix solution is then finally obtained from $\mathbf{vec}\,(\mathbf{H})$ by reversing the vectorization operation. Note that taken individually none of the matrices $(\tilde{\mathbf{S}}_p^T \otimes \mathbf{f}_p)^\dagger(\tilde{\mathbf{S}}_p^T \otimes \mathbf{f}_p) = \tilde{\mathbf{S}}_p^*\tilde{\mathbf{S}}_p^T \otimes \mathbf{f}_p^\dagger\mathbf{f}_p$ in (IV.13) is invertible since $\mathbf{f}_p^\dagger\mathbf{f}_p$ has rank 1. If all combinations of symbols from the joint constellation $\mathscr{C}$ appear in $\tilde{\mathbf{S}}_p$ then $\mathrm{rk}\,(\tilde{\mathbf{S}_p}) = K$, with $\mathrm{rk}\,(\cdot)$ the matrix rank operator, so $\mathrm{rk}\,(\tilde{\mathbf{S}}_p^*\tilde{\mathbf{S}}_p^T \otimes \mathbf{f}_p^\dagger\mathbf{f}_p) = \mathrm{rk}\,(\tilde{\mathbf{S}}_p^*\tilde{\mathbf{S}}_p^T)\,\mathrm{rk}\,(\mathbf{f}_p^\dagger\mathbf{f}_p) = K$. This is most often verified in practice for equally likely constellation symbols, provided that N is large enough. As the sum of P matrices of rank K does not generally yield a matrice of rank KL, the inversion operation in (IV.13) is not ensured, but seems to be verified in our simulations under the short chanel memory assumpion, $P \gg L$.

The overall complexity of the ILSE-OFDM algorithm can be computed as follows: the complexity of the enumeration step requires, for each subcarrier p and each symbol matrix $\tilde{\mathbf{S}}$, computation of $\mathbf{f}_p\mathbf{H}\tilde{\mathbf{S}}$, which is in $\mathcal{O}\,((K+1)LN)$, and computation of a norm over $\mathbb{C}^N$, which is in $\mathcal{O}\,(N)$. Hence the complexity of (IV.7) is in $\mathcal{O}\,(KLMNP)$ As for the estimation step, from (IV.13) the complexity is given by the sum of $\mathcal{O}\left(K^2L^2NP\right)$ (sum of the matrices $(\tilde{\mathbf{S}}_p^T \otimes \mathbf{f}_p)^\dagger(\tilde{\mathbf{S}}_p^T \otimes \mathbf{f}_p)$), $\mathcal{O}\left(K^3L^3\right)$ (matrix inversion), $\mathcal{O}\,(KP(N+L))$ (sum of the matrices $\mathbf{f}_p^\dagger\tilde{\mathbf{r}}_p\tilde{\mathbf{S}}_p^\dagger$) and $\mathcal{O}\left(K^2L^2\right)$ (matrix-vector multiplication). Altogether the complexity of one whole iteration of the algorithm is, retaining only the dominant terms, in $\mathcal{O}\,(KLNP(M+KL))$. In most settings the total number of symbols in the joint constellation M is greater than KL, so the overall complexity is dominated by the enumeration step, as in the single-carrier case.

IV.3 Initialization strategies for ILSE-OFDM

The importance of providing ILSE with an initial channel estimate has already been highlighted in the two previous chapters. This is even more crucial in the multi-carrier case, as $\mathbf{H} \in \mathbb{C}^{LK}$, so the number of degrees of freedom involved is considerable. Inasmuch as the initial channel predictors derived from the method of moments were previously shown to be in many cases reliable enough for ensuring convergence of ILSE towards its global minimum, it would seem then natural to apply the same strategy to multicarrier transmissions. That is, for each subcarrier p we solve the moment problem for $\tilde{\mathbf{h}}_p$ using the received sequence $\mathbf{r}_p$, and build column by column an estimator for $\tilde{\mathbf{H}}$. The major difference here is that the ILSE-OFDM algorithm directly estimates the channel in the time domain. The simplest solution to get a temporal channel estimate from a spectral one consists in taking the IDFT of the latter and retaining only the first L rows. Without additional care however this strategy is very likely to yield poor channel estimates as:

- the multiuser moment method predictors are in general not unique: each subcarrier is then subject to an ambiguity in the choice of the predictor;

- even in the SISO case, the discrete circular invariance of the source symbols implies that the predictors are only defined up to discrete rotations.

Hence, applying the inverse Fourier transform without addressing beforehand any of these indeterminacies will result in a spurious temporal channel matrix predictor. While for the single-carrier case it was not too unrealistic to suppose that the receiver could acquire the actual phase and decoding order, for multi-carrier transmissions this would require this information to be available for each sub-carrier. As the number of subcarriers P can be very large, this ideal framework does not seem reasonable. Consequently, we will propose in the following several strategies attempting to reduce the problem of solving all subcarrier phases and ordering ambiguities to that of acquiring this information for only one sub-carrier, just as in the MISO flat-fading case.

IV.3.1 Phase sorting strategies

Root-finding algorithms

The phase indeterminacies of blind channel estimators constitute a well known problem in OFDM transmissions, and several algorithms have been proposed in the literature to address it [110], [111]. Many of them rely on the convolution property of the Fourier Transform, namely, the DFT of a cyclic convolution is given by the product of the DFTs. In the following we consider without loss of generality a SISO-OFDM transmission with P subcarriers. Applying the moment method estimator II.4 to each subcarrier independently yields the $P \times 1$ vector of q-th power channel frequency estimates $\tilde{\boldsymbol{\xi}} \triangleq \tilde{\mathbf{h}}^q$ where the power exponent applies component-wise and the "hat" notation for estimators has been dropped for convenience. Taking the IDFT of $\tilde{\boldsymbol{\xi}}$, denoted by $\boldsymbol{\xi}$, we obtain by the (cyclic) q-th fold convolution of the temporal channel with itself, denoted by $\mathbf{h}_q^{\circledast}$:

$$\boldsymbol{\xi} = \mathbf{h}^{\circledast q} \triangleq \underbrace{\mathbf{h} \circledast \mathbf{h} \circledast \cdots \circledast \mathbf{h}}_{q \text{ times}} \tag{IV.14}$$

To be accurate, since the channel impulse response has L taps, its q-th autoconvolution has length $L_{\mathbf{h}^{\circledast q}} = q(L-1)+1$, so $\boldsymbol{\xi}$ is actually obtained from the IDFT of $\tilde{\boldsymbol{\xi}}$ and by retaining the $L_{\mathbf{h}^{\circledast q}}$ first coefficients. Note that this requires $P \geq q(L-1)+1$ which is compatible with the short impulse response assumption, $L \ll P$. Let us further define, for any vector $\mathbf{a}$ with length $L_{\mathbf{a}}$, the complex polynomial $P_{\mathbf{a}}(z) \triangleq \sum_{\ell=0}^{L_{\mathbf{a}}-1} a_\ell z^\ell$, known for $z \to 1/z$ as the Z-transform of $\mathbf{a}$. It is then not difficult to check that $P_{\mathbf{a}\circledast\mathbf{a}}(z) = P_{\mathbf{a}}^2(z)$, so $P_{\boldsymbol{\xi}}(z) = P_{\mathbf{h}}^q(z)$ and the $L_{\mathbf{h}^{\circledast q}} - 1 = q(L-1)$ roots of $P_{\boldsymbol{\xi}}(z)$ are the $L-1$ roots of $P_{\mathbf{h}}(z)$ with multiplicity q. In other words, recovering the impulse channel response $\mathbf{a}$ reduces to finding the L distinct roots of the polynomial $P_{\tilde{\boldsymbol{\xi}}}(z)$. In practice things are obviously not so simple because $\boldsymbol{\xi}$ is derived from the moment estimator of $\tilde{\boldsymbol{\xi}}$ which has a non-zero residual error. Consequently the roots of $P_{\tilde{\boldsymbol{\xi}}}(z)$ are in general all distinct, requiring additional treatment for the multiple roots to be identified. Several strategies have been proposed in [95]. The solution we will adopt here is to cluster the roots of $P_{\tilde{\boldsymbol{\xi}}}(z)$ in $L-1$ groups with the k-means algorithm, initialized with the k-products algorithm, presented in Section II.2.1. This choice may not

be optimal in terms of computational load but has the desirable property of always converging.

Autodeconvolution

Another possibility to recover the channel taps from the q-th power channel frequency estimator is the so-called autodeconvolution proposed in [112], which aims at directly solving (IV.14) in $\mathbf{h}$. Expanding the q-th power autoconvolution results in an overdetermined non linear system of $L_{\mathbf{h}^{\circledast q}}$ equations in the coefficients h_ℓ, $\ell \in \{1, \cdots, L\}$. The Gauss substitution method allows to turn this system into a linear one as

$$\mathbf{M}\mathbf{h} = 0 \tag{IV.15}$$

with $\mathbf{M}$ the $L_{\mathbf{h}^{\circledast q}} \times L$ matrix defined by $\mathbf{M}_{p,\ell} \triangleq (p-(q+1)\ell+1)\,\boldsymbol{\xi}_{p-\ell+1}$ and $\mathbf{M}_{p,\ell} = 0$ for indices such that $p-\ell+1 \notin \{1, \cdots, L_{\mathbf{h}^{\circledast q}}\}$. Again, because $\boldsymbol{\xi}$ is an estimator (IV.15) does not hold exactly. The estimator of $\mathbf{h}$ is then obtained from the minimum norm solution. To avoid the trivial solution $\mathbf{h} = 0$ the first coefficient $\mathbf{h}_1$ can be separately estimated as $\mathbf{h}_1 = \sqrt[q]{\widehat{\boldsymbol{\xi}}_1}$, and the remaining coefficients, denoted by the vector $\widehat{\mathbf{h}}_{|1} \triangleq (\widehat{\mathbf{h}}_2, \cdots, \widehat{\mathbf{h}}_L)$ are obtained as

$$\widehat{\mathbf{h}}_{|1} = -\left(\mathbf{M}_{|1}^{\dagger}\mathbf{M}_{|1}\right)^{-1}\mathbf{M}_{|1}^{\dagger}\mathbf{M}_{\{1\}}\widehat{\mathbf{h}}_1 \tag{IV.16}$$

where $\mathbf{M}_{|1}$ and $\mathbf{M}_{\{1\}}$ denote the matrices obtained by extracting the $L-1$ last columns of $\mathbf{M}$ and the first column of $\mathbf{M}$, respectively. Equivalently the L-th coefficient $\mathbf{h}_L$ can be separately estimated as $\mathbf{h}_L = \sqrt[q]{\boldsymbol{\xi}_{L_{\mathbf{h}^{\circledast q}}}}$ and the remaining coefficients deduce by an equation similar to (IV.16). The latter method is termed backward autodeconvolution, as the channel coeffcients are estimated in reverse order, while the former is referred to as forward autodeconvolution. An improvement of the algorithm was proposed in [113] based on an iterative WLS resolution of (IV.15) to account for heteroscedasticity in the residual estimation errors. In the following though we will restrict to the original formulation of the autodeconvolution.

Autodeconvolution by Singular Value Decomposition

It has been observed that the performance of algorithms such as the above forward/backward autodeconvolution are very sensitive to noise, inasmuch as they are subject to error propagation. More specifically, if the first (respectively last) channel tap $\mathbf{h}_1$ ($\mathbf{h}_L$) has a low power, the resulting estimation error made on $\mathbf{h}_1$ ($\widehat{\mathbf{h}}_L$) is likely to be important, and (back)-propagates through Eq.(IV.16). To counter this effect another way of finding the minimal norm solution of $\mathbf{M}\mathbf{h}$ consists in considering the Singular Value Decomposition (SVD) of $\mathbf{M}$ and taking the right singular vector associated with the smallest singular value. Denoting by $\mathbf{h}_s$ this vector, with $\| \mathbf{h}_s \|^2 = 1$ by definition of the SVD, the temporal channel estimator $\mathbf{h}$ is obtained as $\mathbf{h} = \lambda \mathbf{h}_s$. The real coefficient λ is then derived by imposing the

q-th power of the DFT of $\mathbf{h}$ to be the closest, in the complex distance sense, to $\tilde{\boldsymbol{\xi}}$ leading to

$$\mathbf{h} \triangleq \sqrt[q]{\frac{\langle \tilde{\boldsymbol{\xi}}_s | \tilde{\boldsymbol{\xi}} \rangle}{\| \tilde{\boldsymbol{\xi}}_s \|^2}} \mathbf{h}_s \tag{IV.17}$$

where $\tilde{\boldsymbol{\xi}}_s$ is the q-th power of the DFT of $\mathbf{h}_s$.

Qualitative comparison

We have seen several possible ways of finding an initial estimate for the temporal channel $\mathbf{h}$. The advantage of such methods is that by operating in the time domain they implicitely solve the phase ambiguities for each subcarrier, except for one global phase shift. We have then reduced the problem of determining P phases to just a single one. The performances of the three presented temporal estimation strategies can be compared on the basis of the temporal NRMSE, defined similarly as in (III.40) for a given temporal channel estimator $\widehat{\mathbf{h}}$ as

$$\mathrm{NRMSE}(\widehat{\mathbf{h}}) \triangleq \frac{\sqrt{\mathbb{E}\left[\| \mathbf{h} - \widehat{\mathbf{h}} \|^2\right]}}{\mathbb{E}\left[\| \mathbf{h} \|^2\right]} \tag{IV.18}$$

Comparative Monte-Carlo simulations performed on $P = 128$ independent circular complex normal subcarriers and various channel memories $L \in \{3, 5, 10, 15, 20\}$ reveal that in more than 90% of cases the SVD-based estimation outperforms by large the k-means root clustering and the forward/backward algorithm. This percentage increases with the number of taps, reaching more than 99% when $L = 20$. On the other hand the autodeconvolution does not generally yield good results because of noise propagation. In rare cases (less than 10% for $L = 3$ and 1% for $L = 20$), the clustering scheme happens to produce the better estimate in terms NRMSE. These results suggest that we can in almost all cases have access to a reliable initial temporal channel estimate by simultaneously applying the SVD and the root clustering, and selecting the best outcome. Since the NRMSE is actually unobservable, in practice the choice is based on the distance between the q-th power initial frequency channel estimate provided by the moment method and the q-th power DFT of the temporal estimates. Regarding complexity, the computational costs of the root-clustering, autodeconvolution and SVD are roughly given by $\mathcal{O}\left(qL^2 N_{ite}\right)$ for the former, where N_{ite} denotes the number of iterations needed for k-means to converge, and $\mathcal{O}\left(qL^3\right)$ for the two other methods. Considering that convergence of k-means is usually fast and that the channel memory L is short, the three methods have thus quite comparable complexities.

Finally, this whole discussion was based on a single-user OFDM transmission. In the case of several users, the presented algorithms will be capable of providing good results only if there is no permutation ambiguity between the channels q-th power of each subcarrier. Otherwise expressing $\tilde{\boldsymbol{\xi}}_p$ as a q-th power DFT does not make much sense. In practical uses it is then crucial to address the permutation ambiguities prior to the phases resolution step.

IV.3.2 Permutation sorting

Classification of permutation problems

As we have seen in Chapter III for single-carrier MISO transmissions, in many cases the channel power predictors derived from the method of moment are not unique. According to the discussion made in Section (III.3), three possible cases can occur, depending on the users constellations and the corresponding rotational order vector $\mathbf{q}$:

- the simplest scenario occurs when all entries of $\mathbf{q}$ are distinct, *i.e.* each constellation has its own unique discrete rotational symmetry. In that case the moment method channel predictor $\widehat{\boldsymbol{\xi}}$ was shown to be unique, so the receiver can without ambiguity identify each source based on the estimated symbol sequences constellation, provided that prior knowledge of each user's constellation is available;

- some entries of $\mathbf{q}$ are equal, but the associated constellations are distinct. This happens for instance when several users modulate their symbols according to different QAM schemes. The moment-based channel predictors associated to identical rotational orders are then no longer unique, but the estimated symbols can still be associated without ambiguity to their respective source;

- the most general case consists in some sources to use the same constellations. Such sources are defined as indistinguishable, and without additional assumption or a priori information there is no blind way for the receiver to differentiate them.

The first case is ideal but of limited practical interest, as the rotational orders typically range from 2 to 16 by powers of two, strongly limiting the number of users that can be dealt with. The second case was addressed in Section III.3.5 by applying ILSE on each of the possible channel predictors and selecting the best one, in the ILSE cost function sense. The same strategy can readily be extended to the multicarrier framework in a per-subcarrier fashion. This scenario imposes less stringent conditions on the sources constellations than the first one, making identification of a moderate number of users possible. As for the most general case, while blind single-carrier strategies are at a standstill, the diversity induced by the channel frequency selective nature provides us with additional information that may help to recover all sources without ordering ambiguity.

Full-search criterion

In the previous section we expressed the single-user moment method frequency channel $\tilde{\boldsymbol{\xi}}$ as the DFT of the temporal channel q-fold cyclic convolution $\mathbf{h}^{\circledast q}$, Eq.(IV.14). Because of the channel finite memory L, the Inverse Fourier Transform of $\tilde{\boldsymbol{\xi}}$ has its last $P-L+1$ coefficients equal to zero. Consequently, if for K users we define L as the longest channel impulse response, *i.e.* $L \triangleq \max_k(L_k)$, denoting by $\tilde{\boldsymbol{\Xi}}$ the $P \times K$ matrix whose k-th column is the DFT of $\mathbf{h}_k^{\circledast q_k}$, and by $\boldsymbol{\Xi}$ the (column-wise) IDFT of $\tilde{\boldsymbol{\Xi}}$, *i.e.* $\boldsymbol{\Xi} \triangleq \mathbf{F}^{\dagger}\tilde{\boldsymbol{\Xi}}$, then the $(P-L+1) \times K$ submatrix $\mathbf{T}_{\boldsymbol{\Xi}}$ obtained from $\boldsymbol{\Xi}$ by restriction to its last $P-L+1$ rows is null. Apart from full column permutations, any permutation of one or more elements between any two

columns of $\tilde{\mathbf{\Xi}}$ is likely to result in the introduction of non zeros entries in the associated subblock $\mathbf{T}_{\mathbf{\Xi}}$. This provides a way of detecting permutations of channel frequency coefficients from subsets of indistinguishable users, and of recovering the right ordering up to a global permutation. Again, as the coefficients in $\tilde{\mathbf{\Xi}}$ are estimated from the method of moments, their residuals with respect to the actual channel frequency coefficients imply that $\mathbf{T}_{\mathbf{\Xi}}$ will be filled with non zeros entries, regardless of the permutation. It is however reasonable to assume that in most cases those entries should be minimal when the correct ordering is considered. The appropriate criterion for identification of the optimal permutation is then the norm of $\mathbf{T}_{\mathbf{\Xi}}$. Note that here for simplicity we considered the whole submatrix $\mathbf{T}_{\mathbf{\Xi}}$, but only those columns associated with identical sources are actually concerned by permutation ambiguities. A more accurate formulation of our sorting criterion is thus given as follows:

Let us consider k indistinguishable sources with the same constellation, and denote by $\tilde{\mathbf{\Xi}}$ the associated $P \times k$ channel matrix estimated from the method of moments. For each subcarrier p from 2 to P, we define τ_p as a permutation of k elements, and $\boldsymbol{\tau}$ the associated $(P-1) \times 1$ vector. We further define $\tilde{\mathbf{\Xi}}_{\boldsymbol{\tau}}$ as the matrix obtained from $\tilde{\mathbf{\Xi}}$ by permuting the elements in the $P-1$ last rows according to $\boldsymbol{\tau}$, and $\mathbf{\Xi}_{\boldsymbol{\tau}} = \mathbf{F}^{\dagger}\tilde{\mathbf{\Xi}}_{\boldsymbol{\tau}}$ its Inverse Fourier Transform. Finally, we denote by $\mathbf{T}_{\mathbf{\Xi}_{\boldsymbol{\tau}}}$ the submatrix of $\mathbf{\Xi}_{\boldsymbol{\tau}}$ composed of its $P - \max_{k \leq m}(L_k) + 1$ last rows, where L_k denotes the memory of the k-th user channel. Then the "best" permutation $\boldsymbol{\tau}_*$ among the k users is defined as the permutation vector which minimizes the Frobenius norm of $\mathbf{T}_{\mathbf{\Xi}_{\boldsymbol{\tau}}}$:

$$\boldsymbol{\tau}_* \triangleq \underset{\boldsymbol{\tau} \in \mathscr{S}_k^{P-1}}{\operatorname{argmin}} \left(\| \mathbf{T}_{\mathbf{\Xi}_{\boldsymbol{\tau}}} \|_F \right) \tag{IV.19}$$

where $\mathscr{S}_k$ is the permutation set of k elements. The reason why we only consider permutations on subcarriers from 2 to P is to discard vectors $\boldsymbol{\tau}$ that are related to each other by a global permutation of the columns of $\tilde{\mathbf{\Xi}}_{\boldsymbol{\tau}}$, as they result in the same value for $\| \mathbf{T}_{\mathbf{\Xi}_{\boldsymbol{\tau}}} \|_F$. This way the optimal permutation τ_* is (almost surely) unique. It is important to note that the above criterion is only suboptimal: it was observed in simulations that the permutation providing the closest channel estimate to the actual one, in the squared distance sense, can differ from the permutation $\boldsymbol{\tau}_*$ achieving the lowest cost. Finally, by definition the sorting procedure can be applied to each subset of identical sources independently, allowing use of parallel architectures in practical implementations.

Partial search strategy

The main limitation of the above criterion is that, for a given k there are $(k!)^{P-1}$ possible permutation vectors. As the number of subcarriers P is typically greater than 32, even for just two users having the same constellation an exhaustive search would require as much as $2^{31} = \mathcal{O}\left(10^9\right)$ permutations, which in regard to practical delay requirements is not reasonably feasible. A solution consists then in resorting to an iterative partial search: starting from a given subcarrier p, we search for all permutations of k elements only for subcarriers from p to $p + p_0$, with $p_0 < P$. The best of the associated permutation vectors, in the sense of (IV.19) is then used as an indication of the best permutation for the p-th

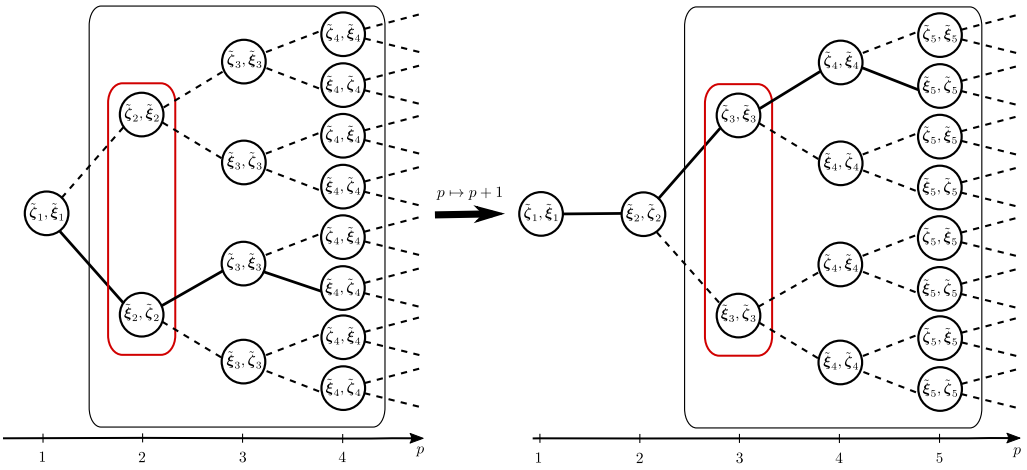

Figure IV.3 – *First two iterations of the troncated search with $K = 2$ users and a horizon $p_0 = 4$. Dashed lines represent transitions between states obtained by permutations in the subsequent subcarrier, and the solid lines show the path that yields the lowest cost function* (IV.19)

subcarrier. In other words, the decision of the best ordering for the channel coefficients of subcarrier p is based on the permutations of the coefficients in the subsequent p_0 subcarriers. The motivating idea is that permutations of coefficients in rows that are far from p should intuitively not significantly alter the IDFT of $\tilde{\boldsymbol{\Xi}}$. The procedure is then iterated until all (but the first) subcarriers have been sorted, thus constructing the "best" matrix $\tilde{\boldsymbol{\Xi}}$ row by row. The resulting algorithm can be thought of as a forward troncated Viterbi algorithm [114], where each state corresponds to a possible permutation for a given subcarrier, and p_0 is referred to as the *horizon* of *depth* of the algorithm. Note that the cost function for a given subcarrier p is still computed from the full $P \times k$ matrices $\tilde{\boldsymbol{\Xi}}_{\boldsymbol{\tau}}$ and not just from the first $p+p_0$ rows.

An illustrative example of the troncated search is shown on Fig.IV.3 for $k = 2$ indistinguishable users and a horizon $p_0 = 2$. The algorithm starts at $p = 2$ since the first subcarrier only accounts for a global permutation. The two columns of $\tilde{\boldsymbol{\Xi}}$ are respectively denoted by $\tilde{\boldsymbol{\zeta}}$ and $\tilde{\boldsymbol{\xi}}$. At the first iteration the minimal troncated path with respect to (IV.19) suggests to permute coefficients $\tilde{\zeta}_2$ and $\tilde{\xi}_2$. The procedure is then repeated from the retained state $(\tilde{\xi}_2, \tilde{\zeta}_2)$, and the resulting minimal path indicates to leave unchanged the coefficients in the third subcarrier. At this stage, the first three rows of the suboptimal $\tilde{\boldsymbol{\Xi}}$ thus read $(\tilde{\zeta}_1, \tilde{\xi}_1)$, $(\tilde{\xi}_2, \tilde{\zeta}_2)$ and $(\tilde{\zeta}_3, \tilde{\xi}_3)$, respectively.

With an appropriate choice of the horizon p_0, the troncated search allows to considerably reduce the complexity of the sorting strategy. For a given subcarrier p, there are $k!^{p_0}$ possible permutations. Neglecting the fact that for the last $P - p_0 + 1$ subcarriers this number is reduced to $k!^{P-p+1}$, the total number of permutations is roughly given by $P(k!)^{p_0}$ instead of $(k!)^{P-1}$ for the full search. For two users with 32 subcarriers and horizon 4 for instance, this gives only 512 permutations, and 131072 for a horizon 12, far below the billion permutations

required by the exhaustive strategy. To approximate the induced computational complexity, each tested permutation requires k IDFT and computation of the matix norm in (IV.19). The former operation is efficiently implemented by the Fast Fourier Transform (FFT) algorithm with complexity in $\mathcal{O}(P\log(P))$, and the latter has complexity $\mathcal{O}(k(P-L+1))$. Altogether the computational load of the troncated search for k indistinguishable sources and horizon p_0 is then in $\mathcal{O}\left(P^2k(k!)^{p_0}\right)$ operations.

IV.4 Simulations

IV.4.1 General settings

We have carried out several Monte-Carlo simulations on the ILSE-OFDM algorithm using the above strategies for phase and permutation resolution. The $L\times K$ channel matrix $\mathbf{H}$ is assumed to have independent, circularly-symmetric complex normal random entries with variance N_0, so the users channels are mutually independent and no time correlation between the multiple paths of a given user is assumed either. The chosen performance measures are the joint SER (III.39) and the temporal NRMSE of the estimated channel matrix $\widehat{\mathbf{H}}$, defined similarly to (IV.18) by replacing channel vectors by the corresponding matrices and the complex norm by the Frobenius norm. Two different mixtures with $K=2$ users have been considered: a double QAM 4 and a QAM 16-QAM 4. In both settings the number of taps for all channels is $L=3$, and the number of subcarriers $P=32$. The number of consecutive OFDM symbols has been chosen to 400 for the first setting and 1000 for the second. The overall channel estimation strategies slightly differ and are summarized in the two functional block diagrams of Fig.IV.4. In both cases the starting point for initialization of ILSE-OFDM is the moment method estimator of matrix $\widetilde{\mathbf{\Xi}}$ whose P rows are independently obtained from Eq.(III.23). The permutation ambiguities are addressed either by the troncated Viterbi algorithm, either by applying single-carrier MISO-ILSEs on each subcarrier, as explained in Section IV.3.2. The three temporal channel estimations strategies proposed in Section IV.3.1 are then applied and the best result is obtained by comparing the initial and final channel frequency power matrices. The ILSE-OFDM is then computed and the resulting temporal channel matrix estimator is Fourier transformed to perform the received sequences threshold decoding independently on each subcarrier.

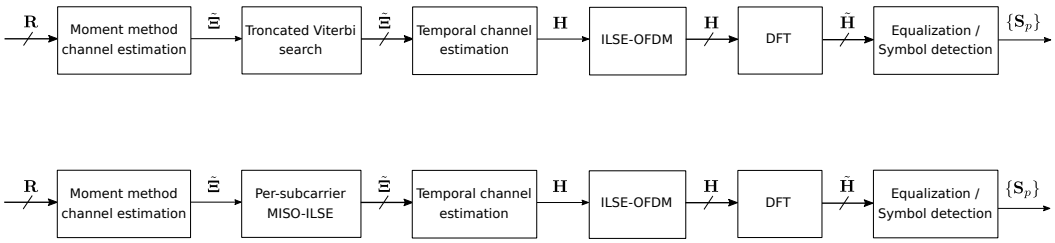

Figure IV.4 – *Functional block diagrams of the ILSE-OFDM channel estimation procedure. Top: identical constellations; Bottom: distinct constellations with equal rotational orders. Crossed arrows indicate parallelization of the pointed block over subcarriers.*

IV.4.2 Results

Two-QAM4 mixture

In the case of two QAM4 the sources cannot be distinguished based on single-carrier strategies, so the troncated Viterbi algorithm is applied to find a suboptimal sorting. The obtained performances are displayed on Fig.IV.5 as a function of the SNR E_b/N_0 (with $E_b = 1$) along with the reference perfect CSI curve and the following method variations:

ILSE-OFDM with perfect phases/permutation refers to the ideal initialization case where all permutation and phase ambiguities have been exactly resolved. In simulations this is done by comparison with the actual channel realizations to extract the optimal source/phase ordering;

ILSE-OFDM corresponds to the basic application of the method with a troncated Viterbi search with horizon 12;

per-sub carrier ILSE introduces an additional step before the partial search by applying the MISO-ILSE algorithm for each subcarrier. The objective is to reduce the estimation noise introduced by the moment method at the input of the pemutation and phase solving steps. The channel estimation procedure is stopped after the phase resolution, *i.e.* no ILSE-OFDM is applied in this case;

per-sub carrier ILSE + ILSE-OFDM is the same strategy as the previous one but with the additional use of the ILSE-OFDM.

It appears clear from both figures that the proposed strategies to solve permutation and phase ambiguities cannot ensure convergence of ILSE-OFDM towards its global minimum. Prior application of the MISO-ILSE algorithm on each subcarrier alone is not sufficient to appreciably improve the estimation either, but together with ILSE-OFDM a substantial gain can be obtained, at the cost of a significant increase in complexity. Only when all sources ordering and phase ambiguities are perfectly resolved does the resulting SER closely match the perfect CSI curve for the whole considered SNR range. This is in neat contrast with the single-carrier MISO-ILSE of Chapter III as no asymptotic error floor is observed here. From

a general perspective all the achieved error rates are quite poor, even for the ideal curve. This can be imputed to the extremely unfavorable transmission conditions, with a SIR equal to 0dB on each subcarrier and with completely uncorrelated path fadings. We recall however that the presented performances are uncoded, meaning they do not include any channel encoding at the transmitter nor error correction scheme at the receiver. Implementing such additional safeguards would hopefully lead to singificantly lower error rates, closer to the reliability requirements of practical wireless transmissions.

QAM4-QAM16 mixture

For a mixture composed of a QAM 4 and a QAM 16 the troncated Viterbi search is unnecessary and is replaced by a bank of single-carrier ILSEs applied on each subcarrier and for each possible moment channel predictor. According to Section III.3.4 there are two such possible predictors, totalizing $2P$ runs of the algorithm. Note that for each subcarrier the ILSE initialized with the correct moment predictor converges most often very quickly – in one or two iterations –, limiting the actual complexity of this stage. Fig.IV.6 displays the results obtained for the perfect CSI and the three following algorithms:

autodeconvolution refers to the use of the strategies in Section IV.3.1 as a self-consistent temporal channel estimation, *i.e.* ILSE-OFDM is not applied afterwards;

autodeconvolution + ILSE-OFDM is the main strategy corresponding to the lower block diagram of Fig.IV.2;

ILSE-OFDM with perfect phases represents the theoretically best achievable averaged outcome of ILSE-OFDM based on the initial moment method predictors and perfectly recovered phases.

By and large the same conclusions as for the previous mixture can be drawn. Application of ILSE-OFDM reveals necessary to approach the 10% error threshold, but without a strongly reliable carrier phases recovery the algorithm cannot do better and quickly saturates. Here again we note how closely the perfect phase ILSE-OFDM performs with respect to a fully known channel scenario. In regard to the performances obtained for the same mixture in Chapter III, applying individually ILSE to each subcarrier without any optimization strategies such as those introduced in Section III.5 is likely to result in an increased probability of not converging to the global minimum. On the opposite, taking into account the full temporal channel matrix structure seems to make the estimation method almost free of spurious fixed points. This suggests that ILSE-OFDM is a suitable and robust strategy to address blind MISO-OFDM transmissions, at least for short impulse responses and provided the phase and ordering ambiguities can be reliably acquired by the receiver. This comes at the cost of a considerable complexity: for the presented simulation the averaged number of iterations for the algorithm to converge was measured to be of order 50 at $E_b/N_0 = 15$dB and only fell below 10 at approximtely $E_b/N_0 \simeq 24$dB. In a nutshell, the method is powerful but requires a stringent framework to fully reveal its efficiency.

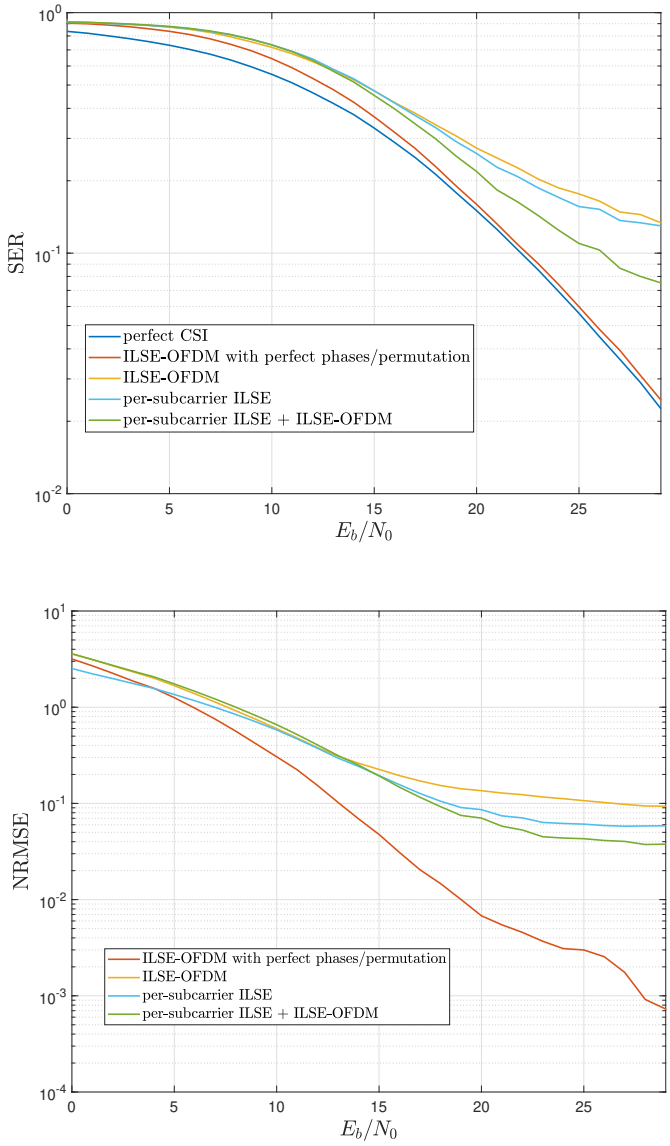

Figure IV.5 – *Joint SER (top) and Temporal NRMSE (bottom) for a two-QAM4 OFDM transmission.*

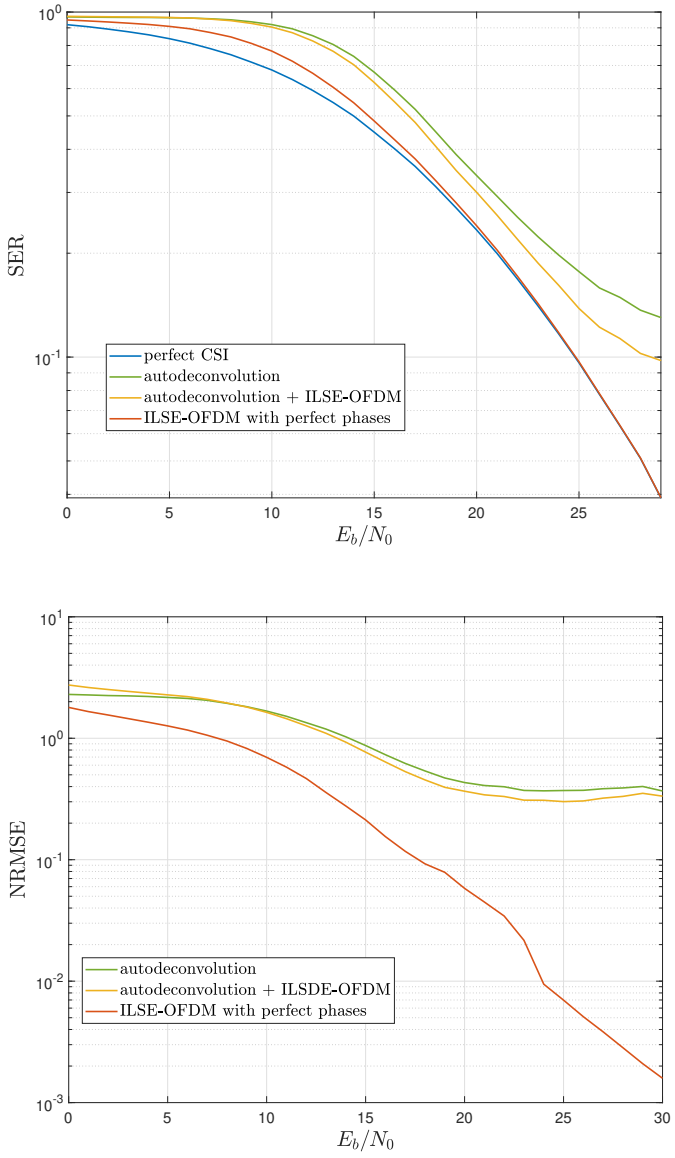

Figure IV.6 – *Joint SER (top) and temporal NRMSE (bottom) for a QAM16-QAM4 OFDM transmission.*

IV.5 Conclusion

We proceeded to enlarge one step further our wireless transmission model by addressing the more realistic scenario of multiuser frequency-selective channels. OFDM revealed as the most natural and convenient extension to consider, with the MISO flat-fading model replaced by several parallel multiuser transmission channels. Based on the short impulse response assumption and the observation that most of the ML-based blind channel estimation techniques proposed in the literature are restricted to the spectral domain, we proposed a generalization of the MISO-ILSE algorithm accounting for the full temporal structure of the channel. Several blind algorithms for solving sources ordering and phase ambiguities introduced by the moment method multiuser channel predictors were used to provide the algorithm with a suitable initial state. Simulations revealed however that the proposed initialization techniques are not reliable enough to ensure convergence of ILSE-OFDM towards its global minimum. Yet the method demonstrated at the same time a real potential in successfully estimating the temporal channels even in extremely harsh transmission settings. The conditions to fully benefit from the method are quite demanding, the most limiting one certainly being the number of OFDM symbols required for the outcome of the algorithm to be meaningful. While for a small number of users these conditions may still be compatible with the channel coherence time and the application delay requirements, as more sources and higher order constellations are involved practical application of the algorithm seems increasingly unlikely. As of now, alternative methods such as recursive algorithms or semi-blind procedures appear more realistic for practical purposes. Still, with the fast evolution in the complexity of the embedded technologies in wireless communication devices, the ILSE-OFDM stands as a powerful potential tool to address high interference and strongly unfavorable related transmission scenarios.

Chapter V

Clustering techniques for entangled data

Contents

Part of this work has been published in the following conference paper:

S. Smith, M. Pischella, M. Terre. "An Elliptical-Shaped Density-based Classification Algorithm for Detection of Entangled Clusters", 25th European Signal Processing Conference (Eusipco 2017), August 2017, pp.1-5, Kos , Greece

V.1 Introduction

In this last chapter we will slightly deviate from the wireless communications framework and adopt a more general point of view by considering a quite fundamental problem in cluster analysis. We have seen in Chapter III how performances of the k-means constrained ILSE algorithm are significantly affected when some points of the joint constellation lie very close to each other. In this particular case it was evidenced that the presence of local minima close to the global one mostly accounted for the incapacity of the algorithm to reliably converge to the optimal solution. More generally, the problem of clustering data in the presence of clusters partially merged or entangled is of both conceptual and practical

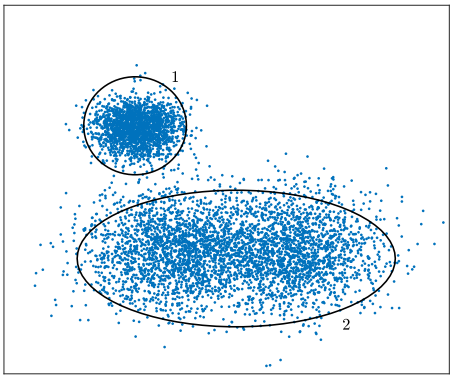

Figure V.1 – *Naive clustering of a gaussian mixture distribution with entangled components.*

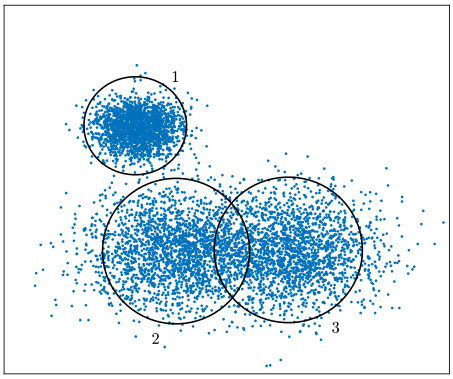

Figure V.2 – *Supervised clustering of a gaussian mixture distribution with entangled components.*

interest. For illustrative purpose, let us consider the two situations depicted on Fig.V.1 and V.2, where the observed data consists in realizations of a mixture distribution with three gaussian components. Two out of the three clusters are partially merged, in such a way that without any a priori knowledge of the underlying data distribution it would be natural to divide the whole dataset into two clusters, as shown on Fig.V.1. Now if we provide a human operator with both the number of components of the mixture and the distribution family of its components, then most likely the resulting clustering will be that of Fig.V.2. A last scenario would consist in assuming only one of the above information to be available. That is, the operator or algorithm either knows that there are only three clusters in the data, or that the data originates from a gaussian mixture distribution with an unknown number of components. In this situation it is not clear what the "optimal" clustering would look like, and several choices of data partitions compatible with the available information may exist.

Through this introductory example we are faced with two major issues. First, the notion of cluster entanglement cannot be given an unified definition, as it heavily depends on the underlying assumptions pertaining to the observed data. What seems clear is that without any constraint on the clustering process such as the number or shapes of the clusters, the ability to separate partially merged data components is most likely doomed to failure. Consequently the cluster entanglement problem has only meaning in the framework of supervised or semi-supervised clustering. Second, even provided with all the relevant hypotheses about the data model, traditional clustering techniques may fail in successfully separating merged clusters, as the entanglement constraint is not direcly taken into account in their operating process.

In light of the above discussion the objective of this chapter is to give a first insight in the treatment of entangled classes in the framework of semi-supervised data clustering. To this end we will propose a density-based algorithm which attempts at identifying entanglement by enforcing the shape of the clusters as ellipsoidal. A first version of the method independent of the actual number of clusters in the data will be first introduced, then a constrained improve-

ment based on iterative merging of spurious clusters will be discussed. The performances of our algorithm will be finally evaluated and compared to reference clustering algorithms from the literature.

V.2 A brief overview of clustering

V.2.1 Definition

A wide diversity of clustering methods and algorithms have been developed and successfully applied in manifold applications including image processing, genetics and data mining [115]. The objective of this section is simply to give a short overview of the most well-known clustering approaches, and is certainly not intended to be exhaustive. Countless textbooks and papers on the subject can be found in the literature. The interested reader can for instance refer to [116] or [117], among many other references.

We formally introduce the clustering problem as follows: given a finite dataset $\mathcal{D}$ of N multidimensional observations denoted by $\mathbf{x}_n$, where $n \in \{1, \cdots N\}$, we aim at classifying the dataset in K meaningful clusters $\mathcal{C}_k$, $k \in \{1, \cdots K\}$, such that all members of any class are more similar to each other than elements taken from different classes. For the sake of simplicity we shall consider from now on that the data points are D-dimensional real vectors, $\mathbf{x}_n \in \mathbb{R}^D$, which allows us to rely on metrics such as the euclidean distance to evaluate similarity between observations.

V.2.2 Properties of clusterings and existing algorithms

From a general point of view clustering techniques can usually be characterized by three properties. First, the number of clusters K required to sort the data may be known in advance or used as a constraint on the algorithm, but may also be a result of the classification process itself. Besides, one may consider by classifying the observations a hard partitioning of the dataset $\mathcal{D}$, meaning that each $\mathbf{x}_n$ exclusively belongs to a single cluster $\mathcal{C}_k$. This is the case of most variations on the k-means algorithm such as k-medians [118], k-modes [116] or k-medoïds [119]. Fuzzy clusterings on the other hand allow data points to belong to several classes with different membership degrees [120]. The c-means fuzzy algorithm for instance can be thought as a fuzzy counterpart to k-means [121]. Finally, some clustering methods are capable of handling the presence of outliers, that is, observations which do not belong to any cluster, *i.e.* $\mathbf{x_n} \in \cap_{k=1}^{K} \mathcal{C}_k^c$. The Fuzzy Clustering by Local Approximation of Membership (FLAME) algorithm is a relatively recent fuzzy algorithm based on a relation graph between neighbouring data points and which accounts for the presence of outliers [122].

More specific distinctions can be made between clustering techniques based on the underlying procedure used to perform the classification. Many algorithms aim at optimizing an objective cost function, the absolute minimum of which corresponds to the best clustering of the dataset. One of the most representative of such methods is the EM algorithm [26] which models the data as realizations from a parametric mixture probability distribution and

aims at iteratively maximizing the log-likelihood Section I.2.5. It is worth mentioning that the k-means algorithm, one of the other well-known representant of this class of methods, can actually be seen as a particular case of EM for equally likely and homoscedastic mixture components. The k-products algorithm proposed in [37] is another example which focuses on estimating the means of the mixture components.

Density-based clustering algorithms represent clusters as dense regions of the observation space. In this framework clusters are identified based on the local density around each observation. The main advantages of such methods are that they do not require a priori information on the number of clusters in the dataset and are suitable for clusters of arbitrary shape, as opposed for instance to k-means which by construction is limited to convex shapes. The Density-Based Spatial Clustering of Applications with Noise (DBSCAN) [123] algorithm and Ordering Points to Identify the Clustering Structure (OPTICS) [124], an extension to clusters with heterogeneous densities, are popular members of this class of methods.

Hierarchical methods define yet another possible approach to clustering, based on iteratively merging or splitting data clusters. They essentially are of two types, namely agglomerative or divisive. [125]. Specifically, divisive hierarchical methods start by considering the whole dataset as a single cluster, and sequentially split it in several smaller clusters based on a predefined dissimilarity measure, until each data point defined its own cluster. Agglomerative techniques proceed in reverse order by starting with singleton clusters and iteravely merging them to the point of obtaining a global cluster. By doing so both methods do not actually result in a specific partition of the dataset but rather in a set of nested partitions represented as a dendrogram. Additional criteria and partition quality measures are then usually required to extract an optimal clustering. Different metrics to measure the dissimilariy between clusters lead to various algorithms, the most well-known being the Single-Link (SINK) [126] and Complete-Link (CLINK) [127], respectively based on the nearest and farthest neighbor distance. Application of hierarchical clustering to large data sets has also been proposed with the Balanced Iterative Reducing and Clustering using Hierarchies (BIRCH) algorithm, an agglomerative method suitable for equally likely and spherical clusters with the additional ability to take outliers into account [128].

More recently, spectral clustering has attracted much interest in the field of data analysis. Spectral clustering techniques are based on the concepts of graph theory and on the so-called similarity matrix, which encapsulates the pairwise measures of similarity between the points in the dataset. The clustering problem can be then turned into an eigenvalue problem [129]. Advantages of spectral clustering include its applicablity to large datasets and to clusters with arbitrary shapes, but the results can be very sensitive to the choice of the similarity measure. Normalized cut stands as a reference example of spectral algorithms that was initially applied to image processing [130].

A last family of clustering techniques that we can mention is the class of search-based algorithms, which are designed to solve complex optimization problems where traditional methods are subject to the recurent problem of convergence towards local minima. Among

others, evolutionary techniques and in particular Genetic Algorithms (GA) address the considered optimization problem by applying the fundamental principles of natural selection [131]. Starting from a population of potential solutions to the problem, several operations inspired from genetics are applied to the population to produce new solutions, called offsprings. The new populations are then evaluated according to the problem requirements and only those which best fulfill them are selected, then used as a new basis for the next generation of solutions. In particular, a mutation operator introduces randomness in the passage to the next generation, allowing new solutions to emerge and preventing the algorithm from being trapped in local minima.

Clustering methods may usually encounter two major limitations. First, the classification produced by a given algorithm can be very sensitive to its initialization configuration, thus requiring several runs to extract the best possible result. Classification approaches relying on the minimization of non convex functions like k-means are typically concerned with this difficulty. Another persistent drawback of classification procedures is that they often experience difficulty in the detection and handling of entangled clusters. We attempt to address the latter by introduction of our elliptical clustering technique.

V.3 The elliptical clustering algorithm

We now introduce the elliptical clustering algorithm, a density-based classification technique which performs a covering of the dataset by elliptical-shaped structures. In its original version this classification technique does not require any assumption on the number of real classes, but it also admits a constrained version which aims at improving the final clustering by a post-processing of the raw result. In the first two sections we describe the underlying concepts motivating the elliptical clustering as well as the classification process, while in Section V.3.3 we adress how the knowledge of the number of real clusters K can be enforced in the resulting clustering. Section V.3.4 provides a complete overview of the algorithm by means of a pseudo-code.

V.3.1 The weighted density function

The elliptical clustering method is based on a representation of clusters as dense regions of the observation space. Similarly to the DBSCAN algorithm, it alternates two steps: firstly detecting a new cluster, then expanding it, until all or enough data points have been processed. However, while DBSCAN relies on local density criteria, we here adopt a more global point of view and represent the overall density of the dataset by means of weighted hyperbolic tangent kernel functions. The resulting density estimation function, denoted by $\rho_{\mathbf{w}}(\mathbf{x})$ is defined as

$$\rho_{\mathbf{w}}(\mathbf{x}) = \frac{1}{\sum_{n=1}^{N} w_n} \sum_{n=1}^{N} w_n \left(1 - \tanh\left(\| \mathbf{x_n} - \mathbf{x} \|^2\right)\right) \tag{V.1}$$

where $\mathbf{x}$ is a D-dimensional vector and $\mathbf{w}$ a N-dimensional weight vector whose each entry w_n is associated with observation $\mathbf{x_n}$. The function $\rho_{\mathbf{w}}(\mathbf{x})$ takes maximal values for all $\mathbf{x}$ lying

in regions with a high concentration of observations, and cancels when $\mathbf{x}$ is far enough from the data. In the context of probability distribution mixtures, these maxima correspond to the modes of each mixture's component, which for unimodal symmetric probability densities such as gaussian distributions coincide with the mean value, provided that the components are separated enough so that their respective modes are still modes of the overall mixture. Hence, by finding all the maxima of the density function, one can in principle recover the centroids of all the clusters in the dataset. Since in general extracting the maxima of a density function such as $\rho_{\mathbf{w}}$ in one row is analytically impossible, we rather try to find them successively, so that a new cluster is extracted at each iteration of the algorithm. Computing the gradient of (V.1) with respect to $\mathbf{x}$, we find that the locations of the maxima obey an auto-coherent equation that we solve iteratively. Given an estimation $\mathbf{x^{(c)}}$ of the location of one of the maxima of $\rho_{\mathbf{w}}$ computed at the current iteration c of the maximization process, the updated estimation at the next iteration $c+1$ is given by

$$\mathbf{x}^{(c+1)} = \frac{\sum_{n=1}^{N} w_n C_n(\mathbf{x}^{(c)})\mathbf{x_n}}{\sum_{n=1}^{N} w_n C_n(\mathbf{x}^{(c)})} \tag{V.2}$$

where $C_n(\mathbf{x}) = 1 - \left(\tanh\left(\|\mathbf{x_n} - \mathbf{x}\|^2\right)\right)^2$. Since the variations of the density function only occur close to the data points, a random observation point is chosen as the initial estimation $\mathbf{x}^{(0)}$. The maximization step stops when the variations of $\mathbf{x}^{(c)}$ with respect to the iteration counter c are small enough, and the resulting vector, denoted by $\mathbf{x}^*$, defines the centroid of the new cluster to be expanded. As the starting point to find a cluster is to randomly pick a data point to initialize the maximization step, it is necessary to find the members of a given cluster as soon as its centroid has been extracted in such a way that all observations found to be part of this cluster can be removed from the possible initialization set for the next centroid detection step.

V.3.2 Elliptical-shaped classification

In an attempt to circumvent the tendency of density-based algorithms to merge entangled clusters, we constrain the classes generated during the expansion step to have ellipsoidal shapes. The motivation behind this choice is to encapsulate enough data points in a simple geometrical shape so that the cluster is well-represented, without assimilating points that would possibly belong to another class, hence giving the algorithm the ability to better distinguish entangled clusters. We thus need to specify both the orientation or principal axes $\{\mathbf{u_d}\}_{d\in\{1,\cdots,D\}}$ and the corresponding semi-axes $\{a_d\}_{d\in\{1,\cdots,D\}}$ to fully parametrize the cluster. In a D-dimensional space, $D-1$ orthonormal direction vectors are chosen, the last one being imposed by orthogonality. A possible choice for the first direction is the vector defined by the initial and final estimations of the centroid of the current cluster, *i.e.* $\mathbf{u}_1 = \frac{(\mathbf{x^{(0)}} - \mathbf{x^*})}{\|\mathbf{x^{(0)}} - \mathbf{x^*}\|^2}$, so that if $D = 2$ the orientation of the ellipse is systematic, while additional arbitrary choices may have to be made in higher dimension. Then, starting from the centroid $\mathbf{x}^*$ and for each previously defined direction $\mathbf{u_d}$, the corresponding semi-axis a_d is obtained by sequentially searching for the closest point in that direction for which either a minimum of the density function is found, revealing the presence of an entangled cluster, or a given threshold value is

reached. This critical value, denoted by ρ_{th}, serves as a maximal extension that an isolated class can achieve, and is adaptative of the inner density of the cluster under consideration, which is related to the amplitude of its maximum, $\rho_{\mathbf{w}}(\mathbf{x}^*)$. We express this threshold value as $\rho_{th} = \rho_{\mathbf{w}}(\mathbf{x}^*)(1 - T_h)$, where T_h is an external parameter strictly lying between 0 and 1. T_h acts as a balance between the typical size of the ellipsoids found by the algorithm and its ability to split partially merged clusters. In our applications the value 0.7 has shown to be a good compromise, but specific applications where for instance a priori knowledge on the relative positions of the clusters is available would lead to other choices.

$$a_d = \min\left(t^*, \{|t| \leq t^* | \tilde{\rho}'_{\mathbf{w}}(t) = 0, \tilde{\rho}''_{\mathbf{w}}(t) \geq 0\}\right) \tag{V.3}$$

where $t^* = \inf\{|t| \in \mathbb{R}^+ | \tilde{\rho}_{\mathbf{w}}(t) \geq \rho_{th}\}$ and $\tilde{\rho}_{\mathbf{w}}(t) = \rho_{\mathbf{w}}(\mathbf{x}^* + t\,\mathbf{u_d})$. We finally define the cluster $\mathcal{C}$ as the set of data points lying inside the generated ellipsoid

$$\mathcal{C} = \{\mathbf{x_n} \in \mathcal{D} | (\mathbf{x_n} - \mathbf{x}^*)^T \mathbf{P}^T \mathbf{A}^{-2} \mathbf{P} (\mathbf{x_n} - \mathbf{x}^*) \leq 1\} \tag{V.4}$$

where $\mathbf{P} = (\mathbf{u_1}, \cdots, \mathbf{u_D})$ is the orthogonal change of basis matrix induced by the orientation chosen for the ellipsoid, and $\mathbf{A}$ is the diagonal matrix whose entries are the semi-axes, $A_{ij} = a_i \delta_{ij}$ with δ_{ij} the Kronecker delta. The list of possible initialization points for the next centroid detection step is then updated by removal of the identified class members.

The weight vector $\mathbf{w}$ introduced in (V.1) allows to tune the relative contribution of each data point to the overall density. It is used to provide a higher weight to the clusters that have not yet been identified, which leads to a better detection of entangled classes. We then choose $w_n = \frac{1}{|\mathcal{C}_k|}$ if $\mathbf{x_n}$ belongs to the class $\mathcal{C}_k$, and $w_n = 1$ if $\mathbf{x_n}$ does not belong to any class yet. By convention, if a given point is found to belong to several classes, its weight is defined as the inverse cardinal of the last cluster it has been assigned to. The weight vector is updated as soon as the membership of the current cluster is established using (V.4), so that data points that have not been classified yet contribute more and more to the density profile. Adding this weight vector may however generate spurious clusters due to the remaining points neglected by the elliptical clustering in the class expansion process. Besides, as more clusters are discovered the set of unclassified points tends to get sparser, leading also to the apparition of few-membered, irrelevant classes of outlier observations. These two cumulative effects result in an overestimation of the number of clusters in the dataset. This is illustrated in Fig. V.3 where a clustering of a two-dimensional gaussian mixture with two components has been performed. The black and red ellipses on the top plot correspond to irrelevant and meaningful clusters, respectively. The bottom plot shows how the extraction of the right component and update of the weight vector allows both an easier detection of the second class and the emergence of excess clusters. A first solution to prevent the algorithm from generating residual clusters is to impose beforehand the percentage of points we want to be clustered, and use it as a stopping criterion for the whole classification procedure. This is another external parameter of the algorithm, that we denote η. In the following section we also propose an additional pruning phase aiming at removing those irrelevant clusters.

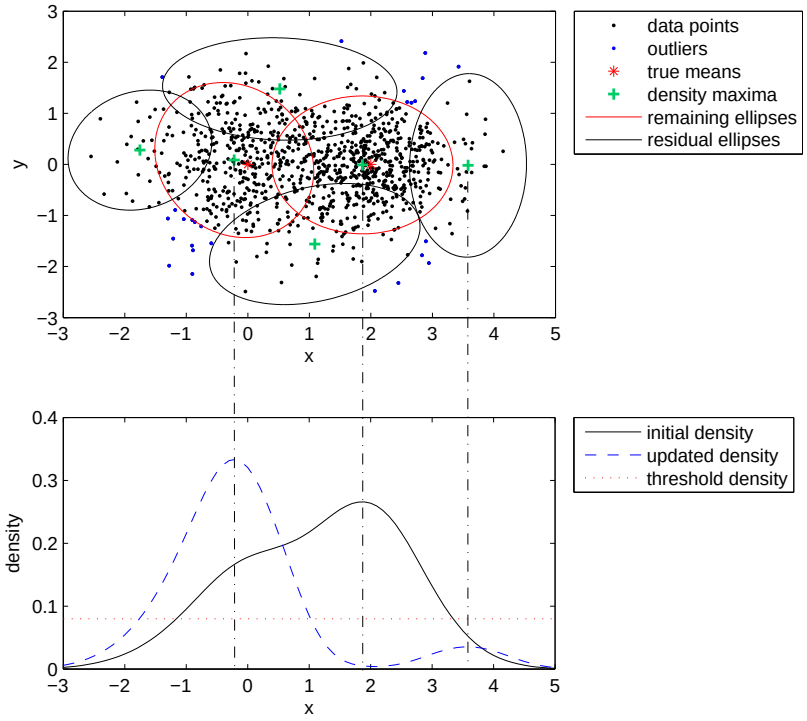

Figure V.3 – *Top: Elliptical classification of two entangled bi-dimensional gaussian distributions with weights* $(0.5, 0.5)$*, means* $(0, 0)$*,* $(2, 0)$ *and spherical covariance matrices* 0.7 *and* 0.5*, respectively. Bottom: Density profile* $\rho_{\mathbf{w}}$ *in the* x *direction at the initial state (black curve) and after the extraction of the first cluster (blue curve) using the density threshold* ρ_{T_h} *(red line).*

V.3.3 Post-processing of the elliptical clustering

The raw classification returned by the elliptical algorithm can be thought of as a covering of the dataset by K' ellipsoidal structures. A first immediate preliminary step to reduce the number of classes is to remove those clusters that only have a single member, and which actually correspond to outlier observations. Then, we enforce the number of real classes K as a constraint to further reduce the number of clusters. Among all pairs of clusters having a non-empty intersection, we select the one which achieves the maximum intersection relatively to the size of the smaller cluster.

$$(k_1, k_2) = \underset{\substack{k \in \{1, \cdots K'\} \\ k' > k}}{\operatorname{argmax}} \left(\frac{|\mathcal{C}_k \cap \mathcal{C}_{k'}|}{\min\left(|\mathcal{C}_k|, |\mathcal{C}_{k'}|\right)} \right) \tag{V.5}$$

The most irrelevant cluster $\mathcal{C}_{k^*}$ is then defined as the smaller one in the resulting pair

$$k* = \operatorname{argmin}\left(|\mathcal{C}_{k_1}|, |\mathcal{C}_{k_2}|\right) \tag{V.6}$$

Finally, we remove $\mathcal{C}_{k^*}$ by redistributing its members among all clusters that share a non empty intersection with it. Let $\mathcal{V}_{k^*} = \{k \in \{1, \cdots, K'\} \backslash \{k^*\} | \mathcal{C}_{k^*} \cap \mathcal{C}_k \neq \emptyset\}$ be the corre-

sponding class labels, and $d_M(\mathbf{x_n}, \mathcal{C}_k)$ the Mahalanobis distance between observation $\mathbf{x_n}$ and class $\mathcal{C}_k$, defined as

$$d_M(\mathbf{x_n}, \mathcal{C}_k) = (\mathbf{x_n} - \mathbf{x_k}^*)^T \, \mathbf{\Sigma}_k^{-1} \, (\mathbf{x_n} - \mathbf{x_k}^*) \tag{V.7}$$

with $\mathbf{x_k}^*$ and $\mathbf{\Sigma}_k$ the centroid and covariance matrix of $\mathcal{C}_k$ respectively. We assign to each class $\mathcal{C}_k$ of $\mathcal{V}_{k^*}$ all data points of $\mathcal{C}_{k^*}$ for which the minimum of the Mahalanobis distance with respect to all other classes of $\mathcal{V}_{k^*}$ is achieved. We can thus write the update of cluster $\mathcal{C}_k$ as

$$\mathcal{C}_k \leftarrow \mathcal{C}_k \cup \{\mathbf{x_n} \in \mathcal{C}_{k^*} | \underset{k' \in \mathcal{V}_{k^*}}{\operatorname{argmin}} \, d_M(\mathbf{x_n}, \mathcal{C}_{k'}) = k\} \tag{V.8}$$

These two steps of detection of residual clusters and reassignment of the corresponding data points is repeated until either $K' = K$, or there are no more non-empty intersection between any pair of clusters. Finally, a last optional phase consists in classifying the outlier observations to the remaining clusters replacing $\mathcal{C}_{k^*}$ and $\mathcal{V}_{k^*}$ by $\cap_{k=1}^{K'} \mathcal{C}_k^{\mathsf{c}}$ and $\{1, \cdots, K'\}$ in (V.8), respectively. An important point to mention is the fact that even after the above pruning phase, the algorithm may still overestimate the number of clusters. Moreover, if the raw classification of the algorithm is such that $K' < K$, no further processing is performed. The knowledge of K is then rather used as a guide to improve the bare elliptical classification than as an absolute requirement. As a matter of fact, in situations where the true number of classes is out of reach, the algorithm may still yield satisfying results using an estimation of K instead.

V.3.4 Pseudo-code and additional comments

The elliptical algorithm takes the three input parameters $\mathcal{D}$, T_h and η in its unconstrained version, as well as the number of real classes K in its constrained form. A summary of how the algorithm proceeds is given in Algorithm 2 as a pseudo-code. The post-processing phase can be considered to begin with the suppression of single-element clusters, but this step can also be included in the unconstrained version of the algorithm since it does not require the parameter K. The outliers classification step is optional as well. Because the observations used as the initial points for the maximization of $\rho_{\mathbf{w}}$ are chosen randomly, the resulting classification is non deterministic, and thus one may have to perform several runs in order to achieve the best possible clustering accessible by the algorithm.

Algorithm 2 Pseudo-code of the elliptical clustering algorithm

function elliptical_clustering($\mathcal{D}$, η, T_h, K)
  // Phase 1: elliptical clustering of the data
$K' \leftarrow 0$, $\mathbf{w} \leftarrow (1, \cdots, 1)$
while $|\cup_{k=1}^{K'} \mathcal{C}_k| < N \times \eta$ **do**
  choose $\mathbf{x}^{(0)}$ as a random $\mathbf{x_n}$ in $\cap_{k=1}^{K'} \mathcal{C}_k^{\complement}$
  find $\mathbf{x}_{K+1}^*$ by iteratively maximizing $\rho_{\mathbf{w}}(\mathbf{x})$ using (V.2)
  for $d = 1 \cdots D$ **do**
    choose $\mathbf{u}_d$ orthogonal to $\{\mathbf{u}_1, \cdots \mathbf{u}_{d-1}\}$
    compute a_d using (V.3)
  end for
  define $\mathcal{C}_{K'+1}$ using (V.4)
  update $\mathbf{w}$
  $K' \leftarrow K' + 1$
end while
  // Phase 2: pruning of irrelevant clusters
add all single-element clusters to the set of outliers
while $K < K'$ **and** $\cup_{k=1}^{K'} \mathcal{V}_k \neq \emptyset$ **do**
  select the cluster to remove using (V.5) and (V.6)
  reassign members of the removed cluster using (V.8)
  $K' \leftarrow K' - 1$
end while
  // Phase 3: classification of outliers
reassign outlier points using (V.8)

end

V.4 Performance evaluation

V.4.1 Clustering validity metrics

The performance of the proposed algorithm is evaluated comparatively to an ideal, gold standard classification of the dataset using two different metrics based on the so-called confusion matrix. Given the target classification $\mathcal{C} = \{\mathcal{C}_k\}_{k\in\{1,\cdots K\}}$ and the clustering under evaluation $\mathcal{C}' = \{\mathcal{C}'_{k'}\}_{k'\in\{1,\cdots K'\}}$ the $K \times K'$ entries of the confusion matrix are defined as $m_{kk'} = |\mathcal{C}_k \cap \mathcal{C}'_{k'}|$. Starting from this general tool a wide variety of clustering evaluation criteria can be derived. For our performance tests we selected two indices, namely the normalized Myrkin index and the Variation of Information.

The Myrkin index [132] is a pair-counting based metric which evaluates the number of misclassified data points. It is defined as

$$M_{\mathcal{C},\mathcal{C}'} = \sum_{k=1}^{K} |\mathcal{C}_k|^2 + \sum_{k'=1}^{K'} |\mathcal{C}'_{k'}|^2 - 2\sum_{k=1}^{K}\sum_{k'=1}^{K'} |\mathcal{C}_k \cap \mathcal{C}'_{k'}|^2 \tag{V.9}$$

The resulting expression is always positive and null if the two classifications are equal. An additional normalization of the Myrkin index can be achieved in order to grant it the N-invariance property, meaning that the index is dependant on the relative proportions of the classes and not directly on the number of data points N. This normalized version is obtained by dividing the bare Myrkin index by N^2.

The Variation of Information [133] is an information-based measure which evaluates the gain and loss of uncertainty about a given classification under the assumption that the other is known. Formally speaking, it is defined as

$$VI_{\mathcal{C},\mathcal{C}'} = H(\mathcal{C}|\mathcal{C}') + H(\mathcal{C}|\mathcal{C}') \tag{V.10}$$

where $H(\mathcal{C}|\mathcal{C}') = -\sum_{k=1}^{K}\sum_{k'=1}^{K'} \frac{m_{kk'}}{N} \log_2\left(\frac{m_{kk'}}{m_{k\cdot}}\right)$ is the conditional entropy of classification $\mathcal{C}$ knowing classification $\mathcal{C}'$ and $m_{k\cdot} = \sum_{k'=1}^{K'} m_{kk'}$. The Variation of Information is zero if and only if both classifications are equal (up to a permutation in the class labels) and is naturally N-invariant.

V.4.2 Simulation assumptions and results

To evaluate the quality of the classifications produced by the elliptical algorithm we have generated 200 random sets of 1000 two-dimensional sample points using gaussian mixture distributions for each value of the mixture component number K from 1 to 10. The weights, means and covariance matrices of each gaussian component are randomly chosen according to a uniform distribution for each independant parameter. The means range from -10 to 10 in each direction, and the maximum value for the covariance matrices entries is set to 1. For each dataset the Normalized Myrkin index and the Variation of Information are computed, then averaged over all datasets having the same number of classes.

Fig. V.4 shows the performance curves for k-means, k-product, EM and the constrained elliptical clustering. For these initialization-dependant algorithms the best result over 100 runs have been extracted before the averaging. Both plots tend to show that our algorithm provides better classification results than k-means and k-product. We also note how similar the performance curves of the elliptical and EM algorithms are, though E-M seems slighty better. This could be an illustration of the fact that for gaussian mixtures the probability distribution components actually are of ellipsoidal shape, so in some sense the two approaches rely on the same underlying principle.

Fig. V.5 depicts the normalized Myrkin index obtained for the unconstrained elliptical algorithm and DBSCAN for two sets of its parameters *Eps* and *MinPts*. While DBSCAN tends to yield better clusterings for a small range of K values, it then considerably drifts in accuracy. This is because as the number of clusters increases while the observation space range is fixed, more and more entangled classes appear and DBSCAN considers them as single entities. The bare elliptical clustering on the opposite overestimates the number of classes but doing so carries more relevant information about the actual clustering of the data. This

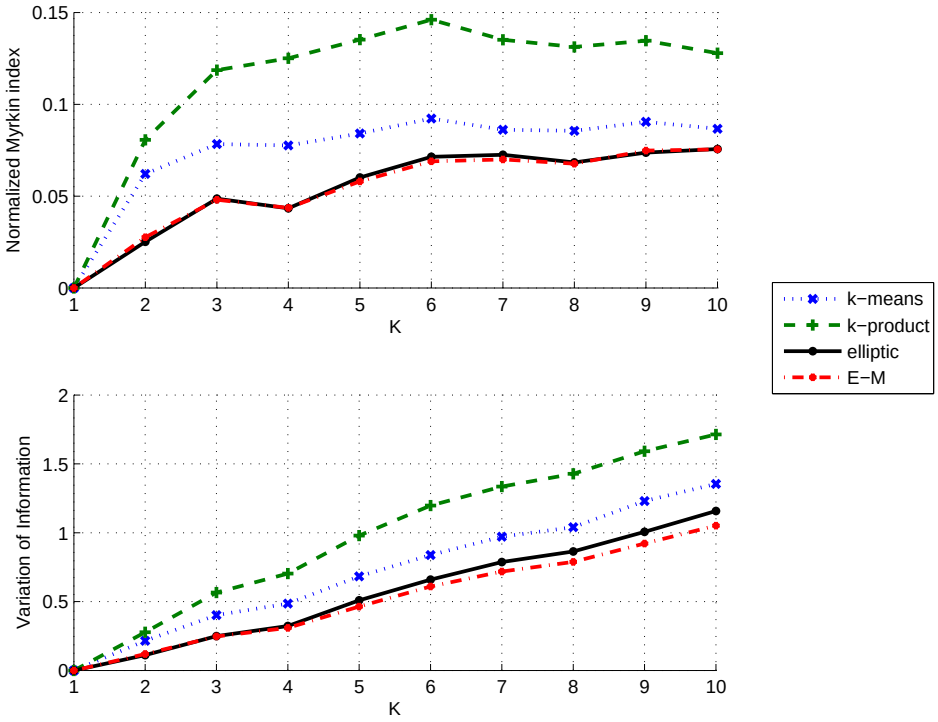

Figure V.4 – *Performance of the constrained elliptical clustering with parameters* $\eta = 0.95$, $T_h = 0.7$ *using the normalized Myrkin index (top) and the Variation of Information (bottom)*

also explains why in the trivial case $K = 1$ and without any post-processing the Myrkin index of the elliptical method is non zero.

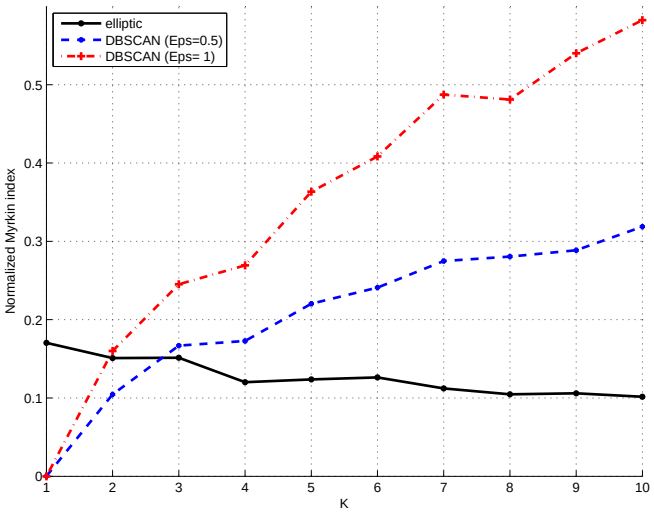

Figure V.5 – *Performance of the unconstrained elliptical clustering with parameters* $\eta = 0.95$, $T_h = 0.7$ *and DBSCAN with* $MinPts = 5$ *using the normalized Myrkin index*

V.5 Conclusion

We have considered the problem of clustering data in the presence of partially merged or entangled clusters, and introduced a density-based clustering approach relying on ellipsoidal-shaped clusters to improve the detection of entangled classes. Simulations have shown that the algorithm yields comparable performance with several standard algorithms in both its constrained and unconstrained versions. This work only gives a first insight on the possibilities of our method and foresees future improvements as well as further comparisons with more advanced existing clustering techniques.

General conclusion

Conclusions

In this thesis we investigated the blind channel estimation and symbol detection problem of wireless multiuser simultaneous transmissions in the presence of high interference and with a single sensor available at reception. Minimum information on the transmitted waveforms was assumed on the receiver side and essentially consisted in the knowledge of the number of sources and their respective modulation schemes. Based on the finite-alphabet nature of the constellations and the Maximum Likelihood approach, we applied and generalized an existing algorithm of the literature called Iterative Least Squares with Enumeration [5], closely related to the k-means clustering algorithm [35]. Our main efforts have focused on the proposition of initialization strategies to prevent the considered algorithm from converging to spurious local minima, a well-known problem in iterative ML minimization techniques. Starting from an oversimplified communication scenario, several analyses on the position of fixed points and their relations to the constellations geometry were provided while progressively complexifying the underlying transmission model.

First the point-to-point transmission scenario with a flat-fading channel was considered. Based on the structure and symmetries of the constellation, several theoretical results on the position of the ILSE fixed points were derived in the noise-free case. In particular, it was shown that for PSK modulations there was essentially a single fixed point, and that the hierarchical structure of regular QAMs induced local minima that could be easily identified and related to the global minimum. A complete characterization of the fixed points for the QAM 16 modulation was provided and validated by simulation, and from the study of higher order QAMs two strategies were proposed to limit the number of random tries needed to reach the global minimum. Two initialization procedures relying on the received data were also discussed: the first one is based on the k-products algorithm and aims at estimating the channel-transformed symbols. The prohibitive bias exhibited by the original method for QAMs was resolved using the hierarchical structure of these constellations. The second consists in a channel estimator derived from the method of moments. Simulations demonstrated the relevance of all proposed initialization methods compared to a fully-random strategy, with the data-based strategies achieving error rates identical to the perfect channel knowledge case.

Next, multiple users communication scenarios were introduced. The resulting model was expressed as a particular instance of the underdetermined Blind Source Separation problem for a single linear mixture. Capitalizing on the assumed mutual independence and known distribution of the sources, a cumulant-based moment problem for estimating the channels was derived, and exactly solved in several mixture settings. The non-uniqueness of the channel estimators for constellations with identical rotational orders was discussed, and possible strategies to resolve it were presented. The resulting channel estimators were used as initial states for the ILSE algorithm. Simulations with maximal interference

levels and comparison with other multiuser detection methods showed that the proposed initialization strategy achieved very good results for a small number of sources and constellation sizes. For higher order constellations and more sources the asymptotic error floor exhibited by the method becomes prohibitive to ensure a reliable symbol detection. A more in-depth analysis of the two-users case revealed that the error floor stems from channel realizations for which the mixed constellation is close to non-identifiability. In these cases the presence of local minima near the global one makes the algorithm very sensitive to its initialization. From these results several strategies for identifying spurious solutions and correcting them were proposed and tested on the two QAM 4 mixture, with promising results. More general considerations on issues pertaining to practical implementations and fundamental assumptions of the method were discussed at the end of the chapter.

Finally we extended our communication model to frequency-selective propagation environments by considering multiuser, Orthogonal Frequency Division Multiplexing transmissions. A new generalization of ILSE to this framework was carried out, based on a direct estimation of the channel in the time domain. The initialization of the algorithm was then addressed, and several strategies were proposed based on existing algorithms and the channel moment method estimators previously derived. For the phase ambiguities, a joint use of a root-clustering algorithm, the autodeconvolution algorithm [113] and its SVD-based refinement was suggested. As for the permutation ambiguities, a partial search algorithm reminiscent of a troncated Viterbi algorithm was presented. Conducted simulations showed that the novel ILSE-OFDM approach is capable of achieving the same error rates than the perfect channel knowledge case even in maximal interference and completely uncorrelated channels, but only when the permutation and phase ambiguities are perfectly resolved. Otherwise the algorithm demonstrated mitigated performances, in addition to being quite restrictive in its operating assumptions.

The last part of the presented work adopted a somehow more general viewpoint and introduced a quite fundamental problem in cluster analysis, namely identification and treatment of entangled data clusters. A first insight to address this issue was provided in the framework of mixture distributions, and an algorithm based on probability density estimation by kernel functions was proposed. For the main part the algorithm aims at successively identifying each mode of the mixture and weight the corresponding cluster so as to intensify the contributions of the remaining components to the overall density profile. By doing so the method tends to produce more clusters than expected, hence a postprocessing of the obtained data partition was discussed, based on an iterative merging of clusters identified as spurious. The proposed algorithm was compared by simulations on random gaussian mixtures to well-known clustering techniques from the literature and showed encouraging results in regard to the selected cluster evaluation metrics.

Perspectives

Each axis developed in the thesis opens several perspectives for further refinements and future work. Some possible directions are listed below:

- the study of fixed points proposed in Chapter II was conducted in the noise-free case and in the asymptotic limit of infinite sample sizes. Several heuristic observations regarding introduction of noise and finite sample size effects were made but lack a rigorous framework to be precisely described. In particular, a characterization of the fixed points uncovered by the asymptotic regime and their relative probabilities of occurrence would provide a precious insight for a better understanding of the possible outcomes of ILSE in noisy scenarios, as well as additional freedom in the design of both robust and optimal initialization strategies;

- in the multiuser case, the number of considered sources was chosen quite small so that the proposed moment problem channel predictors have analytical expressions. More generally numerical algorithms should be implemented so as to address an arbitrary number of sources. Additionally, one of our most promising result concerns the theoretical identification of high-risk channel ratios for which ILSE is likely to fail converging to its global minimum, based on the identifiability condition of finite-alphabets mixtures [47]. Extension of this analysis to more than two sources would be insightful to determine whether the proposed initialization strategies are still likely to be relevant. Finally, a strong inherent assumption of our multiuser transmission model is the perfect mutual synchronicity between the sources. This hypothesis is quite stringent and its relaxation should be considered for practical implementation;

- as the ILSE-OFDM algorithm presented in Chapter IV is highly sensitive to its initialization, alternative algorithms for solving phase and permutation ambiguities should be considered. Also, a recursive, time domain version of the method could be proposed so as to accomodate for time-varying channel coefficients. The recursive version of ILSE proposed in [5] stands as a reasonable basis to start with. It would also be enlightening to perform the same time domain extension for SML approaches such as the EM algorithm, which because they are based on a stochastic representation of the data have often more desirable properties than decision-directed approaches [107];

- the algorithm presented in Chapter V belongs to the class of density-based clustering. In that respect clusters were represented by the modes of the underlying data mixture distribution. This clustering approach may not be the most relevant to address partially merged clusters. Among other possibilities, the choice of hierarchical clustering would appear as a natural candidate for further considerations, as its very foundation precisely lies in the iterative merging or splitting of clusters. Constrained clustering, a relatively recent branch of semi-supervised clustering in which some data pairs are constrained to belong to the same cluster (must-link) or to distinct clusters (cannot-link), constitutes an interesting perspective for further development of this work as well [134].

Bibliography

[1] Z. Ding, X. Lei, G. K. Karagiannidis, R. Schober, J. Yuan, and V. K. Bhargava, "A Survey on Non-Orthogonal Multiple Access for 5G Networks: Research Challenges and Future Trends," *IEEE Journal on Selected Areas in Communications*, vol. 35, no. 10, pp. 2181–2195, Oct. 2017. [Online]. Available: http://ieeexplore.ieee.org/document/7973146/

[2] "Multiple Access Techniques: FDMA, TDMA, AND CDMA," in *RF Measurements for Cellular Phones and Wireless Data Systems*. Hoboken, NJ, USA: John Wiley & Sons, Inc., Jan. 2008, pp. 413–429. [Online]. Available: http://doi.wiley.com/10.1002/9780470378014.ch30

[3] L. Dai, B. Wang, Y. Yuan, S. Han, C.-l. I, and Z. Wang, "Non-orthogonal multiple access for 5G: solutions, challenges, opportunities, and future research trends," *IEEE Communications Magazine*, vol. 53, no. 9, pp. 74–81, Sep. 2015. [Online]. Available: http://ieeexplore.ieee.org/document/7263349/

[4] J.-F. Cardoso, "Blind signal separation: statistical principles," *Proceedings of the IEEE*, vol. 86, no. 10, pp. 2009–2025, Oct. 1998. [Online]. Available: http://ieeexplore.ieee.org/document/720250/

[5] S. Talwar, M. Viberg, and A. Paulraj, "Blind separation of synchronous co-channel digital signals using an antenna array. I. Algorithms," *IEEE Transactions on Signal Processing*, vol. 44, no. 5, pp. 1184–1197, May 1996. [Online]. Available: http://ieeexplore.ieee.org/document/502331/

[6] S. P. Boyd and L. Vandenberghe, *Convex optimization*. Cambridge, UK; New York: Cambridge University Press, 2004, oCLC: 863221741. [Online]. Available: https://doi.org/10.1017/CBO9780511804441

[7] J. Eriksson, E. Ollila, and V. Koivunen, "Essential Statistics and Tools for Complex Random Variables," *IEEE Transactions on Signal Processing*, vol. 58, no. 10, pp. 5400–5408, Oct. 2010.

[8] R. Remmert, *Theory of complex functions*, ser. Graduate texts in mathematics ; Readings in mathematics. New York: Springer-Verlag, 1991, no. 122.

[9] F. Neeser and J. Massey, "Proper complex random processes with applications to information theory," *IEEE Transactions on Information Theory*, vol. 39, no. 4, pp. 1293–1302, Jul. 1993. [Online]. Available: http://ieeexplore.ieee.org/document/243446/

[10] B. Picinbono, "On circularity," *IEEE Transactions on Signal Processing*, vol. 42, no. 12, pp. 3473–3482, Dec. 1994.

[11] N. R. Goodman, "Statistical Analysis Based on a Certain Multivariate Complex Gaussian Distribution (An Introduction)," *The Annals of Mathematical Statistics*, vol. 34, no. 1, pp. 152–177, Mar. 1963. [Online]. Available: http://projecteuclid.org/euclid.aoms/1177704250

[12] D. C. Montgomery and G. C. Runger, *Applied statistics and probability for engineers*, sixth edition ed. Hoboken, NJ: John Wiley and Sons, Inc, 2014.

[13] M. Abramowitz and I. A. Stegun, Eds., *Handbook of mathematical functions: with formulas, graphs, and mathematical tables*, 9th ed., ser. Dover books on mathematics. New York, NY: Dover Publ, 2013, oCLC: 935935300.

[14] P. Comon and C. Jutten, Eds., *Handbook of blind source separation: independent component analysis and applications*, 1st ed. Amsterdam ; Boston: Elsevier, 2010, oCLC: ocn430842957.

[15] M. G. Kendall, A. Stuart, and J. K. Ord, *The advanced theory of statistics in 3 volumes. 1 1.* London: Griffin, 1994, oCLC: 1071028235.

[16] G. Grimmett and D. Stirzaker, *Probability and random processes*, 3rd ed. Oxford ; New York: Oxford University Press, 2001.

[17] A. W. v. d. Vaart, *Asymptotic statistics*, 1st ed., ser. Cambridge series in statistical and probabilistic mathematics. Cambridge: Cambridge Univ. Press, 2007, oCLC: 838749444.

[18] S. M. Kay, *Fundamentals of statistical signal processing*, ser. Prentice Hall signal processing series. Englewood Cliffs, N.J: Prentice-Hall PTR, 1993.

[19] W. M. Bolstad and J. M. Curran, *Introduction to Bayesian Statistics, Third Edition*. Hoboken, NJ, USA: John Wiley & Sons, Inc., Aug. 2016. [Online]. Available: http://doi.wiley.com/10.1002/9781118593165

[20] J. D. Gibbons and S. Chakraborti, *Nonparametric statistical inference*, 5th ed., ser. Statistics, textbooks & monographs. Boca Raton: Taylor & Francis, 2011.

[21] K. M. Ramachandran and C. P. Tsokos, *Mathematical statistics with applications*. Amsterdam ; Boston: Academic Press, 2009, oCLC: ocn261174186.

[22] T. Hastie, R. Tibshirani, and J. H. Friedman, *The elements of statistical learning: data mining, inference, and prediction*, 2nd ed., ser. Springer series in statistics. New York, NY: Springer, 2009.

[23] E. S. Keeping, *Introduction to statistical inference*, dover ed ed., ser. Dover books on mathematics. New York: Dover Publications, 1995.

[24] T. Strutz, *Data fitting and uncertainty: a practical introduction to weighted least squares and beyond*. New York, NY: Springer Berlin Heidelberg, 2015.

[25] A. R. Hall, *Generalized method of moments*, ser. Advanced texts in econometrics. Oxford ; New York: Oxford University Press, 2005, oCLC: ocm57502898.

[26] A. P. Dempster, N. M. Laird, and D. B. Rubin, "Maximum Likelihood from Incomplete Data Via the EM Algorithm," *Journal of the Royal Statistical Society: Series B (Methodological)*, vol. 39, no. 1, pp. 1–22, Sep. 1977. [Online]. Available: http://doi.wiley.com/10.1111/j.2517-6161.1977.tb01600.x

[27] S. Benedetto and E. Biglieri, *Principles of Digital Transmission: With Wireless Applications*, 2002, oCLC: 1050921977. [Online]. Available: https://doi.org/10.1007/b117711

[28] J. G. Proakis and M. Salehi, *Digital communications*, 5th ed. Boston: McGraw-Hill, 2008.

[29] D. Le Ruyet and M. Pischella, *Bases de communications numériques*, 2015, oCLC: 1119888783.

[30] A. Goldsmith, *Wireless communications*. Cambridge ; New York: Cambridge University Press, 2005.

[31] D. Tse and P. Viswanath, *Fundamentals of Wireless Communication*. Cambridge: Cambridge University Press, 2005, oCLC: 938994463. [Online]. Available: https://doi.org/10.1017/CBO9780511807213

[32] S. Verdú, *Multiuser detection*. CambridgeK ; New York: Cambridge University Press, 1998.

[33] A. Okabe, *Spatial tessellations: concepts and applications of Voronoi diagrams*, 2nd ed., ser. Wiley series in probability and statistics. Chichester ; New York: Wiley, 2000.

[34] H. Liu, G. Xu, L. Tong, and T. Kailath, "Recent developments in blind channel equalization: From cyclostationarity to subspaces," *Signal Processing*, vol. 50, no. 1-2, pp. 83–99, Apr. 1996. [Online]. Available: https://linkinghub.elsevier.com/retrieve/pii/0165168496000138

[35] S. Lloyd, "Least squares quantization in PCM," *IEEE Transactions on Information Theory*, vol. 28, no. 2, pp. 129–137, Mar. 1982. [Online]. Available: http://ieeexplore.ieee.org/document/1056489/

[36] A. Manesh, C. R. Murthy, and R. Annavajjala, "Physical Layer Data Fusion Via Distributed Co-Phasing With General Signal Constellations," *IEEE Transactions on Signal Processing*, vol. 63, no. 17, pp. 4660–4672, Sep. 2015.

[37] N. Paul, M. Terre, and L. Fety, "A global algorithm to estimate the expectations of the components of an observed univariate mixture," *Advances in Data Analysis and Classification*, vol. 1, no. 3, pp. 201–219, Nov. 2007. [Online]. Available: http://link.springer.com/10.1007/s11634-007-0014-z

[38] D. Arthur and S. Vassilvitskii, "k-means++: The Advantages of Careful Seeding," *SODA '07 Proceedings of the eighteenth annual ACM-SIAM symposium on Discrete algorithms*, p. 11, 2007.

[39] I. Fijalkow, C. Manlove, and C. Johnson, "Adaptive fractionally spaced blind CMA equalization: excess MSE," *IEEE Transactions on Signal Processing*, vol. 46, no. 1, pp. 227–231, Jan. 1998.

[40] K. Ireland and M. Rosen, *A classical introduction to modern number theory*, 2nd ed., ser. Graduate texts in mathematics. New York: Springer, 1998, no. 84, oCLC: 247306386.

[41] B. Ottersten, R. Roy, and T. Kailath, "Signal waveform estimation in sensor array processing," in *Twenty-Third Asilomar Conference on Signals, Systems and Computers, 1989.* Pacific Grove, California, USA: IEEE, 1989, pp. 787–791. [Online]. Available: http://ieeexplore.ieee.org/document/1201006/

[42] A. Hyvärinen, J. Karhunen, and E. Oja, *Independent Component Analysis*. S.l: Wiley-Interscience, 2001, oCLC: 845874768. [Online]. Available: http://site.ebrary.com/lib/alltitles/docDetail.action?docID=10272411

[43] L. Tong, R.-w. Liu, V. Soon, and Y.-F. Huang, "Indeterminacy and identifiability of blind identification," *IEEE Transactions on Circuits and Systems*, vol. 38, no. 5, pp. 499–509, May 1991.

[44] Xi-Ren Cao and Ruey-Wen Liu, "General approach to blind source separation," *IEEE Transactions on Signal Processing*, vol. 44, no. 3, pp. 562–571, Mar. 1996. [Online]. Available: http://ieeexplore.ieee.org/document/489029/

[45] J. Eriksson and V. Koivunen, "Identifiability, separability, and uniqueness of linear ICA models," *IEEE Signal Processing Letters*, vol. 11, no. 7, pp. 601–604, Jul. 2004.

[46] ——, "Complex random vectors and ICA models: identifiability, uniqueness, and separability," *IEEE Transactions on Information Theory*, vol. 52, no. 3, pp. 1017–1029, Mar. 2006.

[47] M. Behr and A. Munk, "Identifiability for Blind Source Separation of Multiple Finite Alphabet Linear Mixtures," *IEEE Transactions on Information Theory*, pp. 1–1, 2017, arXiv: 1505.05272. [Online]. Available: http://arxiv.org/abs/1505.05272

[48] P. Comon, "Independent component analysis, A new concept?" *Signal Processing*, vol. 36, no. 3, pp. 287–314, Apr. 1994. [Online]. Available: https://linkinghub.elsevier.com/retrieve/pii/0165168494900299

[49] G. Chabriel, M. Kleinsteuber, E. Moreau, H. Shen, P. Tichavsky, and A. Yeredor, "Joint Matrices Decompositions and Blind Source Separation: A survey of methods, identification, and applications," *IEEE Signal Processing Magazine*, vol. 31, no. 3, pp. 34–43, May 2014. [Online]. Available: http://ieeexplore.ieee.org/document/6784078/

[50] Y.-X. Wang and Y.-J. Zhang, "Nonnegative Matrix Factorization: A Comprehensive Review," *IEEE Transactions on Knowledge and Data Engineering*, vol. 25, no. 6, pp. 1336–1353, Jun. 2013.

[51] A.-J. van der Veen and A. Paulraj, "An analytical constant modulus algorithm," *IEEE Transactions on Signal Processing*, vol. 44, no. 5, pp. 1136–1155, May 1996.

[52] C. Papadias and A. Paulraj, "A constant modulus algorithm for multiuser signal separation in presence of delay spread using antenna arrays," *IEEE Signal Processing Letters*, vol. 4, no. 6, pp. 178–181, Jun. 1997.

[53] A. Belouchrani and M. Amin, "Blind source separation based on time-frequency signal representations," *IEEE Transactions on Signal Processing*, vol. 46, no. 11, pp. 2888–2897, Nov. 1998. [Online]. Available: http://ieeexplore.ieee.org/document/726803/

[54] A. Aissa-El-Bey, N. Linh-Trung, K. Abed-Meraim, A. Belouchrani, and Y. Grenier, "Underdetermined Blind Separation of Nondisjoint Sources in the Time-Frequency Domain," *IEEE Transactions on Signal Processing*, vol. 55, no. 3, pp. 897–907, Mar. 2007. [Online]. Available: http://ieeexplore.ieee.org/document/4099541/

[55] F. Gamboa and E. Gassiat, "Source separation when the input sources are discrete or have constant modulus," *IEEE Transactions on Signal Processing*, vol. 45, no. 12, pp. 3062–3072, Dec. 1997. [Online]. Available: http://ieeexplore.ieee.org/document/650266/

[56] Tao Li and N. Sidiropoulos, "Blind digital signal separation using successive interference cancellation iterative least squares," *IEEE Transactions on Signal Processing*, vol. 48, no. 11, pp. 3146–3152, Nov. 2000. [Online]. Available: http://ieeexplore.ieee.org/document/875471/

[57] S. Cruces, "Bounded Component Analysis of Linear Mixtures: A Criterion of Minimum Convex Perimeter," *IEEE Transactions on Signal Processing*, vol. 58, no. 4, pp. 2141–2154, Apr. 2010.

[58] A. T. Erdogan, "A Class of Bounded Component Analysis Algorithms for the Separation of Both Independent and Dependent Sources," *IEEE Transactions on Signal Processing*, vol. 61, no. 22, pp. 5730–5743, Nov. 2013.

[59] S. Cruces, "Bounded Component Analysis of Noisy Underdetermined and Overdetermined Mixtures," *IEEE Transactions on Signal Processing*, vol. 63, no. 9, pp. 2279–2294, May 2015.

[60] H. A. Inan and A. T. Erdogan, "A Convolutive Bounded Component Analysis Framework for Potentially Nonstationary Independent and/or Dependent Sources," *IEEE Transactions on Signal Processing*, vol. 63, no. 1, pp. 18–30, Jan. 2015.

[61] L. De Lathauwer, J. Castaing, and J.-F. Cardoso, "Fourth-Order Cumulant-Based Blind Identification of Underdetermined Mixtures," *IEEE Transactions on*

Signal Processing, vol. 55, no. 6, pp. 2965–2973, Jun. 2007. [Online]. Available: http://ieeexplore.ieee.org/document/4203062/

[62] P. Comon, G. Golub, L.-H. Lim, and B. Mourrain, "Symmetric Tensors and Symmetric Tensor Rank," *SIAM Journal on Matrix Analysis and Applications*, vol. 30, no. 3, pp. 1254–1279, Jan. 2008. [Online]. Available: http://epubs.siam.org/doi/10.1137/060661569

[63] L. De Lathauwer and J. Castaing, "Blind Identification of Underdetermined Mixtures by Simultaneous Matrix Diagonalization," *IEEE Transactions on Signal Processing*, vol. 56, no. 3, pp. 1096–1105, Mar. 2008. [Online]. Available: http://ieeexplore.ieee.org/document/4430007/

[64] J.-F. Cardoso, "Super-symmetric decomposition of the fourth-order cumulant tensor. Blind identification of more sources than sensors," in *[Proceedings] ICASSP 91: 1991 International Conference on Acoustics, Speech, and Signal Processing*. Toronto, Ont., Canada: IEEE, 1991, pp. 3109–3112 vol.5. [Online]. Available: http://ieeexplore.ieee.org/document/150113/

[65] A. Ferreol, L. Albera, and P. Chevalier, "Fourth-order blind identification of underdetermined mixtures of sources (FOBIUM)," *IEEE Transactions on Signal Processing*, vol. 53, no. 5, pp. 1640–1653, May 2005. [Online]. Available: http://ieeexplore.ieee.org/document/1420806/

[66] L. Albera, A. Ferréol, P. Comon, and P. Chevalier, "Blind Identification of Overcomplete MixturEs of sources (BIOME)," *Linear Algebra and its Applications*, vol. 391, pp. 3–30, Nov. 2004. [Online]. Available: https://linkinghub.elsevier.com/retrieve/pii/S0024379504002435

[67] L. Albera, P. Comon, P. Chevalier, and A. Ferreol, "Blind identification of underdetermined mixtures based on the hexacovariance," in *2004 IEEE International Conference on Acoustics, Speech, and Signal Processing*, vol. 2, May 2004, pp. ii–29, iSSN: 1520-6149.

[68] Te-Won Lee, M. Lewicki, M. Girolami, and T. Sejnowski, "Blind source separation of more sources than mixtures using overcomplete representations," *IEEE Signal Processing Letters*, vol. 6, no. 4, pp. 87–90, Apr. 1999. [Online]. Available: http://ieeexplore.ieee.org/document/752062/

[69] M. Zibulevsky and B. A. Pearlmutter, "Blind Source Separation by Sparse Decomposition in a Signal Dictionary," *Neural Computation*, vol. 13, no. 4, pp. 863–882, Apr. 2001. [Online]. Available: http://www.mitpressjournals.org/doi/10.1162/089976601300014385

[70] P. Georgiev, F. Theis, and A. Cichocki, "Sparse component analysis and blind source separation of underdetermined mixtures," *IEEE Transactions on Neural Networks*, vol. 16, no. 4, pp. 992–996, Jul. 2005.

[71] Y. Li, S. Amari, A. Cichocki, D. Ho, and S. Xie, "Underdetermined blind source separation based on sparse representation," *IEEE Transactions on Signal Processing*, vol. 54, no. 2, pp. 423–437, Feb. 2006.

[72] P. Pajunen, "Blind separation of binary sources with less sensors than sources," in *Proceedings of International Conference on Neural Networks (ICNN'97)*, vol. 3, Jun. 1997, pp. 1994–1997 vol.3.

[73] K. I. Diamantaras, "A clustering approach for the blind separation of multiple finite alphabet sequences from a single linear mixture," *Signal Processing*, vol. 86, no. 4, pp. 877–891, Apr. 2006. [Online]. Available: https://linkinghub.elsevier.com/retrieve/pii/S0165168405002392

[74] M. Rostami, M. Babaie-Zadeh, S. Samadi, and C. Jutten, "Blind source separation of discrete finite alphabet sources using a single mixture," in *2011 IEEE Statistical Signal Processing Workshop (SSP)*. Nice, France: IEEE, Jun. 2011, pp. 709–712. [Online]. Available: http://ieeexplore.ieee.org/document/5967801/

[75] K. Diamantaras, T. Papadimitriou, and G. Vranou, "Blind separation of multiple binary sources from one nonlinear mixture," in *2011 IEEE International Conference on Acoustics, Speech and Signal Processing (ICASSP)*. Prague, Czech Republic: IEEE, May 2011, pp. 2108–2111. [Online]. Available: http://ieeexplore.ieee.org/document/5946742/

[76] K. Diamantaras, "Blind channel identification based on the geometry of the received signal constellation," *IEEE Transactions on Signal Processing*, vol. 50, no. 5, pp. 1133–1143, May 2002.

[77] S. Talwar and A. Paulraj, "Blind separation of synchronous co-channel digital signals using an antenna array. II. Performance analysis," *IEEE Transactions on Signal Processing*, vol. 45, no. 3, pp. 706–718, Mar. 1997. [Online]. Available: http://ieeexplore.ieee.org/document/558489/

[78] W. Hoeffding, "Probability Inequalities for Sums of Bounded Random Variables," *Journal of the American Statistical Association*, vol. 58, no. 301, pp. 13–30, Mar. 1963. [Online]. Available: http://www.tandfonline.com/doi/abs/10.1080/01621459.1963.10500830

[79] A. Abdelmutalab, K. Assaleh, and M. El-Tarhuni, "Automatic modulation classification using hierarchical polynomial classifier and stepwise regression," in *2016 IEEE Wireless Communications and Networking Conference*. Doha, Qatar: IEEE, Apr. 2016, pp. 1–5. [Online]. Available: http://ieeexplore.ieee.org/document/7565127/

[80] V. Gouldieff, J. Palicot, and S. Daumont, "Blind automatic modulation classification in multipath fading channels," in *2017 22nd International Conference on Digital Signal Processing (DSP)*. London: IEEE, Aug. 2017, pp. 1–5. [Online]. Available: http://ieeexplore.ieee.org/document/8096116/

[81] J. Bingham, "Multicarrier modulation for data transmission: an idea whose time has come," *IEEE Communications Magazine*, vol. 28, no. 5, pp. 5–14, May 1990.

[82] R. v. Nee and R. Prasad, *OFDM for wireless multimedia communications*, ser. Artech House universal personal communications series. Boston: Artech House, 2000.

[83] Zhendao Wang and G. Giannakis, "Wireless multicarrier communications," *IEEE Signal Processing Magazine*, vol. 17, no. 3, pp. 29–48, May 2000. [Online]. Available: http://ieeexplore.ieee.org/document/841722/

[84] G. Stuber and M. Russell, "Terrestrial digital video broadcasting for mobile reception using OFDM," in *Proceedings of GLOBECOM '95*, vol. 3. Singapore: IEEE, 1995, pp. 2049–2053. [Online]. Available: http://ieeexplore.ieee.org/document/502766/

[85] J. Rault, D. Castelain, and B. Le Floch, "The coded orthogonal frequency division multiplexing (COFDM) technique, and its application to digital radio broadcasting towards mobile receivers," in *IEEE Global Telecommunications Conference, 1989, and Exhibition. 'Communications Technology for the 1990s and Beyond.* Dallas, TX, USA: IEEE, 1989, pp. 428–432. [Online]. Available: http://ieeexplore.ieee.org/document/64008/

[86] J. A. C. Bingham, *ADSL, VDSL, and multicarrier modulation*, ser. Wiley series in telecommunications and signal processing. New York: Wiley, 2000.

[87] A. Scaglione, G. Giannakis, and S. Barbarossa, "Redundant filterbank precoders and equalizers. II. Blind channel estimation, synchronization, and direct equalization," *IEEE Transactions on Signal Processing*, vol. 47, no. 7, pp. 2007–2022, Jul. 1999.

[88] T. Pollet and M. Moeneclaey, "Synchronizability of OFDM signals," in *Proceedings of GLOBECOM '95*, vol. 3, Nov. 1995, pp. 2054–2058 vol.3.

[89] B. Muquet, M. de Courville, and P. Duhamel, "Subspace-based blind and semi-blind channel estimation for OFDM systems," *IEEE Transactions on Signal Processing*, vol. 50, no. 7, pp. 1699–1712, Jul. 2002. [Online]. Available: http://ieeexplore.ieee.org/document/1011210/

[90] R. Heath and G. Giannakis, "Exploiting input cyclostationarity for blind channel identification in OFDM systems," *IEEE Transactions on Signal Processing*, vol. 47, no. 3, pp. 848–856, Mar. 1999.

[91] C. Li and S. Roy, "Subspace-based blind channel estimation for OFDM by exploiting virtual carriers," *IEEE Transactions on Wireless Communications*, vol. 2, no. 1, pp. 141–150, Jan. 2003.

[92] D. Pham and J. Manton, "A subspace algorithm for guard interval based channel identification and source recovery requiring just two received blocks," in *2003 IEEE International Conference on Acoustics, Speech, and Signal Processing, 2003. Proceedings. (ICASSP '03).*, vol. 4, Apr. 2003, pp. IV–317, iSSN: 1520-6149.

[93] B. Su and P. P. Vaidyanathan, "Subspace-Based Blind Channel Identification for Cyclic Prefix Systems Using Few Received Blocks," *IEEE Transactions on Signal Processing*, vol. 55, no. 10, pp. 4979–4993, Oct. 2007.

[94] M. de Courville, P. Duhamel, P. Madec, and J. Palicot, "Blind equalization of OFDM systems based on the minimization of a quadratic criterion," in *Proceedings of ICC/SUPERCOMM '96 - International Conference on Communications*, vol. 3, Jun. 1996, pp. 1318–1322 vol.3.

[95] S. Zhou and G. Giannakis, "Finite-alphabet based channel estimation for OFDM and related multicarrier systems," *IEEE Transactions on Communications*, vol. 49, no. 8, pp. 1402–1414, Aug. 2001.

[96] Y. Song, S. Roy, and L. Akers, "Joint blind estimation of channel and data symbols in OFDM," in *VTC2000-Spring. 2000 IEEE 51st Vehicular Technology Conference Proceedings (Cat. No.00CH37026)*, vol. 1, May 2000, pp. 46–50 vol.1, iSSN: 1090-3038.

[97] Tao Cui and C. Tellambura, "Semi-blind Channel Estimation and Data Detection for OFDM Systems Over Frequency-Selective Fading Channels," in *Proceedings. (ICASSP '05). IEEE International Conference on Acoustics, Speech, and Signal Processing, 2005.*, vol. 3. Philadelphia, Pennsylvania, USA: IEEE, 2005, pp. 597–600. [Online]. Available: http://ieeexplore.ieee.org/document/1415780/

[98] Y. Li, "Pilot-symbol-aided channel estimation for OFDM in wireless systems," *IEEE Transactions on Vehicular Technology*, vol. 49, no. 4, pp. 1207–1215, Jul. 2000.

[99] H. Zamiri-Jafarian and S. Pasupathy, "EM-based recursive estimation of channel parameters," *IEEE Transactions on Communications*, vol. 47, no. 9, pp. 1297–1302, Sep. 1999.

[100] M.-A. Khalighi and J. J. Boutros, "Semi-blind Channel Estimation Using EM Algorithm in Iterative MIMO APP Detectors," p. 9, 2006.

[101] X. Wautelet, C. Herzet, A. Dejonghe, J. Louveaux, and L. Vandendorpe, "Comparison of EM-Based Algorithms for MIMO Channel Estimation," *IEEE Transactions on Communications*, vol. 55, no. 1, pp. 216–226, Jan. 2007.

[102] A. Zia, J. Reilly, and S. Shirani, "Information geometric approach to channel identification: a comparison with EM-MCMC algorithm," in *2004 IEEE International Conference on Communications (IEEE Cat. No.04CH37577)*, vol. 4, Jun. 2004, pp. 2452–2456 Vol.4.

[103] R. Chen, H. Zhang, Y. Xu, and H. Luo, "On MM-Type Channel Estimation for MIMO OFDM Systems," *IEEE Transactions on Wireless Communications*, vol. 6, no. 3, pp. 1046–1055, Mar. 2007.

[104] K. Naskovska, M. Haardt, and A. L. de Almeida, "Generalized Tensor Contractions for an Improved Receiver Design in MIMO-OFDM Systems," in *2018 IEEE International*

Conference on Acoustics, Speech and Signal Processing (ICASSP), Apr. 2018, pp. 3186–3190, iSSN: 2379-190X.

[105] Chiu Shun Wong, D. Obradovic, and N. Madhu, "Independent component analysis (ICA) for blind equalization of frequency selective channels," in *2003 IEEE XIII Workshop on Neural Networks for Signal Processing (IEEE Cat. No.03TH8718)*. Toulouse, France: IEEE, 2003, pp. 419–428. [Online]. Available: http://ieeexplore.ieee.org/document/1318041/

[106] L. Sarperi, X. Zhu, and A. K. Nandi, "Blind OFDM Receiver Based on Independent Component Analysis for Multiple-Input Multiple-Output Systems," *IEEE Transactions on Wireless Communications*, vol. 6, no. 11, pp. 4079–4089, Nov. 2007.

[107] C. Aldana, E. de Carvalho, and J. Cioffi, "Channel estimation for multicarrier multiple input single output systems using the EM algorithm," *IEEE Transactions on Signal Processing*, vol. 51, no. 12, pp. 3280–3292, Dec. 2003.

[108] P. Lancaster and M. Tismenetsky, *The theory of matrices: with applications*, 2nd ed., ser. Computer science and applied mathematics. Orlando: Academic Press, 1985.

[109] L. Hogben and a. O. M. C. Safari, *Handbook of Linear Algebra, Second Edition, 2nd Edition*, 2013, oCLC: 1105801736.

[110] S. Zhou, G. Giannakis, and A. Scaglione, "Long codes for generalized FH-OFDMA through unknown multipath channels," *IEEE Transactions on Communications*, vol. 49, no. 4, pp. 721–733, Apr. 2001.

[111] H. Shiratsuchi and H. Gotanda, "Frequency domain blind channel estimation without phase ambiguity for QAM-OFDM systems," in *2015 9th International Conference on Signal Processing and Communication Systems (ICSPCS)*, Dec. 2015, pp. 1–8.

[112] R. Maoudj, I. Ahriz, A. Savarit, L. Féty, and M. Terre, "4th order statistics based blind channel estimation for multicarrier transmission," in *2014 21st International Conference on Telecommunications (ICT)*, May 2014, pp. 140–144.

[113] R. Maoudj, A. Dziri, and M. Terre, "Blind propagation channel estimation with enhanced auto-deconvolution," in *2016 24th International Conference on Software, Telecommunications and Computer Networks (SoftCOM)*. Split, Croatia: IEEE, Sep. 2016, pp. 1–6. [Online]. Available: http://ieeexplore.ieee.org/document/7772124/

[114] G. Forney, "The viterbi algorithm," *Proceedings of the IEEE*, vol. 61, no. 3, pp. 268–278, 1973. [Online]. Available: http://ieeexplore.ieee.org/document/1450960/

[115] R. Xu and D. WunschII, "Survey of Clustering Algorithms," *IEEE Transactions on Neural Networks*, vol. 16, no. 3, pp. 645–678, May 2005. [Online]. Available: http://ieeexplore.ieee.org/document/1427769/

[116] A. K. Jain and R. C. Dubes, *Algorithms for clustering data*, ser. Prentice Hall advanced reference series. Englewood Cliffs, N.J: Prentice Hall, 1988.

[117] C. M. Bishop, *Pattern recognition and machine learning*, ser. Information science and statistics. New York: Springer, 2006.

[118] Z. Huang, "Extensions to the k-Means Algorithm for Clustering Large Data Sets with Categorical Values," *Data Mining and Knowledge Discovery*, vol. 2, no. 3, pp. 283–304, 1998. [Online]. Available: http://link.springer.com/10.1023/A:1009769707641

[119] E. Schubert and P. J. Rousseeuw, "Faster k-Medoids Clustering: Improving the PAM, CLARA, and CLARANS Algorithms," in *Similarity Search and Applications*, G. Amato, C. Gennaro, V. Oria, and M. Radovanović, Eds. Cham: Springer International Publishing, 2019, vol. 11807, pp. 171–187. [Online]. Available: http://link.springer.com/10.1007/978-3-030-32047-8_16

[120] J. C. Bezdek, *Pattern recognition with fuzzy objective function algorithms*, ser. Advanced applications in pattern recognition. New York: Plenum Press, 1981.

[121] J. C. Dunn, "A Fuzzy Relative of the ISODATA Process and Its Use in Detecting Compact Well-Separated Clusters," *Journal of Cybernetics*, vol. 3, no. 3, pp. 32–57, Jan. 1973. [Online]. Available: http://www.tandfonline.com/doi/abs/10.1080/01969727308546046

[122] L. Fu and E. Medico, "FLAME, a novel fuzzy clustering method for the analysis of DNA microarray data," *BMC Bioinformatics*, vol. 8, no. 1, p. 3, Dec. 2007. [Online]. Available: https://bmcbioinformatics.biomedcentral.com/articles/10.1186/1471-2105-8-3

[123] M. Ester, H.-P. Kriegel, J. Sander, and X. Xu, "A Density-Based Algorithm for Discovering Clusters in Large Spatial Databases with Noise," *KDD'96 Proceedings of the Second International Conference on Knowledge Discovery and Data Mining*, pp. 226–231, Aug. 1996.

[124] M. Ankerst, M. M. Breunig, H.-P. Kriegel, and J. Sander, "OPTICS: ordering points to identify the clustering structure," in *Proceedings of the 1999 ACM SIGMOD international conference on Management of data - SIGMOD '99*. Philadelphia, Pennsylvania, United States: ACM Press, 1999, pp. 49–60. [Online]. Available: http://portal.acm.org/citation.cfm?doid=304182.304187

[125] J. C. Gower and G. J. S. Ross, "Minimum Spanning Trees and Single Linkage Cluster Analysis," *Applied Statistics*, vol. 18, no. 1, p. 54, 1969. [Online]. Available: https://www.jstor.org/stable/10.2307/2346439?origin=crossref

[126] R. Sibson, "SLINK: An optimally efficient algorithm for the single-link cluster method," *The Computer Journal*, vol. 16, no. 1, pp. 30–34, Jan. 1973. [Online]. Available: https://academic.oup.com/comjnl/article-lookup/doi/10.1093/comjnl/16.1.30

[127] D. Defays, "An efficient algorithm for a complete link method," *The Computer Journal*, vol. 20, no. 4, pp. 364–366, Apr. 1977. [Online]. Available: https://academic.oup.com/comjnl/article-lookup/doi/10.1093/comjnl/20.4.364

[128] T. Zhang, R. Ramakrishnan, and M. Livny, "BIRCH: an efficient data clustering method for very large databases," in *Proceedings of the 1996 ACM SIGMOD international conference on Management of data - SIGMOD '96*. Montreal, Quebec, Canada: ACM Press, 1996, pp. 103–114. [Online]. Available: http://portal.acm.org/citation.cfm?doid=233269.233324

[129] U. von Luxburg, "A tutorial on spectral clustering," *Statistics and Computing*, vol. 17, no. 4, pp. 395–416, Dec. 2007. [Online]. Available: http://link.springer.com/10.1007/s11222-007-9033-z

[130] Jianbo Shi and J. Malik, "Normalized cuts and image segmentation," *IEEE Transactions on Pattern Analysis and Machine Intelligence*, vol. 22, no. 8, pp. 888–905, Aug. 2000. [Online]. Available: http://ieeexplore.ieee.org/document/868688/

[131] J. Ribeiro Filho, P. Treleaven, and C. Alippi, "Genetic-algorithm programming environments," *Computer*, vol. 27, no. 6, pp. 28–43, Jun. 1994.

[132] B. Mirkin, *Mathematical Classification and Clustering*. New York, NY: Springer, 2013, oCLC: 1066197090. [Online]. Available: http://public.ebookcentral.proquest.com/choice/publicfullrecord.aspx?p=5575463

[133] M. Meilă, "Comparing clusterings—an information based distance," *Journal of Multivariate Analysis*, vol. 98, no. 5, pp. 873–895, May 2007. [Online]. Available: https://linkinghub.elsevier.com/retrieve/pii/S0047259X06002016

[134] D. Dinler and M. K. Tural, "A Survey of Constrained Clustering," in *Unsupervised Learning Algorithms*, M. E. Celebi and K. Aydin, Eds. Cham: Springer International Publishing, 2016, pp. 207–235. [Online]. Available: http://link.springer.com/10.1007/978-3-319-24211-8_9

le cnam

Stanley SMITH

Optimization strategies for blind multiuser detection in strong interference scenarios

le cnam

Résumé : Dans cette thèse nous étudions la détection aveugle de sources pour des mélanges linéaires à un seul capteur et dans des situations dominées par l'interférence. Nos hypothèses de travail portent uniquement sur l'indépendance des sources et le caractère fini et uniforme de leur distribution. Centrant notre étude autour d'un algorithme itératif de la littérature, plusieurs méthodes d'initialisation sont proposées afin d'en améliorer la robustesse quant aux cas les plus défavorables. En particulier, la relation entre les minima locaux vers lesquels les algorithmes considérés peuvent converger et la géométrie des constellations sous-jacentes aux mélanges est étudiée. Plusieurs méthodes visant à intégrer cette information au processus de détection global sont analysées. Les résultats obtenus par simulation sur des configurations de mélange variées attestent de l'efficacité des stratégies proposées via à vis des algorithmes de détection aveugle traditionnels. Une extension de notre méthode à des canaux sélectifs en fréquence et pour des transmissions multi-porteuses est également effectuée, conduisant à de nouvelles propositions d'initialisation. Notre étude se conclut par des considérations plus générales quant à l'aptitude des algorithmes de classification à pouvoir discerner des ensembles de points exhibant une forte proximité.

Mots clés : Analyse statistique de données, traitement du signal, télécommunications

Abstract : In this thesis we address the blind channel estimation and source detection of linear mixtures with a single sensor in scenarios strongly dominated by interference. In this framework our only assumptions relate to the sources mutual independence, as well as the discrete and uniform nature of their probability distribution. Based on existing iterative algorithms from the literature, we propose several initialization strategies so as to enhance both their overall performance and robustness to highly unfavorable mixture configurations. We provide a detailed analysis of the relation between the spurious fixed points these algorithms are known to possibly converge to and the underlying mixtures geometry. Possible strategies to account for this additional information in the overall detection process are discussed as well. Simulation results attest to a significant improvement of the achieved error rates compared to all tested traditional detection schemes. An extension of the method to the estimation of frequency-selective channels in multiuser and orthogonal multicarrier transmissions is then performed, along with several initialization propositions. We conclude our study by more general considerations on clustering algorithms and their ability to discriminate between partially entangled data classes.

Keywords : Statistical data analysis, signal processing, wireless communications